Finite Element Characterization of the Behaviour of Masonry Infill Shear Walls With and Without Openings

by

Mohammed Ashraf Nazief

A thesis submitted in partial fulfillment of the requirement for the degree of

Doctor of Philosophy

In

Structural Engineering

Department of Civil and Environmental Engineering

University of Alberta

ABSTRACT

The current design practice is to ignore the interaction between masonry infill walls and containing frames due to the inadequate and incomplete guidance in current codes and standards. Most investigations on the behaviour of masonry infill shear walls were performed on scaled specimens and restricted by budget and time to a limited number of parameters. This research aims to help fill the knowledge gap in the understanding of the lateral load-lateral displacement response of masonry infill walls with and without openings.

A finite element (FE) technique was developed to model masonry infilled frames using the simplified micro-modelling approach. Behaviour of contact between the different masonry units and between the masonry infill wall and containing frame was idealized by a traction–separation law that accounts for separations due to tension and shear cracks. The commercially available FE package, ABAQUS, was used to build 3D models for 9 steel and 8 RC masonry infilled frames with and without openings from four major experimental programs. The lateral load–displacement response and failure mechanism of the FE models were in strong agreement with the experimental results. The validated FE technique was used to study some of the most influential parameters such as: infill wall aspect ratio, size and location of gaps between the frame and the infill wall, presence and size of frame haunches, and size and location of window and door openings. The FE analysis was carried out using two master full-size masonry infilled steel and RC frame models representing a 3-storey building designed to the 2010 NBCC.

In addition to the 17 models used to validate the FE technique, 34 solid

infilled frames and 50 infilled frames with openings were built and analyzed for the effect of the parameters under investigation. It was found that a full separation gap up to 5 mm between the infill wall and the frame does not significantly impact the behaviour; to ensure a complete separation, a full separation gap of 10 mm or higher is needed. Another finding is that frame haunches could increase the lateral load resistance by more than 50% compared to frames with no haunches. A single diagonal compression strut was formed in infill walls with openings 10% or less of the wall surface area. Sliding shear was the dominating failure mode for infill walls with large opening size and/or low aspect ratios. Openings that are 15–20% of the infill wall surface area resulted in 50% and more reduction in the lateral load resistance. Still, much research is needed to gain better understanding of the true behaviour of this complex lateral load resisting system.

DEDICATIONS

To my Mother and Father,

To my Brother and Sister,

To Everyone who supported me

ACKNOWLEDGMENTS

I wish to express my sincere thanks to my supervisor Dr. Yasser Korany for his interest and continuous support during the entire length of my program. I would, also, like to thank Dr. Samer Adeeb for assisting me to overcome technical difficulties regarding modelling using ABAQUS. I would, also, like to thank my family at GRACOM represented in Mr. Karl Binder, Mr. Mark Labas and Mr. Kerry Donaghey with whom I was honored to spend amazing time learning about masonry and their way of construction during my internship period at GRACOM.

The financial support of this project was provided by Natural Sciences and Engineering Research Council of Canada (NSERC) together with Canada Masonry Design Centre, the Canadian Concrete Masonry Producers Association (CCMPA) and the University of Alberta; and was gratefully acknowledged.

The analysis of the finite element models were performed on Westgrid High Performance Computing Machines by Compute Canada which made the analysis of the problem possible.

At last and definitely not least, thanks to my mum and dad for believing in me and for their continuous support and encouragement throughout my life.

TABLE OF CONTENTS

LIST OF TABLES

LIST OF FIGURES

LIST OF SYMBOLS AND ABBREVIATIONS

Symbols:

a	:	Small positive constant used to quantify direction of plastic flow when σ & τ equal to zero
A	:	Total area of the diagonal strut
A_{open}	:	Opening size
A_{panel}	:	Area of the masonry infill panel
A_n	:	Net cross-section area of masonry
A_{uc}	:	Uncracked portion of the effective cross-section area of the wall that provide shear bond capacity
b_w	:	Width of the wall
$\mathrm{B_i^I}$	:	Centroidal strain formulation at node *i*
$\dot{d}$	:	First derivative of the displacement with respect to time
d^e	:	Elastic relative displacement vector
d^g	:	Geometric relative displacement vector
d^p	:	Plastic relative displacement vector
d_n^*	:	Relative displacement normal the interface surface
d_t^*	:	Relative displacement tangential to the interface surface
d_v	:	Effective depth for shear calculation
D^e	:	Diagonal matrix of elastic constants
$\mathrm{D_n}$	:	Elastic normal stiffness
E_f	:	Modulus of elasticity of frame material
E_m	:	Modulus of elasticity of mortar joint
E_u	:	Modulus of elasticity of masonry unit

E_θ : Masonry modulus of elasticity in the diagonal direction

E_0 : Masonry modulus of elasticity in a parallel direction to the bed joint

E_{90} : Masonry modulus of elasticity in a normal direction to the bed joint

f_m : Masonry compressive strength

$f'_{m\text{-}0}$: Compressive strength of masonry panel parallel to bed joints

$f'_{m\text{-}90}$: Compressive strength of masonry panel normal to bed joints

F : Force in the diagonal strut

G_f^I : Mode-I fraction energy

G_f^{II} : Mode-II fracture energy

G_m : Shear modulus of mortar joint

G_u : Shear modulus of masonry unit

h : Height of the masonry infill wall

h_m : Thickness of mortar joint

H : Height of frame measured centerline to centerline between beams

I : Node of the element under consideration

I_b : Moments of inertia of the beam sections of the frame

I_c : Moments of inertia of the column sections of the frame

J_2 : Second invariant of deviatoric stress

k_n : Normal stiffness of the interface element

k_s : Shear stiffness of the interface element

K : Elastic Stiffness matrix of the cohesive element

K_{ini} : Initial stiffness of the masonry infilled frame

l : Length of the masonry infill wall

l_a : Opening width

M_f : Factored moment at the section under consideration

M_{pb} : Plastic moment capacity of the beam

M_{pc} : Plastic moment capacity of the column

M_{pj} : Minimum of the column's, beam's or the connection's plastic moment capacity

N^I : Isoparametric shape function

N_i^I : Isoparametric shape function of node *i*

N_u : Factor compressive force acting normal to shear surface that is associated with ultimate horizontal loading

P_1 : Compressive force in masonry acting normal to the sliding plane

P_{cr} : Cracking load for the masonry infilled frame

P_d : Axial compressive load on the section under consideration based on 0.9 times the dead load plus any axial load arising from bending in coupling beam

P_{ult} : Ultimate load for masonry infilled frame

$Q(\sigma)$: Plastic Potential

R_1 : Reduction factor to account for presence of openings

t : Net thickness of masonry infill wall

t_n : Normal traction stress in the interface element

t_s : Shearing traction stress in the s-direction

t_t : Shearing traction stress in the t-direction

T_o : Original Thickness of the cohesive element

u^I : Interpolation function for each node of the element

v_m : Shear strength attributed to masonry

V_{el} : Element volume

V_f : Factored shear at the section under consideration

V_r : Shear Capacity of the masonry

w_{eff} : Diagonal strut effective width

x_i : Spatial position of the point under consideration in the original configuration

α_c : Ratio of column contact length to height of the column

α_b : Ratio of beam contact length to span of the beam

α_h : Vertical contact length between the diagonal strut and the frame

α_L : Horizontal contact length between the diagonal strut and the frame

χ : Factor to account for direction of the compressive strength in masonry member relative to the direction used for the determination of f_m and equal to 0.5

δ_n : Separation in the normal direction

δ_s : Separation in s-direction

δ_t : Separation in t-direction

Δ_{ult} : Displacement corresponding to the ultimate load for masonry infilled frames

ε_p : Plastic strain tensor

φ_m : Masonry resistance factor (equal to 0.6)

η : Parameter controlling direction of flow

γ_g : Factor to account for partial grouted or ungrouted walls that are constructed from hollow or semi-solid units.

$\dot{\lambda}$	:	Plastic multiplier
μ	:	Factor equal to 1.0 for masonry to masonry contact or masonry to roughened concrete sliding plane
ϑ	:	Poisson's ratio
Π	:	Total potential energy
σ	:	Stress vector
σ_e	:	Effective plastic strain
τ	:	shear stresses
Γ_i^I	:	Deformation modes associated with no energy in the point
ξ	:	tan the angle of inclination of asperieties

Abbreviations:

DDA: Discrete Deformation Analysis

FE: Finite element

FEM: Finite Element Method

DT: Diagonal Tension Crack

SS: Sliding Shear

CC: Corner Crushing

FF: Plastic Hinge in the column

SC: Shear Cracks

RC: Reinforced Concrete

NBCC: National Building Code of Canada

COV: Coefficient of Variation

CHAPTER 1

INTRODUCTION

1.1. General

Masonry walls are used extensively as exterior walls to form part of the building envelope and as interior partition in steel/concrete frame structures. Masonry infill walls are mostly considered non-structural elements, and their lateral resistance is not accounted for in current design practices. Engineers neglect the contribution of masonry infill shear walls to resist lateral loads due to the complexity of the analysis and lack of sufficient design information. This practice does not always lead to conservative designs. Infill walls can greatly stiffen flexible frames and can significantly affect the distribution of lateral loads to the members of the resisting system. Higher than expected loads will be attracted to the infilled sections of the frame, which may lead to cracking of the wall and overstressing of the frame. Furthermore, unequal distribution of infill walls will lead to redistribution of lateral loads due to torsional effects. Completely separating infill walls from the surrounding frames requires complex and costly measures to ensure the out-of-plane stability of the infill walls which is otherwise compromised. Therefore, accounting for the presence of masonry infill walls in the analysis of framed structures is necessary for developing efficient designs and to ensure that neither the wall nor the frame is overstressed.

The response of existing buildings provides ample evidence of the ability of masonry infill walls to increase the lateral resistance of buildings. During the 1990 Manjil earthquake in Iran, several buildings did not collapse although they were not appropriately designed to resist earthquake loads because of the presence of the masonry infill walls. A similar situation was reported during the 1992 earthquake in Egypt. The presence of masonry infill walls contributed to resist the lateral load. Moreover, most of the damage took place in the masonry infill walls and not the frame.

Some of the current Codes/Standards Such as Canadian Standard (CSA S304.1-04), New Zealand standard (NZS 4230-04), Mexican Code (2004) and

American Code (MSJC-11) provide design provisions for masonry infill shear walls, but these provisions are restricted to ideal cases that are hard to achieve. Other Codes/Standards neglect the structural effect of the masonry infill wall in resisting lateral loads.

1.2. Problem Definition

The current Canadian Standard for the Design of Masonry Structures (CSA S304.1-04) provides some guidance for the design of masonry infill walls but limited to ideal cases that can hardly be achieved. The masonry infill shear wall has to be in full contact with the containing frame; in other words, no gap between the frame and the masonry infill wall and no openings are allowed. The current edition of CSA S304.1 stated that in case of the presence of opening, a detailed finite element modelling should be performed to show the development of struts within the wall. This is not a feasible way of conducting the analysis.

A study carried out by Nazief and Korany (2013) had shown that CSA S304.1-04 is not consistent in computing the initial stiffness and the ultimate resistance of masonry infill walls. They reported that the initial stiffness and resistance were overestimated for masonry infill walls bounded by steel frames, and underestimated for walls bounded by concrete frames.

Although numerous investigations have been carried out on the in-plane behaviour of masonry infill walls, there is still a lack in understanding of its behaviour. There is a need for a rational approach to account for the contribution of masonry infill shear walls with openings to the lateral load resistance.

1.3. Scope and Objectives

1.3.1. Scope

This study deals with the in-plane behaviour of concrete masonry unit infill shear walls with and without openings bounded by steel and reinforced concrete frames. The behaviour of the frame itself is not part of this study. The investigation was performed numerically using the commercially available finite element program, ABAQUS. The loading considered in this study is in-plane quasi-static

loading condition. The study does not include infill walls subjected to out-of-plane loading or combined loadings.

1.3.2. Objectives

Although the focus of the current study is the in-plane behaviour of masonry infill walls with openings, the research will necessarily cover the behaviour of solid masonry infill walls (i.e.: no window openings). The main objectives of this investigation are to:

- Develop finite element technique capable of predicting the load-displacement response of masonry infilled frames with and without openings with adequate accuracy.
- Use the finite element technique to investigate the effect of the most influential parameters on the behaviour of masonry infill walls. These influential parameters include: Infill wall's aspect ratio, opening size and location, partially and fully grouted infill, presence of gaps between the masonry infill wall and the containing frame, and frame hunched corners (i.e.: hunched column-beam connection)

1.4. Thesis Organization

In Chapter 1, a brief overview of the problem is provided and the motivation behind the current study. The research scope and objectives were also presented in this chapter.

In Chapter 2, the behaviour of masonry infill shear walls was reviewed from available literature. The effect of different parameters on the resistance of the masonry infill shear walls were discussed. Also, the design methodologies presented in different codes and standards for these types of walls were summarized.

The non-linear finite element modelling technique used for the assessment of masonry infilled frames under in-plane loading was described in Chapter 3. The material models used to characterize the frame and masonry wall materials were presented.

Chapter 4 discussed validation of the developed finite element models against published test results. A summary for the finite element models built to study the effect of the most influential parameters (masonry wall aspect ratio, gap size and location, stiffness of infill wall, effect of haunches, and opening size and location) was given in Chapter 5. Description of different material properties used for the steel and masonry material were also included.

The effect of the infill wall aspect ratio, gap size and location, stiffness of infill wall and haunches on the lateral load-lateral displacement behaviour of solid infill walls (no openings) were presented in Chapter 6; whereas the behaviour of masonry infill walls with opening were presented in Chapter 7. Finally, Chapter 8 included the main conclusions and recommendations for future work.

CHAPTER 2

LITERATURE REVIEW

2.1. Introduction

In modern construction, masonry walls are used extensively to fill concrete and steel frames due to high impact resistance and heat and sound insulation properties. These walls are called *masonry infill shear walls*. Due to the lack of design information, the practice has been to ignore the interaction between the masonry infill wall and the containing frame to simplify the design. Considering the interaction between the infill walls and the containing frame may not be beneficial for the frame (Karayannis et al., 1998). It may also lead to unsafe and/or uneconomical design (Drysdale and Hamid, 2005). It is worth mentioning that infill walls have poor seismic performance against moderate and high seismic loads. This is attributed to the high degradation of stiffness, strength and low dissipation in the energy that results from brittle failure of the masonry infill walls (El-Dakhakhni, 2002).

The behaviour of the masonry infill shear walls has been studied experimentally and analytically. Smith (1966) investigated the behaviour using finite element models. Smith and Carter (1969), Stafford-Smith and Coull (1991) and Mainstone (1971) used the strut approach to simulate the behaviour of solid infill walls (no openings) under monotonic loading. The infill walls were presented by single strut. Asteris (2008) reported that presenting the wall with one single strut element is ineffective in modelling the complex behaviour of infilled frames. Nazief and Korany (2013) compared different codes/standards expressions in computing the diagonal strut width, initial stiffness and infill wall resistance relative to experimental testing.

Liauw (1972) adopted a method for analyzing the infilled frame through using an equivalent frame to represent the infilled system. Liauw and Kwan (1983) developed a plastic collapse theory for the masonry infill based on testing micro-concrete infill. It was noted that the presence of the infill panels leads to increase the stiffness of the containing frames and the dissipating energy; however, the

frame-infill system becomes less ductile even in cases of defective infilled frames (Asteris, 2008).

Masonry infill shear walls could fail in one of these main modes: i) Diagonal cracking, ii) Sliding shear along bed joints or iii) Compression failure in the diagonal strut (Maan and Müller, 1982, Drysdale and Hamid, 2005, Kaltakc et al., 2006). These walls must also be designed to resist the out-of-plane loading that might be exerted on them. Kaltakc et al. (2006) reported that failure will take place in frame's legs and beam prior to the infill in case of having a infill wall with high strength. Researchers indicated that walls are capable of resisting more loads although a diagonal crack has formed within the wall; thus, diagonal cracking should not be considered to be structural mode of failure (El-Dakhakhni et al., 2003 and Flanagan and Bennett, 2001).

Although there is significant amount of research carried out on the topic, All of them was limited to small set of parameters that can affect the behaviour. None of the researchers considered the effect of all possible parameters on the in-plane behaviour of both steel and RC infilled frames. The investigations did not cover large pool of window and door openings that could influence the behaviour.

2.2. Experimental Testing of Masonry Infill Walls

Several experimental investigations were performed to investigate the effect of numerous parameters on the performance of infill steel frames. Dawe and Seah (1989) conducted an experimental investigation on 28-full-scale, single storey, single bay specimens infilled with 200×200×400 mm hollow concrete blocks. The specimens were built using steel frame of a total height of 2800 mm and center-to-center length between columns of 3600 mm. The frame's column was constructed using W250×58 steel-section placed along its week axis, while the beam's section was W200×46 steel-section. The average compressive and tensile strength for masonry was 22 and 2.5 MPa, respectively. Several parameters that affects the load carrying capacity were investigated including: frame to wall boundary conditions, opening size, joint reinforcement, reinforcing the diagonal strut, presence of bond beam within the infill, and frame rigidity. Dawe and Seah (1989) recognized the

most influential parameters that affects the behaviour of masonry infill shear walls, yet they did not test ranges for these parameters.

It was reported that absence of mortar between the frame flanges and the infill wall has a small effect on the initial stiffness of the system, but the ultimate load was reduced by 16%. The presence of ties between the frame and the infill walls did not affect the initial stiffness of the infill wall compared to those without ties; however, the ultimate load was reduced by 20%. In addition, the cracking pattern of the infill wall was not the same as the standard specimen; this was attributed to the restrain provided by the presence of ties. The presence of gaps or bond breaker between the infill wall and the roof beam led to reduction in the major cracking and ultimate load by 50%. A similar conclusion was reached when poor quality mortar was used between the frame and the infill. This was attributed to elimination of the interface shear which helps in narrowing the size of the developed cracks. Joint reinforcement had no significant effect on the capacity and initial stiffness. A completely hinged frame experienced a reduction in the ultimate load as well as the initial major cracking by 50% and 25%, respectively. The deflected shape of hinged frames led to separation between the infill and the containing frame (similar to the case where a gap is present).

The presence of door opening location was investigated and found that for central door openings, the reduction in the initial stiffness and ultimate capacity was 54% and 40%, respectively; when the opening was located away from the loading side the reduction in the initial stiffness and carrying capacity was less than the previous case (32% and 34% respectively). The worst location for the openings was reported to be near the loading point which led to reduction of 54% and 56% in the initial stiffness and carrying capacity of the infill wall respectively. Reinforcing the compression strut led to increase in the initial stiffness and ultimate capacity by 76% and 31%, respectively compared to unreinforced walls. Using bond beams had a minor effect on the ultimate load carrying capacity of infill walls (only 3% more in ultimate capacity than the ordinary masonry infill).

Mehrabi et al. (1996) tested twelve ½-scale single storey, single bay, RC

frames experimentally infilled with hollow and solid concrete masonry units of dimensions 92.075×193.675×92.075 mm. Two RC frames were designed according to ACI 318 (1989): strong frame capable of resisting the high lateral loading, and weak frame that resists basic wind speed of 100 mph. During the design of the frames, the contribution of the masonry wall was ignored. The hollow and solid concrete blocks were used in the experimental testing to simulate strong and weak infill. The masonry panel was constructed after the frame construction as in the common construction practice. During testing, the level of vertical loading was kept constant; some specimens had the vertical load acting on the column, while others had ⅓ of the load being applied to the beam and ⅔ applied to the columns. In their experimental testing, Mehrabi et al. (1996) did not consider on the effect of openings or gap size between the frame and the wall in the behaviour. Also, scaled specimens are not a good representative for the true behaviour of large scale buildings.

It was reported that infill panels with lower aspect ratios (*h/l*) sustained higher lateral loading than those of higher aspect ratio. For *h/l* of 1/2, the lateral resistance is 17% higher than *h/l* of 2/3. It was also reported that using strong infill led to the increase in the infill wall stiffness 35 times more than weak infill. Higher vertical loads on the masonry infill walls was found to increase the stiffness and lateral load resistance of the infill wall. The presence of the vertical loading led to increasing the confinement of the specimen; hence, increasing its lateral load capacity.

Al-Chaar (1998) studied the performance of reinforced concrete frames infilled with concrete masonry units as well as clay brick units. The investigation was conducted on ½ scale specimens. The frames were single, double and triple bay width with typical bay width of 2032 mm between centerlines of columns; the height of the infill walls was 1524 mm. The column cross-section was 203×127 mm, while the beam cross-section was 197×127 mm. The slenderness of the concrete masonry wall (*h/l*) is 13.9**,** while that for clay brick was 23.13. Type N mortar was used in all the investigations. Unlike other researchers, Al-Chaar looked at multiple bay frames. He did not look at the effect of gaps (top gap and full

separation gap) between the frame and the infill wall.

It was stated that the presence of stiffer masonry infill wall enables the system of carrying more load than the case of the bare frame. For multiple bay frames the stiffness increases nonlinearly with the increase of the number of infilled bays. Most of the damage in the infill walls will take place in the infill wall located at near the loaded side. It was reported that increasing the prism strength of the infill wall led to enhancement of the strength of the infill wall.

Another experimental investigation was conducted by Chiou et al. (1999) on clay brick infilled concrete frames. The length of the containing frame was 3000 mm, and its height was 2700 mm. The column cross-section was 300×350 mm, while the beam cross-section was 350×400 mm. Two specimens were considered in their investigation. The first specimen was built using brick units with full height and in full contact with the containing frame, while the other specimen had a partial height wall (1100 mm height) to resemble the presence of large window openings. Chiou et al. (1999) looked only on one size of window in their investigation.

It was reported that presence of the partial height wall decreased the ultimate lateral load capacity of the system by 47% compared to full infilled frames. The presence of partial height walls introduced to new supporting condition to the frame's column which led to new straining actions (bending moment and shear force) not account for in the orginal design; this led to cracking in the frame at this location.

Flanagan and Bennett (1999) studied infill steel frames with clay tile units experimentally. In their work, 8 different specimens with different column and beams sizes were tested till failure. The infill wall thickness was also varied between being single wythe (195 mm thick) and double wythe (330 mm thick). The sizes of the steel frame sections as well as the length and height of the infilled wall varied from one frame to another to study the effect of frame stiffness on infill wall behaviour. Flanagan and Bennett investigated only clay tile infilled steel frames, and their findings cannot be extended to other types of masonry infilled frames.

Three frames with aspect ratios of 1.0, 0.79 and 0.65 were tested. It was

reported that decreasing the infill walls aspect ratio led to increase in the infill ultimate capacity by 5% and 11%, respectively. The presence of gaps between the frame and infill wall was found to reduce the initial stiffness by 40%; however, the ultimate load capacity of the infilled frame was not affected. The presence of openings within the infill wall led to reduction 50% of in the infill wall capacity if it was located near the loaded side, and 25% if it was away from the loaded side. The ultimate capacity of infill walls were increased when using fixed frames. This was attributed to the larger contact between the frame and the infill which led to higher confinement to the infill wall.

When the infill wall was placed eccentrically with respect with the containing frame, spalling of mortar took place in the infill wall. The load was applied in the centerline of the containing frame which led to introducing out-of-plane loading to the infill wall. It was observed that the in-plane initial stiffness and peak loading was reduced by 30% and 25%, respectively, compared to specimens having the infill wall at the centre of the wall.

El-Dakhakhni et al. (2004) tested two infilled frames with hollow concrete masonry units of nominal dimensions 400×200×150 mm: one had solid infill, while the other had an opening within the infill. They compared their results to the case of bare frame. The dimensions of the test specimens were 3600 mm in length between centerlines of supports, while the height of the frame till the top of the beam was 3000 mm. the columns and beams of the frame were constructed using W250×33 I-beam section. The size of the door opening was 1000×1500 mm. The average compressive strength of the blocks was found to be 21.4 MPa based on the net area of the block; the average compressive strength of mortar was found to be 20.7 MPa, while that of the masonry prism was found to be 13.4 MPa (face-shell area only). The specimens were subjected to cyclic quasistatic loading at one end. The behaviour was limited to one frame in full contact and another having one size of window opening; hence, the conclusion cannot be used to describe the behaviour and failure mode appropriately.

El-Dakhakhni et al. (2004) indicated that the presence of the opening within

the wall leads to degradation in the carrying capacity of the wall. Due to the presence of a major crack above the door opening, the infill wall would behave as if it is three different parts. The first part will be the one above the opening (above the lintel), while the second and third parts would be the parts to the left and right of the door opening. The side walls would act as struts. Diagonal cracking on those side parts would occur once the maximum tensile capacity of the wall is exceeded.

Moghaddam (2004) studied the behaviour of concrete frame infilled with brick masonry units. The study focused on the effect of different masonry units on the lateral resistance of the masonry infill system. Five specimens were considered in this study having identical frame dimensions. The frame had a height of 1300 mm and length of 1500 mm. Beam and columns were constructed with steel using INP120 steel standard section of area 1420 mm^2 and moment of inertia of 3280000 mm^4. The first specimen was infilled with solid brick units with total infill dimensions (length × width × thickness) 1240×1380×110 mm. The dimension of the individual brick unit was 60×210 mm. The second specimen is considered to be a repaired specimen for the first one where the crushed materials were replaced with concrete. In addition to that, a small knee tie was provided at the beam-column joint to repair the weld at this location. The third specimen is identical to the first one except that the masonry units used were perforated masonry units. The fourth specimen was a repaired specimen for the third one; the repair was performed by applying a wire mesh and a micro-concrete shotcrete of thickness 2.5 mm on each face of the infill panel. For the fifth sample, it is the same as the third specimen except that concrete units were used at the compressed corners. Moghaddam (2004) did not look at the behaviour of masonry infilled frames when there is gap between the wall and the containing frame, or when there is a window/door opening in the masonry wall. It was reported that using perforated clay brick units led an increase 41% in the ultimate capacity than using solid units. This conclusion contradicts with what was reported by Mehrabi et al. (1996).

Yàñez et al. (2004) carried out experimental testing on sixteen full-scale, single-bay, single-storey masonry infilled reinforced concrete frames. The type of masonry units used in this investigation where of concrete blocks and clay bricks.

Four of the test specimens were constructed using solid infills, whereas the rest had opening within with different size to account for window and door openings. The specimens were subjected to cyclic loading. Their work focused only on the behaviour of weak frames. They reported that all specimens failed due to diagonal tension cracking initiation in the wall. The presence of window and door opening led to increasing the ductility of the system compared to solid infill frames; however, the ultimate load was reduced.

Kakaletsis and Karayannis (2009) conducted experimental study on the effect of the presence of infill within single-storey, one-bay, ⅓-scale reinforced concrete frames. The masonry infill was constructed using clay tile units. The length of the infill wall was 1200 mm, while its height was 800 mm. The column cross-section was 150×150 mm, while the beam cross-section was 100×200 mm. Three specimen having centered windows opening (height equal to 333 mm) with different width were tested (opening width to wall length (l_a/l) equals 0.25, 0.38 and 0.5, respectively). Additional three specimens with door openings having the same l_a/l were tested as well (height of door opening was 666 mm). The frame was designed so that the column had closer ties along its length. The beam was reinforced with more stirrups in the critical regions. The beam-column connection was reinforced with five horizontal stirrups to prevent its brittle failure. The masonry properties were chose to be weak in resisting lateral loads. All specimens were scaled specimens, which is not a good representative for the behaviour. The study focused only on the behaviour of clay brick tiles.

It was reported that the presence of openings within the infill wall led to reduction in its capacity as found by Dawe and Seah (1989) and Flanagan and Bennett (1999). Moreover, the infilled frames were affected more by the presence of door openings more than window openings. This is due to the formation of small piers with lower stiffness when doors were introduced.

Blackard et al. (2009) tested ⅔-scale, single bay, single storey masonry infilled concrete frames with clay brick units of dimensions 197×95.3×57.2 mm. The frame was constructed to behave in a non-ductile manner; the masonry infill

wall was not reinforced. Four specimens were considered in this study: solid infill, infill with small window opening (978×749 mm), infill with door opening (711×1422 mm) and infill with large window opening (1524×787 mm). The door and windows opening were placed with an eccentricity with respect to the containing frame. Similar to the previous researches, scaled specimens are not a good representative to the true behaviour of the system. The research focused only on one size for a door and a window opening and did not cover effect of gaps between the frame and the infill wall. It was found that the presence of opening led to reduction in the capacity of infill frame systems; the peak plateau was longer (more ductile) than the case of solid infill.

Tasnimi and Mohebkhah (2011) studied the performance of clay brick infilled steel frames with openings. The steel frame was of length 2400 mm centerline to centerline, while the height was 1870 mm. Both the column and the beam were constructed using I-beam of section IPE 140. The masonry infill was constructed using brick units of dimensions 219×110×66 mm (the thickness of the wall is 110 mm). Six specimens were considered in their investigation: bare frame, solid frame and four frames with different opening sizes (500×500 mm window opening, 700×800 mm window opening, 1200×600 mm window opening and 700×1450 mm door opening). All openings were centered with the containing frame, and off-centre locations was not investigated. The investigation looked at the effect of opening sizes on the lateral capacity of the infill wall. The same conclusion regarding the effect of openings within the infill wall was found; however, it was stated that openings would not increase the ductility of the system (unlike other researches).

2.3. Numerical Modelling of Masonry Infill Walls

The in-plane behaviour of masonry infill shear walls has been investigated numerically. Numerical analysis has benefits over experimental testing as it is a less expensive way to carry out the investigation rather than testing lots of specimens. Also, numerical modelling enables study of the most influential parameters that affects the behaviour of this type of walls. However, these models

had to be calibrated and validated against experimental testing.

In general, there are two different techniques to study the behaviour of masonry numerically: Micro and Macro level modelling. Micro-modelling deals with modelling all the masonry components (i.e.: the masonry unit, mortar and the interface between them). This type of modelling requires full description of the material used which is obtained from experimental testing of material samples of masonry units and mortar. This type of modelling is complicated; however, it allows tracing the developed stresses and cracks developed within the wall assembly.

Macro-modelling lumps the masonry unit, the mortar joint and the interface together to form one homogenous material. It treats the masonry as a homogenous continuum having an anisotropic behaviour. Macro-modelling is useful when studying large walls where the developed stresses are likely to be uniform; it cannot be used in studying the failure patterns of masonry walls.

According to Lourenço (1996), masonry micro-model can take one of the following techniques: i) detailed micro-modelling or ii) simplified micro-modelling.

The first modelling scheme requires the knowledge of all material properties of masonry unit and mortar. The interface between the two materials is a potential crack/slip surface. This model enables studying different element behaviour in a detailed manner. One of the drawbacks of this modelling technique is the large computational time. The second scheme simplifies the problem by lumping the mortar joint and the interface into an average interface. In this case, the masonry unit has to be expanded to keep the geometry unchanged. This model is less accurate than the previous one (Poisson's ratio for mortar is ignored), but it saves time in computation.

In the simplified micro-modelling technique, all the damage is concentrated in the weak mortar joint, and in pure tension surface in the masonry unit at vertical plane in the middle of the block to simulate cracks that could occur in the head joints, bed joints and/or masonry units. Two dimensional interface element is

provided between the masonry units to create discontinuity in the displacement field. Lourenço (1996) provides approximate formulas for the computation of the normal and shear stiffness (k_n, k_s) of the interface element used between masonry elements as:

$$k_n = \frac{E_u E_m}{h_m(E_u - E_m)} \quad \text{2-1}$$

$$k_s = \frac{G_u G_m}{h_m(G_u - G_m)} \quad \text{2-2}$$

Where, E_u: Modulus of elasticity of masonry unit

E_m: Modulus of elasticity of mortar joint

h_m: Thickness of mortar joint

G_u: Shear modulus of masonry unit

G_m: Shear modulus of mortar joint

In the past years, analysis of infill shear walls was complicated; however, the presence of modern computer software and powerful computing machines has facilitated the analysis of these walls numerically. Modelling masonry infill shear walls is one of the most challenging problems due to the complexity of the modelling scheme that must be followed. Most of the current research was carried out using Finite Element Method (FEM) (Zeinkiewicz and Taylor, 2000) or Discrete Deformation Analysis (DDA) (Shi, 1988).

2.3.1. Micro Modelling

Mehrabi and Shing (1997) developed a finite element model to investigate the behaviour of concrete frame infilled with concrete masonry units. They used the smeared crack element to model the concrete frame and the masonry units. The effect of the mortar joint was accounted for by using constitutive models. The developed constitutive model assumed the nonlinear hardening behaviour of the interface under a compressive stress to be an elastic phenomenon. Shear dilatation was a combination of normal compaction and geometric dilatation as shown:

$$d = \dot{d^e} + \dot{d^p} + \dot{d^g} \quad \text{2-2a}$$

Where:

$$d^e = \begin{Bmatrix} d_n^e \\ d_t^e \end{Bmatrix} \quad \text{2-2b}$$

$$d^p = \begin{Bmatrix} d_n^p \\ d_t^p \end{Bmatrix} \quad \text{2-2c}$$

$$d^g = \begin{Bmatrix} d_n^g \\ d_t^g \end{Bmatrix} \quad \text{2-2d}$$

Where:

d^e, d^p, d^g: Elastic, Plastic & Geometric relative displacement vectors.

d_n^*, d_t^*: Relative displacement normal and tangential to the interface surface

$\dot{d}$: First derivative of the displacement with respect to time.

The elastic behaviour of the system was expressed using Equation 2-3; as for the plastic behaviour, yield criterion and non-associate flow rule that was introduced by Lotfi and Shing (1994) was considered in this study. Equation 2-4 and 2-5 demonstrated these rules.

$$\sigma = D^e d^e \quad \text{2-3}$$

Where:

σ: Stress vector

D^e: Diagonal matrix of elastic constants

d^e: Relative displacement vector

$$Q(\sigma) = \frac{1}{2}[\eta\tau^2 + (\sigma + a)^2] \quad \text{2-4}$$

Where:

$Q(\sigma)$: Plastic Potential

η: Parameter controlling direction of flow

σ, τ: Normal & shear stresses

a: Small positive constant used to quantify direction of plastic flow when σ & τ equal to zero

$$\dot{d}^p = \dot{\lambda}\frac{\partial Q}{\partial \sigma} \qquad 2\text{-}5$$

Where:

$\dot{\lambda}$: Plastic multiplier

Contraction of the interface would occur under compressive stress greater than *a*. It was reported that the geometric dilatation would not occur till fracture took place. The shear dilatancy is given as the sum of the normal plastic compaction and the geometric dilatation. Equation 2-6 shows the expression used for the computation of the shear dilatation.

$$\dot{d}^g = A\dot{d}^p \qquad 2\text{-}6a$$

$$A = \begin{bmatrix} 0 & \text{Sign}(d_t^p)\dot{d}_t^p\xi \\ 0 & 0 \end{bmatrix} \qquad 2\text{-}6b$$

Where:

ξ: tan the angle of inclination of asperieties

Mehrabi and Shing (1997) reported a variation in the obtained results in case of having a bond slip element between the frame element and the masonry infill. The results when bond slip interface elements were considered in the analysis were closer than when it was ignored. The computed peak capacity was close to those of experimental testing (variation of about 10%); however, the entire behaviour of the system was not the same as experimental testing. This could be attributed to the choice of element used in modelling the concrete frame and masonry elements.

A simplified computer model was proposed by Dawe et al. (2001a). This model was developed using linear finite element. The load-deflection response of the infill wall can be further used in modelling multi-bay multi-storey frames by replacing the infill panel by diagonal members having the same load-deflection response as the proposed model.

Their proposed model took into account different parameter as gaps, interface bond and friction, separation and re-contact at the frame infill interface. Moreover, the model took into account the nonlinear behaviour due to shear and tension cracking in the infill panel as well as crushing in the infill. The development of plastic hinge within the frame members was accounted for in their models. The load was increased in a stepwise manner at the selected nodes of the analytical model. At each load step, the stresses in the infill panel were determined and checked for failure. When failure was reported, the stiffness matrix of the system was modified to take into account this failure, and the analysis was repeated until no failure was detected. When the model became in equilibrium, the deflection of the system was recorded. The load was increased after reaching the peak load to ensure that failure took place. In order to reach equilibrium after failure, additional springs having stiffness of same order of magnitude as the frame were introduced. Figure 2-1 shows a schematic for the proposed model.

To determine the force in the infill panel, the force in the spring is subtracted from the total applied force of the system. The load deflection-behaviour of the infill panel can then be developed. This small approximation has a slight effect on the load deflection behaviour of the system. In modelling the frame, a plane linear elastic frame element having three degrees of freedom at each joint was used. Different frame elements were joined together by a zero length elements having two translational and one rotational spring; the same spring elements were used to join the frame to the support. All nonlinearity in the frame behaviour was concentrated in these joints presented in Figure 2-2.

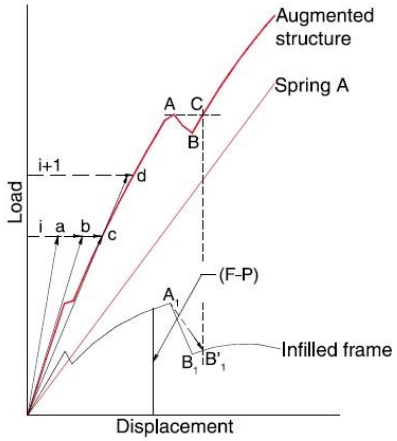

Figure 2-1: Schematic for computing the force in the infill (Source: Dawe et al., 2001a)

The masonry panel was assembled using rectangular elastic zones of plane stress elements joined together with joint element having limited shear and tensile capacity. The joints have infinite compressive stiffness and capacity, low tensile strength and shear capacity depending on mortar bond strength and joint friction to simulate cracking in masonry.

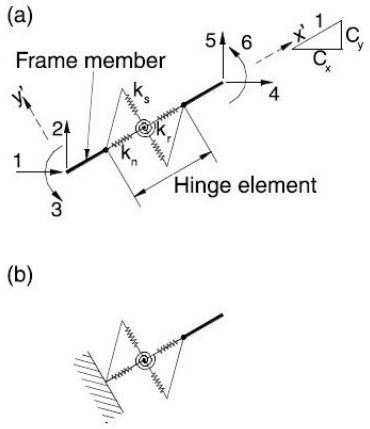

Figure 2-2: Schematic for: a) hinge element connecting frame elements and b) hinge element at support (Source: Dawe et al., 2001a)

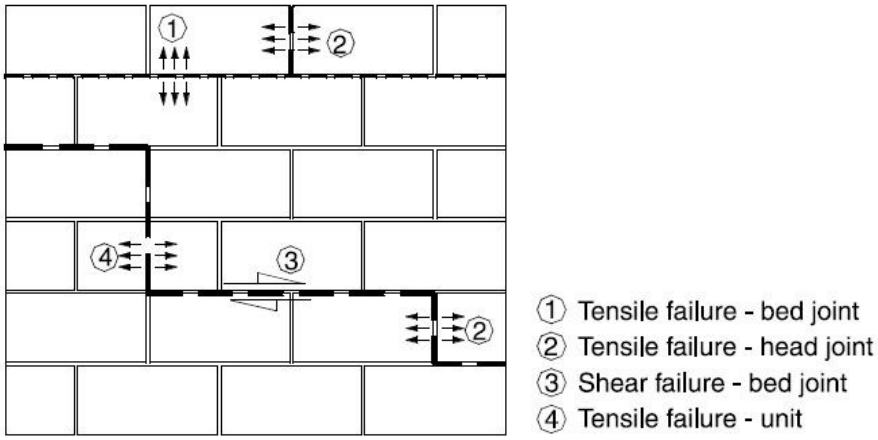

Figure 2-3: Failure modes in the masonry infill wall (Source: Dawe et al., 2001a)

The interface between frame and infill panel was presented by a pair of normal and tangential springs attaching the infill to the frame element presented in Figure 2-4; its properties were identified according to the bond between the frame and the infill. The normal spring will identify the amount of compression transferred at the interface. Consequently, the tangential stiffness of the interface element will simulate the bond and friction between the panel and the frame. The effect of the joint reinforcement was implemented by adding its effect to the global stiffness matrix of the infill system.

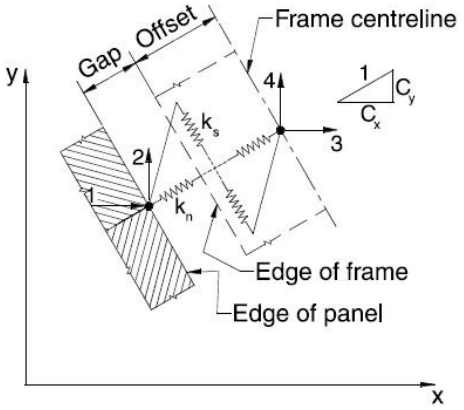

Figure 2-4: Interface element between the masonry infill and the frame element (Source: Dawe et al., 2001a)

The masonry panel is assumed to be homogenous and linear elastic up to cracking and orthotropic in direction parallel and normal to bed joints. Their

proposed model was in good agreement with the experimental data (maximum Error of 20%). The difference between the experimental and the proposed results may be attributed to the approximation used when not enough information is available for the model. In addition, material properties are not always constant all over the specimen. Another drawback of the proposed modelling technique is: it just works for steel infilled frames and not RC ones.

Moghaddam (2004) developed a finite element model to study the behaviour of brick infilled steel frames. His study focused on the behaviour of the system in the elastic range; the peak and post peak behaviour of infilled walls was not considered in this study. Three types of elements were used in modelling the problem: three degree of freedom beam element, two degrees of freedom panel element and rigid short interface element with pin ends. The choice of the panel element was taken equal to ½ the size of the brick element used in the investigation to predict and capture all possible failure mechanisms that could take place in the masonry infill wall. The effect of the mortar joint was not considered in this investigation.

It was reported that shear stresses reached its maximum value closer to the development of the compression strut. He stated that his model is limited for cases where the failure of the wall is not dominated by crushing of the masonry infill at its corners.

Al-Chaar et al. (2008) introduced a modelling technique for masonry infilled RC frames. Their analysis was performed using commercially available software, DIANA. Both, the RC frame and the masonry infill wall were modelled using continuum elements with a smeared-crack constitutive models; the mortar joint were modelled using structural interface as specified by Lourenço (1996) to capture the cohesion, separation and shear degradation at the interface. In their model, they relied on Coulomb friction model combined with a tension cutoff and elliptical compression cap shown in Figure 2-5. One of the draw backs of this modelling technique is that it fails in capturing cumulative damage taking place in a mortar joint.

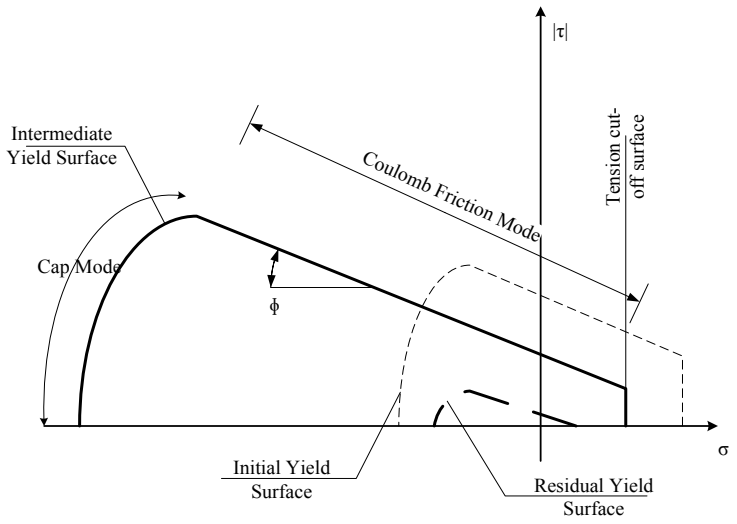

Figure 2-5: Interface model used by Al-Chaar et al. (2008)

The problem of concrete frames infilled with masonry units was studied by Alam et al. (2009). Unlike other researchers, the infill wall was modelled using detailed micro-modelling. The infill was modelled using 2D plane stress elements. Interface elements capable of transmitting shear and normal forces were used between the RC frame and the infill wall. A Coulomb friction model was assigned to the interface elements. If the shear stress exceeded limiting value, sliding would take place between the two surfaces relative to each other.

Stavridis and Shing (2010) used the FEM to study the lateral load behaviour of RC frames infilled with concrete masonry units. Their modelling technique combines smeared and discrete cracking approaches to capture different failure modes of the frame-infill system. Their analysis was carried out using commercial available software "FEAP" (Taylor 2007). The RC frame was modelled using a four triangular smeared-crack elements connected with four double-nodded interface elements, shown in Figure 2-6, to model the shear cracking in the RC frame. Horizontal and vertical interface elements were used to capture cracks developed at 0°, 90° and ± 45° (as modelled). Truss elements were used in modelling the vertical reinforcement; while the shear reinforcement, presented in Figure 2-6, was placed in a zigzag pattern to prevent sliding along the horizontal interface, which is not a realistic mode of failure.

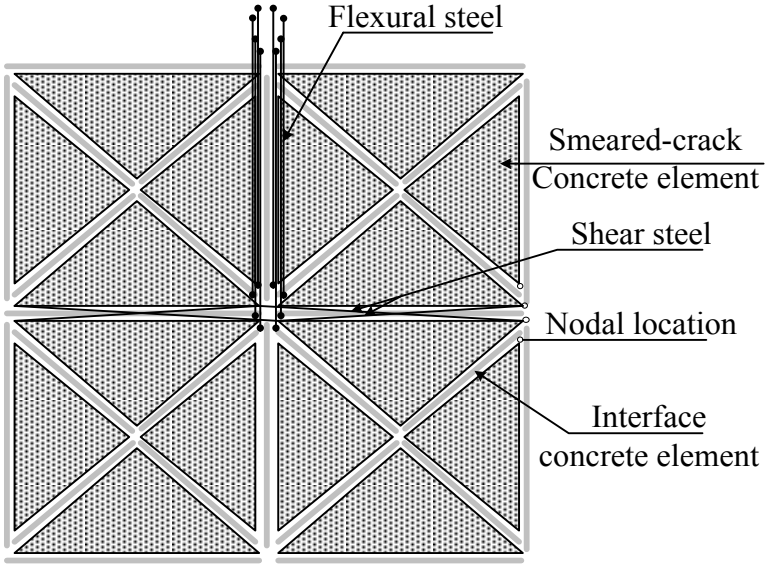

Figure 2-6: Finite element model (developed from: (Stavridis and Shing 2010))

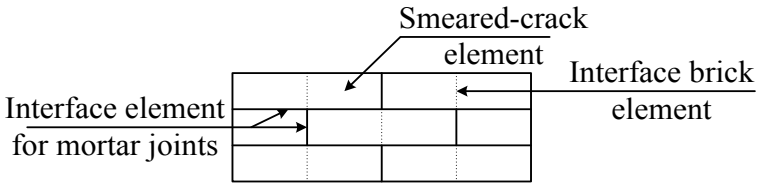

Figure 2-7: Stavridis and Shing (2010) finite element model for infill panel

The masonry units were modelled using the smeared-crack elements as the RC frame. Interface brick element was introduced at the middle of each the block to account for possible splitting of each block. Different elements were connected together using interface elements to account for the presence of mortar joint. Figure 2-7 shows a schematic for Stavridis and Shing (2010) proposed modelling scheme for masonry.

A simple nonlinear orthogonal material law was used to simulate the tensile fracture of the materials. The materials are modelled using elastic-plastic law identified by Von-Mises failure surface together with the tension cutoff. The Von-Mises surface is given by:

$$J_2 - {}^1\!/_3\,\sigma_e^2 \varepsilon_p = 0 \qquad 2\text{-}7$$

$$\varepsilon_p = \sqrt{(2/3) d\varepsilon_{ij}^p d\varepsilon_{ij}^p} \qquad 2\text{-}8$$

Where:

J_2: Second invariant of deviatoric stress

σ_e: Effective plastic stress tensor

ε_p: Plastic strain tensor

Figure 2-8 shows the strain hardening/softening as well as the orthotropic material laws adopted by Stavridis and Shing (2010). A crack was initiated perpendicular to the direction of the maximum principle stress when maximum tensile strength (f_t') was exceeded; hence, the orthogonal material law was used to simulate the nonlinear behaviour in tension and compression. The constitutive model used simulates the fracture modes given by Lotfi and Shing (1994).

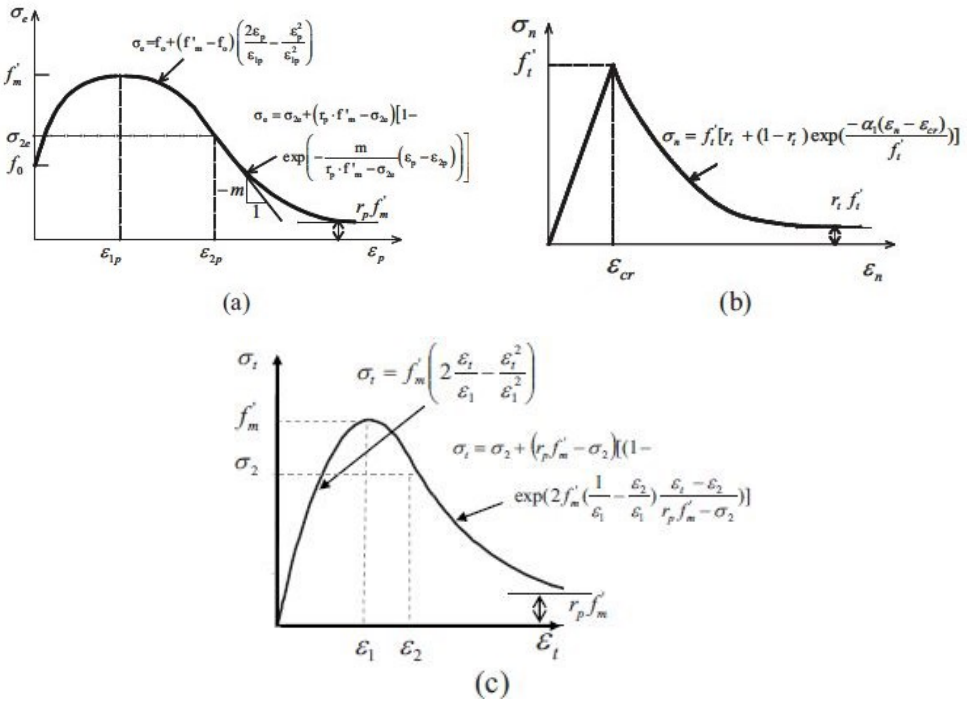

Figure 2-8: Constitutive models: a) Plasticity model effective stress vs strain, b) tensile behaviour model and c) full compressive behaviour model (Source: Stavridis and Shing, 2010)

The concrete material model was calibrated using fracture mode-I and

Mode-II, G_f^I and G_f^{II}. Fracture mode-I, G_f^I, was obtained from fracture testing and test data available in literature. The value of G_f^{II} was assumed to be ten times that of G_f^I. The additional parameters controlling the shape of failure surface (α, β, μ, η and r) depend on the aggregate size and the composition of concrete mixes. These parameters were determined from the mixed mode fracture test given by Hassanzadeh (1990). The orthogonal model of the concrete was determined from compressive stress-strain relation of a concrete cylinder. The mortar behaviour parameters were determined using the beam test or the bond wrench test (Stavridis and Shing, 2010). The shearing strength at the mortar joint could be obtained by conducting the direct or triple shear test. Mode-II fracture energy, G_f^{II}, was determined from sliding shear test; while Mode-I fracture energy, G_f^I, is taken to be one-tenth of G_f^{II}. The elastic normal stiffness, D_n, was determined to simulate accurately the compressive behaviour of the masonry assembly. The value of the tangential stiffness was taken $D_n/(2(1+\vartheta))$, where ϑ is Poisson's ratio for mortar. Masonry elements were modelled as the concrete element. The tensile strength was determined using the splitting test and/or modulus of rapture test. Mode-I fracture energy was taken as reported in literature (Van der Pluijm, 1992).

In their investigation, some parameters were assumed. They carried out sensitivity analysis for these assumed parameters to see the effect of their assumption on the obtained results. It was reported for some parameters, the variation could impact the results of the model significantly. The main drawback of the proposed model is that it is only suitable for analysis under the action of monotonic loading (Koutromanos et al., 2011).

2.3.2. Macro Modelling

Macro-model is a simplified method that studies the global behaviour of infilled frame system; its intention is not to model local failures that might take place within the masonry infill panel. Usually, a masonry infill wall is simulated by diagonal strut(s) joining the corners of frame's columns together (Smith and Carter (1969), Stafford-Smith and Coull (1991); Mainstone (1971)). Several researches have proposed different ways to account of the masonry infill wall. Different

width(s) for the diagonal strut varied considerably between them. The following section covers this modelling technique.

The behaviour of masonry infilled frames was investigated by Al-Chaar (2002). A push over analysis was carried out on infill panels using nonlinear finite element analysis. The masonry panel was modelled using an equivalent strut model shown in Figure 2-9. In case of the presence of openings, Al-Chaar (2002) proposed using a factor to be multiplied by the width of the full infill to account for the infill presence. The same diagonal strut width of the diagonal strut as indicated by Smith and Carter (1969) and Mainstone (1971) was considered in his work for solid infill (i.e.: no openings). An additional reduction factor was implemented to the previous equations to account for cracking that are present within the infill wall when loading.

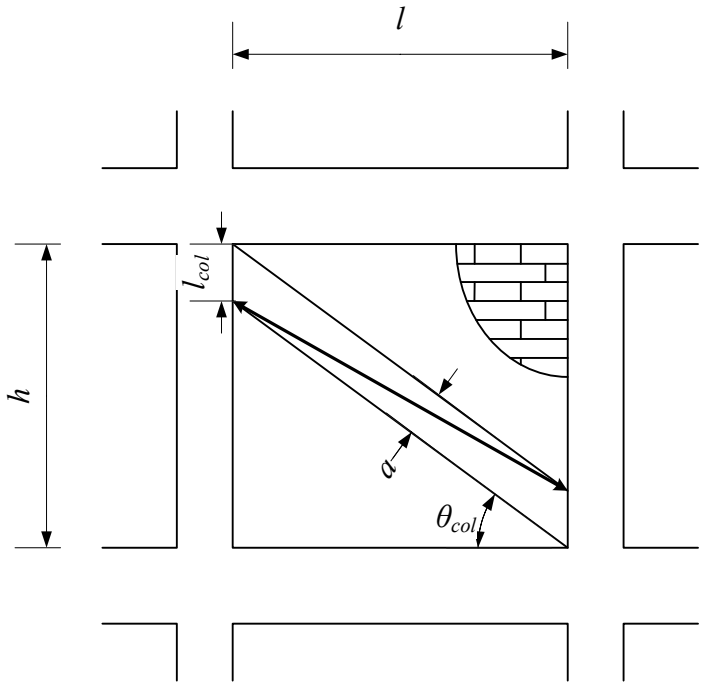

Figure 2-9: Proposed strut model by (Al-Chaar 2002)

The proposed width of the diagonal strut is given as shown in the following equations:

$$\lambda_1 = \left(\frac{E_m t \sin 2\theta}{4EI_{col}h}\right)^{\frac{1}{4}} \qquad 2\text{-}9a$$

$$\theta = \tan^{-1}\frac{h}{l} \quad \text{2-9b}$$

$$D^2 = h^2 + l^2 \quad \text{2-9c}$$

$$a = 0.175D(\lambda_1 H)^{0.4} \quad \text{2-9d}$$

$$\tan\theta_{col} = \frac{h - a/\cos\theta}{l} \quad \text{2-9e}$$

$$l_{col} = \frac{a}{\cos\theta_{col}} \quad \text{2-9f}$$

Where:

E_m: Masonry modulus of elasticity

t: Net thickness of masonry infill wall

H: Height of frame measured centerline to centerline between beams

Two reduction factors were introduced to the width of the diagonal strut to account for the presence of opening in the infill panel and the presence of cracks in the infill wall, R_1 and R_2 respectively. Table 2-1 shows his proposed values for R_2.

$$R_1 = 0.6\left(\frac{A_{open}}{A_{panel}}\right)^2 - 1.6\left(\frac{A_{open}}{A_{panel}}\right) + 1.0 \quad \text{2-10}$$

Where, R_1: Reduction factor to account for presence of openings

A_{open}: Opening size

A_{panel}: Area of the masonry infill panel

Table 2-1: Values of R_2 (Al-Chaar, 2002)

	R_2 for Type of Damage	
h/t	Moderate	Severe
≤ 21	0.7	0.4
> 21	Requires Repair	

El-Dakhakhni et al. (2003) presented the masonry infill wall with three diagonal struts to model the infill panel. They stated that this modelling technique

has better capability in simulating the stiffness of the infill wall as well as the developed stresses within the frame members. The proposed model was an approximation of a finite element model that was carried out using commerically available software, ANSYS, in which they noted that the contact between the infill and the frame took place in a region and not a single point. Figure (2-10) shows their proposed model.

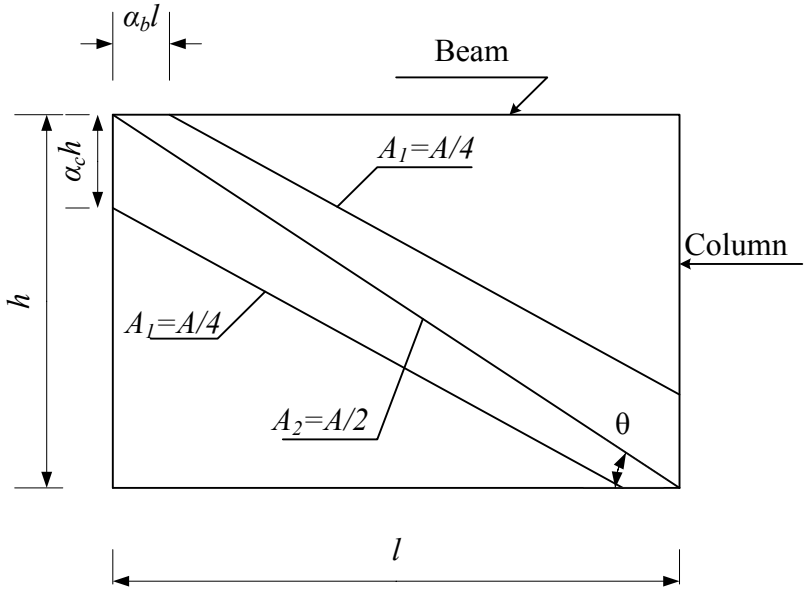

Figure 2-10: El-Dakhakhni et al. (2003) proposed three strut model

The width of the overall diagonal strut was determined using contact length between the masonry infill wall and the containing frame as proposed by Saneinejad and Hobbs (1995) near failure of the infill wall. This expression was modified to be in terms of the compressive strength of the prism in direction normal and parallel to the bed joint as follows:

$$\alpha_c h = \sqrt{\frac{2\,(M_{pj} + 0.2\,M_{pc})}{f'_{m\text{-}0}\;t}} \leq 0.4h \qquad 2\text{-}11a$$

$$\alpha_b l = \sqrt{\frac{2\,(M_{pj} + 0.2\,M_{pb})}{f'_{m\text{-}90}\;t}} \leq 0.4l \qquad 2\text{-}11b$$

Where:

α_c: Ratio of column contact length to height of the column

α_b: Ratio of beam contact length to span of the beam

h: Height of the column

l: Length of the beam

M_{pj}: Minimum of the column's, beam's or the connection's plastic moment capacity

M_{pc}, M_{pb}: Plastic moment capacity of the column and beam

f'_{m-0}, f'_{m-90}: Compressive strength of masonry panel parallel and normal to bed joints

t: Thickness of infill wall

El-Dakhakhni et al. (2003) suggested that the total area (A) of the diagonal strut to be divided to 3 parts; the edge areas shall be presented by a diagonal strut having area $A_1 = A/4$. The middle strut was taken to have an area A_2 equal to twice the edge strut. The value of A took the following form:

$$A = \frac{(1 - \alpha_c)\,\alpha_c\, h\, t}{\cos\theta} \qquad 2\text{-}12$$

Where:

A: Total area of the diagonal strut

α_c: Ratio of column contact length to height of the column

h: Height of the column

t: Thickness of infill wall

θ: $\tan^{-1}(h/l)$

El-Dakhakhni et al. (2003) modelled the frame using elastic elements. The nonlinearity in the frame's behaviour was lumped in the beam-column joint through the use of nonlinear springs. The joint capacity was taken as the minimum of column's, beam's or connection ultimate plastic capacity. Thus, the ultimate capacity of the bare frame (H_u) is given in terms of minimum of the column's, beam's or the connection's plastic moment capacity; and the frame height as:

$$H_u = \frac{\sum_{n=1}^{4} M_{pj}}{h} \quad \text{2-13}$$

Since the diagonal strut are acting at an angle, El-Dakhakhni et al. (2003) proposed an equation for the computation of the modulus of elasticity of the masonry in terms of its angle of inclination. In their computation, masonry was treated as an orthotropic material. The value of the modulus of elasticity acting at an angle θ is given as:

$$E_\theta = \frac{1}{\frac{1}{E_0}\cos^4\theta + \left[-\frac{2\nu_{0-90}}{E_0} + \frac{1}{G}\right]\cos^2\theta \sin^2\theta + \frac{1}{E_{90}}\sin^4\theta} \quad \text{2-14}$$

Where:

E_θ: Masonry modulus of elasticity in the diagonal direction

E_0, E_{90} : Masonry moduli of elasticity in a parallel and normal direction to the bed joint

ν_{0-90}: Poisson's ratio defined as the ratio of the strain in the direction normal to bed joint due to strain in direction parallel to bed joint

G: Shear modulus

θ: Angle of inclination of the diagonal strut

Furthermore, the stress strain relation for the masonry infill panel was simplified to account for the peak stress as shown in Figure 2-11. The idealization was achieved by joining different points by straight lines. The values of the strains ε_1, ε_2 and ε_p are computed as follows:

$$\varepsilon_1 = \varepsilon_p - 0.001 \quad \text{2-15a}$$

$$\varepsilon_2 = \varepsilon_p + 0.001 \quad \text{2-15b}$$

$$\varepsilon_u = 0.01 \quad \text{2-15c}$$

El-Dakhakhni et al. (2003) indicated that that the proposed macro-model was capable of simulating some of El-Dakhakhni (2002) experimental test results but not all of them.

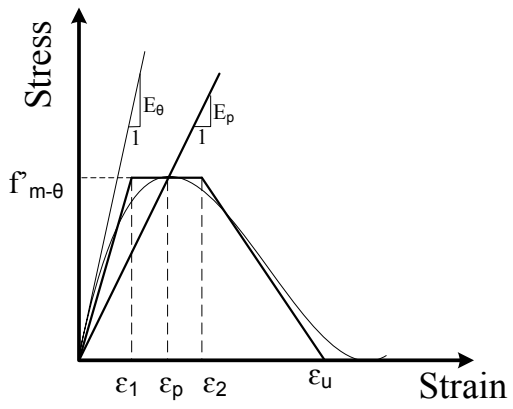

Figure 2-11: El-Dakhakhni et al. (2003) simplified stress-strain tri-linear relations

Asteris (2008) developed a 2D finite element model in which plane beam elements were used to model the frame. The masonry infill was modelled using a four element isoparametric rectangular element with 8 degrees of freedom. He assumed the masonry material to be homogenous anisotropic material. A new methodology to account for contact/separation between the infill wall and the containing frame was achieved iteratively. Preliminary, the infill panel is tied to the containing frame at two corner points (end points of the compression strut). When the lateral loading is applied, the nodal forces, displacement and stresses were calculated at the Gauss points; then a check is performed to make sure that the infill nodes do not overlap with the frame. In case of no overlap, another check is required to make sure that there is no tension developed. In case of presence of tension forces, these points should not be linked. In contrast, if the nodes overlapped the frame, these points are then linked with the overlapped location; the analysis is repeated again until there is no overlap. Despite the simplicity of the proposed model, it deals with the masonry infill as a homogenous isotropic material which is not the case. Masonry infill walls are formed from to different materials. The interface between them is considered to be a plane of weakness. In most of the cases it is the location at which failure is initiated. The proposed model fails in reflecting this kind of behaviour.

Rodrigues et al. (2010) adopted a simplified macro-model based on the strut approach to model infill walls. The infill wall was modelled using four rigid strut

elements connected with a central element. All the nonlinearity in the behaviour of the masonry infill shear wall is lumped into the central element. The proposed model and properties of the central element is shown in Figure 2-12. The load displacement response of the masonry infill shear wall must be known in advance of modelling. Also, the proposed model fails in capturing the behaviour of partial height walls.

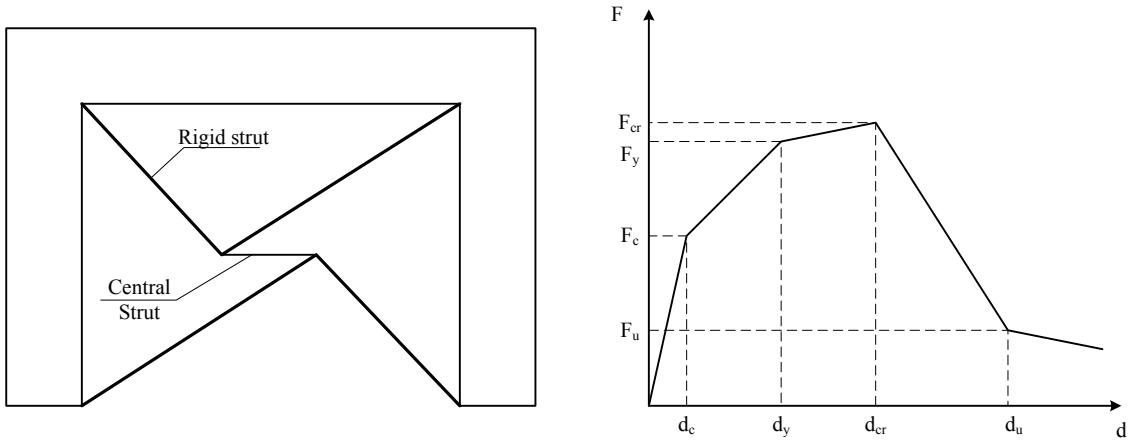

(a) Strut Model (b) Material model for central element

Figure 2-12: Proposed model by Rodrigues et al. (2010)

2.3.3. Discontinuous Deformation Analysis Model

Another numerical way to model masonry structure is the use of using Discontinuous Deformation Analysis (DDA). This method was first introduced by Shi (1988). Discontinuous deformation analysis is considered an implicit method that possesses complete block kinematics, first order displacement approximation, postulate of equilibrium and energy consumption. In DDA, no interpenetration or tension is allowed between blocks at any time; the variables in DDA are the displacements.

The equations are solved in the same way as finite-element analysis. Each block in the DDA is independent and connection only exists when blocks are in contact with one another. The interactions between different blocks are simulated by contact springs. Any inadmissible contacts are deleted, and corner-corner

contacts are dealt with using some rules. The solution is computed based on an iterative technique until the contact forces enter equilibrium with time. The Mohr-Coulomb law regulates the contact behaviour by ensuring that the sole source of energy consumption comes from friction losses only. A first-order polynomial is chosen as the displacement function for the 2-D blocks to restrict the block to constant stress.

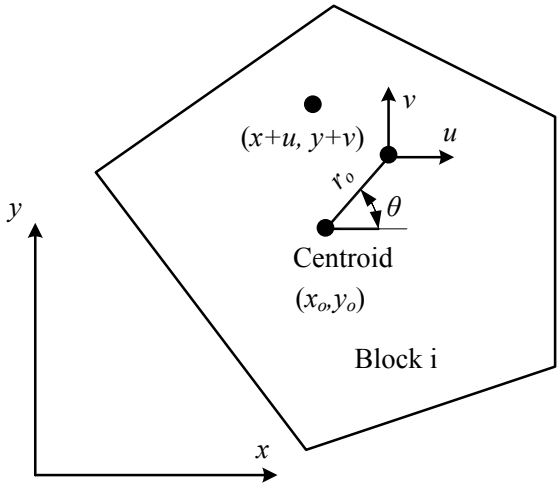

Figure 2-13: Schematic for block configuration as per Chiou et al. (1999)

$$\begin{Bmatrix} u \\ v \end{Bmatrix} = \begin{bmatrix} 1 & 0 & -(y-y_o) & (x-x_o) & 0 & (y-y_o)/2 \\ 0 & 1 & (x-x_o) & 0 & (y-y_o) & (x-x_o)/2 \end{bmatrix} \times \begin{Bmatrix} u_o \\ v_o \\ r_o \\ \varepsilon_x \\ \varepsilon_y \\ \gamma_{xy} \end{Bmatrix} \quad \text{2-16a}$$

$$\begin{Bmatrix} u \\ v \end{Bmatrix} = [T_i][D_i] \quad \text{2-16b}$$

Where:

x_o, y_o: Coordinate of block centroid

x, y: Any point in block i

u_o, v_o: Rigid body translation

r_o: Rigid body rotation

u, v: Displacement at any point in block i

ε_x, ε_y, γ_{xy}: Strain component in the 2D

T_i: First order displacement function

D_i: Displacement vector of block i

Shi (1988) derived the equilibrium equation by minimizing the total potential energy. The equilibrium equations for n blocks are given as:

$$\begin{bmatrix} K_{11} & K_{12} & \cdots & K_{1n} \\ K_{21} & K_{22} & \cdots & K_{2n} \\ \vdots & \vdots & \ddots & \vdots \\ K_{n1} & K_{n2} & \cdots & K_{nn} \end{bmatrix} \begin{Bmatrix} D_1 \\ D_2 \\ \vdots \\ D_n \end{Bmatrix} = \begin{Bmatrix} F_1 \\ F_2 \\ \vdots \\ F_n \end{Bmatrix} \quad \text{2-17}$$

Where:

K_{ii}: Depends on material modulus and inertia effect of Block i

K_{ij} $(i \neq j)$: Depends on the contact between block i and j.

F_i: Force vector of Block i

The coefficient for K_{ij} and F_i are written as:

$$(K_{rs})_{ij} = \frac{\partial^2 \Pi}{\partial d_{ri} \partial d_{sj}}, r, s = 1,2,\ldots\ldots,6 \quad \text{2-18}$$

$$(F_r)_i = \frac{\partial \Pi(0)}{\partial d_{ri}}, r = 1,2,\ldots\ldots,6 \quad \text{2-19}$$

Where Π is the total potential energy that includes the contribution of the inertia forces, initial stresses, internal strains, point loading, body forces, contact spring deformation... etc. The force in the contact springs will increase with the increase in the level of the applied load until it reaches its capacity. Failure will occur when the capacity is reached.

Chiou et al. (1999) studied the behaviour of masonry infill walls using DDA. In addition, they carried out experimental testing to verify the proposed technique. The DDA results were found to be in good agreement with the experimental testing (about 4% variation); however, it is worth mentioning that this

method does not provide any post cracking information on the infill panel. In addition, it is a 2D analysis.

2.4. Factors Affecting the Behaviour of Masonry Infill Shear Walls

2.4.1. Wall Aspect Ratio

The masonry infill wall aspect ratio is defined as the wall's height to length ratio. Mehrabi et al. (1996) studied the effect of the masonry infill aspect ratio on the performance of masonry infill frames. They reported that infill panels with lower aspect ratios sustained higher lateral loading that those of higher aspect ratios. For *h/l* of 1/2, the lateral resistance is 17% higher than *h/l* of 2/3.

Flanagan and Bennett (1999) conducted a similar investigation on three identical steel infilled frames with clay tiles with aspect ratios of 1.0, 0.79 and 0.65. They reached the same conclusion as Mehrabi et al. (1996). It was observed that decreasing the infill walls aspect ratio led to increase in the infill ultimate capacity by 5% and 11%, respectively, compared to walls with h/l of 1.0. Similarly, an increase of 6% and 9% was recorded for the load causing tile failure. Decreasing the aspect ratio of the infill wall means increase of its length; hence, increase of its stiffness and ability to sustain more lateral load.

Dawe et al. (2001a) investigated the effect of changing the aspect ratio numerically using FEM. The same material and frame section present in Dawe and Seah (1989) were used in their investigation. Three infilled frames having *h/l* of 0.5, 1 and 1.5 were considered. They reported that infill walls with small aspect ratios had higher first peak resistance (increase of 4% and 14% compared to infill with *h/l* of 1.0 and 1.5, respectively). Dawe et al. (2001a) stated that after the first peak (crushing of the corners) was reached, the infilled frame with aspect ratio 1.0 sustained higher load; this load is even higher than the first peak. This contradicts what was published in previous experimental work, and it can be attributed to the occurrence of singularities at some nodes after failure of the corner took place.

2.4.2. Frame to Masonry Infill Wall Boundary Conditions

Dawe and Seah (1989) observed that there is no significant change in the initial stiffness of the masonry infill wall when no mortar was placed between column flanges and infill wall. Only the ultimate load was reduced by 16% was reported due to the decrease in the compressive strength of the used masonry prism. They also looked at the performance of infill walls when they were tied with the adjacent columns with flat-bars and L-shaped ties. The presence of ties did not affect the initial stiffness of the masonry infill panel compared to those without ties; however, the ultimate load was reduced by 20%. In addition, the cracking pattern of the infill wall was not the same as the standard specimen; this was attributed to the restrain provided by the presence of ties between the column and the infill walls. The diagonal compression strut was not developed completely due to these extensive cracking. A similar conclusion was reported by Dawe et al. (2001a) through FEM modelling. Dawe et al. (2001a) indicated that the interface condition between the frame and the masonry infill has a little effect (can be ignored) on the capacity.

The presence of gaps between the infill wall and the roof beam had a significant effect on the initial stiffness as well as the ultimate strength of the masonry. Dawe and Seah (1989) compared four specimens together; specimen WB2 and WB3 were similar specimens built from steel frames and having masonry infill of same properties. No mortar was present between the panel and the flange. Specimen WB4 was similar to the previous once, except there was 20 mm gap between the beam and the infill wall. Specimen WB5 was similar to WB4, but the infill was tied to the column flanges. It was reported that the presence of the gap led to reduction in the major cracking and ultimate load by 50%. If the quality of the mortar used between the frame and the infill was poor, a similar conclusion was reached as the case of the gap. This could be attributed to the presence of cracks in the mortar due to shrinkage when it hardened. The performance of infill walls separated from the frames with bond breakers would behave as the case of gaps. This was attributed to elimination of the interface shear which helps in narrowing the size of the developed cracks.

Flanagan and Bennett (1999) studied the performance of steel infilled frame with clay tiles where there was no mortar joint between the frame and the infill wall. It was observed that the initial stiffness of the wall was less than when the wall was in full contact. Once the gaps were closed, the stiffness increased remarkably. The presence of these gaps did not affect the ultimate load capacity of the infilled frame.

2.4.3. Masonry Infill Wall Stiffness

Mehrabi et al. (1996) studied the effect of using strong infill in enhancing the infill wall behaviour. A comparison between strong infill constructed from solid concrete blocks and weak infill constructed from hollow concrete blocks was conducted. It was reported that the use of strong infill led to the increase in the infill wall stiffness 35 times more than weak infill; strong infills carried more load prior to failure.

Al-Chaar (1998) and Al-Chaar et al. (2002) stated that the presence of stiffer masonry infill wall enables the system of carrying more load than the case of the bare frame. Moreover, the stiffness increases with the increase of the number of infilled bays of a multi bay frame; however, this increase does not follow a linear pattern. It was also reported that the masonry infill was capable of sustaining load even after damage took place (compared to the bare frame case). The same behaviour was reported by Dawe et al. (2001a). In their numerical investigation, it was found that increasing the prism strength of the infill panel led to enhancement of the strength of the infill wall.

Moghaddam (2004) carried out a similar investigation using infilled steel frames with brick units. He stated that the use of perforated brick infill led to increase in the lateral stiffness by 43% more than using solid ones. Although the compressive strength of solid prisms was higher than those of perforated ones, the later was found to have higher shear rigidity. This had an effect on the overall ultimate capacity; perforate units leads to 41% increase in the ultimate capacity than using solid units. He reported that the first crack load was the same for both types of brick units.

2.4.4. Openings in the Masonry Infill Wall

The effect of presence of openings was studied experimentally by several researchers. Dawe and Seah (1989) investigated the behaviour of infill walls having door openings in several locations. They found that presence of door opening reduces initial stiffness as well as ultimate capacity of masonry infill walls. The reduction was found to be more when opening is located near by the loading point rather than having it away from it.

Chiou et al. (1999) observed failure in the frames column near the loading edge for partially infilled RC frames with clay brick units. Most of the cracks were located at the center of the column. The partial height wall introduced additional supporting condition which was not taken into consideration in the design of the RC frame. For full height walls, cracking took place at the corner of the frame's column near the loading side. Horizontal cracking on the interface between containing frame base and the infill wall was also reported. The presence of the partial height wall led to decrease in the ultimate capacity of the system by 47% than the case of full infill; however, the mode of failure of the two specimens were not the same.

Flanagan and Bennett (1999) introduced a window opening of dimensions 600×600 mm placed in the corner of the clay tile infill wall within steel frame. They reported that presence of the opening reduced the stiffness of the infilled frame significantly. They reached the same conclusion given by Dawe and Seah (1989). The reduction in the infill capacity is more when the opening is near the loaded side than away from it (50% and 25% reduction, respectively).

El-Dakhakhni et al. (2004) indicated that the presence of the opening within the wall leads to degradation in the carrying capacity of the wall. Due to the presence of a major crack above the door opening, the infill wall behaved as three different parts. The first part will be the one above the opening (above the lintel), while the second and third parts would be the parts to the left and right of the door opening. The side walls would act as struts. Diagonal cracking on those side parts would occur once the maximum tensile capacity of the wall is exceeded.

Kakaletsis and Karayannis (2009) reached a similar conclusion as the previous researchers. The presence of openings led to decrease in the capacity of the masonry infill wall. Kakaletsis and Karayannis (2009) stated that the infill frame system is affected more by the presence of door opening than windows. This is due to the formation of small piers with lower stiffness when doors are introduced. A similar conclusion was reached by Yáñez et al. (2004).

Blackard et al. (2009) stated that although the presence of opening reduces the capacity of infill frame systems, the peak plateau is longer (more ductile) than the case of solid infill. The presence of window openings within the infill did not reduce the ultimate capacity of the infill wall significantly (Shing et al., 2009). The presence of infill affected the failure mode of frame's columns (shear and flexural failures at unexpected locations). Another observation was the presence of window openings led to reduction in the ultimate carrying capacity of the wall by 15% compared to the solid case (Blackard et al., 2009 and Shing et al., 2009).

Unlike other researchers, Tasnimi and Mohebkhah (2011) stated that presence of the openings within the infilled frames did not increase the ductility of the system. They reported that the ductility of the system relies on the mode of failure of the infill panel. Infill panels failing in diagonal tension or toe crushing would have less ductility than solid infills. They defined the ductility to be the post peak response till complete failure of the system. All the other researchers considered ductility to be the ability of the system to carry the load till peak load. After peak load is reached, spalling and deterioration of the masonry material is more likely to take place in infill with openings (not confined as solid infill).

2.4.5. Joint Reinforcement

Dawe and Seah (1989) studied the effect of the presence of joint reinforcement on the capacity of masonry infill shear walls. They report that the presence of the joint reinforcement in the infill panel had a minor effect on the ultimate carrying load capacity. However, absence of horizontal joint reinforcement led to the increase in cracking in the infill panel; hence, decrease in the initial stiffness of the wall.

2.4.6. Reinforcing the Diagonal Strut

Dawe and Seah (1989) studied the effect of the presence of diagonal reinforcement on the carrying capacity of the masonry infill shear walls. They grouted vertical reinforcement bars of length equal to the expected diagonal compression strut width. It was reported that this technique led to increase in the initial stiffness and ultimate capacity by 76% and 31% respectively of the infill panel.

2.4.7. Presence of Bond Beams

In an experimental investigation to study the effect of bond beams on the behaviour of masonry infill shear walls, Dawe and Seah (1989) reported that using bond beams had a minor effect on the ultimate load carrying capacity of infill walls (only 3% more than the ordinary masonry infill). It was observed that the first major crack coincided with the attainment of the ultimate load. In addition, the pre-peak stiffness was found to be 38% more than the ordinary masonry infill wall which was in full contact with the wall and no joint reinforcement was provided.

2.4.8. Gravity Loading

Mehrabi et al. (1996) mentioned that the increase in the value of the vertical loading led to the increase in the stiffness and the maximum resistance of the specimen. The presence of the vertical loading led to increasing the confinement of the specimen; hence, increasing its capacity. This statement is true till a certain limit. If the applied gravitational load exceeds an optimum value cracking in the infill would occur reducing the capacity of the system (Dawe et al., 2001a). When the specimen was subjected to cyclic loading, lower resistance than the case of the monotonic loading was recorded. The same conclusion was reported by Liu and Manesh (2013).

2.4.9. Frame Rigidity

Some researchers studied the effect of frame rigidity on infill walls. Dawe and Seah (1989) and Dawe et al. (2001b) studied this behaviour experimentally and numerically. They studied the performance of seven different infill frames with different rigidity. Specimen WD7 was built of masonry infill wall and a rigid frame.

The infill wall was reinforced with horizontal truss-type joint reinforcement (Blok-Trus BL30) placed in alternate bed joints. No mortar was provided between column flanges and infill wall. Four specimens (WD8, WD9, WD 10 and WD13) where similar to WD7, except that they were built inside a completely hinged frame. Another two masonry specimens were constructed within a completely hinged frame, the first havmg a 20 mm gap between the infill and the roof beam (WD11); while the other had a central door opening of dimensions 0.8x2.2 m and no vertical reinforcement was provided along the sides of the wall (WD12). All the specimens were tested till complete failure.

Dawe and Seah (1989) reported that the use of a completely hinged frame led to reduction in the ultimate load as well as the initial major cracking by 50% and 25%, respectively. An interesting observation was found in the behaviour of WD8 and WD11. Although WD11 had a 20 mm gap between the infill and the roof beam, the behaviour was similar to WD8 (except for the ductility). The way in which the hinged frames deflected led to separation between the infill and the containing frame; which made it close to the case where a gap is being provided in advance of the testing. The same conclusion was reached by Dawe et al. (2001b).

Flanagan and Bennett (1999) looked at the effect of frame rigidity on the performance of masonry infill shear walls. Four different frames were considered in this case, where the dimensions of the infill wall were kept constant. Only, the frame's column cross-sectional size and orientation were varied in this case. It was observed that increasing the stiffness of the frame led to an increase in the ultimate capacity of the containing frames. Increasing the stiffness of the frame led to increase in the contact between the frame and the masonry infill wall; hence, increase in the confinement exerted on the masonry infill wall leading to increase in the ultimate capacity.

2.4.10. Position of the Infill Wall Relative to the Frame

Flanagan and Bennett (1999) studied the behaviour of infill frames when the wall position was not in the centerline of the containing frame. The infill wall was offset from the centerline so that approximately 65% of the panel thickness

was within the frame. Since the loading was applied at the frame centerline, the wall was subjected to a combination of in-plane and out-of-plane bending. It was observed that considerable spalling of the mortar took place due to the out-of-plane effect. The in-plane initial stiffness and peak loading was reduced by 30% and 25%, respectively, compared to the specimen where the wall was at the centre of the frame.

2.5. Design Approach in Different Codes and Standards

Most of the current design codes and standards ignores the contribution of the masonry infill wall in resisting the lateral load applied on the structure. This section reviews the information currently available about these codes and standards.

2.5.1. Canadian Standard for Masonry Structures (CSA S304.1, 2004)

The Canadian Standard relies on the masonry infill shear wall to participate in carrying the lateral loading. The standard provides design equations when the masonry infill shear wall is in full contact with the containing frame which is hard to achieve in actual construction.

The Standard does not provide any guidance for the design of the masonry infill shear walls where there are gaps between the frame and the wall. Also, there is no design provision in case of the presence of openings. The standard recommends the performance of experimental or analytical investigations for the wall showing the development of the diagonal strut for both cases.

In the current version of the standard, masonry walls fail due to one of the following failure mechanism: (i) shear slip along bed joint, (ii) diagonal tension cracking failure and (iii) failure in the compression strut. Most of the experimental research has shown that diagonal tension failure is not a realistic failure mode as the wall can still carry more load even though they are cracked. The following section summarizes the different provisions presented in the standard.

a. Shear Slip Failure Along Bed Joints

The failure takes place at the mid-height of the wall. This failure leads to

the formation of a knee-braced frame which may lead to premature failure of the column in the supporting frame. The factored in-plane resistance is given by the following equation:

$$V_r = 0.16\varphi_m\sqrt{f_m}A_{uc} + \varphi_m\mu P_1 \qquad 2\text{-}20$$

Where:

V_r: Shear Capacity of the masonry

φ_m: Masonry resistance factor (equal to 0.6)

f_m: Masonry compressive strength

A_{uc}: Uncracked portion of the effective cross-section area of the wall that provide shear bond capacity

μ: Factor equal to 1.0 for masonry to masonry contact or masonry to roughened concrete sliding plane

P_1: Compressive force in masonry acting normal to the sliding plane, taken as the dead load plus 0.9 of the vertical component of the compressive force resulting from the diagonal strut action

b. Diagonal Tension Failure

This type of failure is the most common mode of failure. Although the wall can still resist lateral loading after the formation of the first diagonal crack, these cracks might be not acceptable in some applications. The diagonal tension capacity is given by the following formula:

$$V_r = \varphi_m(v_m b_w d_v + 0.25P_d)\gamma_g \qquad 2\text{-}21a$$

$$v_m = 0.16\left(2 - \frac{M_f}{V_f d_v}\right)\sqrt{f_m} \qquad 2\text{-}21b$$

Where:

v_m: Shear strength attributed to masonry

b_w: Width of the wall

d_v: Effective depth for shear calculation (shall not be taken less than 0.8 the length of the wall)

P_d: Axial compressive load on the section under consideration based on 0.9 times the dead load plus any axial load arising from bending in coupling beam

γ_g: Factor to account for partial grouted or ungrouted walls that are constructed from hollow or semi-solid units. The value equal to 1.0 for fully grouted masonry, fully solid concrete block masonry or solid brick. Otherwise, this value can be taken as the effective area divided by gross area; but shall not be taken greater to 0.5

M_f: Factored moment at the section under consideration

V_f: Factored shear at the section under consideration

It should be mentioned that the value of $\frac{M_f}{V_f d_v}$ shall not be less than 0.25 nor more than 1.0.

c. Compression failure in the Compression Strut

This mode of failure happens when the stresses in the compressive strut (from the strut and tie model) exceeds the ultimate capacity of the masonry. The Canadian standard gives a value for the width of the diagonal strut

$$w_{eff} = \sqrt{{\alpha_h}^2 + {\alpha_l}^2}/2 \qquad \text{2-22a}$$

$$\alpha_h = \frac{\pi}{2} \sqrt[4]{\frac{4E_f I_c h}{E_m t_e \sin 2\theta}} \qquad \text{2-22b}$$

$$\alpha_L = \pi \sqrt[4]{\frac{4E_f I_c h}{E_m t_e \sin 2\theta}} \qquad \text{2-22c}$$

$$\theta = \tan^{-1}\frac{h}{l} \qquad \text{2-22d}$$

Where:

w_{eff}: Effective width of the diagonal strut

α_h: Vertical contact length between the diagonal strut and the frame

α_L: Horizontal contact length between the diagonal strut and the frame

E_m, E_f: The moduli of elastic of the masonry and the frame material

I_c, I_b: Moments of inertia of the column and the beam sections of the frame

h, l: Height and length of the masonry infill shear wall

t_e: Sum of the thickness of two face shells for the hollow or semi-solid block units and is equal to the thickness of the wall for solid or fully grouted units

The effective width of the diagonal strut, w_{eff}, shall not exceed a value of quarter the diagonal length. The expression for the diagonal compressive force (F) is given as:

$$F = 0.85\varphi_m \chi f_m A_e \qquad 2\text{-}23$$

Where:

χ: Factor to account for direction of the compressive strength in masonry member relative to the direction used for the determination of f_m and equal to 0.5

The Canadian masonry standard, also, considers the effect of slenderness in the computation of the force developed in the diagonal strut.

2.5.2. American Building Code Requirement for Masonry Structures (MSJC, 2011)

Previous versions of MSJC did not include any guideline on the design of infill walls. In the current version, masonry infill walls were classified into two categories: Non-Participating infill walls and Participating infill walls. Non-participating infill walls are those walls surrounded by gaps; the size of these gaps is large enough to prevent the containing frame and the masonry infill wall from coming in contact (not less than 9.5 mm). This type of masonry infill wall does not share in resisting lateral loading; the gaps are filled with uncompressible materials

to avoid the transfer of any lateral load to the infill. Non-participating infill walls should only be designed to resist the out-of-plane loading.

Participating infill walls are walls that participate in resisting lateral loads. Small gaps, which are closed when lateral loading is applied on the wall, may exist between infill wall and the containing frame. For such a case, the code requires reduction in the strength and stiffness by 50%. A restriction on the height to thickness ratio of 30 is given by the code to insure construction stability of the wall.

The code does not allow partial height walls and walls with openings in sharing lateral resistance. According to MSJC (2011), infill walls are expected to fail due to diagonal failure in the compression strut, corner crushing in the infill panel material, or sliding shear; but, eventually, the wall is going to fail due to corner crushing of the masonry materials. The capacity of the infill wall is taken as the least of the following equations:

$$V_{n\,inf} = \min \begin{cases} 150\, t_{net\,inf} f'_m \\ \text{Horizontal component of the force in the equivalent strut at a racking displacement of 25 mm} \\ \frac{V_n}{1.5} \end{cases} \qquad \text{2-24a}$$

$$V_n = \text{smaller of} \begin{cases} 0.33 A_n \sqrt{f'_m} \\ 0.83 A_n \\ 0.26 A_n + N_u \end{cases} \qquad \text{2-24b}$$

Where:

A_n: Net cross-section area of masonry

f'_m: Compressive strength of masonry

N_u: Factor compressive force acting normal to shear surface that is associated with ultimate horizontal loading

$t_{net\,inf}$: Net thickness of infill wall

$V_{n\,inf}$: Nominal horizontal in-plane shear strength of infill walls

V_n: Nominal shear strength

The width of the strut, w_{inf}, used in MSJC (2011) is given as:

$$w_{inf} = {0.3}/{\lambda_{strut} \cos \theta_{strut}} \quad \text{2-25a}$$

$$\lambda_{strut} = \sqrt[4]{{(E_m t_{net\ inf} \sin 2\theta_{strut})}/{(4E_{bc} I_{bc} h_{inf})}} \quad \text{2-25b}$$

Where:

E_{bc}: Modulus of elasticity for bounding columns

E_m: Modulus of elasticity for masonry

h_{inf}: Height of infill wall

I_{bc}: Moment of inertia of bounding column

λ_{strut}: Characteristic stiffness parameter

2.5.3. Evaluation of Earthquake Damaged Concrete and Masonry Wall buildings (FEMA 306, 2000)

Another design manual that is issued in the United States considers the infill wall to contribute in the resistance of lateral load. The values presented in this design manual are different than what is currently present in the MSJC (2011). The width of the diagonal strut that simulates the masonry infill shear wall's stiffness was based on the work performed by Mainstone (1971) and Mainstone and Weeks (1971). FEMA 306 (2000) does not allow presence of gaps between the masonry wall and the containing frame. Also, no window and door openings are allowed to be present in the masonry infill shear wall.

$$a = 0.175 r_{inf} (\lambda_1 h_{col})^{0.4} \quad \text{2-26a}$$

$$\lambda_1 = \sqrt[4]{{(E_m t_{inf} \sin 2\theta)}/{(4E_{fe} I_{col} h_{inf})}} \quad \text{2-26b}$$

$$\theta = \tan^{-1} {h_{inf}}/{L_{inf}} \quad \text{2-26c}$$

Where:

a: The width of the diagonal strut (in)

r_{inf}: Diagonal length of the masonry infill wall (in)

h_{col}: Column height between centerlines of beams (in)

E_m: Modulus of elasticity of masonry infill material (psi)

t_{inf}: Thickness of the masonry infill panel (in)

E_{fe}: Modulus of elasticity of frame material (psi)

I_{col}: Moment of inertia of column (in^4)

h_{inf}: Height of the masonry infill wall (in)

L_{inf}: Length of the masonry infill wall (in)

Similar to the Canadian Standard, this design manual allows the wall to fail in the same failure mechanisms (i.e.: diagonal tension cracking, sliding shear failure and compression failure in the diagonal strut). The equations for these failure modes are summarized as follows.

$$V_{slide}^{i} = \mu\, L_{inf}\, t_{inf}\, E_m \rho^2 \qquad 2\text{-}27$$

$$V_{cr}^{i} = 40\sqrt{2\, f'_{me}}\; t_{inf} \Big/ \left({L_{inf}}/{h_{inf}} + {h_{inf}}/{L_{inf}} \right) \qquad 2\text{-}28$$

$$V_c = a\, t_{inf}\, f'_{m90}\, \cos\theta \qquad 2\text{-}29$$

Where:

V_{slide}^{i}: Sliding shear capacity for masonry infill shear walls (lb)

V_{cr}^{i}: Diagonal tension shear capacity for masonry infill shear walls (lb)

V_c: Compression failure in the diagonal strut for masonry infill shear walls (lb)

μ: Coefficient of sliding friction along the bed joint

ρ: Interstory drift angle

f'_{me}: Compressive strength of the masonry prism (psi)

f'_{m90}: Compressive strength of the masonry prism parallel to bed joint (psi)

2.5.4. Mexican Norm for Masonry Structures (Mexican Code, 2004)

The Norm defines the masonry infill shear walls to be those surrounded by beams and columns of the structural frames to which they provide stiffness against lateral loading. The masonry infill shear walls may be reinforced or unreinforced walls.

There is a restriction on the thickness of the wall given by the Mexican Code. The wall shall not be less than 100 mm in thickness. The wall shall be designed to resist the in-plane and the out-of-plane loading. The in-plane shear resistance of the masonry is given as

$$V_{mR} = F_R(0.85\, v_m^*\, A_T) \qquad 2\text{-}30$$

Where:

V_{mR}: The shear resistance for masonry

F_R: Strength reduction factor (equal to 0.7)

v_m^*: Design diagonal compressive strength of the wall specimen over the gross area

A_T: Gross area of the wall

When using horizontal reinforcement in the wall, its effect should be taken into consideration in carrying the horizontal loading. The contribution of the horizontal reinforcement is given by:

$$V_{SR} = F_R \eta P_n f_{yh} A_T \qquad 2\text{-}31$$

Where:

V_{SR}: Shear resistance of the reinforcement

η: Efficiency factor

P_n: Amount of horizontal reinforcement used

f_{yh}: Yielding stress of horizontal reinforcement

The overturning of the wall in the out-of-plane direction shall be prevented by constructing connections between the frame and the masonry infill shear wall, or the wall should be reinforced with ties columns or internal columns.

The containing frame's columns must be design to resist a shear force equal to one half the lateral loading acting on the infill. This force shall be distributed over a distance of quarter the height of the column measured from the horizontal side of the beam.

2.5.5. New Zealand Standard for Masonry Structures (NZS 4230, 2004)

This design standard is only intended to be used for concrete masonry blocks. Similar to the Canadian Standard, the New Zealand Standard (NZS 4230, 2004) requires that infill walls be in full contact with containing frames. The standard realized the reduction of the stiffness that would occur in case of presence of gaps between the frame and the infill wall; yet, it did not provide any guidance on the expected amount of reduction or the maximum permissible size. The failure modes of the masonry infill shear walls are the same as CSA S304.1 (2004) (i.e.: diagonal tension failure, failure in the compression strut, and sliding shear failure); however, the standard did not provide any design equation for sliding shear failure. The equation used in the computation of diagonal tension cracking is:

$$V_r = \emptyset v_n b_w d_v \qquad 2\text{-}32$$

Where:

V_r: Shear capacity for the masonry

b_w: Bedded width of the masonry wall

d_v: Length of the wall in the direction of the applied load

v_n: Shear strength of the masonry infill

Ø: Strength reduction factor

The other mode of failure that is identified by NZS 4230 (2004) is failure in the diagonal compression strut. Equation (2-33) gives the expression used for the computation of this type of failure.

$$F = 0.85\emptyset f_m A_e \quad \text{2-33a}$$

$$A_e = w\ t \quad \text{2-33b}$$

Where:

F: Force in the compression strut

A_e: Masonry effective area

t: Effective depth of the infill wall

w: Effective width of the diagonal strut

$\emptyset$: Strength reduction factor

The previous expression is similar to that in CSA S304.1 (2004). The difference between both is χ factor that accounts for the direction of the applied compression force in CSA S304.1-04. The width of the compression strut in NZS 4230 (2004), unlike the Canadian standard, was set to a constant value equal to quarter the length of the developed compression strut.

The New Zealand standard recommends experimental and analytical investigation showing the development of diagonal struts capable of bracing the frame as the case of the Canadian standard. In the case of a reinforced masonry panel, the reinforcement must be connected to the adjacent beams and columns by lapped starter bars, welding or any mean that ensures the development of the composite action.

2.6. Code Comparison

The adequacy of the design expressions presented in the Canadian standard, New Zealand standard, and the American code in predicting the capacity of masonry infill shear walls were examined in this section. This was done by relying on experimental results for masonry infilled frames from five large investigations (Dawe and Seah, 1989; Mehrabi et al., 1996; Flanagan and Bennett, 1999; El-

Dakhakhni, 2002; and Tasnimi and Mohebkhah, 2011). Only specimens that failed by corner crushing of the masonry infill wall were considered in this analysis. All material reduction factors were set to unity in resistance calculations. Table 2-2 summarizes the properties of frames and infill walls of the specimens used.

In determining the width of the compression strut, the Canadian standard takes into account the relative stiffness between the infill wall and the containing frame and places a limit of ¼ the diagonal length of the wall. The New Zealand standard takes the width of the compression strut to be ¼ the diagonal length of the wall and ignores the effect of the relative stiffness between the infill wall and the frame. The American Code considers the stiffness of the frame's columns but not its beam; a similar expression to the American code was represented by FEMA 306 (2000), which also considers only the column's stiffness.

Diagonal strut width computed from standard and code expressions as well as FEMA's equation was used to estimate the initial stiffness of the infilled frames investigated in this study using 2D SAP 2000 elastic analysis. The frame elements as well as diagonal strut were modelled using beam elements. For the diagonal strut, the moment at the beam-column intersection was released to act as link member. The real cross-sectional area of the beam and column are assigned to these elements. The diagonal strut member was given the cross-sectional area equal to the effective width as given by the standards/codes and the effective thickness of the infill wall. The computed initial stiffness values for different codes/standards (K_{CSA}, K_{NZS}, K_{MSJC}, K_{FEMA}) were compared to the initial stiffness values determined from experimental results (K_{Exp}). This comparison aims to assess the accuracy of the standard/code expressions in estimating the width of the diagonal strut.

Table 2-3 summarizes the initial stiffness results for all masonry infilled frames investigated compared to the initial stiffness values determined from the experimental results. The diagonal strut width values computed according to the Canadian and New Zealand standards and used in the elastic analysis resulted in much higher initial stiffness values than measured for infilled steel frames. The

stiffness of the concrete masonry infilled steel frames was overestimated by 174% and 203% on average by the Canadian standard and the New Zealand standard, respectively. The estimated initial stiffness was even higher (570% app.) for steel frames filled with clay masonry. The Canadian and New Zealand standards underestimated the initial stiffness of concrete frames filled with concrete masonry by 48%.

Table 2-2: Properties of the frames and masonry infill used in the analytical study

Ref	Spec	Frame			Masonry Infill Wall				
		Type E (MPa)	I-Column (10^6 mm^4)	I-Beam (10^6 mm^4)	Unit Type & Size (mm)	Thick (mm)	f'_m (MPa)	l_w (mm)	h_w (mm)
[15]	WA1*	Steel 200,000	18.80	45.40	Concrete block 200×200×400	64.00	27.40	3592	2597
	WA2*						27.70		
	WA3*						26.50		
	WA4						24.40		
	WB1*						23.70		
[18]	D1	Steel 200,000	48.90	48.90	Conc. block 400×200×150	60.00	13.40	3342	2742
[54]	T	Steel 200,000	5.41	5.41	Clay brick 219×110×66	110.00	7.4	2260	1800
[25]	F1	Steel 200,000	0.913	119.00	Clay tile 300×200×300	195.00	5.6	2240	2240
	F2		7.03	119.00	Clay tile 300×200×300	195.00	5.6	2240	2240
	F4		4.04	556.00	Clay tile 300×200/100×300	330.00	2.3	2240	2240
	F5		12.00	295.00	Clay tile 300×200/100×300	330.00	2.3	2240	2240
	F9		71.10	119.00	Clay tile 300×200×300	195.00	5.6	2240	2240
	F17		7.03	1.19	Clay tile 300×200×300	195.00	5.6	3450	2240
	F21		7.03	119.00	Clay tile 300×200×300	195.00	5.6	2840	2240
[41]	M4	Conc 17,225	83.30	152.00	Conc. block 100×100×200	31.76	10.62	2123	1422
	M7	Conc 18,603	142.00	152.00	Conc. brick 100×100×200	92.07	13.57	2123	1422
	M8	Conc 17,225	83.30	152.00	Conc. block 100×100×200	31.76	9.51	2123	1422
	M10	Conc 20,119	83.30	152.00	Conc. block 100×100×200	31.76	10.61	2963	1422

*Specimens with truss type joint reinforcement.

The American code overestimated the initial stiffness of clay masonry infilled steel frames by 63% on average. It underestimated the initial stiffness for steel frames filled with concrete masonry by 35%. Initial stiffness values predicted using FEMA's expression were comparable to the measured values for concrete masonry infilled steel frames. However, FEMA's expression overestimated the initial stiffness for steel frames filled with clay masonry by 182% on average. Both the American code and FEMA's expression exceptionally underestimated the stiffness of concrete frames filled with concrete masonry walls by 80% and 71% of the measured values, respectively.

It is clear from Figure 2-14 that the Canadian standard overestimates the resistance of masonry infilled steel frames with concrete and clay masonry infills by 26% and 42% on average, respectively. This is likely due to overestimating the width of the diagonal strut. On the other hand, the Canadian standard underestimates the capacity of concrete frames filled with concrete masonry by 51%. While standards and codes are intended to be conservative, significant underestimation of resistance is uneconomical.

The New Zealand standard overestimates the resistance of concrete block and clay brick walls filling steel frames by almost two multiples. This may be attributed to the higher values of the diagonal strut width and the absence of any reduction factor to account for the fact that compressive stresses act at an angle to bed joints. Conversely, the predicted resistances for concrete frames filled with concrete masonry walls are in good agreement with the measured values. If a stress factor of 0.5 is applied to the New Zealand standard's expression, estimated resistances would be comparable to those computed using the Canadian standard.

The American code predicted the resistance of masonry infilled shear walls better than both the Canadian and New Zealand standards as its estimates were consistently below the measured values. The code's best prediction with an average of 83% of measured resistance is for steel frames filled with clay masonry. The average predicted resistance for concrete masonry infilled steel frames is 59% of the measured resistance. However, the American code greatly underestimated the

resistance of concrete frames filled with concrete masonry, only 30% of the measured resistance on average.

From the previous findings it clear that the diagonal strut design equations for masonry infill shear walls in the Canadian standard, the New Zealand standard, and the American code failed to provide consistent estimate for the lateral load resistance. This will lead to unsafe/uneconomical design for the frames. The current equations should be updated to reflect the behaviour of different materials used in constructing the masonry infill wall and the frame material as well.

Table 2-3: Initial stiffness based on diagonal strut width given in different codes/standards

Frame	Infill	Spec #	K_{Exp} *kN/mm*	CSA S304.1-04 [2]		NZS 4230-04 [3]		2011 MSJC [4]		FEMA 356 [11]	
				K_{CSA} *kN/mm*	K_{CSA} / K_{Exp}	K_{NZS} *kN/mm*	K_{NZS} / K_{Exp}	K_{MSJC} *kN/mm*	K_{MSJC} / K_{Exp}	K_{FEMA} *kN/mm*	K_{FEMA} / K_{Exp}
Steel	Concrete units	WA1	73.00	167.20	2.29	193.89	2.66	33.93	0.46	75.33	1.03
		WA2	82.00	167.20	2.04	193.89	2.36	33.93	0.41	75.33	0.92
		WA3	74.00	167.20	2.26	193.89	2.62	33.93	0.46	75.33	1.02
		WA4	63.00	170.94	2.71	193.89	3.08	34.83	0.55	75.88	1.20
		WB1	72.00	171.96	2.39	193.89	2.69	35.00	0.49	76.24	1.06
		D1	19.60	93.00	4.74	93.00	4.74	29.43	1.50	44.57	2.27
		Average			2.74		3.03		0.65		1.25
		COV+ (%)			33.49		26.29		59.64		37.08
	Clay units	T	22.24	69.81	3.14	79.53	3.58	20.71	0.93	36.21	1.63
		F1	13.19	79.15	6.00	79.15	6.00	14.23	1.08	30.48	2.31
		F2	14.37	105.42	7.34	105.42	7.34	26.36	1.83	42.66	2.97
		F4	20.19	142.18	7.04	142.18	7.04	36.36	1.80	60.52	3.00
		F5	25.75	161.89	6.29	161.89	6.29	50.32	1.95	72.62	2.82
		F9	30.33	118.96	3.92	118.96	3.92	58.37	1.92	66.86	2.20
		F17	17.27	160.50	9.29	160.50	9.29	25.49	1.48	61.37	3.55
		F21	12.94	135.80	10.49	135.80	10.49	26.33	2.03	53.07	4.10
		Average			6.69		6.74		1.63		2.82
		COV+ (%)			34.52		33.03		24.10		25.93
Concrete	Concrete units	M4	75.30	32.60	0.43	32.60	0.43	14.16	0.19	18.87	0.25
		M7	255.70	140.88	0.55	140.88	0.55	40.56	0.16	67.48	0.26
		M8	57.80	35.17	0.61	35.17	0.61	14.97	0.26	20.13	0.35
		M10	69.20	34.35	0.50	34.35	0.50	13.63	0.20	20.07	0.29
		Average			0.52		0.52		0.20		0.29
		COV+ (%)			12.65		12.65		17.93		13.56

*K_{Exp}: Experimental initial stiffness, K_{CSA}: initial stiffness computed from the diagonal strut width given in CSA S304.1-04, K_{NZS}: initial stiffness computed from the diagonal strut width given by NZS 4230-04, K_{MSJC}: initial stiffness computed from diagonal strut width given by 2011 MSJC, and K_{FEMA}: initial stiffness computed from diagonal strut width given by FEMA 306-00.

+COV: Coefficient of Variation

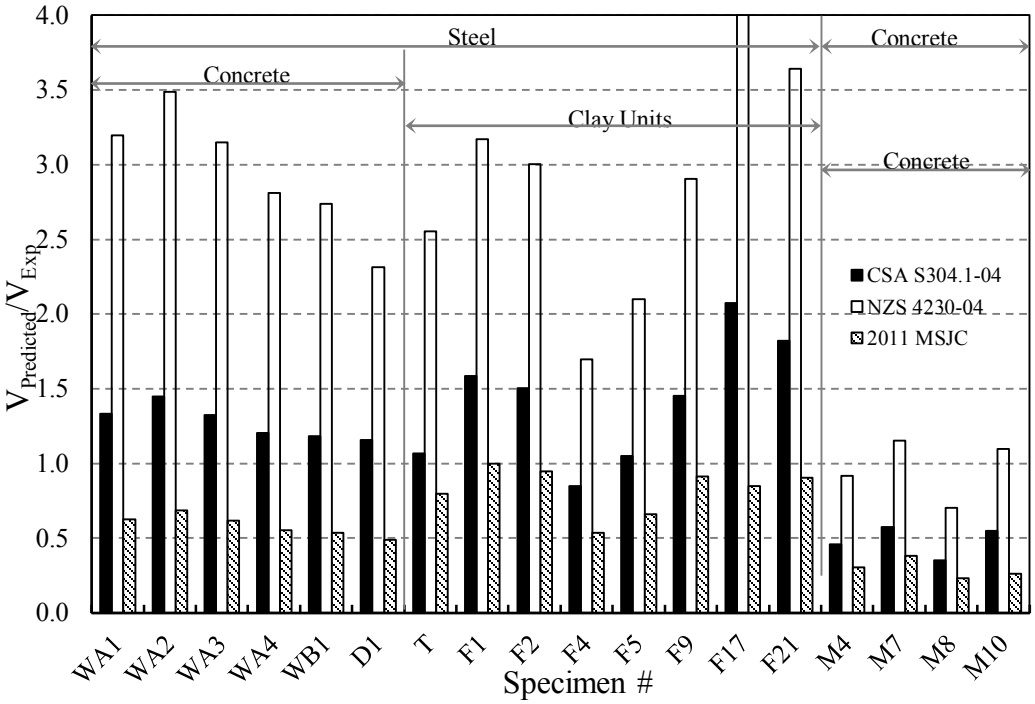

Figure 2-14: Diagonal Strut resistance predicted from different Codes/Standards

2.7. Closure

Masonry infill walls are used extensively in the construction industry as internal partitioning and external boundary for skeletal RC and steel framed buildings. Accounting for this type of walls in increasing the stiffness of the structural frames leads to economical design, and hence saving in the construction cost. A detailed literature review for the problem of the in-plane behaviour of masonry infill shear walls was carried out in this chapter. Guidelines for the design of these types of walls in different codes/standards were also presented.

A comparison of the in-plane resistance of masonry infill shear walls computed using the diagonal strut models in the Canadian, New Zealand, and American standards and codes showed failure in predicting the lateral load resistance. The equation provided in those design codes/standards failed in providing consistent estimate for the initial stiffness and ultimate resistance of the masonry infill wall regardless of the type of frame and masonry material used. This will lead to unsafe design when considering the masonry infill wall in sharing the

lateral load. These equations needs to be updated to reflect the behaviour of all materials used in constructing the frame and masonry infill wall.

The results of this study clearly demonstrated that much research is still needed to gain better understanding of the behaviour of masonry infilled frames and develop design expressions that are capable of predicting the lateral load resistance of this type of wall with greater accuracy.

Accounting for the presence of the masonry infill walls in analysis of frames may lead to safe and/or economical design and enhance the overall performance of the structural system. This can be satisfied by introducing a simplified design approach which incorporates all the factors affecting the infill panels' performance. The following chapter gives a brief review on the finite element method which will be used in investigating the behaviour of masonry infill walls.

CHAPTER 3

FINITE ELEMENT MODELLING

3.1. Introduction

The finite element method is a powerful tool that can be used to study the behaviour of structures under different loading conditions. This chapter presents the modelling scheme and the material properties used to analyze the behaviour of masonry infilled frames. Masonry was modelled using the simplified micro-modelling approach to trace the developed stresses in it.

3.2. Description of the Finite Element Technique

Finite element modelling of masonry is challenging as masonry is a non-homogenous material formed from masonry units and mortar joints. It requires knowledge of all the possible failure mechanisms that can take place in the unit, mortar or the interface between the units and mortar.

The simplified micro-modelling technique discussed in Chapter 2 is used in this study. In this technique, masonry units are extended from all directions by half the thickness of the mortar joint. An interface element is placed in between the units representing the mortar joint behaviour. This technique in modelling has been successfully used by many researchers (e.g.: Stavridis and Shing, 2010; Mehrabi and Shing, 1997; and Al-Chaar et al., 2008).

In order to capture the true behaviour of masonry infill shear walls, 3D models were needed. 3D modelling helps identifying all possible failure mechanisms that can take place within the infill wall. It also enables modelling the exact geometry of masonry units. The webs in the concrete blocks are accounted for in 3D models, and hence the effective supporting condition of the face shells. Three dimensional modelling also allows accurate modelling of the contact between the masonry blocks and the mortar joint as contact takes place in two separate planes. The downside of 3D modelling is the large number of elements in the model which requires a longer time for analysis. In order to minimize computational time, High Performance Computing (HPC) was used through

Compute Canada which reduces the analysis time required for each problem by 70%. ABAQUS 6.10-EF2, a commercially available finite element package by SIMULIA (2010), was used in building the finite element models. Elements available in ABAQUS library were used to model the masonry infilled frames. The following section summarizes the characteristics of these elements. Also, built-in material models in ABAQUS were used to describe the behaviour of steel, concrete and masonry units is presented.

3.2.1. Masonry, Concrete and Steel Elements

Three-dimensional 8-node solid element, C3D8R, was used to model reinforced concrete and steel frames, grout columns, and the masonry infill walls. This element has three translational degrees of freedom for each node in the global directions. This solid element is capable of modelling complex geometry and performing nonlinear analyses involving contact, plasticity, and large deformations. The reinforcement for RC frames and masonry bond beams was modelled using the Beam Element, B31. This beam element has three translation and three rotational degrees of freedom at each node.

The three dimensional 8 nodes solid element is available through ABAQUS library with full and reduced integration scheme. In the current study, reduced integration scheme was considered for this elements. The reduced integration scheme for these elements is based on a single point uniform strain formulation where the strains are obtained as average strain over the element volume. This uniform strain method (Flanagan and Betytschko, 1981) ensures that the first orfer reduced integration element pass the patch test and attain the accuracy when the element are skewed. Equation 3-1 shows the displacement vector for the element used in the analysis. For uniform strain formulation, the gradient matrix is given in Equation 3-2.

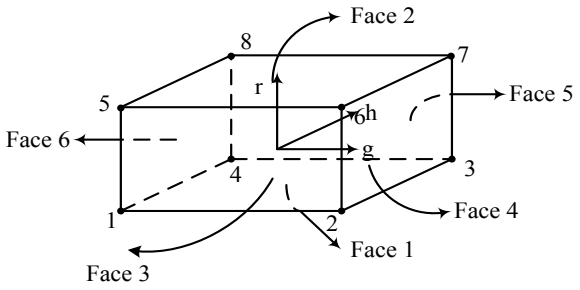

Figure 3-1: Schematic for the solid brick element used in modelling (C3D8R)

$$u = N^I(g, h, r)\, u^I \quad \text{sum on I} \tag{3-1a}$$

$$N^I(g,h,r) = \frac{1}{8}\Sigma^I + \frac{1}{4}\, g\Lambda_1^I + \frac{1}{4}\, h\Lambda_2^I + \frac{1}{4}\, r\Lambda_3^I + \frac{1}{2}\, hr\, \Gamma_1^I + \frac{1}{2}\, gr\, \Gamma_2^I + \frac{1}{2}\, gh\, \Gamma_3^I + \frac{1}{2}\, ghr\, \Gamma_4^I \tag{3-1b}$$

$$\Sigma^I = [+1, +1, +1, +1, +1, +1, +1, +1\ ] \tag{3-1c}$$

$$\Lambda_1^I = [-1, +1, +1, -1, -1, +1, +1, -1\ ] \tag{3-1d}$$

$$\Lambda_2^I = [-1, -1, +1, +1, -1, -1, +1, +1\ ] \tag{3-1e}$$

$$\Lambda_3^I = [-1, -1, -1, -1, +1, +1, +1, +1\ ] \tag{3-1f}$$

$$\Gamma_1^I = [+1, +1, -1, -1, -1, -1, +1, +1\ ] \tag{3-1g}$$

$$\Gamma_2^I = [+1, -1, -1, +1, -1, +1, +1, -1\ ] \tag{3-1h}$$

$$\Gamma_3^I = [+1, -1, +1, -1, +1, -1, +1, -1\ ] \tag{3-1j}$$

$$\Gamma_4^I = [-1, +1, -1, +1, +1, -1, +1, -1\ ] \tag{3-1k}$$

$$B_i^I = \frac{1}{V_{el}} \int_{V_{el}} N_i^I(g, h, r)\, dV_{el} \tag{3-2a}$$

$$N_i^I(g, h, r) = \frac{\partial N^I}{\partial x_i} \tag{3-2b}$$

Where *I* stands for the node of the element under consideration, V_{el} is the element volume, and x_i is the spatial position of the point under consideration in the original configuration, N^I is the isoparametric shape function; N_i^I is the isoparametric shape function of node *i*, $\Gamma_1^I, \Gamma_2^I, \Gamma_3^I$ and Γ_4^I are the deformation modes associated with no energy in the point; g, h, r are the position of the node with respect to the centroid

of the element, u is the interpolation function for the whole element, u^I interpolation function for each node of the element, and B_i^I is the centroidal strain formulation at node *i*.

Using reduced integration cuts down the computation time for solving the problem, specially for large scale problems. This saving in analysis time is significant in problems with relatively small wavefront and for problems where constitutive models require lengthy calculations. A drawback of using the reduced integration is that the element stiffness matrix will be ranked deficient as singular modes might appear in the response. The artificial damping method given by Flanagan and Belytschko (1981) was used to control this response.

3.2.2. Interface Element

Three-dimensional cohesive element, COH3D8, was used to model the interface between masonry units. The thickness of the cohesive element was set to an infinitesimally small value, near zero. A traction separation model that assumes the material to behave linearly until it reaches maximum tensile and shear stresses was assigned to the element; the behaviour of the interface before damage is linear elastic with normal and shear stiffnesses taken as defined by Lourenço (1996). A penalty stiffness that degrades under tension and/or shear loading takes place after the maximum stress is reached to identify damage initiation. The element fails completely when the displacement taking place in the element exceeds a predefined value of twice the displacement value at the maximum tensile stress; hence, the stiffness of the element is set to zero. Figure 3-2 shows a schematic for the shape and deformation modes of the cohesive element. After failure of the cohesive element, the lateral load applied to the infilled frame system will be resisted by friction force developed from the Coulomb-friction model between different elements.

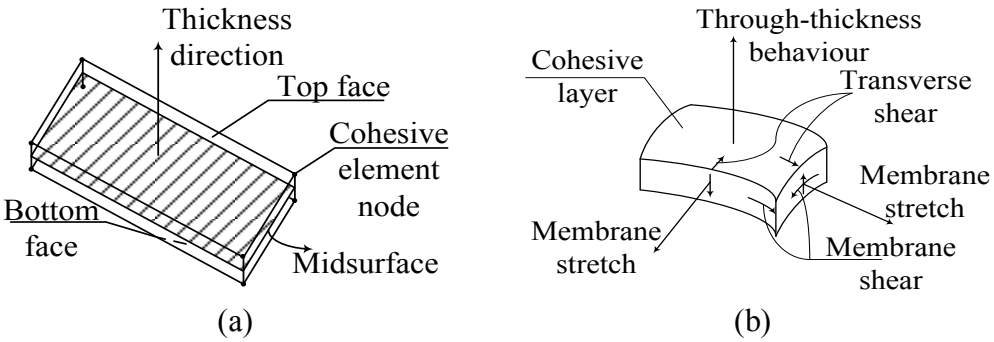

Figure 3-2: Cohesive element (a) schematic and (b) Deformation modes

These elements are usually chosen and placed at location where cracks are expected to be developed. In three dimensional problems, the traction separation model assumes failure to be in a normal direction to the interface, tangential direction (both horizontal directions). The relative change of the position of the top and bottom face of a cohesive element is used to compute the transverse shear behaviour of the element. As shown in Figure 3-3, this element was tied to the adjacent elements using a tie constraint to resemble the adhesion. This tie constrains forces joints of different elements; hence, share the deformation exhibited on the assembly.

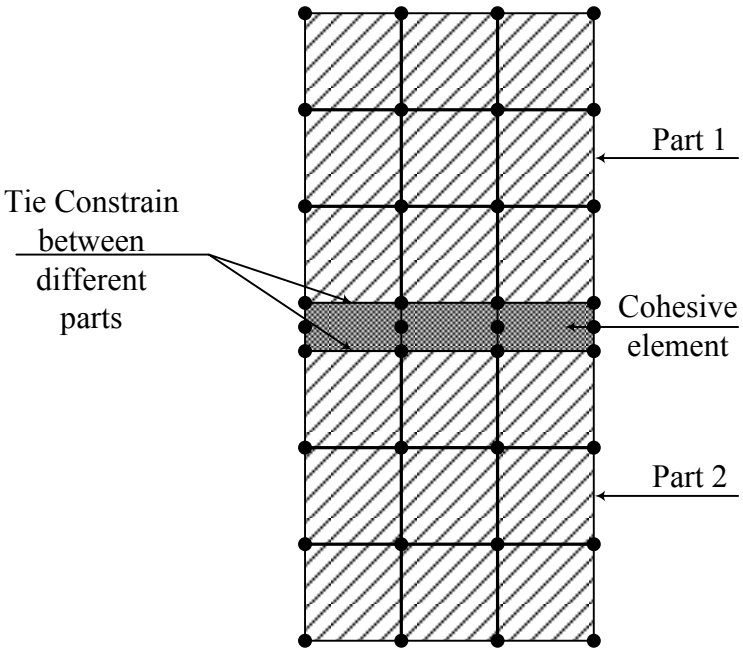

Figure 3-3: Cohesive element between two different parts in ABAQUS

In this research, linear elastic traction separation behaviour was assumed for the interface model followed by initiation and evaluation of the damage. The nominal traction stress vector, t, is defined by three component: a normal stress value (t_n) in the direction of the thickness of the cohesive element, and two transverse shear stresses (t_s and t_t). The corresponding separations (δ_n, δ_s and δ_t) are given as Equation 3-3. The elastic behaviour can be written as shown in Equation 3-4.

$$\varepsilon_n = \frac{\delta_n}{T_o} \quad , \quad \varepsilon_s = \frac{\delta_s}{T_o} \quad , \quad \varepsilon_t = \frac{\delta_t}{T_o} \tag{3-3}$$

$$t = \begin{Bmatrix} t_n \\ t_s \\ t_t \end{Bmatrix} = \begin{bmatrix} K_{nn} & K_{ns} & K_{nt} \\ K_{ns} & K_{ss} & K_{st} \\ K_{nt} & K_{st} & K_{tt} \end{bmatrix} \begin{Bmatrix} \varepsilon_n \\ \varepsilon_s \\ \varepsilon_n \end{Bmatrix} = K\varepsilon \tag{3-4}$$

Where T_o is the original thickness of the cohesive element, K is the elastic stiffness matrix for fully coupled behaviour. The stiffness matrix is going to be reduced to a diagonal matrix if uncoupled behaviour between the normal and shear behaviour is considered. The values of the normal and tangential stiffness coefficients are taken equal to the value indicated by Lourenço (1996):

$$k_n = \frac{E_u E_m}{h_m(E_u - E_m)} \tag{3-5a}$$

$$k_s = \frac{G_u G_m}{h_m(G_u - G_m)} \tag{3-5b}$$

The damage in the cohesive element was assumed to initiate when the maximum nominal stress ratio reaches a value of unity as per Equation 3-6. The damage evaluation is a measure to the rate by which the stiffness of the material will get degraded when the corresponding initiation criterion is reached. The damage variable, d, has an initial value of zero till the damage is initiated. After the damage is initiated, and with further loading, the value of d varies from 0 to 1 monotonically. The stress components for the traction separation behaviour are affected as shown in Equation 3-7

$$\max\left\{\frac{\langle t_n \rangle}{t_n^0} \ , \ \frac{\langle t_s \rangle}{t_s^0} \ , \ \frac{\langle t_t \rangle}{t_t^0}\right\} = 1 \tag{3-6}$$

$$t_n = \begin{cases} (1 - d)\,\bar{t}_n & \bar{t}_n \geq 0 \\ \bar{t}_n & \text{Damage is not initiated} \end{cases} \qquad 3\text{-}7a$$

$$t_s = (1 - d)\,\bar{t}_s \qquad 3\text{-}7b$$

$$t_t = (1 - d)\,\bar{t}_t \qquad 3\text{-}7b$$

Where $\bar{t}_n$, $\bar{t}_s$ and $\bar{t}_t$ are the stress components predicted by the elastic traction-separation behaviour for the current strains without damage. In addition to the damage evaluation, a mixed mode behaviour should be defined for the cohesive element. This behaviour quantifies the relative proportions of normal and shear deformation taking place in the element. An energy-based mixed mode was used in this research. The total work done, G_T, is the summation of the work done by the tractions and their relative displacements in the normal and tangential direction (i.e.: $G_T = G_n + G_s + G_t$). The mixed mode definition follows Equation 3-8. The portion of the work done by the shear tractions is denoted by G_S and is equal to $G_s + G_t$.

As shown in Figure 3-4, a linear damage evaluation was assumed in this analysis where the damage will be computed based on the maximum displacement the element can undergo before complete damage of the element takes place. In this case, the value of the damage parameter, d, is as given in Equation 3-9.

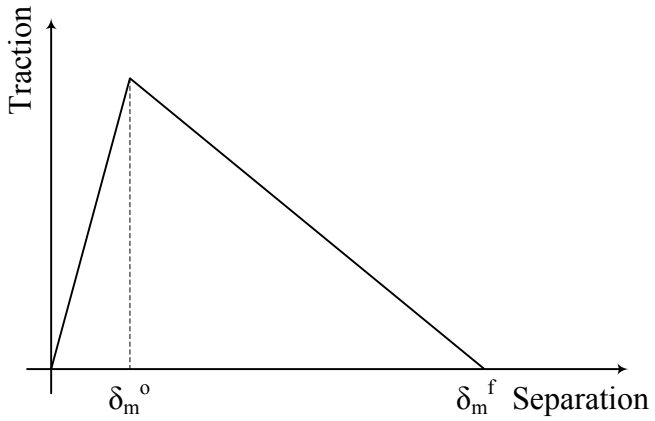

Figure 3-4: Linear damage evaluation for the cohesive element (SIMULIA, 2010)

$$m_1 = \frac{G_n}{G_T}\ ,\ m_2 = \frac{G_s}{G_T}\ ,\ m_3 = \frac{G_t}{G_T} \qquad 3\text{-}8$$

$$d = \frac{\delta_m^f \left(\delta_m^{max} - \delta_m^0\right)}{\delta_m^{max} \left(\delta_m^f - \delta_m^0\right)} \qquad 3\text{-}9$$

Where δ_m^f is the effective displacement at complete failure, δ_m^{max} is the maximum value of the effective displacement attained during the entire loading history, and δ_m^0 is the effective displacement at the instant of damage initiation.

3.2.3. Reinforcement Elements

Beam element (B31) was used to model reinforcement for the RC frame, masonry bond beam, and reinforcement in the grout. This element follows the beam theory in which the element's cross-sectional dimensions are smaller than its length (i.e.: slender element). For 3D analysis, each node of the beam element experiences 6 degrees of rotation (i.e.: 3 rotational and 3 translational degree of freedom at each node).

3.2.4. Constitutive Material Models

The behaviour of steel material used for the steel column and beam sections and reinforcing bars was idealized by an elasto-plastic material response. Figure 3-5 describes this behaviour. The total deformation, ε, is expressed in terms of elastic, ε_{el}, and plastic deformation, ε_{pl}, that the element will experience as shown in Eqution 3-10.

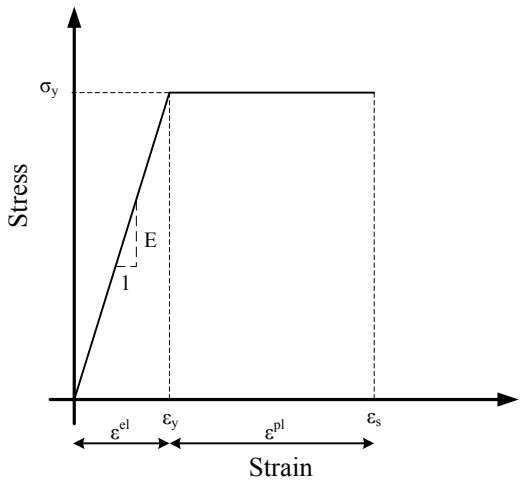

Figure 3-5: Steel material elasto-plastic material model

$$\varepsilon = \varepsilon^{el} + \varepsilon^{pl} \quad 3\text{-}10$$

The elastic response is assumed to be linear and isotropic. It can be expressed through the use of Young's modulus as well as Poisson's ratio. As for the plastic part, it requires satisfaction of a uniaxial-stress plastic strain relationship. The yield condition can be written as follows:

$$q = \sigma^0 \quad 3\text{-}11$$

Where $\sigma^0(\bar{\varepsilon}^{pl}, \theta)$ is the yield stress and the corresponding plastic strain, at a given temperature, θ.

Concrete and masonry behaviours are characterized by a non-linear response. This nonlinear response can be idealized by an elastic part until micro-cracking is initiated in the material followed by a nonlinear plastic response. Concrete damaged plasticity model assumes failure to be due to tensile cracking as well as compressive crushing of the material. The two hardening variables, $\widetilde{\varepsilon_t^{pl}}$ and $\widetilde{\varepsilon_c^{pl}}$, control the yield surface under tension and compression loading, respectively. The plastic behaviour under compression is characterized by stress hardening followed by strain softening after the reaching the ultimate stress, σ_{cu}. Thus, the tensile and compressive stresses can be expressed in terms of the elastic and plastic strains as given in Equation 3-12 (Hillerborg et al., 1976).

$$\sigma_t = \sigma_t \left(\tilde{\varepsilon}_t^{pl}, \tilde{\varepsilon}_t^{\cdot pl}, \theta, f_i\right) \quad 3\text{-}12a$$

$$\sigma_c = \sigma_c \left(\tilde{\varepsilon}_c^{pl}, \tilde{\varepsilon}_c^{\cdot pl}, \theta, f_i\right) \quad 3\text{-}12b$$

Where the subscript t and c refer to tension and compression, respectively; $\tilde{\varepsilon}_t^{pl}$ and $\tilde{\varepsilon}_c^{pl}$ are the equivalent plastic strains in tension and compression, respectively; $\tilde{\varepsilon}_t^{\cdot pl}$ and $\tilde{\varepsilon}_c^{\cdot pl}$ are the equivalent plastic strain rates, θ is the temperature, and f_i is any other predefined variables.

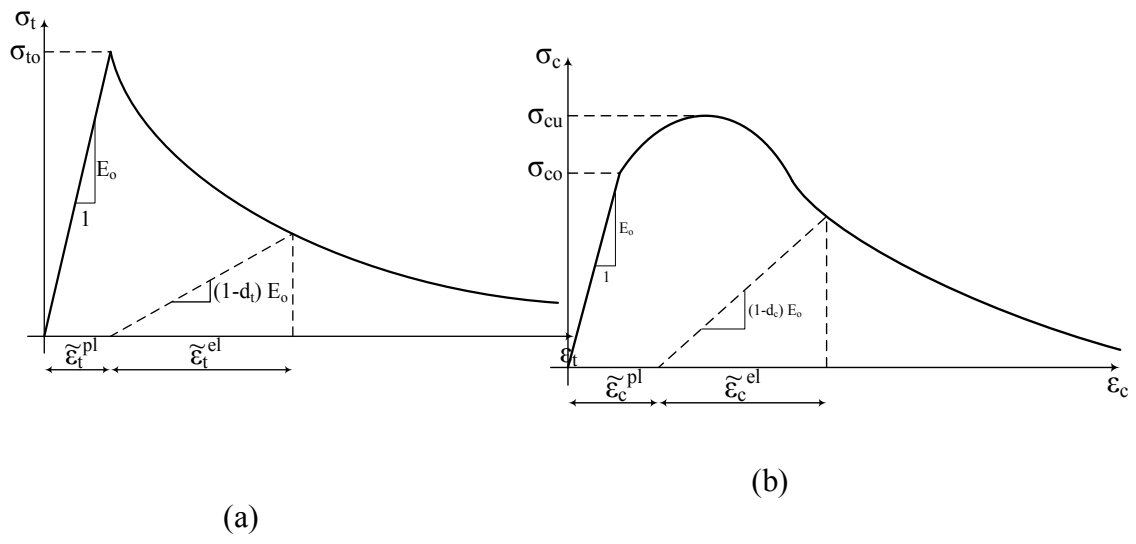

Figure 3-6: Concrete behaviour in (a) tension and (b) compression (Hillerborg et al., 1976)

3.3. Loading and Solver

The solver used in performing the analysis is the dynamic explicit analysis. This solver is very efficient for analyzing large models with a relatively short dynamic response time. It is used to mimic the effect of quasi-static loading. The load is applied in the form of displacement to achieve convergence of the problem; also, to mimic how the load was applied in the experiment. The reaction forces was computed as integration of the nodal reactions at the base of the frame.

3.4. Closure

In this Chapter, a finite element technique for modelling masonry infilled RC and steel frames was presented. The model for the masonry infill wall was carried out based on the simplified micro-model proposed by Lourenço (1996). Steel was modelled as an elasto-plastic material. The concrete and masonry infill wall were modelled using an elastic response followed by a non-linear plastic model using concrete damaged plasticity model. The interface between the masonry units and between the infill wall and containing frame was achieved by using cohesive elements that follow a traction separation law.

The proposed finite element model was validated against experimental test

results of four major investigations as presented in Chapter 4, and it wasused to study the effect of the most influential parameters that affects the behaviour of masonry infilled frames presented in Chapter 5.

CHAPTER 4

VALIDATION OF FINITE ELEMENT MODELLING TECHNIQUE

4.1. Introduction

In this chapter, experimental test results from four major experimental programs were used to validate the adequacy of the finite modelling technique described in Chapter 3 in predicting the behaviour of masonry infill walls with and without openings. The experimental investigations cover steel and RC frames with solid infill walls (i.e.: no openings) and infill walls with window and door openings.

4.2. Experimental Data

In order to validate the developed finite element technique, experimental test results available in 4 major research studies were considered (Dawe & Seah, 1989; Mehrabi et al., 1996; Yàñez et al., 2004; and Liu & Soon, 2012). The infilled frames varied in size from full scale models to 1/3 scale models. Nine masonry infilled steel frames and eight masonry infilled RC frames were analyzed covering cases for frames with solid infills (i.e.: no opening) and frames having infill walls with window/door openings. The steel and RC frames were moment resisting frames. The details and mechanical properties for the frames and infill walls are summarized in Tables 4-1 and 4-2. For information on reinforcement detailing and/or steel sections used for the frame construction, the reader is referred to the publications referenced in Table 4-1.

Mehrabi et al. (1996) applied vertical loading to the frame specimens in addition to the lateral loading. In this investigation, specimens M3 & M4 were subjected to 146.85 *kN* vertical loading on each column; whereas specimens M8 & M9 were subjected to 97.9 *kN* on each column and 97.9 *kN* on the beam. The other researchers did not introduce any vertical confinement on the frame beam or columns. Also, specimen M4 was subjected to cyclic loading; hence, the envelope for the loading history was used to study the equivalent monotonic load displacement behaviour.

Table 4-1: Details of the experimental specimens used to validate the FEM

Ref	Spec #	Frame Type	Frame size	Opening size (mm)	Opening location	Infill wall Dimensions	
						l_w (mm)	h_w (mm)
Dawe & Seah (1989)	WA4	Steel Frame	Full	None	N/A	3592	2597
	WB2			None	N/A		
	WC4			800×2200	Central		
	WC5			800×2200	600 mm$^+$		
	WC7			None	N/A		
Liu & Soon (2012)	N3NA		1/3	None	None	1351	1080
	F3NA			None	None		
	P3WA			537×283	Central		
	P3DA			402×643			
Mehrabi et al. (1996)	M4	RC Frame	1/2	None	None	2123	1422
	M8			None	None		
	M3			None	None		
	M9			None	None		
Yáñez et al. (2004)	Y1		Full	None	None	3250	2050
	Y2			2064×1230	Central		
	Y3			825×1230			
	Y4			645×2050	1922.5 mm$^+$		

$^+$Distance measured from the loaded side.

Table 4-2: Properties of the masonry infilled frames used to validate the FEM

Spec #	Frame Type and properties			Masonry Infill Wall		
	E (MPa)	I-Column ($10^6\ mm^4$)	I-Beam ($10^6\ mm^4$)	t^* (mm)	f'_m (MPa)	Units Dim. (mm)
WA4	Steel 200,000	18.80	45.40	64.00	24.40	Concrete block 200×200×400
WB2					33.30	
WC4					33.10	
WC5					32.50	
WC7					33.40	
N3NA	Steel 199,500	4.77	4.77	22.00	10.50	Concrete block 131×64×67
F3NA					9.40	
P3WA					9.40	
P3DA					9.40	
M4	Concrete 17,225	83.28	152.00	31.76	10.61	Concrete block 100×100×200
M8	Concrete 17,225	83.28	152.00	31.76	9.51	
M3	Concrete 21,910	83.28	152.00	92.08	15.10	Concrete brick 100×100×200
M9	Concrete 17,225	83.28	152.00	92.08	14.19	
Y1	Concrete 22,977	100	100	52	16.26	Concrete block 291×141×115
Y2						
Y3						
Y4						

*t: Thickness of the face-shell of the masonry unit.

4.3. Finite Element Models

The simplified micro-modelling technique discussed in Chapter 3 was used to build models for the FE models for the physical masonry infilled frames listed in Table 4-2. Element used, constitutive material models, and the interface models were discussed in details in Chapter 3. Figure 4-1 shows a schematic for a typical finite element model for a reinforced concrete frame filled with a solid masonry wall.

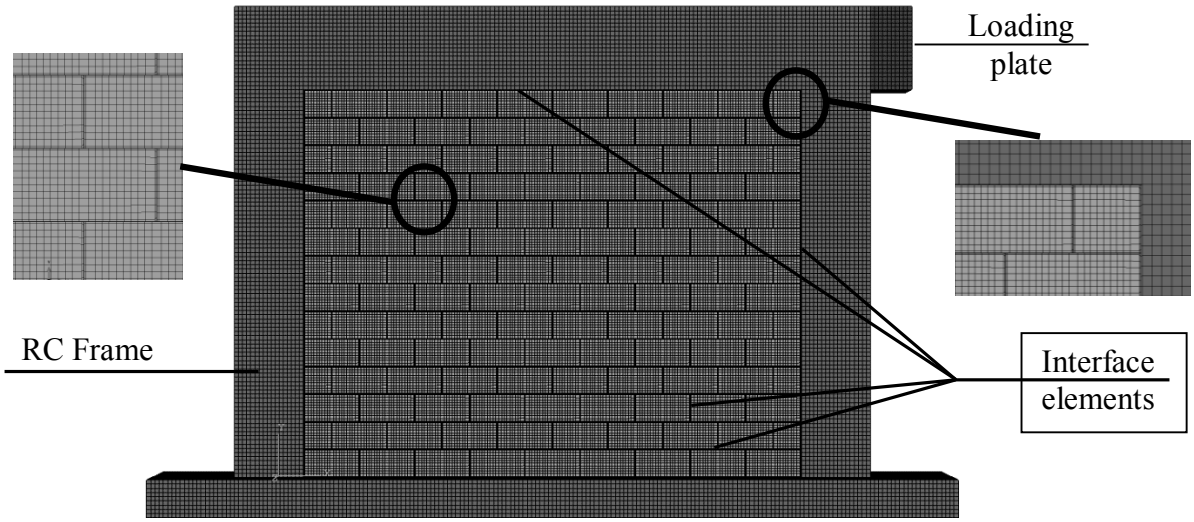

Figure 4-1: Schematic for a typical FEM for a masonry infilled RC frame

Mehrabi et al. (1996) subjected their specimens (M3, M4, M8 and M9) to confinement pressure before the lateral load was applied. In the finite element model, two loading steps were defined that acted in series. In the first load step, the confinement pressure was applied. Once the confinement pressure was reached, the second load step was initiated where the lateral load was applied.

4.4. Numerical Results vs Experimental Results

Figure 4-2 is a schematic for the lateral load-lateral displacement response of masonry infilled frames. The parameters shown in Figure 4-2 were used to evaluate the adequacy of the FEM in predicting the behaviour of the infilled frame system. The initial stiffness (K_{ini}) is defined as the slope of the initial linear portion of the load-displacement curve. The cracking load (P_{cr}) is taken as the instant where a major change in stiffness took place on the load-displacement history. The

ultimate load and ultimate displacement (P_{ult} & Δ_{ult}) are the ultimate lateral load resisted by the system and its associated displacement.

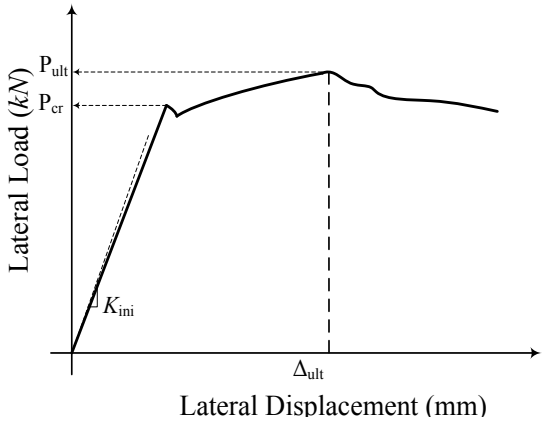

Figure 4-2: Schematic for the lateral load-lateral displacement behaviour of typical masonry infilled frame

In order to assess the adequacy of the FEM in estimating the response of masonry infilled frames, load-displacement behaviours constructed from the FEM were compared to the corresponding ones from experimental testing. The finite element model is stated to be in good agreement when the difference between the experimental and FEM results is less than 15% (difference is not significant on the lateral behaviour). The following sections summarize the comparison between the FEM predictions and the experimental measurements and observations.

4.4.1. Dawe and Seah (1989) Study

Figure 4-3 shows the lateral load-lateral displacement response of the finite element model compared to the physical response of the infilled steel frames. The finite element output was in good agreement with the experimental testing.

For solid infilled frames (WA4, WB2 and WC7), the infilled steel frames behaved linearly at early stages. The ratio between the initial stiffness for the finite element models to the experimental testing was reported as 1.1, 0.94 and 1.14 for specimens WA4, WB2 and WC7, respectively. Separation between the infill wall and the containing frame took place at the loaded side due to failure of the interface element at this location. The first crack that affected the behaviour took the form of

a stepwise diagonal tension crack, similar to experimental testing. Specimen WA4 had a relative value for the cracking load of 1 compared to the experimental testing, while both WB2 and WC7 had a relative cracking load of 1.06 compared to their experimental test value.

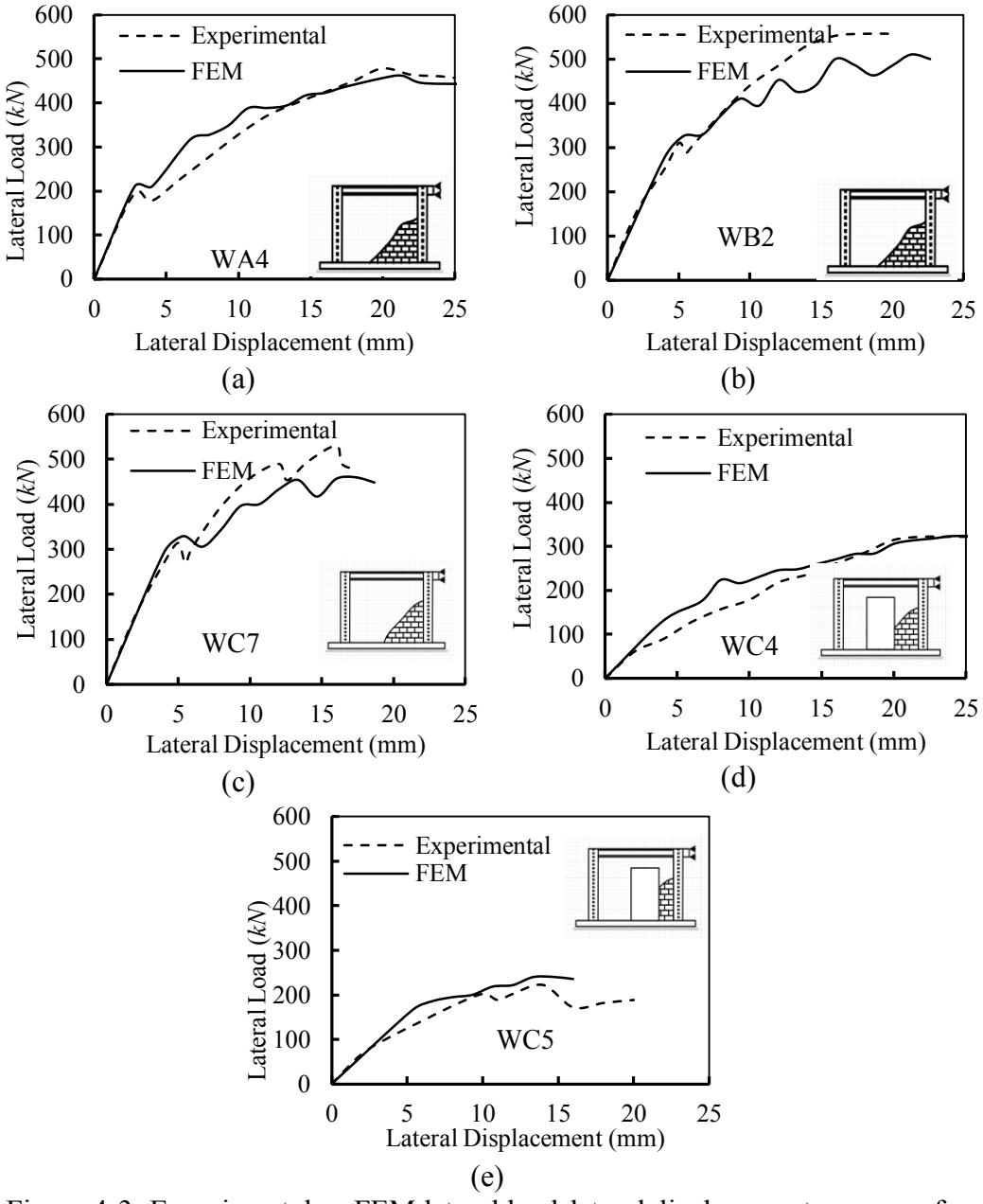

Figure 4-3: Experimental vs FEM lateral load-lateral displacement response for Dawe and Seah (1989) specimens: a, b, c for solid infill walls and d and e for infill walls with door opening

A diagonal compression strut was formed in the masonry infill wall. From

the finite element, it was clear that the width of the diagonal strut is not constant and was dependent on the loading level. Failure was dominated by crushing of masonry at the corners of the developed strut. The predicted value for the ultimate load from the finite element investigation were 0.97, 1.01 and 0.86 relative to the corresponding experimental values for specimens WA4, WB2 and WC7; while the ultimate displacement was predicted with relative values of 1.07, 1.18 and 1.08 for the same specimens. The steel frame did not experience formation of plastic hinges at the joints or in its members. Figures 4-4 through 4-6 show the principal compressive stresses at failure load for specimen WA4, WB2 and WC7, respectively.

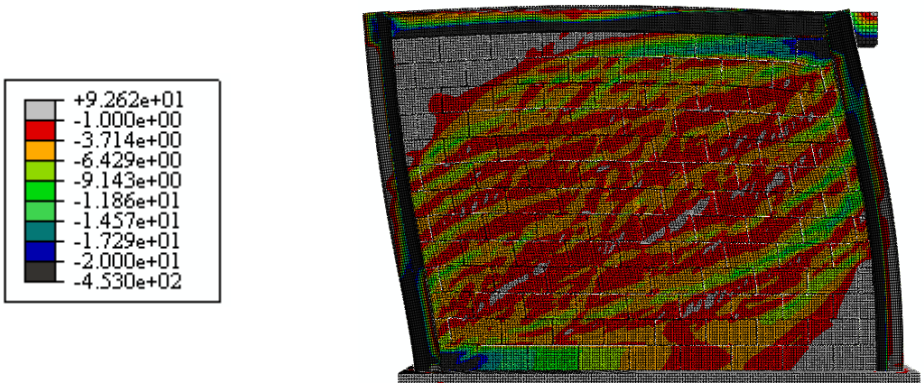

Figure 4-4: Principal compressive stresses at failure for Dawe and Seah (1989) for solid infilled steel frame, WA4 (MPa)

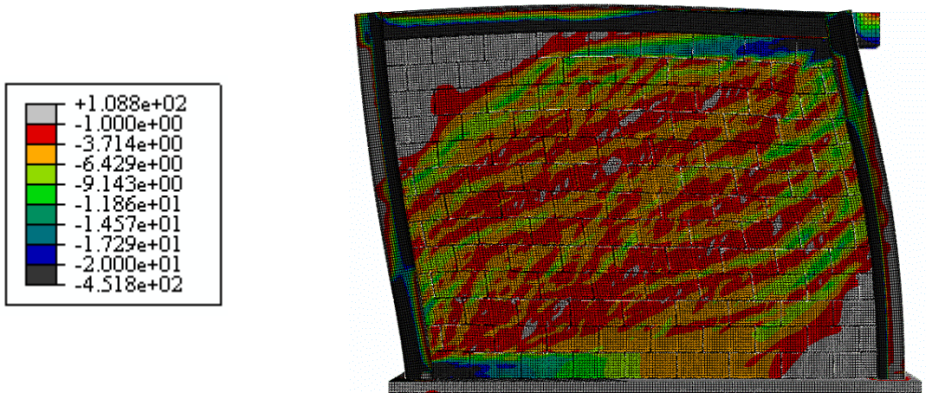

Figure 4-5: Principal compressive stresses at failure for Dawe and Seah (1989) for solid infilled steel frame, WB2 (MPa)

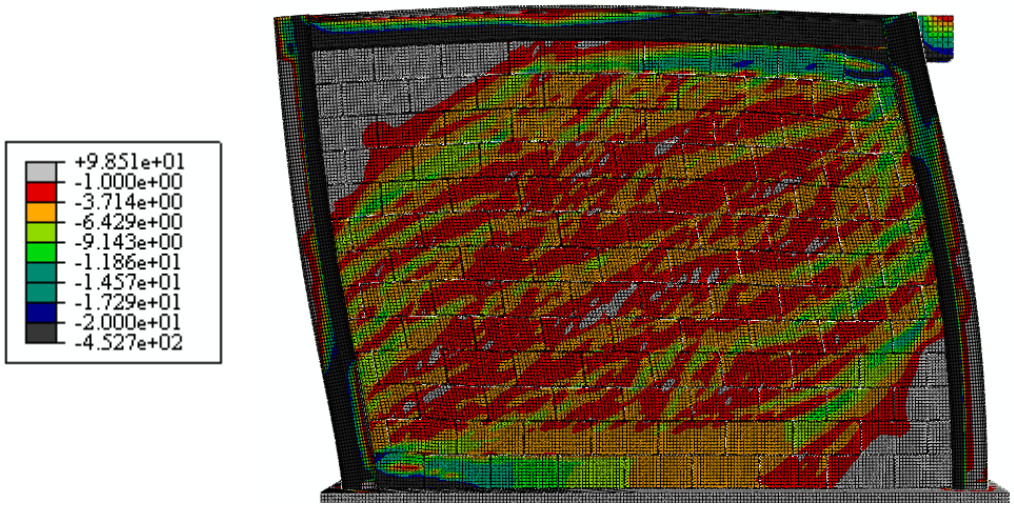

Figure 4-6: Principal compressive stresses at failure for Dawe and Seah (1989) for solid infilled steel frame, WC7 (MPa)

For infilled steel frames with door openings (WC4 and WC5), the presence of the door opening forced the infill wall to behave as two separate piers joined together with a spandrel. The initial stiffness of the infilled frames were 0.96 and 0.80 for WC4 and WC5, respectively, relative to the corresponding experimental testing. The first major crack took the form of a vertical crack at the top corner of the door opening towards the loaded side for both specimens. Specimen WC4 and WC5 gave higher prediction for the cracking load (2.00 and 1.33 compared to the corresponding experimental cracking load); this might be attributed to the non-homogenous nature of masonry and difficulty associated with modelling cracks. Diagonal tension cracks were developed in the pier towards the load side. The presence of the door opening led to the formation of a group of compression struts in the infill wall as shown in Figures 4-7 and 4-8. With continuous loading of the specimens, the infill wall failed due to crushing of masonry at the loaded corner. The ultimate load was predicted as 0.97 and 0.91 for specimen WC4 and WC5, respectively, compared to the experimental ultimate value. The finite element model predicted the ultimate displacement associated with the ultimate load with an average of unity for both infilled frames with opening compared to the experimental test result.

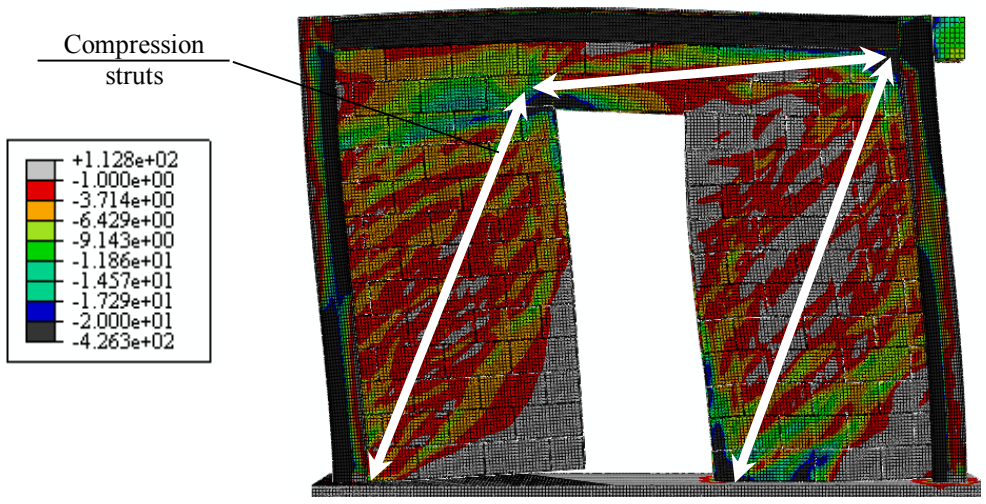

Figure 4-7: Principal compressive stresses at failure for Dawe and Seah (1989) for infilled steel frame with door opening, WC4 (MPa)

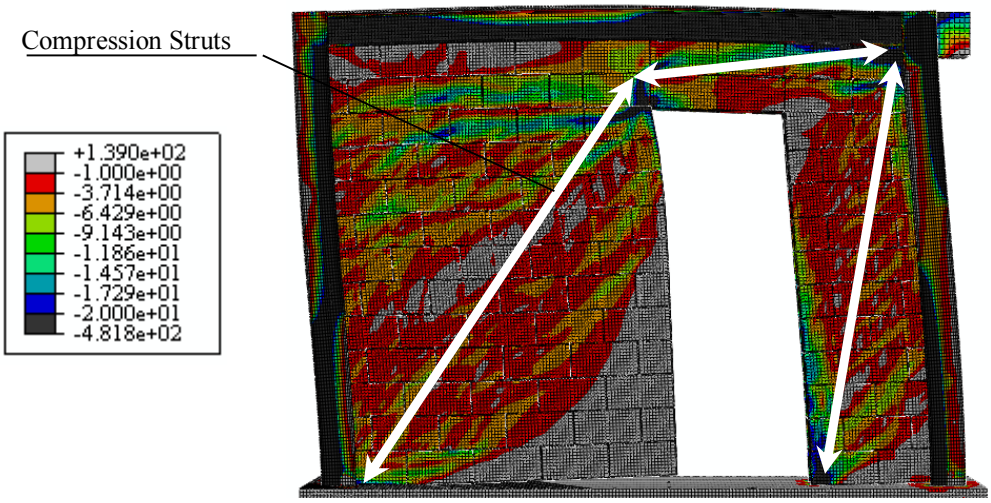

Figure 4-8: Principal compressive stresses at failure for Dawe and Seah (1989) for infilled steel frame with door opening, WC5 (MPa)

4.4.2. Liu and Soon (2012) Study

Liu and Soon (2012) tested 1/3 scale steel frames filled with concrete masonry units. Four of their frames were used to validate the finite element models:

hollow masonry solid infill wall, grouted solid masonry infill wall, an infill wall with a window opening, and an infill wall with door opening. The lateral load-lateral displacement responses for these four frames are shown in Figure 4-9.

Both solid infill walls, constructed using hollow and grouted construction, followed a linear elastic pattern until separation between the frame's top beam and the infill wall took place towards the unloaded side due to tension failure in the interface elements. It is worth mention that the reduction in the stiffness was not significant. The finite element model predicted the initial stiffness with an average of unity for both specimens compared to the physical value. Diagonal shear cracking started to initiate in the infill wall. The finite element models predicted the cracking load with less accuracy than the physical value. For hollow masonry infill wall, the predicted value was 19% less than the experimental cracking load; as for the fully grouted masonry, the prediction was 40% less than the experimental test results. Similar to Dawe and Seah (1989), this variation might be attributed to complexity associated with modelling cracks. Also, in the finite element, the properties of the interface was assumed constant which is not the case in the experimental testing. Both walls failed eventually due to corner crushing of the masonry material at the tip of the developed compression strut. The finite element model gave a good estimate of the ultimate failure load with a value of 0.95 and 1.02 for the hollow infilled frames and fully grouted infilled frames compared to the experimental ultimate load; the corresponding ultimate displacement was predicted with an average of 1.18 and 1.06 for hollow and grouted masonry infilled frames, respectively, compared to the experimental value. Figures 4-10 and 4-11 show the principal compressive stresses developed in the masonry infilled walls.

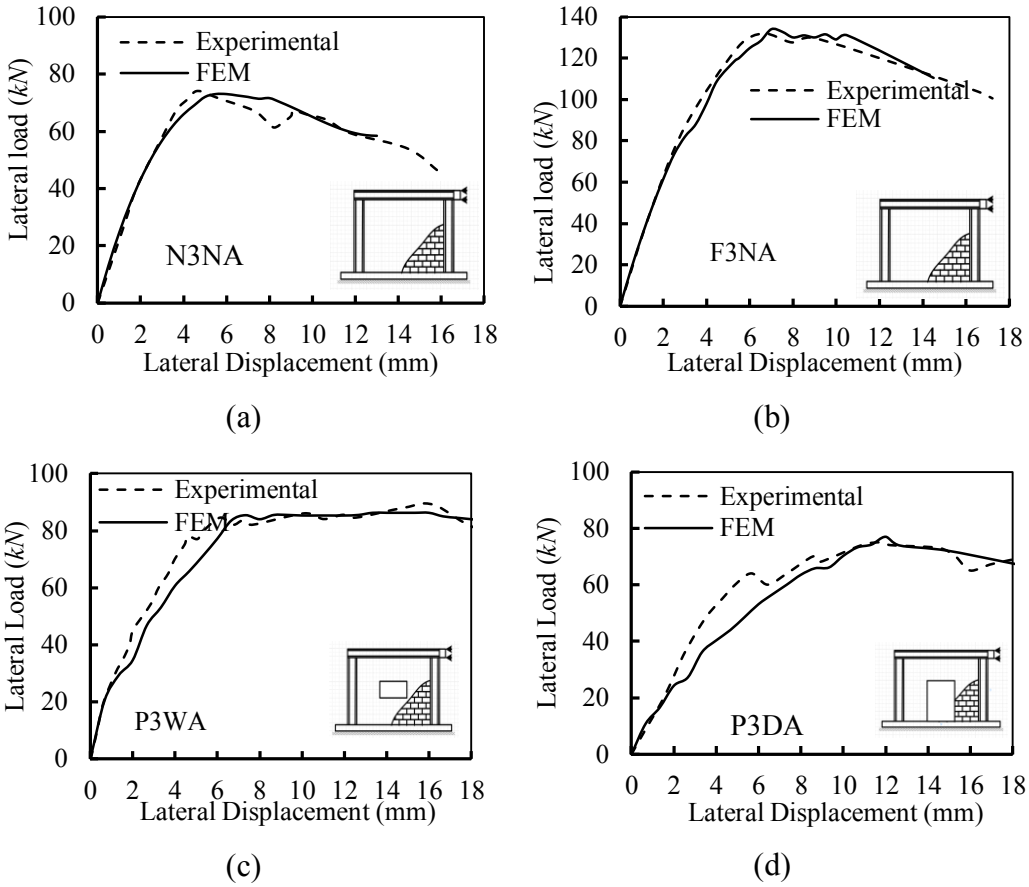

Figure 4-9: Experimental vs FEM lateral load-lateral displacement response for Liu & Soon (2012) specimens; a and b: Solid infill wall; c: infill wall with window opening; and d: an infill wall with door opening

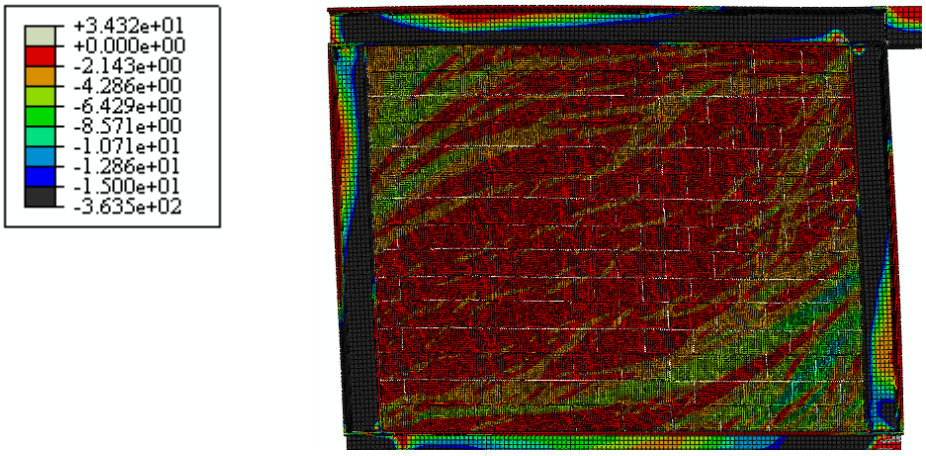

Figure 4-10: Principal compression stresses at failure for Liu and Soon (2012) masonry infilled frame, N3NA (MPa)

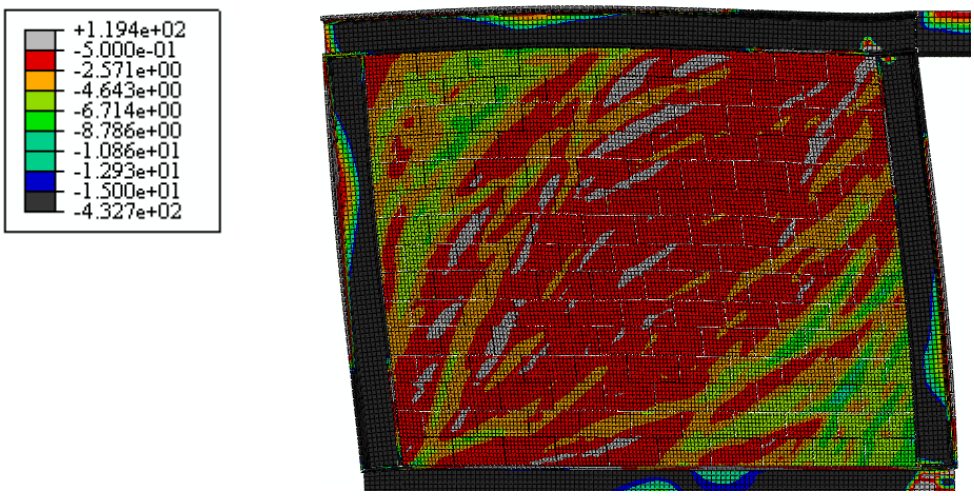

Figure 4-11: Principal compression stresses at failure for Liu and Soon (2012) masonry infilled frame, F3NA (MPa)

The presence of a window or door opening reduced the stiffness of the masonry infill walls compared to solid infill walls. Specimen P3WA had a window opening, while the P3DA had a door opening. Both specimens were partially grouted with grout placed every 198 mm. Similar to the solid infilled frames, separation between the containing frame and the masonry infill wall took place by tension failure of the interface elements towards the unloaded side. The failure of the contact element did not affect the initial stiffness; the finite element model initial stiffness was recorded as 1.08 and 1.18 for specimen P3WA and P3DA, respectively, compared to corresponding experimental value. Diagonal shear cracks were developed in the infill wall leading to reduction in the initial stiffness of the wall with a relative value of 0.9 and 1.03 for P3WA and P3DA, respectively, compared to the experimental value. The number of cracks started to increase till failure. The predicted values for failure load from the finite element were close to the experimental value with relative value of 0.97 and 1.03 for P3WA and P3DA, respectively. Grouted columns acted as stiffeners to the masonry units, which led to redistributing the load along the length of the wall; hence, increase the number of developed cracks. Figures 4-12 and 4-13 show the developed stresses in the infill at failure.

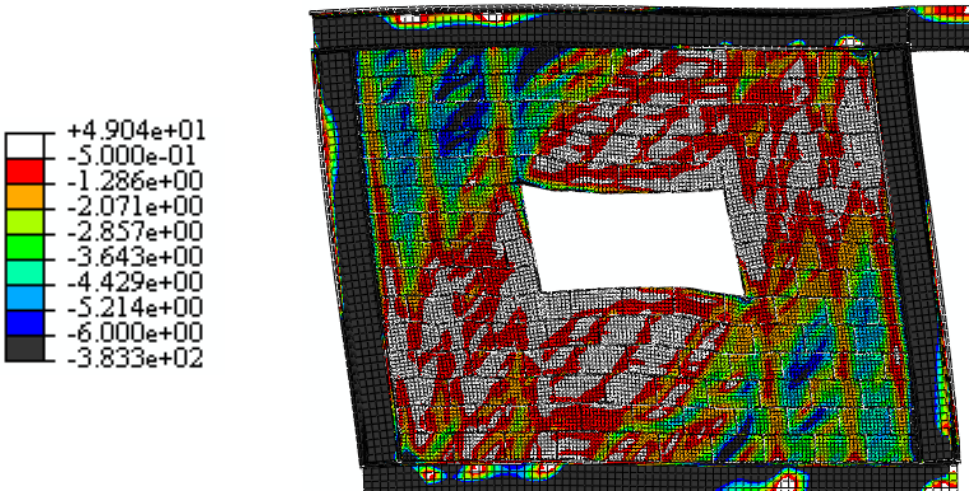

Figure 4-12: Principal compression stresses at failure for Liu and Soon (2012) masonry infilled frame, F3NA (MPa)

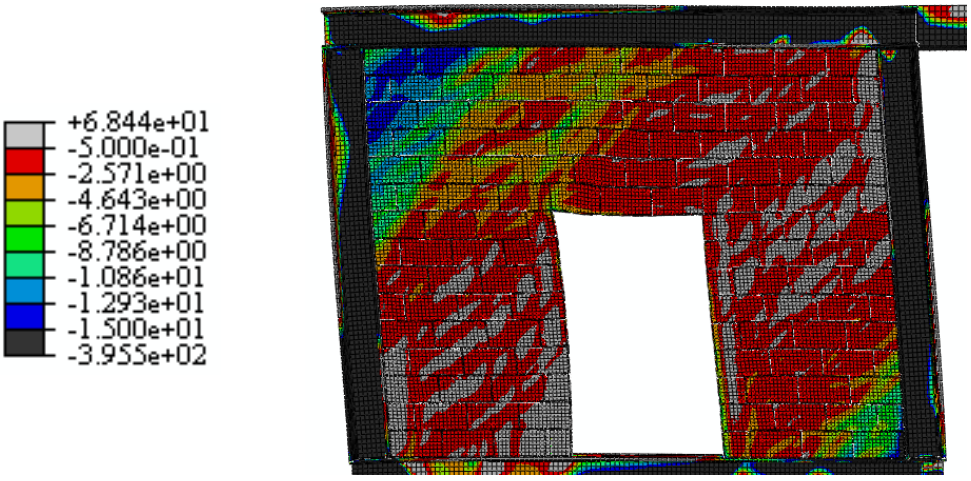

Figure 4-13: Principal compression stresses at failure for Liu and Soon (2012) masonry infilled frame, F3NA (MPa)

4.4.3. Mehrabi et al (1996) Study

The previous two investigations focused on the validating the FEM against experimental testing of infilled steel frames. Mehrabi et al (1996) studied the same behaviour for RC frames. Their experimental program focused on testing ½ scale RC frames filled with concrete masonry units. Figure 4-14 shows the lateral load-lateral displacement response for the specimens used to validate the finite element model.

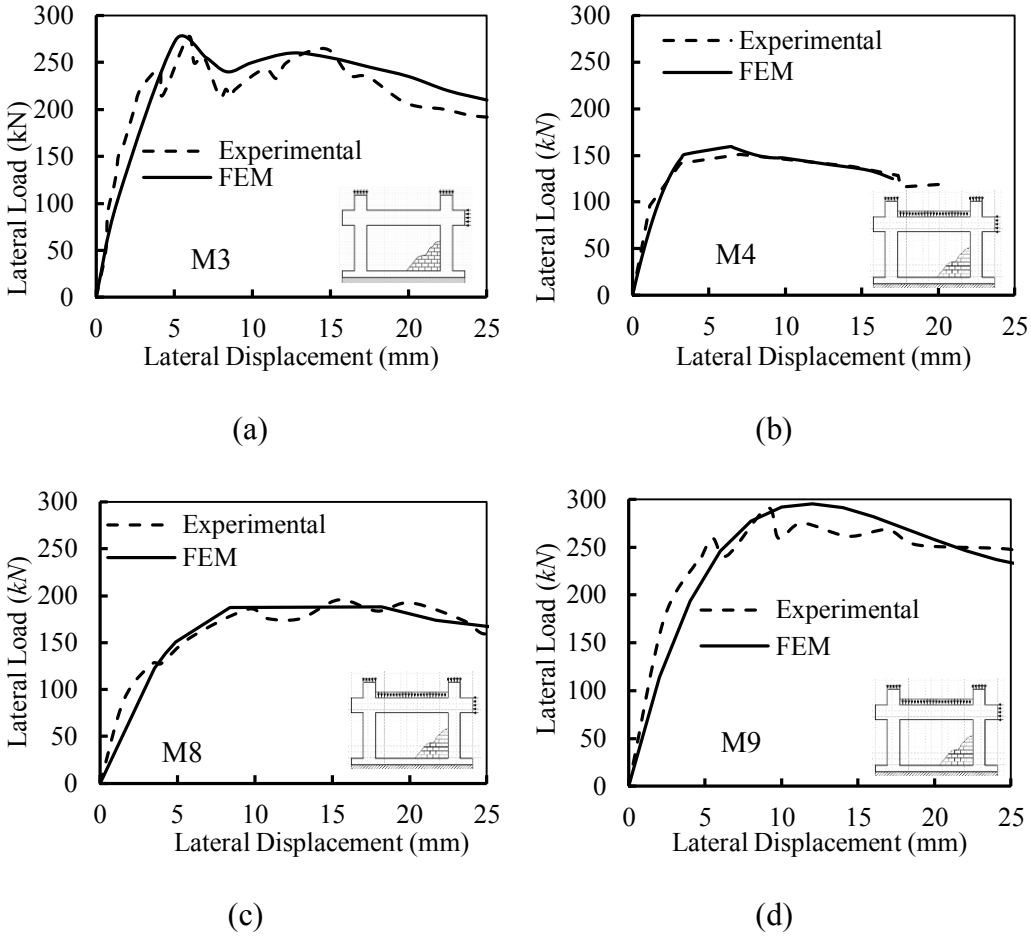

Figure 4-14: Experimental vs FEM lateral load-lateral displacement response for Mehrabi et al. (2004) specimens

Similar to the behaviour of masonry infilled steel frames, separation between the masonry infill and the containing frame took place by tension failure of the interface element. This failure did not affect the lateral load-lateral displacement response for the infilled frame. The initial stiffness computed from the finite element models were less than the experimental results for the different infilled frames by 25% on average. Specimen M3 failed due to the formation of a diagonal tension crack at the same load as what was reported in the experimental testing (cracking load was the same as the ultimate load). For specimen M8, the first crack took the form of a diagonal tension crack at loading level 8% less than the experimental cracking load. With continuous loading, the crack was fully developed in the moasnry infill wall, and failure was reported at the same load level

as the experimental result; however, the corresponding displacement was 30% more than the experimental one. The first crack in specimen M9 was a step wise crack starting from the loaded corner. The finite element model prediction for the cracking load were 25% less than the experimental test. With continuous loading, sliding shear took place along the top two mortar joints. The ultimate load from the finite element model was the same as the experimental testing, but the ultimate 60% more than what was reported in the experiment.

For specimen M4, the initial stiffness of the finite element model was 20% less than the experimental testing. The first crack took the form of diagonal tension crack and was formed at a load level 18% less than the experimental testing. The finite element model showed that sliding shear of the masonry along a bed joint at the top third of the wall was the dominating failure mechanism, unlike the experimental testing which showed corner crushing of the masonry. This might be attributed to the reversible nature of the applied load in conducting the experiment. The finite element model, however, was subjected to monotonic loading. The minimum compression stresses developed in the different infilled RC frames are shown in Figures 4-15 through 4-18.

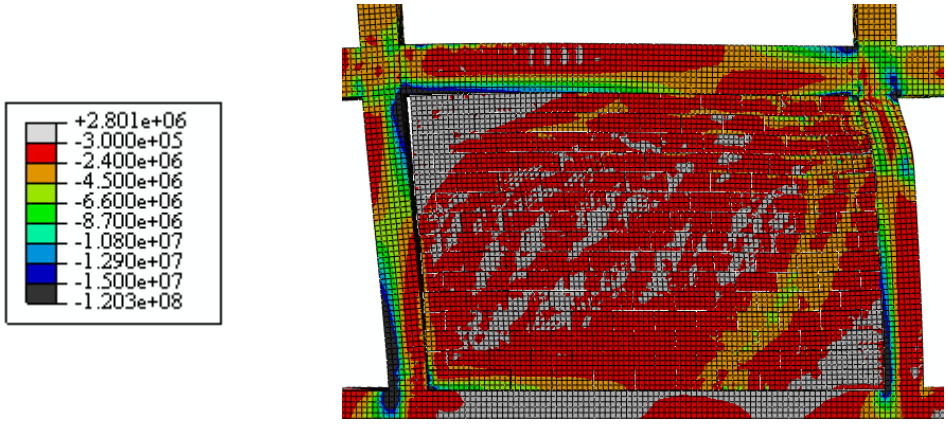

Figure 4-15: Principal compression stresses at failure for Mehrabi et al. (1996) masonry infilled frame, M3 (N/m^2)

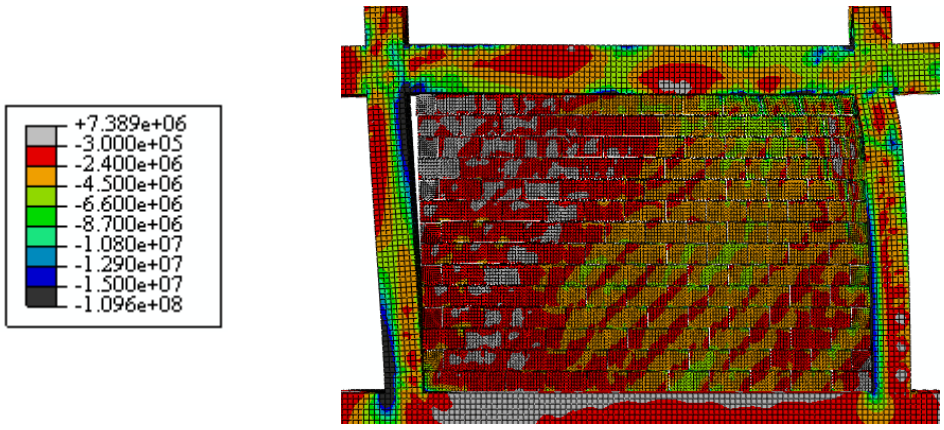

Figure 4-16: Principal compression stresses at failure for Mehrabi et al. (1996) masonry infilled frame, M8 (N/m^2)

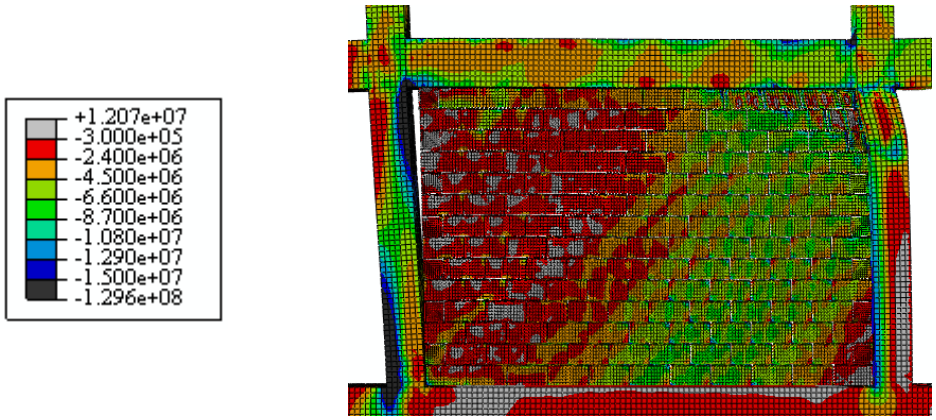

Figure 4-17: Principal compression stresses at failure for Mehrabi et al. (1996) masonry infilled frame, M9 (N/m^2)

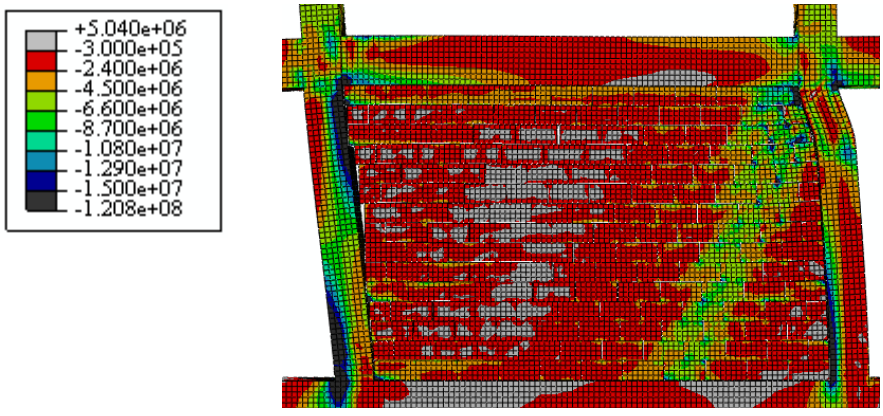

Figure 4-18: Principal compression stresses at failure for Mehrabi et al. (1996) masonry infilled frame, M4 (N/m^2)

4.4.4. Yàñez et al. (2004) Study

Another investigation that dealt with concrete masonry infill wall built in concrete frame was conducted by Yàñez et al. (2004). In their experimental testing, full scale models were constructed and subjected to lateral loading. The lateral load-lateral displacement behaviour for these specimens was compared against the finite element output as shown in Figure 4-19.

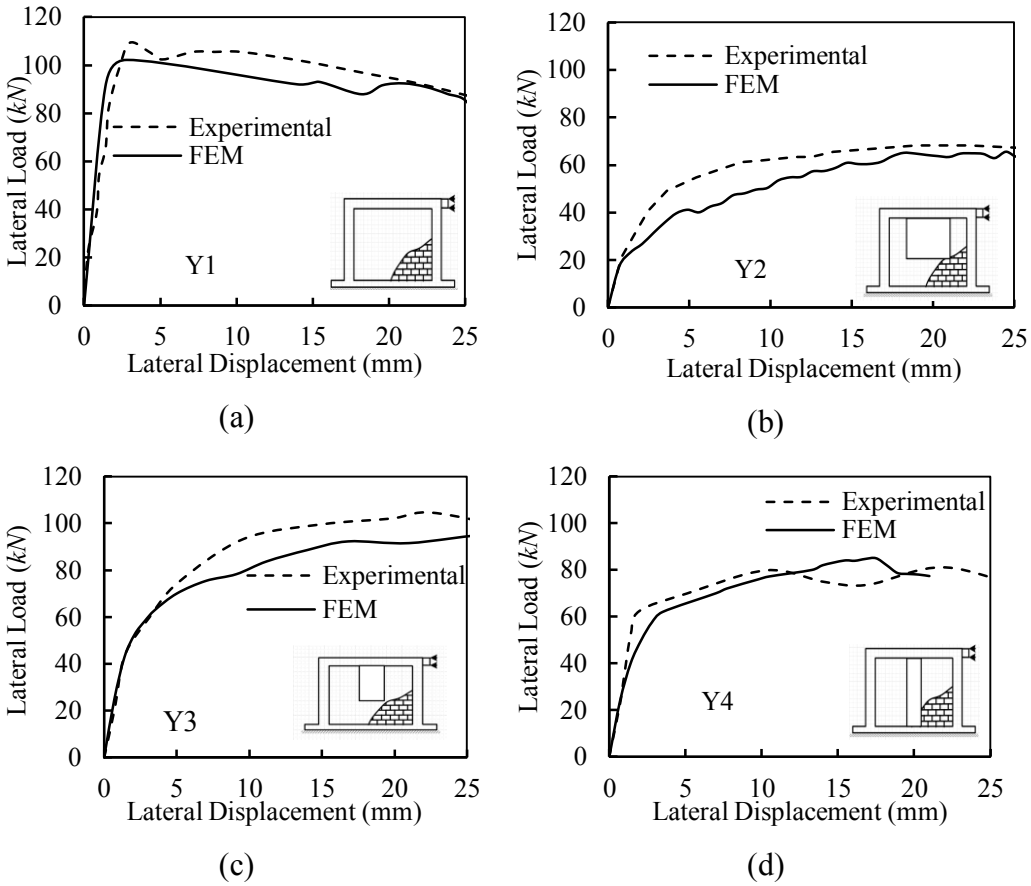

Figure 4-19: Experimental vs FEM lateral load-lateral displacement response for Yàñez et al. (1996) specimens: a) solid infill wall, b) large window opening, c) narrow window opening and d) narrow door opening

All the infill panels failed due to development of diagonal tension cracking in the infill wall. For specimen Y1, the initial stiffness for the finite element model was higher than the experimental testing by 40%; the first crack took the form of a diagonal tension crack at lateral load level 30% higher than the experimental one. Failure of the masonry infill wall was achieved with the full development of the

diagonal tension crack at load level 6% less than the corresponding experimental one; the models prediction for the ultimate displacement corresponding to the ultimate load was less than the experimental value by 12%.

When a window/door opening was introduced in the infill wall, the behaviour of the system was more ductile. The initial stiffness for specimen Y2, Y4 were increased by 4% and 7%, respectively, compared to the experimental testing, while it was reduced by 9% for specimen Y3. The first crack developed in specimen Y2 and Y3 were underestimated from the finite element model by 17% and 15%, respectively, compared to the experimental testing, while specimen Y4 experienced increase in the cracking load of 3%. Similarly, the ultimate load measured from the finite element output was almost the same as the experimental test result for the three specimen. The finite element model overestimated the ultimate displacement for specimen Y2 and Y3 by 20% compared to the experimental testing, while it underestimate the value for Y4 by 21%. Figures 4-20 through 4-23 shows the principal compressive stresses in the four specimens.

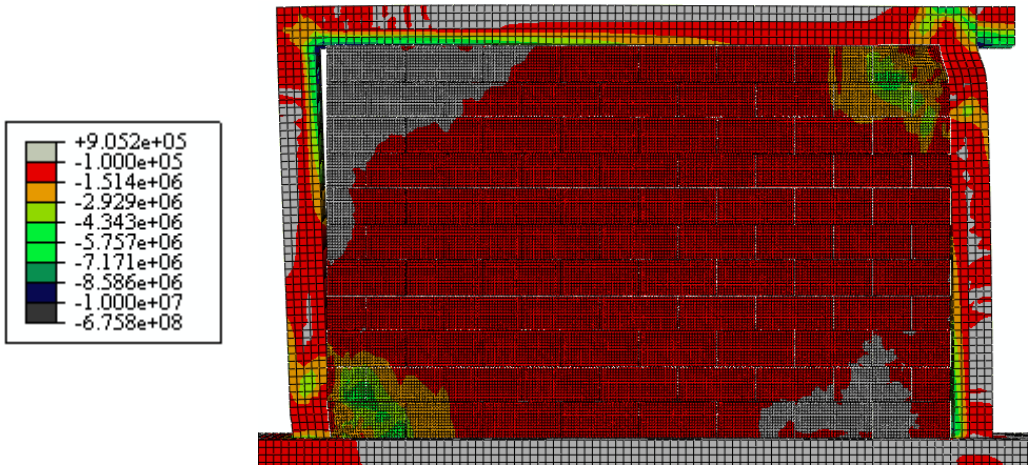

Figure 4-20: Principal compressive stresses at failure load for Yàñez et al. (2004) specimen Y1 (N/m^2)

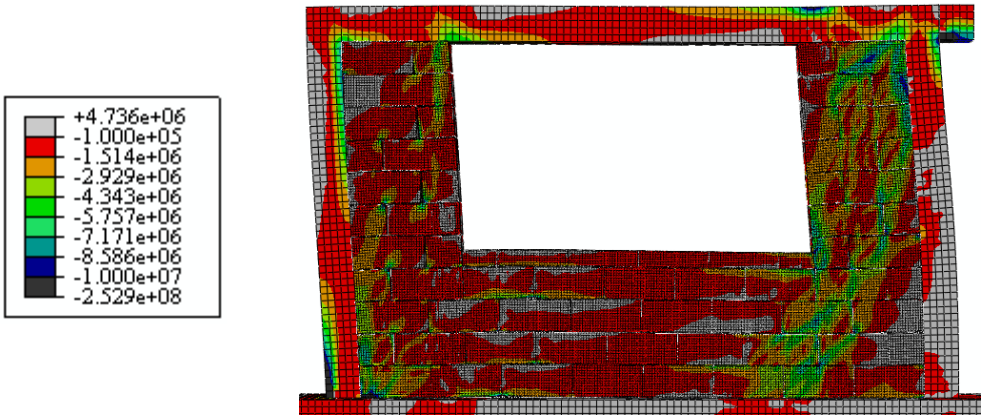

Figure 4-21: Principal compressive stresses at failure load for Yàñez et al. (2004) specimen Y2 (N/m^2)

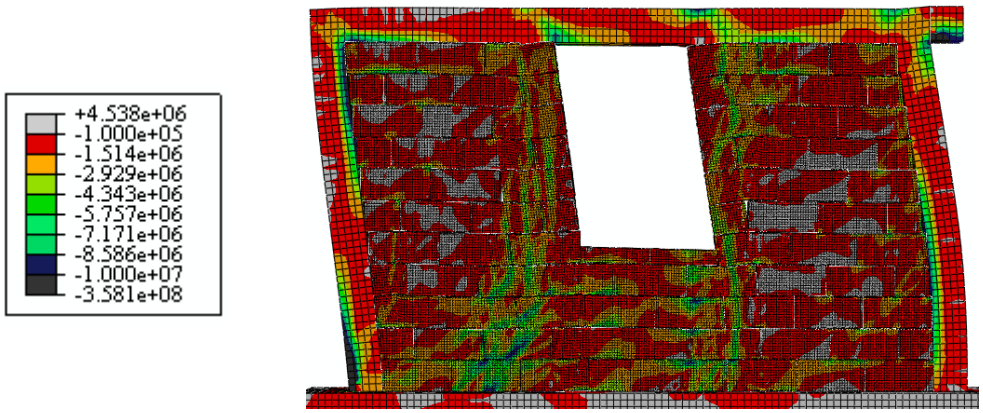

Figure 4-22: Principal compressive stresses at failure load for Yàñez et al. (2004) specimen Y3 (N/m^2)

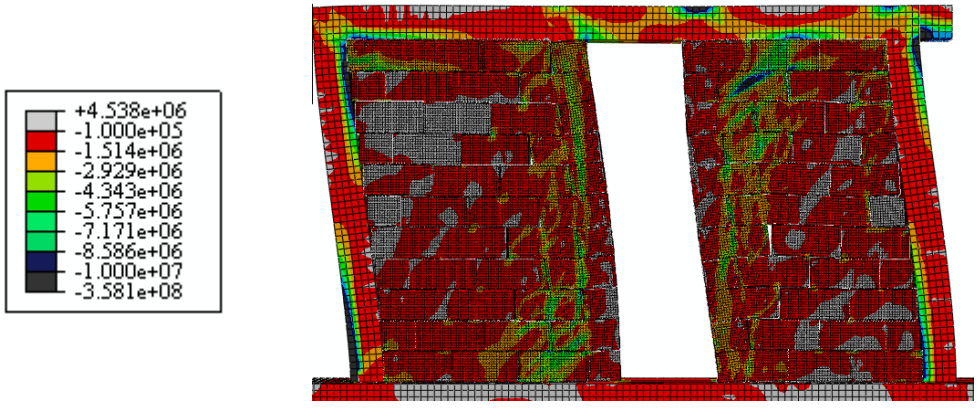

Figure 4-23: Principal compressive stresses at failure load for Yàñez et al. (2004) specimen Y4 (N/m^2)

4.4.5. Validation Summary

Tables 4-3 and 4-4 summarize the results of the FE analysis compared to the experimental results for infilled frames without opening and with opening, respectively. The finite element model was capable of predicting the initial stiffness of solid infilled frame system without opening compared to the measured experimental values with an average value of 0.99 and coefficient of variation of 19.06%; the ultimate load had an average of 0.97 with a coefficient of variation of 4.60% compared to measured values. The associated displacement with the ultimate load had an average of 1.12 with a coefficient of variation of 18.73%. The average predicted value for the cracking load was 0.93 with a coefficient of variation of 19.52% for solid walls.

Table 4-3: Comparison between finite element and experimental results for solid masonry infilled frames without opening

Spec #	$K_{ini\ FEM}$ (*KN*/mm)	$K_{ini\ FEM}$ / $K_{ini\ EXP}$	$P_{cr\ FEM}$ (*kN*)	$P_{cr\ FEM}$ / $P_{cr\ EXP}$	$P_{ult\ FEM}$ (*kN*)	$P_{ult\ FEM}$ / $P_{ult\ EXP}$	$\Delta_{ult\ FEM}$ (mm)	$\Delta_{ult\ FEM}$ / $\Delta_{ult\ EXP}$	Failure Mode*
WA4	70.10	1.11	210	1.00	461.71	0.97	21.30	1.07	CC+DT
WB2	69.25	0.94	325.61	1.06	560.00	1.01	21.30	1.18	CC+DT
WC7	73.14	1.14	329.21	1.06	460.00	0.86	17.33	1.08	CC+DT
N3NA	25.97	1.07	50	0.81	73.00	0.95	5.50	1.18	CC+DT
F3NA	52.15	0.92	81	0.63	134.00	1.02	7.00	1.06	CC
M3	98.90	0.76	275.6	0.99	275.60	0.99	5.10	0.84	DT
M4	60.15	0.80	73	0.82	159.16	0.98	11.40	0.95	SS
M8	45.51	0.79	123	0.92	187.28	0.99	18.20	1.30	DT
M9	94.92	0.92	193.6	0.74	295.47	1.01	12.00	1.63	SS+DT
Y1	65.08	1.40	91	1.3	102.00	0.94	2.86	0.95	DT
Average		0.99		0.93		0.97		1.13	
COV+ (%)		19.09		19.52		4.60		18.73	

* CC: Corner Crushing, DT: Diagonal tension cracking, SS: Sliding shear failure

+COV: Coefficient of Variation

The developed model showed also capability in predicting the lateral load-displacement behaviour for infilled frames with openings. The initial stiffness had an average value of 1.00 with a coefficient of variation of 11.57%; the predicted ultimate load had an average of 0.97 with a coefficient of variation of 4.91%; while the associated ultimate displacement had an average value of 1.03 and coefficient of variation of 15.33%. As for the cracking load, the average predicted value was 1.14 with a coefficient of variation of 34.53%. The higher values for the coefficient of variation are attributed to the nature of the masonry modelling. Masonry

assembly is composed of different materials with different mechanical properties. It is, hence, a highly non-homogenous material. In modelling masonry, cracks were assumed to take place in weak surfaces between different blocks (i.e.: interface element) or through the block itself once the stresses exceeded the allowable permissible values. Also, the properties of the masonry were assumed to be constant all over the assembly; the effect of any slight imperfection is not accounted for in building the FEM which might take place in constructing the wall. These conditions will attribute greatly in the cracking load prediction level of the system.

Table 4-4: Comparison between finite element and experimental results for masonry infilled frames with opening

Spec #	$K_{ini\ FEM}$ (*KN*/mm)	$\frac{K_{ini\ FEM}}{K_{ini\ EXP}}$	$P_{cr\ FEM}$ (*kN*)	$\frac{P_{cr\ FEM}}{P_{cr\ EXP}}$	$P_{ult\ FEM}$ (*kN*)	$\frac{P_{ult\ FEM}}{P_{ult\ EXP}}$	$\Delta_{ult\ FEM}$ (mm)	$\frac{\Delta_{ult\ FEM}}{\Delta_{ult\ EXP}}$	Failure Mode*
WC4	32.50	0.96	130	2.03	323.68	0.97	24.00	1.09	CC+DT
WC5	31.03	0.80	120	1.33	222.50	0.91	14.70	1.05	CC+DT
P3WA	30.62	1.08	46.8	0.9	86.25	0.97	13.33	0.82	DT
P3DA	16.13	1.18	65.86	1.03	77.00	1.03	12.00	1.03	DT
Y2	24.96	1.04	39.64	0.83	67.00	0.99	25.90	1.23	DT
Y3	35.41	0.91	66.5	0.85	95.80	0.92	26.50	1.20	DT
Y4	33.96	1.07	62.00	1.03	85.00	1.05	17.50	0.79	DT
Average		1.00		1.14		0.97		1.03	
COV^{+} (%)		11.57		34.53		4.91		15.33	

* CC: Corner Crushing, DT: Diagonal tension cracking, SS: Sliding shear failure
+COV: Coefficient of Variation

The proposed FE technique was successful in predicting the same failure mechanisms as the experimental testing. Tables 4-3 and 4-4 are a summary for the failure modes of the FE models for different specimens. Failure mechanisms were determined from the stress contours developed in the masonry walls. Cracking took place at locations where stresses exceeded the maximum value. Failure modes determined from the FE models were in full agreement with the observation from experimental testing except for specimen M4. Specimen M4 was reported to fail in sliding shear and corner crushing at the loaded side, while the FE model predicted sliding shear only. In the experimental testing, the lateral load had a reversible nature (cyclic) which led to crushing of the material, unlike the FE analysis which was carried out under quasi-static displacement.

4.5. Closure

In this Chapter, the finite element technique proposed in Chapter 3 was validated against experimental observation from four major research programs. Nine masonry infilled steel frames and eight infilled RC frames were considered in the validation. The experimental data included infilled frames ranging from full size to 1/3 scale and covered cases of hollow and grouted solid infill walls and infill walls with window or door openings.

It was demonstrated that the developed finite element technique is capable of capturing the entire lateral load-lateral displacement history of masonry infilled frames up to failure with acceptable accuracy. In addition, the technique is capable of accurately predicting the failure mechanisms of the infill wall: sliding shear, diagonal tension cracking, and corner crushing. Therefore, the developed modelling technique was used to study the effect of the most influential parameters on the behaviour of masonry infilled frames.

CHAPTER 5

ANALYTICAL INVESTIGATION

5.1. Introduction

The finite element technique described in Chapter 3 and validated in Chapter 4 was used to build two full-size masonry infilled steel and RC master frames to study the system's behaviour under lateral in-plane loading. The analytical investigation covers the most influential parameters that impact the in-plane response of masonry infilled frames. These parameters are: the infill wall aspect ratio, gap size and location between the infill wall and the containing frame, haunched frame response, infill wall relative stiffness, and opening size and location relative to the infill wall.

The full size frame models used in this analysis represent typical construction of multi-storey steel and RC framed buildings. A full description of each frame's geometry, details and materials is presented in this chapter. A summary of the analysis matrix including the value range for the investigated parameters is also provided.

5.2. Master Frame Models

Two full size master steel and RC frames were constructed using ABAQUS 6.10-EF (SIMULIA, 2010). The master frames represent typical construction of a three storey building with the frames spaced 5000 mm apart. The height of the masonry infill wall within the frame was taken as a height of 2800mm, while the length was varied from equal to the height to twice the height to study different values of aspect ratios.

The steel and RC master frames were designed and detailed according to 2010 NBCC. The design yielded a steel frame with a column section of W250×58 and a beam section of W200×46 as shown in Figure 5-1. The frame was detailed to act as an moment resisting frame. This was achieved by welding the beam to the column web; The column was welded at its base to the supporting beam. The RC master frame had a rectangular cross-section of 250×500 mm, while the beam had

dimensions of 250×600 mm. Figure 5-2 shows the geometry and reinforcement detailing of the RC frame. The steel reinforcement detailing resulted in the formation of a moment resisting frame for the RC frame as well. Both steel and RC master frames were checked against wind load applied in Edmonton, AB, and the members sizes and properties were found adequate to resist the applied load. The supporting beam in both the steel and RC frame acts as the solid base upon which the frame is being erected. Also, it acts as the foundation upon which the masonry infill wall would sit on.

The masonry infill wall was constructed using concrete masonry units of nominal dimensions of 400×200×200 mm. The masonry infill wall was placed at the centre of the frame to avoid any out-of-plane loading to be applied on the infill wall.

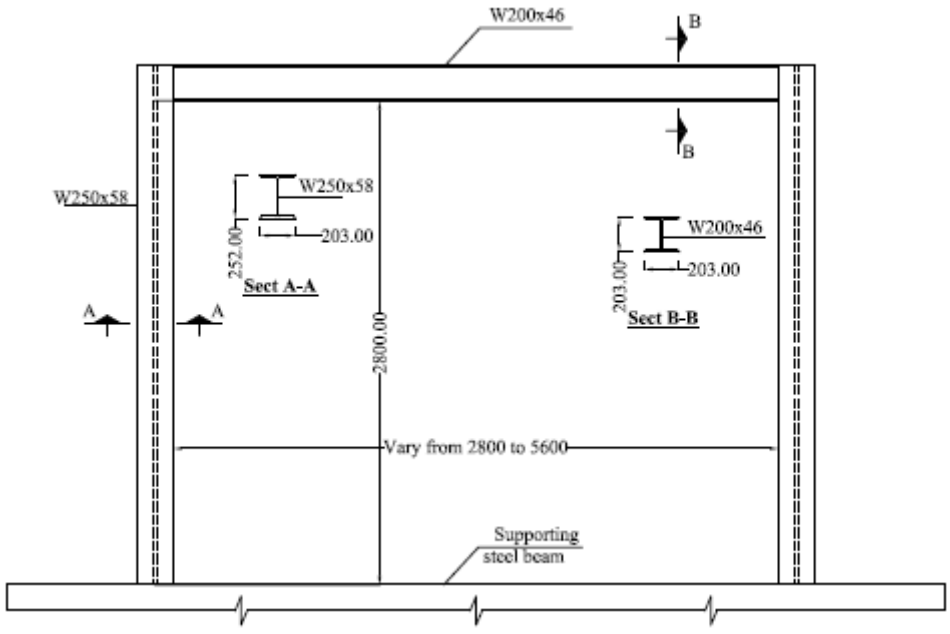

Figure 5-1: Geometry and details of the master steel frame used in the FE investigation

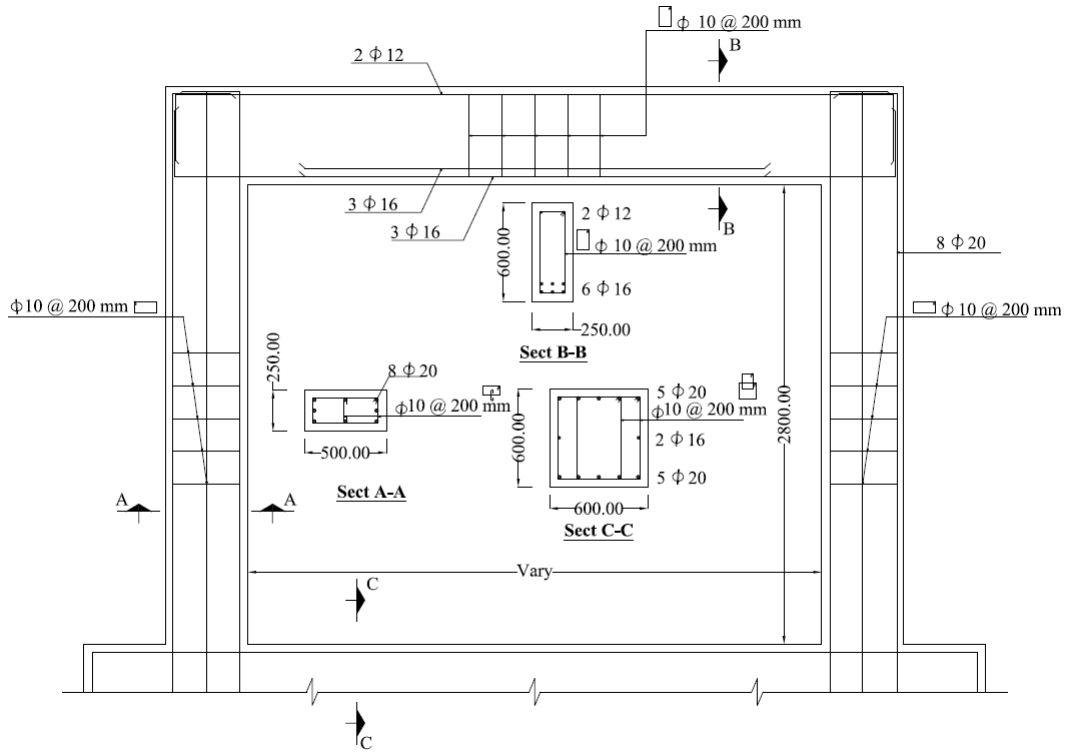

Figure 5-2: Geometry and reinforcement detailing of the master RC frame used in the FE investigation

5.3. Material Characterization

Steel sections and reinforcing bars were assumed to have a yield strength of 350 MPa and an ultimate strength of 450 MPa. The elasto-plastic response described in Chapter 3 and shown in Figure 5-3 was used to model the steel material behaviour. The value of the modulus of elasticity for steel was 200,000 MPa.

Reinforced concrete frames were assumed to be constructed using normal weight concrete having a compressive strength of 30 MPa. The idealized stress stain curve for the concrete is shown in Figure 5-4. The failure strain for the concrete was assumed to occur at strain level of 0.004. The elastic part of the curve was defined by the secant modulus of elasticity at 40% of the peak compressive strength (E_c = 21295 MPa). The Poisson's ratio for the concrete was taken equal to 0.25. The plastic part of the curve was modelled using the concrete damaged plasticity model described in Chapter 3 and given by Equation 3-11. The maximum

tensile stress of the concrete is usually 10% of its allowable compression capacity. The value in this investigation was taken as 3.2MPa.

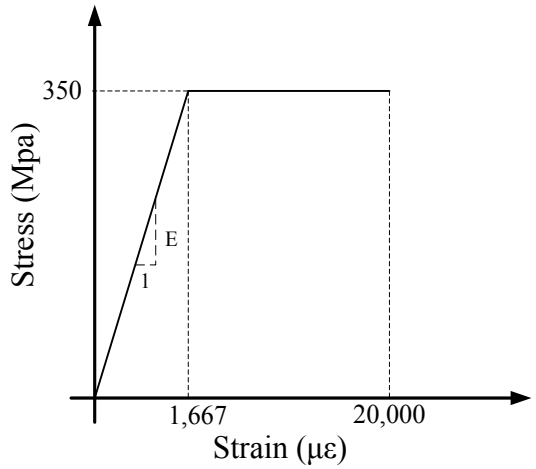

Figure 5-3: Idealized steel material behaviour used in the FE analysis

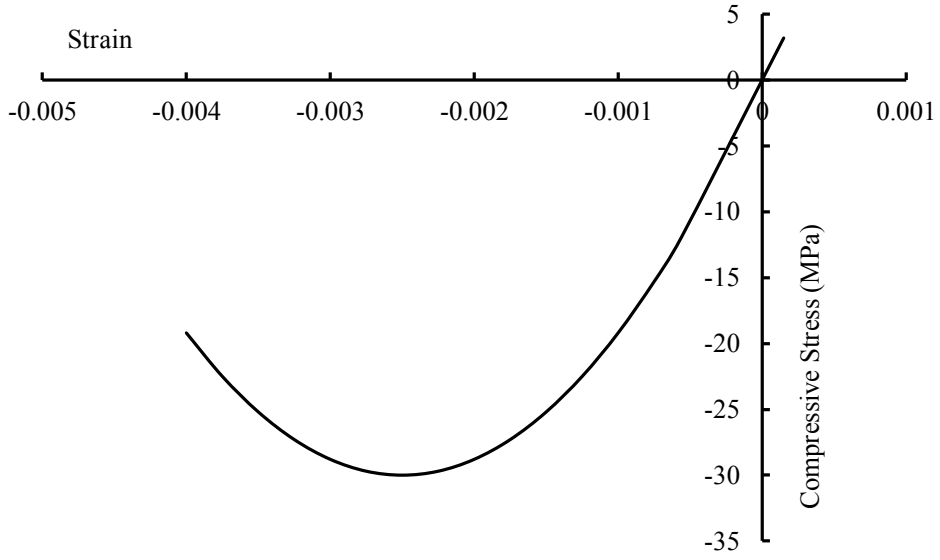

Figure 5-4: Concrete idealized Stress-strain relationship used in the FE analysis

In the current investigation, three types for masonry construction were considered: hollow construction, partially grouted construction and fully grouted construction. Partially grouted walls were modelled using hollow masonry units having the properties of hollow masonry, the grouted cores having the properties

of the grout. Fully grouted walls were modelled using solid masonry units having the properties of grouted masonry. The compressive strength of hollow masonry was assumed to be 25 MPa, that for grouted masonry was assumed 18 MPa, and grout compressive strength was taken as 10 MPa. Masonry strength values are true values measured at the University of Alberta for hollow and grouted prisms constructed of units having a nominal compressive strength of 20 MPa and type S mortar.

The idealized stress-strain relationships for hollow masonry, grouted masonry, and grout are given in Figure 5-5. Similar to concrete, the behaviour of the masonry was divided into two parts: elastic response and nonlinear plastic response. The stress-strain behaviour of the masonry prism was almost linear till a stress level of 80% of the maximum compressive strength of the hollow masonry; The secant modulus that defines the linear response was measured as 21336 MPa. The non-linear response was modelled according to the concrete damaged plasticity model defined in Chapter 3.

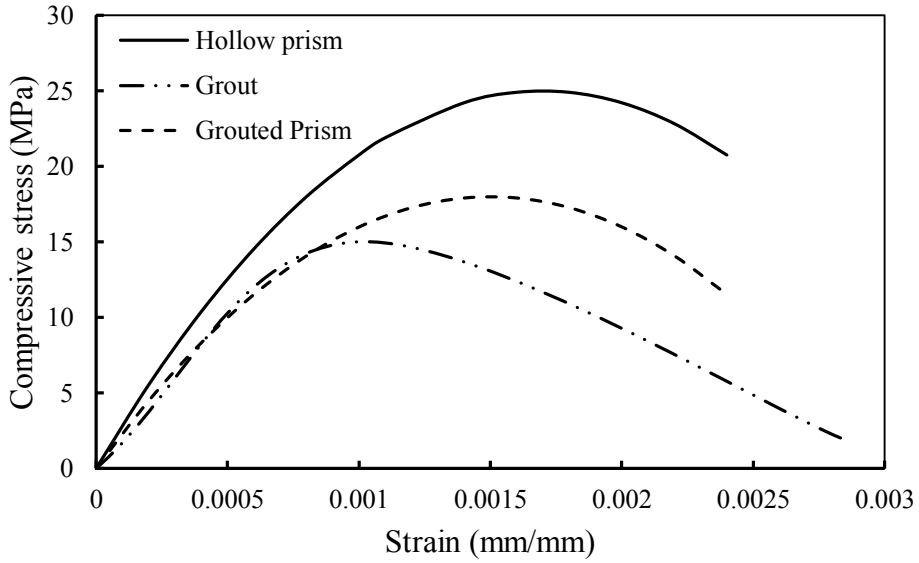

Figure 5-5: Idealized compressive stress-strain relationships for hollow masonry, grouted masonry and grout used in the FE analysis

The properties of the interface elements introduced between the masonry units and between the masonry infill wall and the frame namely, normal stiffness,

K_n, Shear stiffness, K_s, normal tensile stress, σ_t, and shear stress, τ_s, were computed as discussed in Chapter 3 and are summarized in Table 5-1. After failure of the contact elements, friction forces were assumed to develop according to the Coulomb-friction model. The coefficient of friction between the masonry units and between the frame and the masonry infill wall was taken as 0.7 which is a typical value for friction between concrete units forming the masonry infill wall. Finite element analysis results had shown that the contribution of friction between the masonry infill wall and the containing frame is minimal compared to the one between different masonry units; hence, the value was set to a constant value of 0.7 for the whole model for simplicity in computation.

Table 5-1: Characteristic of the interface element used in the FE analysis

Interface	K_n (MPa/mm)	K_s (MPa/mm)	σ_t (MPa)	τ_s (MPa)	Friction coefficient
Unit/Mortar	5051.136	2370.73	0.10	1.20	0.7
Wall/frame	5051.136	2370.73	0.10	1.20	0.7

5.4. Analysis Matrix

Finite element models were built and used to investigate the effect of the most influential parameters on the behaviour of masonry infilled frames. The models were constructed following the simplified micro-model approach discussed in Chapter 3. A summary for the analysis matrix is given in Tables 5-2 and 5-3 for solid infilled frames and infilled frames with openings, respectively. The total number of frames analyzed using ABAQUS 6.10-EF was 84 frames (42 steel and 42 RC frames).

The most influential parameters that affect the response of masonry infilled frames to lateral loads are: infill wall aspect ratio, gap size and location between the infill wall and the containing frame, relative stiffness between the infill wall and the frame, haunch presence in the frame, and opening size and location relative to the infill wall.

Table 5-2: Analysis matrix for solid masonry infilled frames constructed using ABAQUS

Frame designation		*h/l*	Gap size (mm)	Grout	Haunch
Concrete	Steel				
F1C-GA15-76	F1S-GA15-76	0.76	15	N/A	N/A
F2C-GA10-76	F2S-GA10-76		10		
F3C-GA07-76	F3S-GA07-76		7		
F4C-GA05-76	F4S-GA05-76		5		
F5C-GT15-76	F5S-GT15-76		15		
F6C-GT10-76	F6S-GT10-76		10		
F7C-GT07-76	F7S-GT07-76		7		
F8C-GT05-76	F8S-GT05-76		5		
F9C-HC-76	F9S-HC-76		N/A		
F10C-PC-76	F10S-PC-76			Partially	
F11C-FC-76	F11S-FC-76			Fully	
F12C-H1-76	F12S-H1-76			N/A	400√2
F13C-H2-76	F13S-H2-76				200√2
F14C-H3-76	F14S-H3-76				600√2
F28C-HC-59	F28S-HC-59	0.59			N/A
F41C-HC-50	F41S-HC-50	0.5			
F54C-HC-100	F54S-HC-100	1.0			

Refering to Tables 5-2 and 5-3, the infilled frame model consists of 3 sections (FXL-YYYY-UU). The first part (FXL) stands for the frame number and material of construction; for example, “F1C” means infilled RC frame model number 1, whereas “F1S” means infilled steel frame model number 1. The second part (YYYY) stands for the construction type. For example, a full separation gap of width 15 mm all around the infill wall is denoted “GA15”, whereas a top gap with the same size is given the symbol “GT15”. In case of a solid infill wall in full contact with the frame (no gap) of hollow construction is given the symbol “HC”. A partially grouted wall is labeled “PC”, while a fully grouted masonry is given “GC” symbols. The presence of an opening has a different notation depending on the opening size and location. For instance, “OW1C” stands for hollow masonry infill wall with a central window opening of dimensions 1200×1000 mm. When the opening is eccentric towards the loaded side, the symbol “C” is switched to “L”; while when the opening is towards the unloaded side, it takes the symbol “U”. The

last part of the infilled frame designation stands for the infill wall aspect ratio expressed as a percent.

Table 5-3: Analysis matrix for masonry infilled frames with openings constructed using ABAQUS

Frame ID		*h/l*	Opening size[+] (mm)	Open. Loc.[*] (mm)	Grout
Concrete	Steel				
F15C-OW1C-76	F15S-OW1C-76	0.76	1200×1000	Center	Around opening
F16C-OW1L-76	F16S-OW1L-76			400	
F17C-OW1U-76	F17S-OW1U-76			2000	
F18C-OW2C-76	F18S-OW2C-76		800×800	Center	
F19C-OW2L-76	F19S-OW2L-76			400	
F20C-OW2U-76	F20S-OW2U-76			2400	
F21C-OW3C-76	F21S-OW3C-76		2000×1000	Center	
F22C-OW3L-76	F22S-OW3L-76			400	
F23C-OW3U-76	F23S-OW3U-76			1200	
F25C-OD1C-76	F25S-OD1C-76		800×2200	Center	
F26C-OD1L-76	F26S-OD1L-76			400	
F27C-OD1U-76	F27S-OD1U-76			2400	
F42C-OW1C-50	F42S-OW1C-50	0.50	1200×1000	Center	Around opening
F43C-OW1L-50	F43S-OW1L-50			400	
F44C-OW1U-50	F44S-OW1U-50			4000	
F45C-OW2C-50	F45S-OW2C-50		800×800	Center	Around Opening
F46C-OW2L-50	F46S-OW2L-50			400	
F47C-OW2U-50	F47S-OW2U-50			4400	
F48C-OW3C-50	F48S-OW3C-50		2000×1000	Center	
F49C-OW3L-50	F49S-OW3L-50			400	
F50C-OW3U-50	F50S-OW3U-50			3200	
F51C-OD1C-50	F51S-OD1C-50		800×2200	Center	
F52C-OD1L-50	F52S-OD1L-50			400	
F53C-OD1U-50	F53S-OD1U-50			4400	

[+] All window openings are centric with the wall height.
[*] Distance measured from the loaded side till the opening location.

A full example for the frame ID is “F50C-OW3U-50”; the name stands for masonry infilled RC frame number 50 constructed from hollow masonry infill wall in full contact with the containing frame. The wall has a window opening of size 2000×1000 mm located towards the unloaded side. The infill wall had an aspect ratio of 0.50.

The aspect ratios investigated included values of 0.5, 0.59, 0.76 and 1.0. These aspect ratios reflect typical frame sizes used in current practice. The gap between the infill wall and the containing frame can be a top gap between the masonry infill wall and frame's beam or a full separation gap between the infill wall and the containing frame. The gap size investigated for the full separation gap and the top gap were: 5 mm, 7 mm, 10 mm and 15 mm.

To study the effect of the infill wall stiffness on the behaviour, the percentage of grouted cores were chosen as: 0% grout (hollow wall), 27% grout (a partially grouted wall where cores were grouted every 800 mm), and 100 grout (fully grouted wall). The presence of haunch in the frame influences the lateral response and mode of failure of masonry infill walls. Three sizes of haunches were considered: $200\sqrt{2}$ mm, $400\sqrt{2}$ mm and $600\sqrt{2}$ mm. All the haunches were constructed at an angle of 45^{o}. The analysis was performed for both steel and RC infilled frames.

The effect of opening presence within the infill wall was investigated by considering four sizes of openings in the infill wall: 800×800 mm, 1200×1000 mm, 800×2200 mm and 2000×1000 mm. The analysis covered cases were the opening was centric, eccentric towards the loaded side, and eccentric away from the loaded side as shown in Table 5-3.

The load was applied to the finite element models as a quasi-static lateral displacement at the loading point of the infilled frame system. The lateral load was computed by the integration of the reactions at the base of the frame. The dynamic explicit solver in ABAQUS, which is suitable in analyzing structures with relatively short dynamic response, was used to conduct the analysis. Lateral displacement was applied to the infilled frame system untill failure took place.

5.5. Summary

The effect of the most influential parameters on the behaviour of masonry infilled frames were investigated using finite element models for 42 steel and 42 RC infilled frames. The parameters considered are: the infill wall aspect ratio, gap size and location between the infill wall and the containing frame, infill wall

stiffness, presence of haunch in the frame, and opening size and location.

Load was applied to the frame as a lateral displacement in a quasi-static manner, and the lateral load was computed as the integration of the reaction at the base of the frame. The results of the analysis matrix are presented and discussed in Chapter 6 for solid masonry infilled frames and Chapter 7 for infilled frames with openings.

CHAPTER 6

BEHAVIOUR OF SOLID MASONRY INFILL WALLS

6.1. Introduction

In this chapter, the results of the finite element analysis of the solid masonry infill wall models described in Chapter 5 are presented and discussed including: the cracking pattern and failure mechanism of the masonry infill wall, lateral load-lateral displacement response, initial stiffness, cracking load, and ultimate load and corresponding lateral displacement of the masonry infilled frames. Results for the infilled frame models having walls with openings are presented in Chapter 7.

6.2. Effect of Wall Aspect Ratio

The effect of the aspect ratio of the masonry infill wall on the lateral load-lateral displacement behaviour of the infilled frames has been investigated assuming four different aspect ratios (*h/l*) of 0.50, 0.59, 0.76 and 1.00 for a 2800 mm high infill wall. Figures 6-1 and 6-2 show the lateral load-lateral displacement responses for masonry infilled steel and RC frames, respectively. Table 6-1 summarizes the finite element (FE) results for the initial stiffness (K_{ini}), cracking load (P_{cr}), ultimate load (P_{ult}) and corresponding displacement (Δ_{ult}) for the different infilled frame models.

Table 6-1: Summary of the FE results for solid masonry infilled frames with different height-to-length (*h/l*)

Frame ID	*h/l*	K_{ini} (*kN/mm*)	P_{cr} (kN)	P_{ult} (kN)	Δ_{ult} (kN)	Failure mode*
F54S-HC-100	1.00	105.09	269.18	334.76	17.33	CC
F9S-HC-76	0.76	127.42	339.78	424.12	17.33	CC
F28S-HC-59	0.59	132.24	415.82	488.43	16.00	CC
F41S-HC-50	0.50	146.72	450.00	558.55	17.33	CC
F54C-HC-100	1.00	282.37	376.51	505.10	22.67	CC
F9C-HC-76	0.76	293.84	391.80	611.15	22.67	CC
F28C-HC-59	0.59	296.23	395.00	760.61	17.34	CC
F41C-HC-50	0.50	299.96	400.00	757.13	20.00	CC

*CC: Corner crushing.

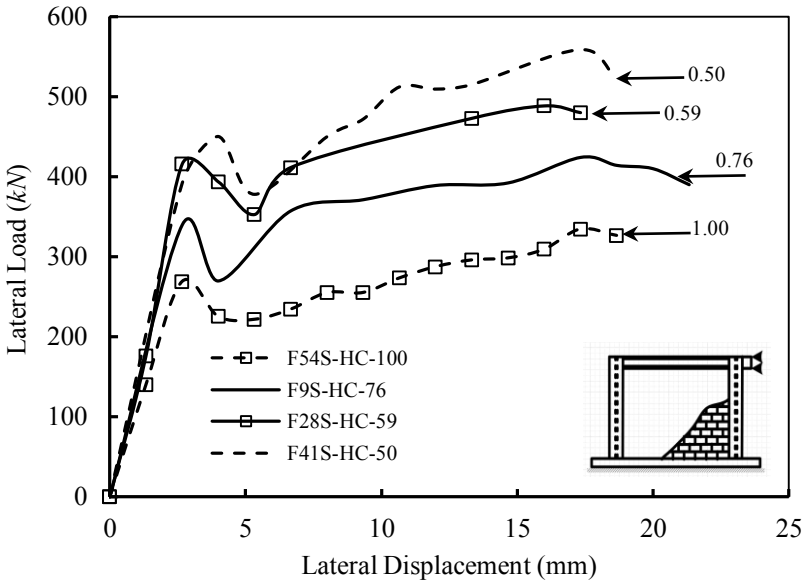

Figure 6-1: Lateral load vs lateral displacement response for solid masonry infilled steel frames with aspect ratios from 0.5 to 1.0

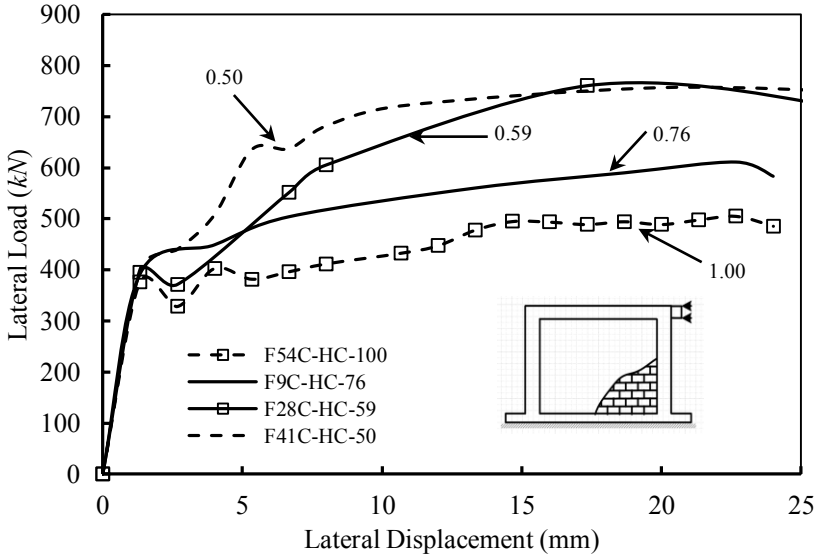

Figure 6-2: Lateral load vs lateral displacement response for solid masonry infilled RC frames with aspect ratios from 0.5 to 1.0

The results of the different aspect ratios were compared to the behaviour of masonry infill wall results of aspect ratio 1.0 as shown in Table 6-2. The initial stiffness of the bare steel frame was 3.2 *kN/mm*, while that for bare RC frame was 22.61 *kN/mm*. The steel frame did not experience the development of plastic hinge due to the constraint provided by the masonry infill wall; however, the RC frame

had experienced the formation of plastic hinge in the loaded top corner of the frame's column followed the formation of the cracks in the infill wall.

Table 6-2: Normalized initial stiffness, cracking load, ultimate load and corresponding displacement relative to results for $h/l = 1.0$

Frame ID	h/l	Frame Type	Ratio to results for $h/l = 1.0$			
			K_{ini}	P_{cr}	P_{ult}	Δ_{ult}
F54S-HC-100	1.00	Steel	1.00	1.00	1.00	1.00
F9S-HC-76	0.76		1.21	1.26	1.27	1.00
F28S-HC-59	0.59		1.26	1.54	1.46	0.92
F41S-HC-50	0.50		1.40	1.67	1.67	1.00
F54C-HC-100	1.00	RC	1.00	1.00	1.00	1.00
F9C-HC-76	0.76		1.04	1.04	1.21	1.00
F28C-HC-59	0.59		1.05	1.05	1.51	0.76
F41C-HC-50	0.50		1.06	1.06	1.50	0.88

The lateral load-lateral displacement response for masonry infilled steel frames was linear elastic until a stepwise diagonal tension cracks were developed in the infill wall. A diagonal compression strut was formed in the masonry infill wall, and failure took place due to crushing of the masonry at the corners of the diagonal strut. The failure mode was the same for all frames having different aspect ratios. Figures 6-3 shows the developed compression stresses acting on the wall at peak load for masonry infilled steel frames with anaspect ratio of 0.76.

Figure 6-4 shows the developed diagonal compression strut and the principal compression stresses at the ultimate loads for masonry infilled RC frames with walls having an aspect ratio of 0.76. The first cracks were observed as stepwise diagonal tension cracks in the wall followed by a formation of a plastic hinge at the top of the column at the loaded end. With continued loading of the infilled RC frame, a diagonal compression strut was formed in the masonry infill wall. The infill wall failed due to crushing of the masonry at the corners of the developed compression strut. Another plastic hinge was formed in the RC frame at the base of the unloaded column after corner crushing of the masonry infill wall leading to the formation of a failure mechanism.

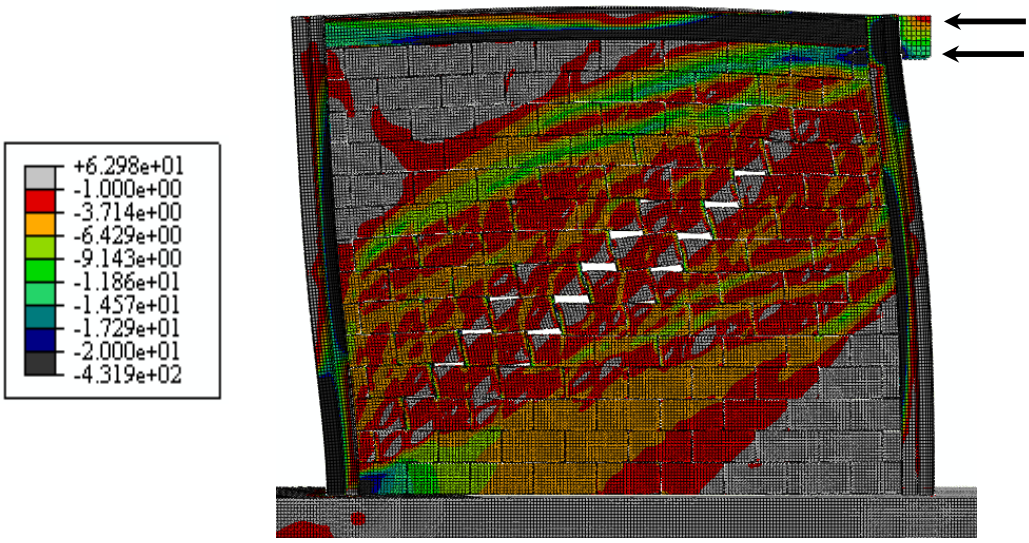

Figure 6-3: Principal compressive stresses at ultimate load in F9S-HC-76 (Steel frame, wall aspect ratio of 0.76) (MPa)

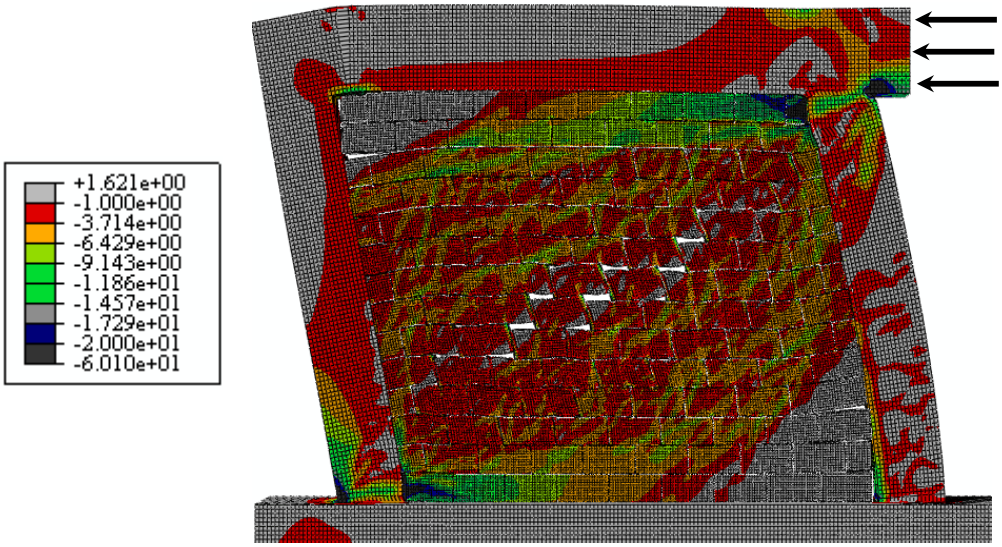

Figure 6-4: Principals compressive stresses at ultimate load in F9C-HC-76 (RC frame, wall aspect ratio of 0.76) (MPa)

Figures 6-5 and 6-6 show the effect of the aspect ratio of the infill wall on initial stiffness, and cracking and ultimate loads, respectively. The base of comparison is the behaviour of the frame filled with masonry infill wall having an aspect ratio of 1.0. Decreasing the aspect ratio from 1.0 to 0.5 led to 40% enhancement in the initial stiffness for the masonry infilled steel frame but only 6%

for the masonry infilled RC frame. The bare RC frame had a higher stiffness (22.61 *kN/mm*) compared to the bare steel frame (3.20 *kN/mm*). The relative stiffness between the masonry infill wall and the steel frame is much higher than for masonry infilled RC frames.

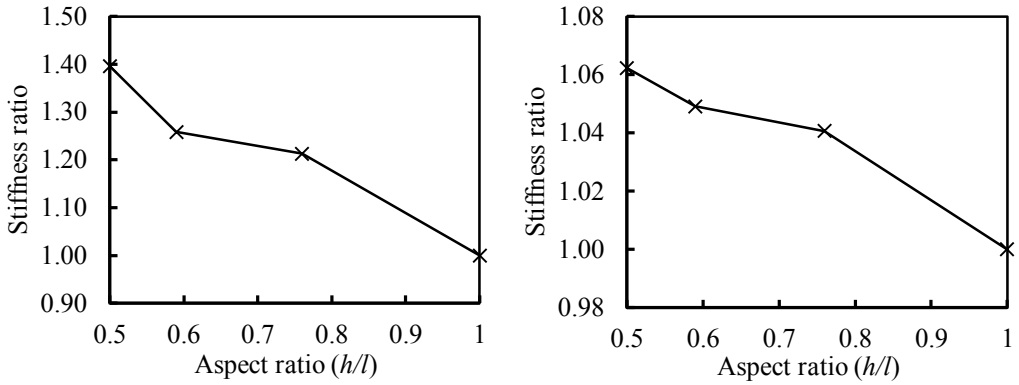

Figure 6-5: Effect of aspect ratio on the initial stiffness for (a) Steel frames and (b) RC frames

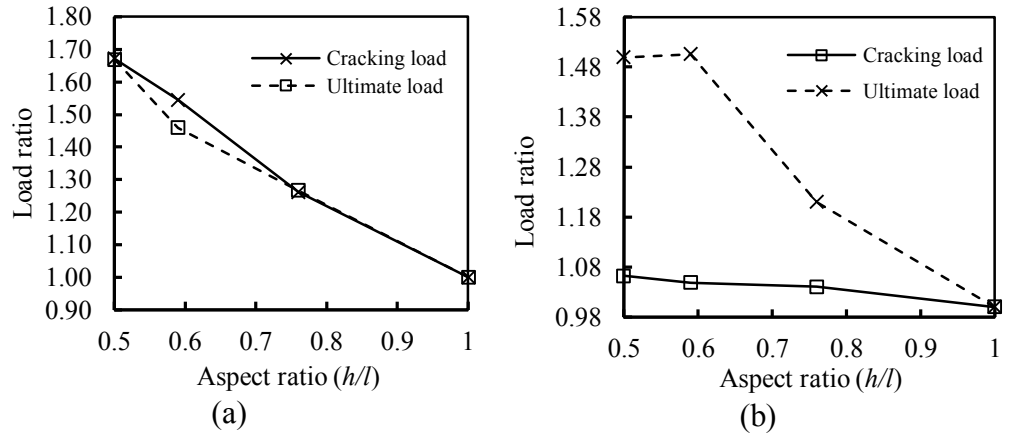

Figure 6-6: Effect of aspect ratio on the cracking and ultimate load for (a) Steel frames and (b) RC frames

Lower infill wall aspect ratios resulted in improvement in the cracking and ultimate loads of the system. The cracking and ultimate loads for the infilled steel frame with 0.50 aspect ratio were 70% higher than for the infilled steel frame with 1.0 aspect ratio. For infilled RC frames, the cracking load increased by 7% and the ultimate load increased by 50% for the aspect ratio of 0.50. Because of the high stiffness of the bare RC frame, the relative stiffness between the masonry infill

walls and the RC frame did not vary much with changing the aspect ratio of the wall; hence, the cracking load was almost the same for all aspect ratios. However, the ultimate load was improved for the lower aspect ratios due to the formation of a plastic hinge mechanism in the frame resulting in the loss of its contribution. In the post-cracking phase, the lateral load was resisted by the masonry infill wall alone. Decreasing the aspect ratio of the infill wall led to a stiffer system; however, the system experienced a reduction of 8% and 12% in the displacement corresponding to the ultimate load for masonry infilled steel and RC frames, respectively.

6.3. Effect of Gap Size and Location

Four masonry infilled steel and four masonry infilled RC frames having a full separation gap between the frame and the masonry infill wall were investigated. Another four infilled steel and four infilled RC frames were analyzed for a top gap between the frame's beam and the masonry infill wall. The width of the gaps considered were 5 mm, 7 mm, 10 mm and 15 mm. All masonry infill walls in this part of the investigation had an aspect ratio of 0.76 representing the most common size for infilled frames. The results were compared with the response of frames in full contact with the masonry infill wall. A summary of the FE results for the initial stiffness (K_{ini}), cracking load (P_{cr}), ultimate load (P_{ult}) and corresponding displacement (Δ_{ult}) for the different infilled frames is given in Table 6-3.

The parameters in Table 6-3 were compared against those for infilled frames in full contact with the infill wall and the ratios are given in Tables 6-4. The lateral load-lateral displacement behaviour of masonry infilled steel and RC frames with different gap sizes is shown in Figures 6-7 through 6-10. The initial stiffness of the system in the case of a gap is defined as the slope to the curve after the infill wall has shared the lateral load with the containing frame. The behaviour of masonry infilled steel and RC frames with a top gap was similar to those with no gaps. On the other hand, the presence of full separation gaps forced the frame to follow the behaviour of bare frame until the gap between the masonry infill wall and the containing frame was closed.

Table 6-3: Summary of the FE results for masonry infilled frames with different gap sizes and locations

Frame ID	Gap size and location	K_{ini} (*kN/mm*)	P_{cr} (kN)	P_{ult} (kN)	Δ_{ult} (mm)	Failure mode*
F9S-HC-76	No gap	127.42	339.78	424.12	17.33	CC
F1S-GA15-76	15 mm, full	27.52	120.17	179.87	22.67	N/A†
F2S-GA10-76	10 mm, full	45.33	154.92	250.00	19.00	CC
F3S-GA07-76	7 mm, full	65.98	155.24	352.53	20.00	DT+CC
F4S-GA05-76	5 mm, full	95.66	181.43	370.00	18.00	DT+CC
F5S-GT15-76	15 mm, top	65.19	255.39	322.19	14.00	DT+CC
F6S-GT10-76	10 mm, top	85.99	223.50	320.53	14.00	DT+CC
F7S-GT07-76	7 mm, top	88.18	310.06	386.57	20.31	CC
F8S-GT05-76	5 mm, top	98.05	315.00	388.40	15.67	CC
F9C-HC-76	No gap	293.84	450.00	611.15	22.67	CC
F1C-GA15-76	15 mm, full	28.51	222.43	222.43	19.25	FF†
F2C-GA10-76	10 mm, full	28.69	299.89	299.89	18.67	DT+CC
F3C-GA07-76	7 mm, full	82.31	328.08	421.16	25.33	DT+CC
F4C-GA05-76	5 mm, full	131.96	382.74	430.22	24.00	DT+CC
F5C-GT15-76	15 mm, top	277.49	498.77	498.77	2.67	DT+CC
F6C-GT10-76	10 mm, top	284.92	482.79	487.65	13.34	DT+CC
F7C-GT07-76	7 mm, top	288.74	437.11	538.86	14.67	CC
F8C-GT05-76	5 mm, top	292.66	440.00	540.85	14.67	CC

*CC: Corner crushing, DT: Diagonal tension cracking and SS: Sliding shear

†N/A: no failure in the masonry infill wall or the containing frame, FF: Plastic hinge in the column.

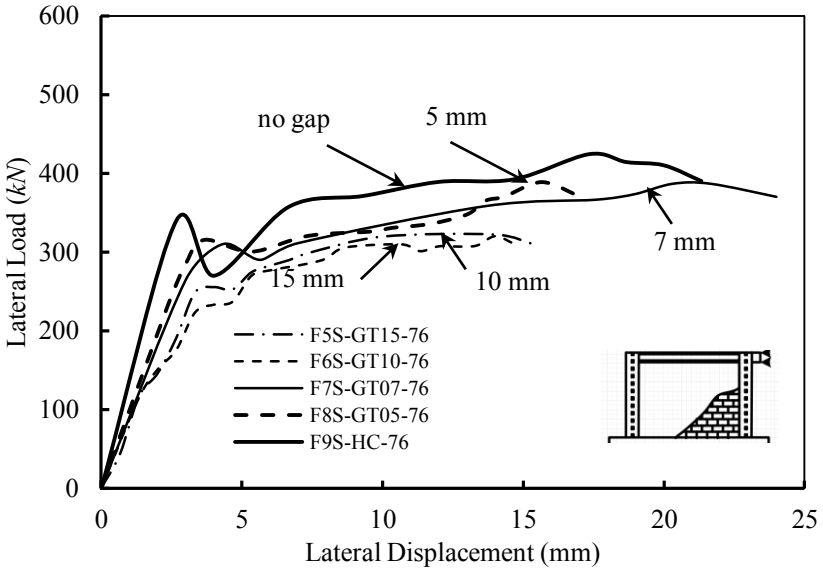

Figure 6-7: Lateral load-lateral displacement response of masonry infilled steel frames with a top gap between the wall and the frame's beam

Table 6-4: Initial stiffness, cracking load, and ultimate load and corresponding displacement for different gap sizes and locations expressed relative to the results for no gap

Frame ID	Ratio to results for frames with no gap			
	K_{ini}	P_{cr}	P_{ult}	Δ_{ult}
F9S-HC-76	1.00	1.00	1.00	1.00
F1S-GA15-76	0.22	0.35	0.42	1.31
F2S-GA10-76	0.36	0.46	0.59	1.10
F3S-GA07-76	0.52	0.46	0.83	1.15
F4S-GA05-76	0.75	0.53	0.87	1.04
F5S-GT15-76	0.51	0.75	0.76	0.81
F6S-GT10-76	0.67	0.66	0.76	0.81
F7S-GT07-76	0.69	0.91	0.91	1.17
F8S-GT05-76	0.77	0.93	0.92	0.90
F9C-HC-76	1.00	1.00	1.00	1.00
F1C-GA15-76	0.10	0.49	0.36	0.85
F2C-GA10-76	0.10	0.67	0.49	0.82
F3C-GA07-76	0.28	0.73	0.69	1.12
F4C-GA05-76	0.45	0.85	0.70	1.06
F5C-GT15-76	0.94	1.11	0.82	0.12
F6C-GT10-76	0.97	1.07	0.80	0.59
F7C-GT07-76	0.98	0.97	0.88	0.65
F8C-GT05-76	1.00	0.98	0.88	0.65

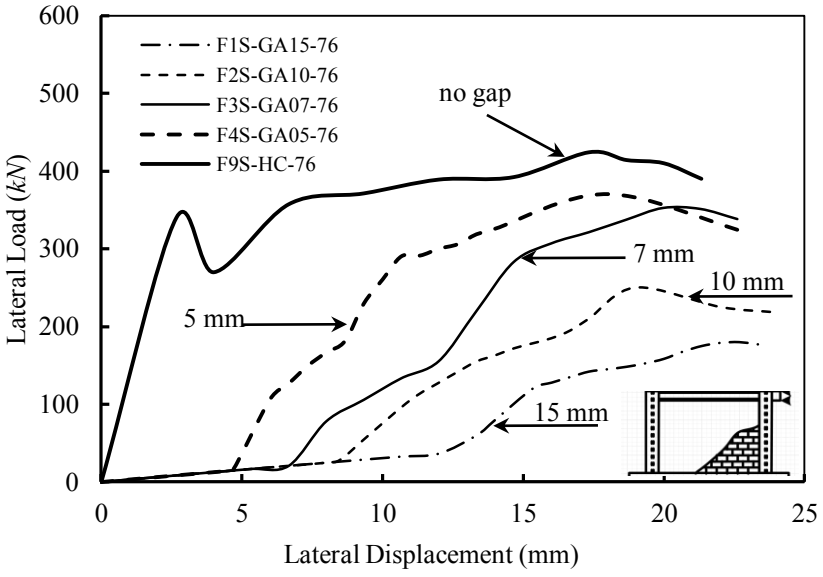

Figure 6-8: Lateral load-lateral displacement response of masonry infilled steel frames with full separation gaps

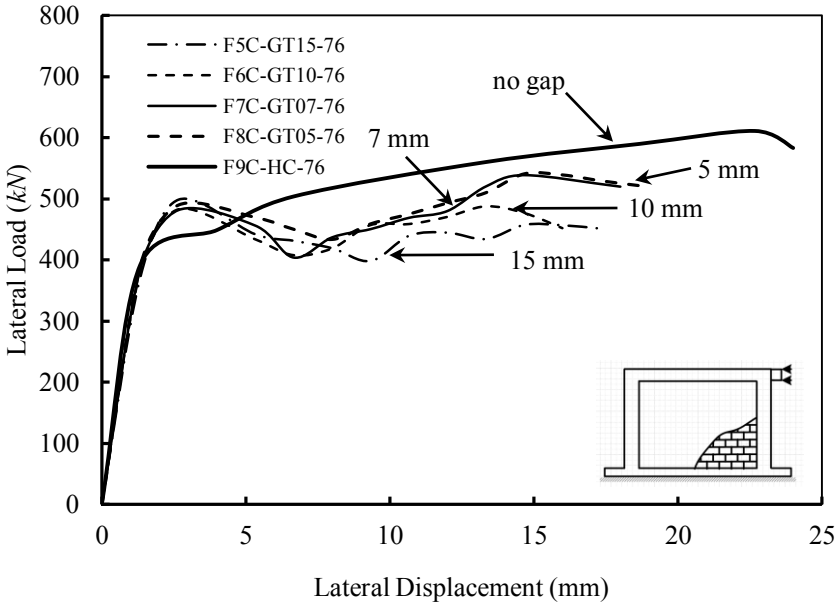

Figure 6-9: Lateral load-lateral displacement response of masonry infilled RC frames with a top gap

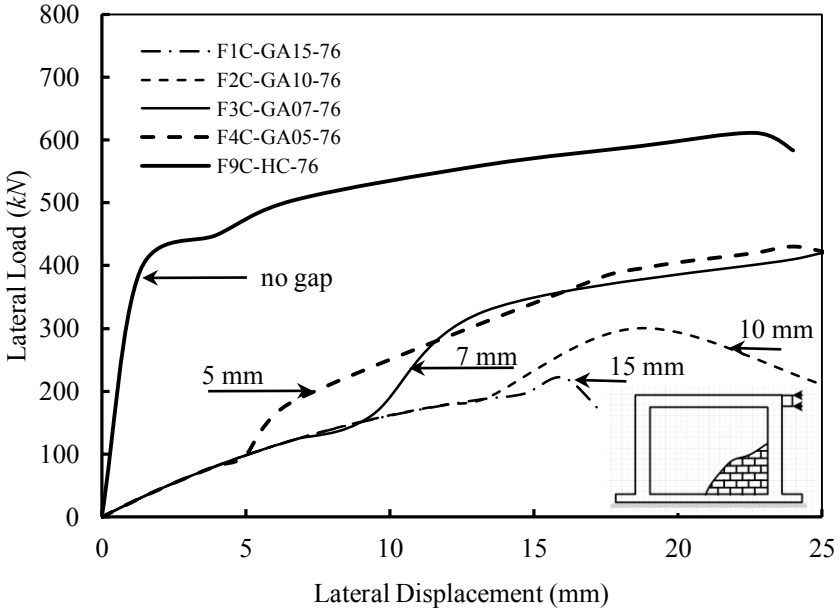

Figure 6-10: Lateral load-lateral displacement response of masonry infilled RC frames with a full separation gap

Similar to the response of masonry infilled steel frame in full contact with the masonry infill wall, the presence of a top or full separation gap between the frame and the masonry infill wall did not result in the development of plastic hinges in the steel frame regardless of the gap size.

When a top gap was introduced between the RC frame's beam and the masonry infill wall, the masonry infilled RC frame behaved in a similar manner to a masonry infilled RC frame with no gap. The RC frame experienced the formation of a plastic hinge in the loaded corner. Failure of the system was dominated by failure in the masonry infill wall. The response of the RC infilled frame was the same when a full separation gap was introduced; however, failure took place in the frame only when the full separation gap had a width of 15 mm. The principal compressive stresses developed at failure for masonry infilled steel and RC frames with full separation gaps of 7 mm and 15 mm are presented in Figures 6-11 through 6-14. For infilled frames having a full separation gap of 7 mm, a diagonal compression strut was formed in the infill wall. The infill wall failed due to the formation of a diagonal tension crack in the infill wall followed by crushing of the masonry at the corners of the compression strut. As shown in Figure 6-14, a full separation gap of 15 mm in masonry infilled RC frame prevented the development of an effective compressive strut. The wall did not share carrying the load, and failure was dominated by the development of plastic hinges at the loaded corner and the base of the column on the unloaded side.

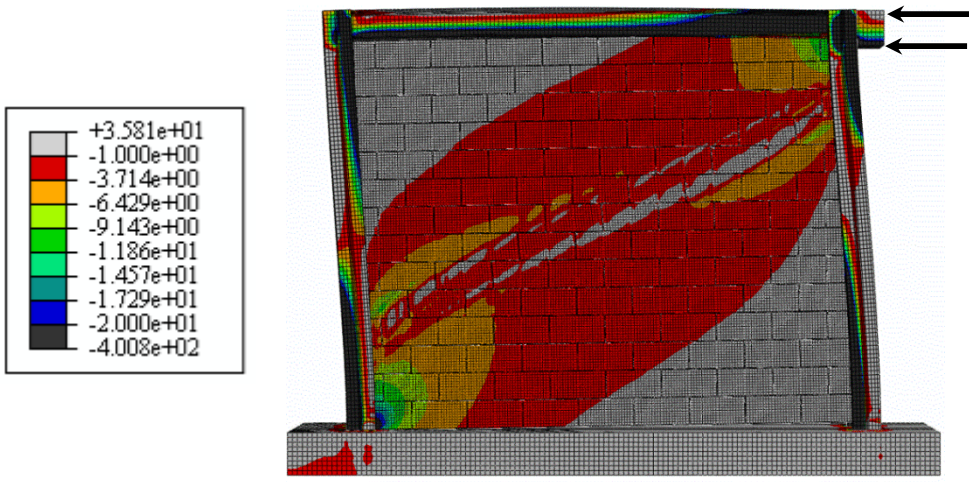

Figure 6-11: Principal compressive stresses at failure load in F3S-GA07-76 (steel frame with a 7 mm full separation gap) (MPa)

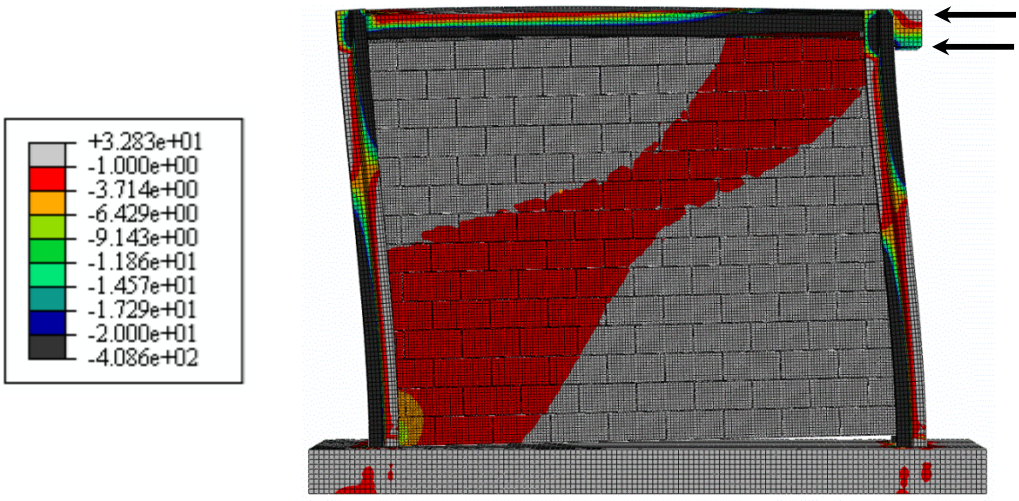

Figure 6-12: Principal compressive stresses at failure in F1S-GA15-76 (steel frame with a 15 mm full separation gap) (MPa)

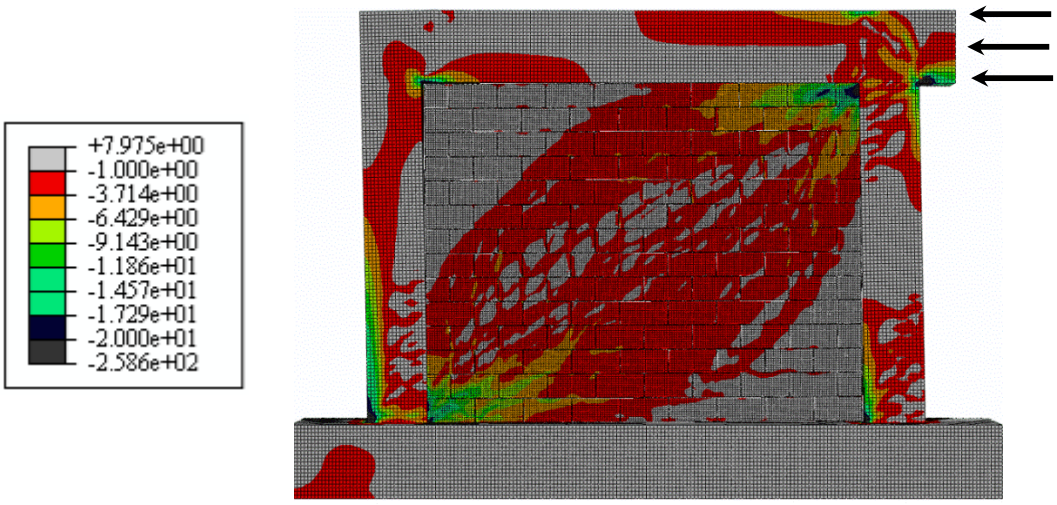

Figure 6-13: Principal compressive stresses at failure in F3C-GA07-76 (RC frame with a 7 mm full separation gap) (MPa)

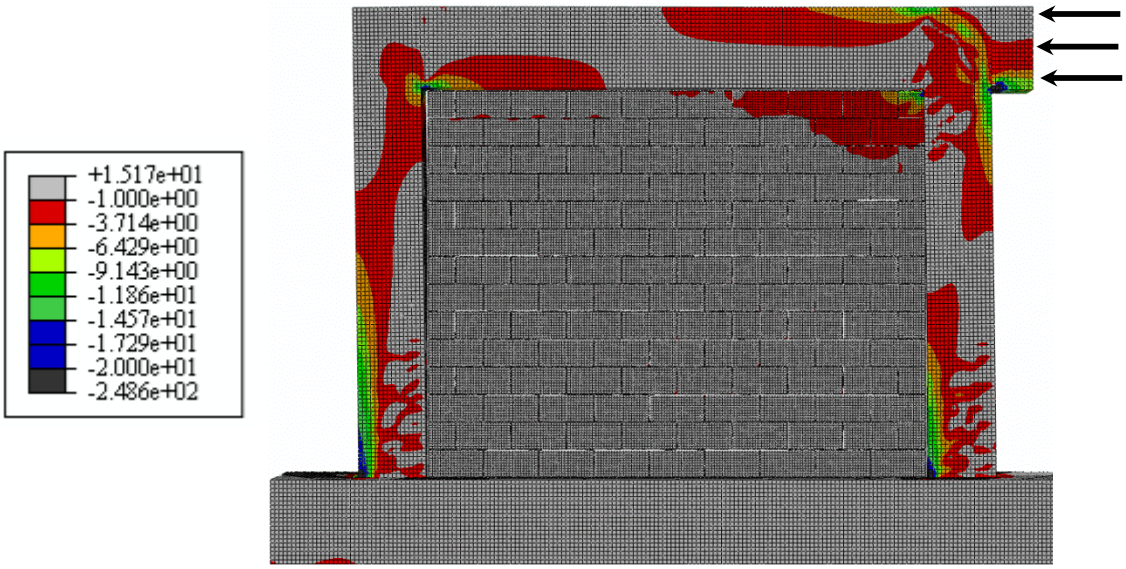

Figure 6-14: Principal compressive stresses at failure in F1C-GA15-76 (RC frame with a 15 mm full separation gap) (MPa)

Figures 6-15 through 6-18 show the principal compressive stresses at failure for masonry infilled steel and RC frames with 15 mm and 7 mm top gaps. For steel frames, the infill wall failed due to crushing of the masonry at the corners of the developed diagonal compression strut. Due to the flexibility of the steel beam-column connection, the frame deflected and the gap between the frame and the masonry infill wall was closed adding a confinement pressure to the masonry infill wall, which prevented the development of a diagonal tension crack in the wall as shown in Figures 6-15 and 6-16.

For masonry infilled RC frames, the rigid beam-column connection prevented the frame's beam from deforming, especially for the case of a 15 mm gap size. The masonry infill wall was not confined in this case leading to the formation of a diagonal tension crack in the infill wall as shown in Figures 6-17 and 6-18. Some residual capacity remained in the wall due to friction; however, the capacity of the wall was reduced after the formation of the diagonal tension crack. In the case of smaller gaps (5 mm and 7 mm), the infill wall failed in crushing of the masonry at the corners of the developed diagonal compression strut. The RC

frame's beam experienced sufficient deformation to close the smaller gaps which added confinement to the developed strut.

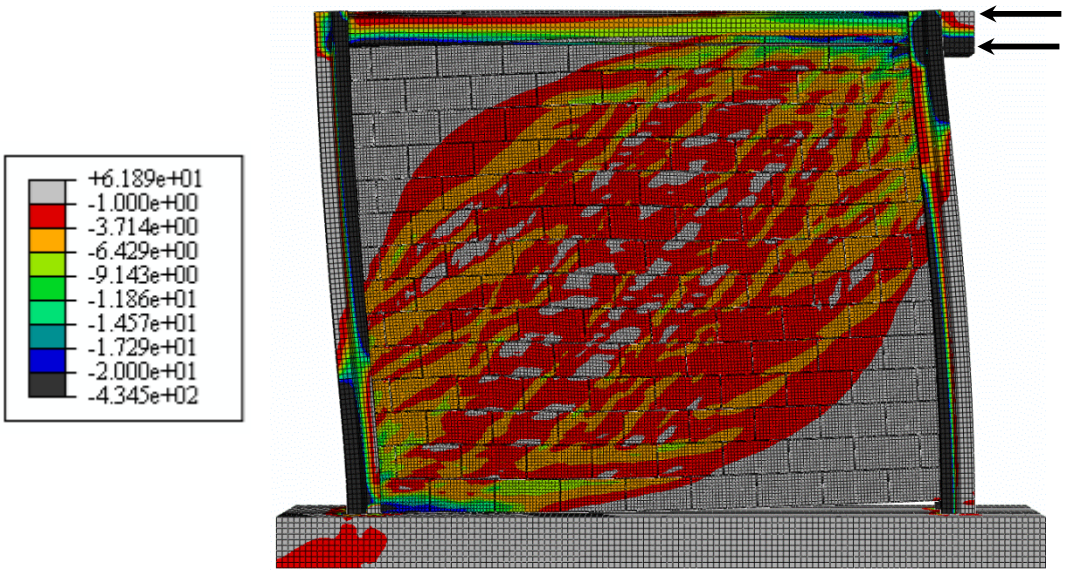

Figure 6-15: Principal compressive stresses at failure in F7S-GT07-76 (steel frame with a 7 mm top gap) (MPa)

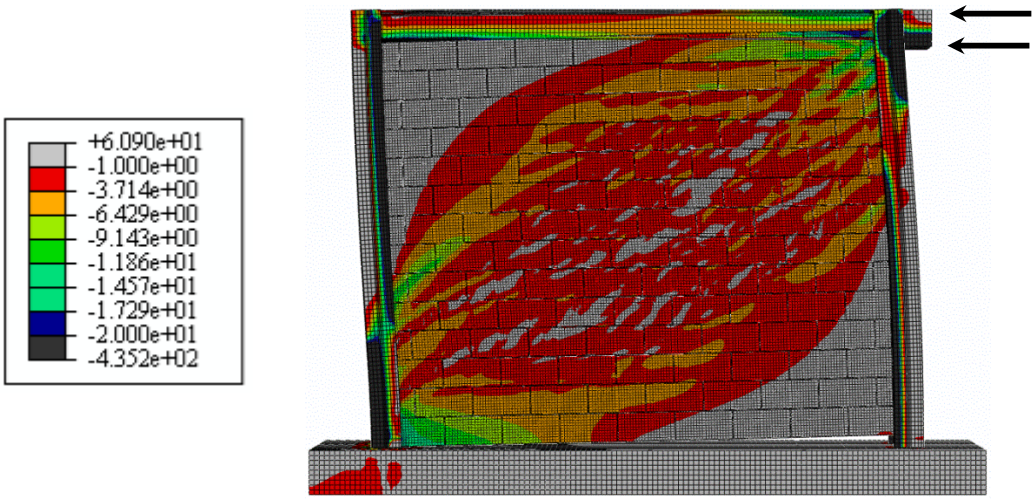

Figure 6-16: Principal compressive stresses at failure in F5S-GT15-76 (steel frame with a 15 mm top gap) (MPa)

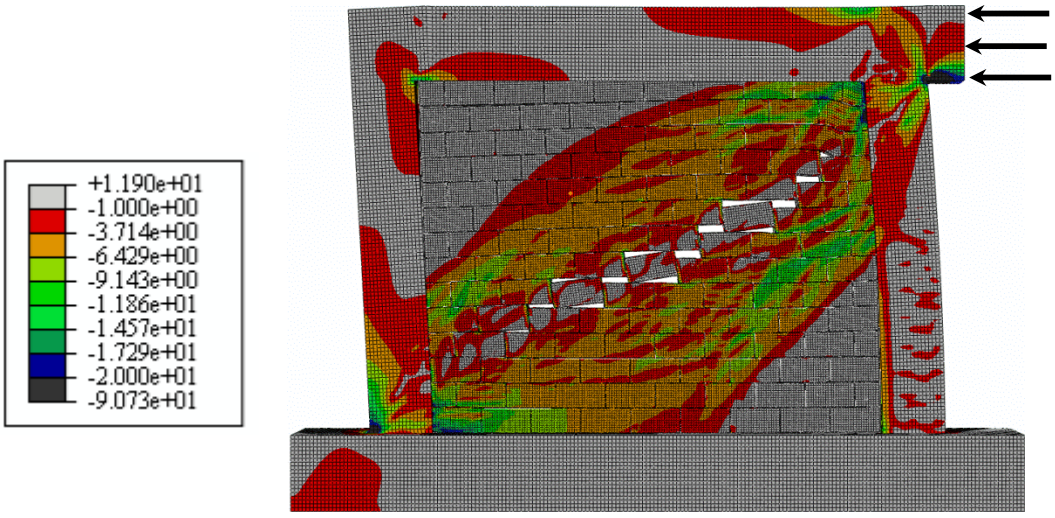

Figure 6-17: Principal compressive stresses at failure load in F7C-GT07-76 (RC frame with a 7 mm top gap) (MPa)

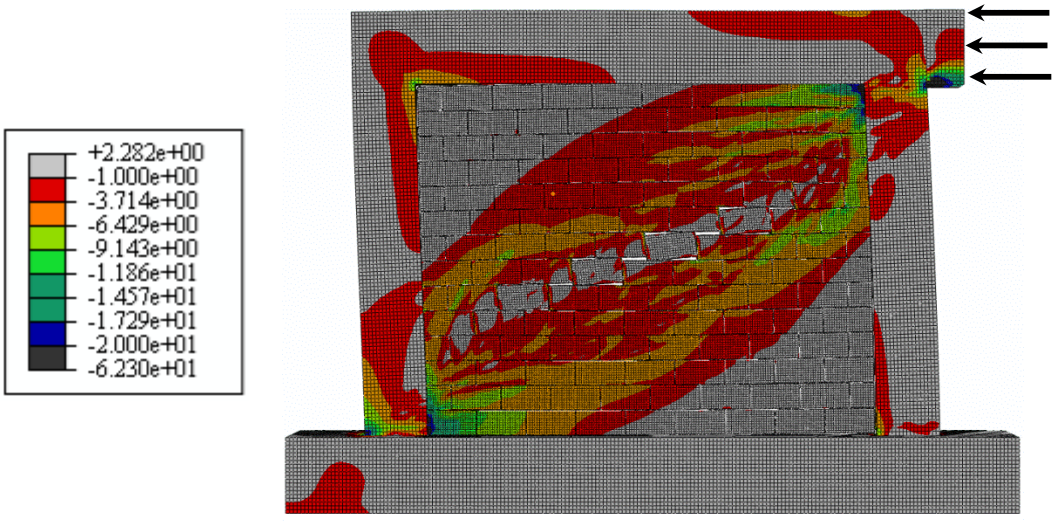

Figure 6-18: Principal compressive stresses at failure load in F5C-GT15-76 (RC frame with a 15 mm top gap) (MPa)

To assess the effect of the gap size and location on the lateral load resistance of the frame system, the computed results for infilled frames with gaps were compared to the case of infill walls in full contact with the surrounding frames (i.e. no gaps) Figures 6-19 and 6-20 show the effect of the presence of a gap and its

location on the initial stiffness and ultimate lateral load, respectively, for masonry infilled steel and RC frames.

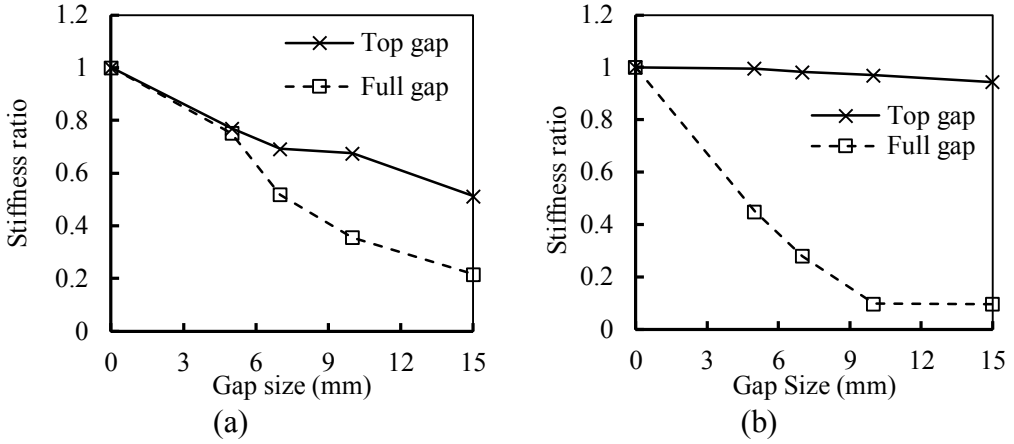

Figure 6-19: Effect of gap size and location on the initial stiffness of: (a) Steel frames, and (b) RC frames

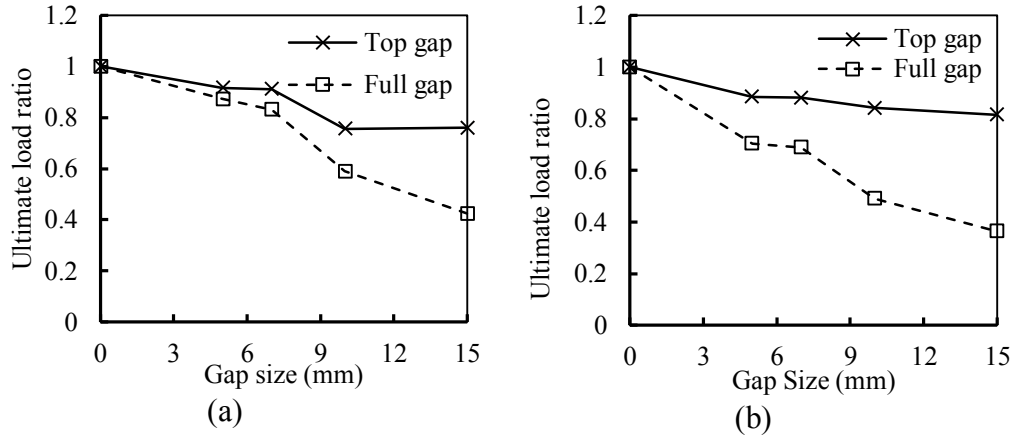

Figure 6-20: Effect of gap size and location on the ultimate load of: (a) Steel frames, and (b) RC frames

The presence of a full separation gap led to a significant drop in the initial stiffness. The reduction in the initial stiffness was 65% for masonry infilled steel frames with a gap size of 10 mm, while the reduction was 90% for masonry infilled RC frames with a gap size of 10 mm. The masonry infill wall had a much higher initial stiffness (2902 *kN/mm*) compared to 22.61 *kN/mm* and 3.20 *kN/mm* for the RC and steel frames, respectively. However, the system did not benefit from this high stiffness due to the presence of a full separation gap. Once the separation gap

was closed, the infill wall shared resisting the load with the frame. The maximum reduction in the ultimate lateral load was found to be 60% for masonry infilled steel frames having a full separation gap of 15mm. The reduction in the cracking load and ultimate lateral load were reduced by 50% and 65%, respectively, for infilled RC frame.

When a top gap was introduced between the masonry infill wall and the containing frame, infilled steel frames experiences a reduction in initial stiffness of 50% for a gap size of 15 mm. Only 7% reduction was recorded for RC frames having the same gap size. The RC frame's beam was more rigid and deformed much less than the steel frame's beam. As a result, the infill wall contact area was always much larger with the column than the beam. Therefore, reduction in the contact between the RC beam and the infill wall did not have any significant effect on stiffness. The cracking load was reduced by 25% for infilled steel frames with a top gap of 15mm compared to the case of no gap. However, the formation of the first crack took place at higher loading level (7% higher load) for masonry infilled RC frame. The rigidity of the beam-column connection prevented sudden transmission of the load from the RC frame to the infill wall. With higher loading levels, the connection start experiencing cracks shedding its load on the wall which led to its cracking

The ultimate lateral load was reduced by 25% for both steel and RC infilled frames for 10 mm top gap. The presence of a top gap between the masonry infill wall and the containing frame led to reduction in the confinement on the masonry infill wall. The beam was not able to deform to close the gap regardless of the stiffness of the beam-column connection which made the reduction almost the same for infilled steel and RC frames. When the top gap size was 15 mm, the ultimate displacement was reduced by 90% compared to the case of no gap for masonry infilled RC frames. For large top gap sizes (10 mm and 15 mm), the failure mode of the masonry infill wall took the form of diagonal tension cracks followed by corner crushing of the masonry at the corner of the diagonal compression strut.

6.4. Effect of Haunches

Three steel frames and three RC frame models with different haunch sizes were built and used to study the effect of haunches. All infilled steel and RC frames investigated had the same aspect ratio of 0.76 representing common dimensions. The finite element models had haunches constructed at 45° angle, and a side length of 200 mm, 400 mm and 600 mm (actual haunch length = side×$\sqrt{2}$). All haunches had the same thickness as the containing frame. As shown in Figures 6-21 and 6-22, the presence of a haunch reduced the drop in the lateral load after the formation of cracks in the infill walls (transition zone between the linear and nonlinear parts of the lateral response). A summary of the FE results for the initial stiffness (K_{ini}), cracking load (P_{cr}), ultimate load (P_{ult}) and corresponding displacement Δ_{ult} for the different infilled frames is given in Table 6-5. The results were compared to masonry infilled frames with no haunch and the ratios are given in Table 6-6.

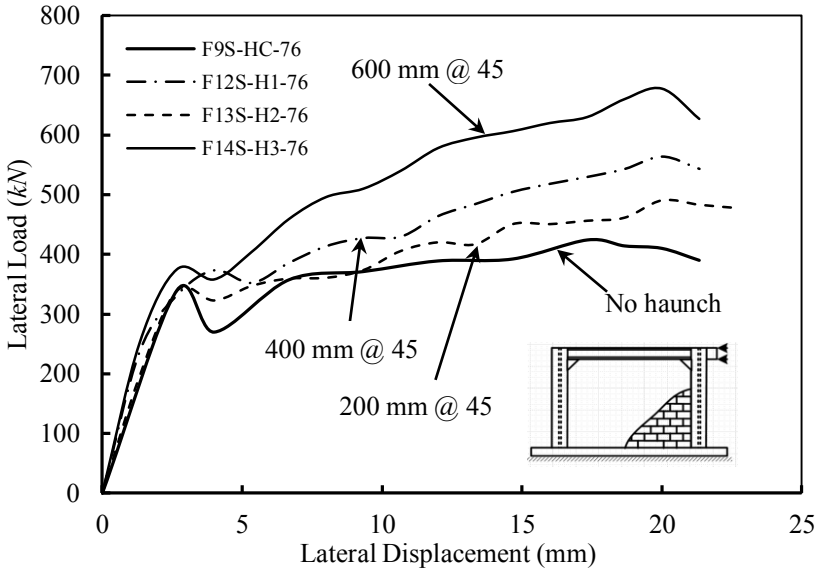

Figure 6-21: Lateral load vs lateral displacement for haunched masonry infilled steel frames

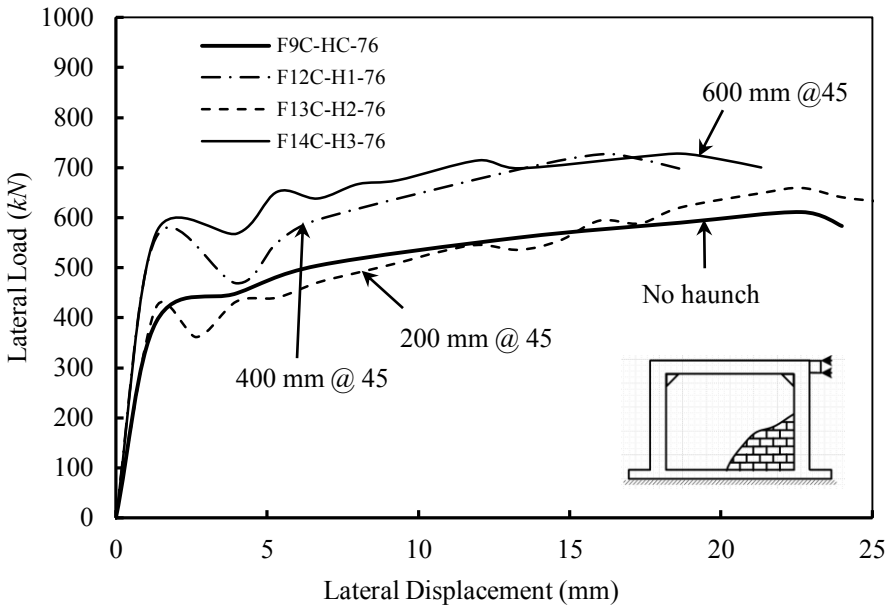

Figure 6-22: Lateral load vs lateral displacement for haunched masonry infilled RC frames

Table 6-5: Summary of the FE results for haunched masonry infilled steel and RC frames

Frame ID	Haunch size & angle (*mm*)	K_{ini} (*kN/mm*)	P_{cr} (*kN*)	P_{ult} (*kN*)	Δ_{ult} (*mm*)	Failure mode*
F9S-HC-76	N/A	127.42	339.78	424.12	17.33	CC
F12S-H1-76	$400\sqrt{2}$@45	178.07	373.50	564.04	20.00	CC
F13S-H2-76	$200\sqrt{2}$@45	147.22	339.37	490.81	20.00	CC
F14S-H3-76	$600\sqrt{2}$@45	188.87	374.93	677.53	20.00	CC
F9C-HC-76	N/A	293.84	450.00	611.15	22.67	CC
F12C-H1-76	$400\sqrt{2}$@45	419.99	560.00	726.51	16.00	CC
F13C-H2-76	$200\sqrt{2}$@45	314.99	420.00	658.90	22.67	CC
F14C-H3-76	$600\sqrt{2}$@45	427.50	570.00	727.98	18.67	CC

*CC: Corner crushing

Table 6-6: Initial stiffness, cracking load, and ultimate load and corresponding displacement for different haunch sizes and angles expressed relative to results of no haunch

Frame ID	Haunch size & angle (*mm*)	Ratio to results of frames with no haunch			
		K_{ini}	P_{cr}	P_{ult}	Δ_{ult}
F9S-HC-76	N/A	1.00	1.00	1.00	1.00
F12S-H1-76	$400\sqrt{2}$@45	1.40	1.10	1.33	1.15
F13S-H2-76	$200\sqrt{2}$@45	1.16	1.00	1.16	1.15
F14S-H3-76	$600\sqrt{2}$@45	1.48	1.10	1.60	1.15
F9C-HC-76	N/A	1.00	1.00	1.00	1.00
F12C-H1-76	$400\sqrt{2}$@45	1.43	1.24	1.19	0.71
F13C-H2-76	$200\sqrt{2}$@45	1.07	0.93	1.08	1.00
F14C-H3-76	$600\sqrt{2}$@45	1.45	1.27	1.19	0.82

The presence of a haunch within the masonry infilled steel and RC frames led to increasing the confinement exerted on the masonry infill wall and delayed crack formation and development. A diagonal compression strut was developed in the infill wall as shown in Figures 6-23 and 6-24. Failure of the masonry infilled frames was governed by crushing of the masonry at the corners of the developed strut and no plastic hinges were formed in the frames. The masonry infilled RC frame behaved similar to the infilled steel frame where no plastic hinge was formed in the frame, and the masonry infill wall failed due to crushing on the masonry at the corner of the developed compression strut. Figures 6-23 and 6-24 show the diagonal compression struts developed within the infill walls of haunched steel and RC frames. The mode of failure of the masonry infill wall was similar to the failure of frames receiving no corner treatment.

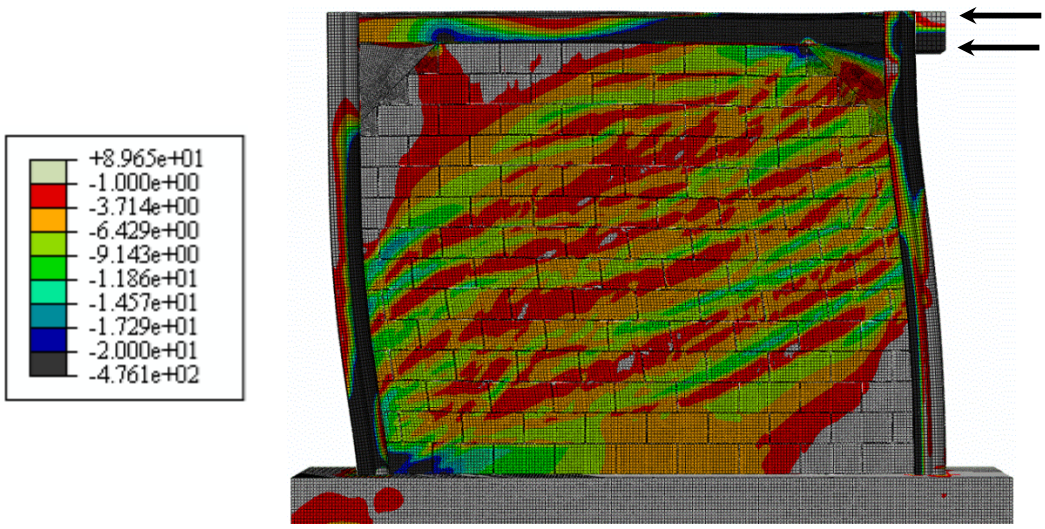

Figure 6-23: Principal compressive stresses at failure load in F14S-H3-76 (haunched steel frame, haunch side length = 600 mm) (MPa)

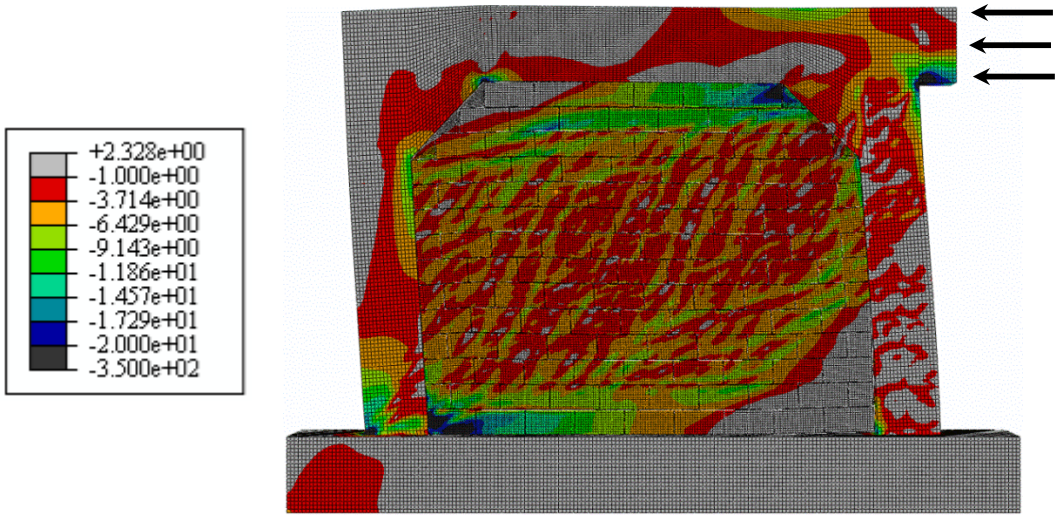

Figure 6-24: Principal compressive stresses at failure load in F14C-H3-76 (haunched RC frame, haunch side length = 600 mm) (MPa)

Improvements in initial stiffness and ultimate lateral load for masonry infilled steel and RC frames with haunches are shown in Figures 6-25 and 6-26, respectively. The basis of comparison is the behaviour of frames with no haunch (F9S-HC-76 and F9C-HC-76). The results show that larger haunch size (side length = 600 mm) increased the initial stiffness by 50% for both steel and RC frames. The problem of stress concentration at the corner of masonry infill wall-frame contact

zone was relieved by the presence of the haunch. The presence of large haunch sizes redistributed the stresses along the contact length preventing stress concentration and, hence, premature failure compared to smaller ones. The maximum increase in the ultimate lateral load was found to be 60% and 20% for infilled steel and RC frames for $600\sqrt{2}$mm, respectively. The presence of haunch in the steel frame increased its stiffness by 60% leading to a corresponding increase in the ultimate load resistance of the infilled steel. The RC frame did not experience a similar increase as cracking in the members took place at high loading level leading to reduction in its stiffness.

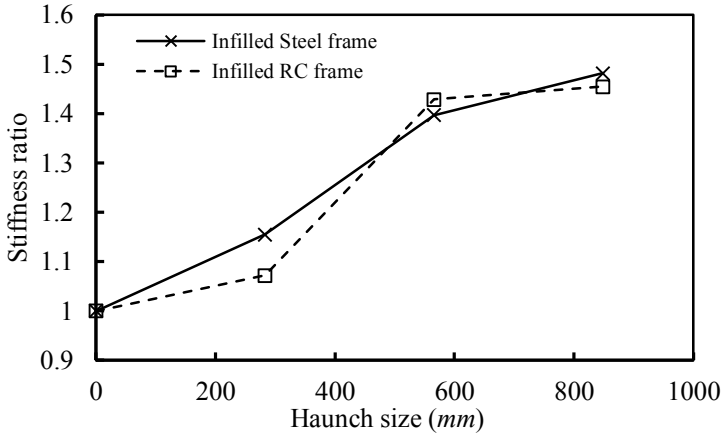

Figure 6-25: Effect of haunch size on the initial stiffness of masonry infilled frames

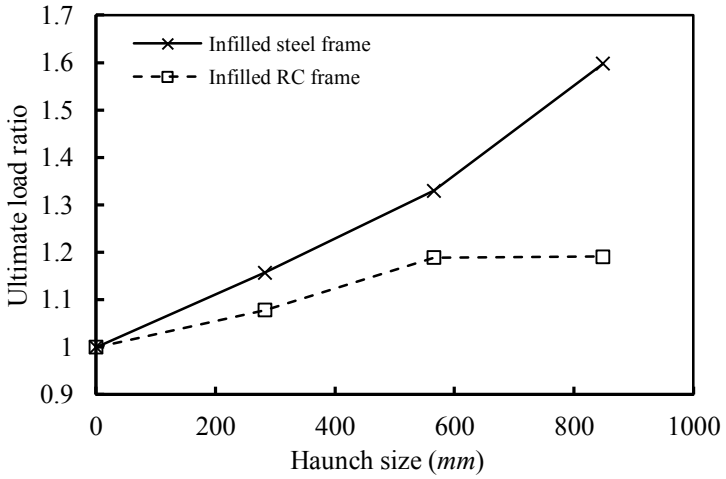

Figure 6-26: Effect of haunch size on the ultimate lateral load of masonry infilled frames

The cracking load in masonry infill walls was delayed due to the presence of the haunch in the steel and RC frame. The haunch added confinement stress to the masonry infill wall leading to the formation of the cracks at higher loading level. The cracking load was increased by 10% for masonry infilled steel frame compared to 27% for masonry infilled RC frame with haunch size of $600\sqrt{2}$ mm. The ultimate displacement of the steel infilled frames was also increased by 15% for $600\sqrt{2}$ mm haunch, while it was reduced by 20% for infilled RC frames. The reduction in the ultimate displacement for masonry infilled RC frames might be attributed to the formation of cracks in the frame specially at the stiff beam-column connection which led to a quick transfer of the load from the frame to the infill wall leading to its failure at lower displacement levels.

6.5. Effect of Infill Wall Stiffness

Three steel and three RC frame models filled with concrete masonry walls having different grouting conditions were used to study the effect of the infill stiffness on the lateral load-lateral displacement response. All masonry infill walls were 2800 mm in height and had an aspect ratio (*h/l*) of 0.76. The masonry infill wall was constructed in full contact with the frame. Three grouting cases were investigated: 0% grout (hollow wall), 27% grout (a partially grouted wall where cores were grouted every 800 mm), and 100 grout (fully grouted wall). Figures 6-27 and 6-28 show the lateral load-lateral displacement response of infilled steel and RC frames having different grouting conditions. A summary of the FE results for initial stiffness (K_{ini}), cracking load (P_{cr}), ultimate load (P_{ult}) and corresponding displacement (Δ_{ult}) for the different infilled frames is given in Table 6-7. These values were compared to the corresponding values for masonry infilled frames with no grout in the cores. The results of the comparisons are listed in Table 6-8.

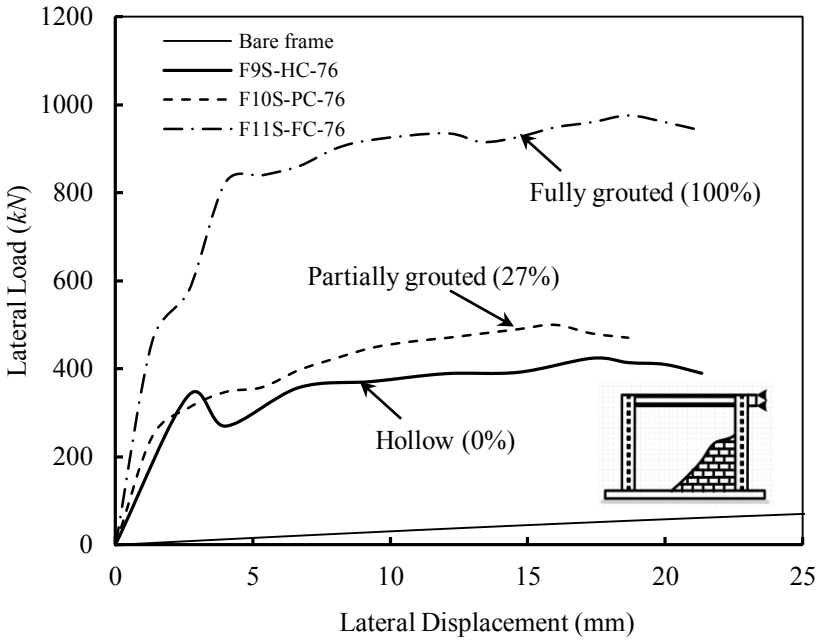

Figure 6-27: Lateral load-lateral displacement response for steel frames filled with masonry walls having different grouting ratios

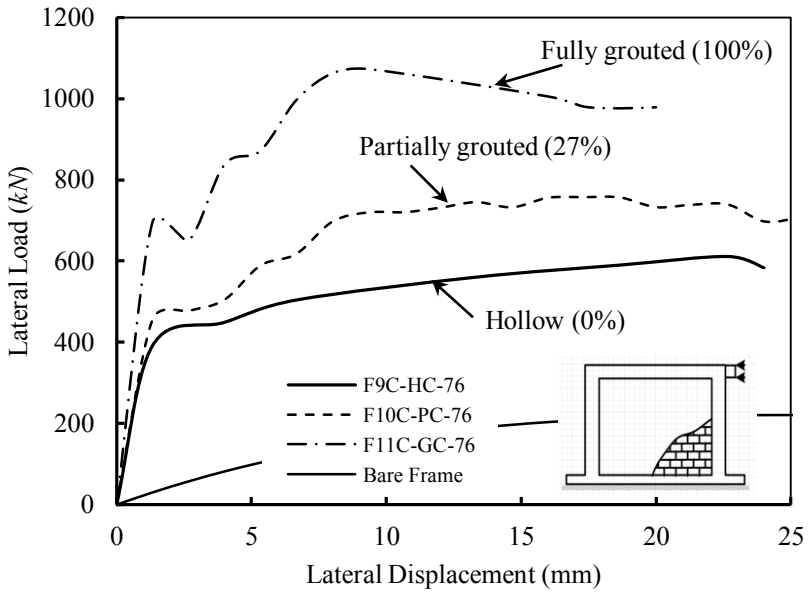

Figure 6-28: Lateral load-lateral displacement response for RC frames filled with masonry walls having different grouting ratios

Table 6-7: Summary of the FE results for masonry infilled steel and RC frames with different grouting ratios

Frame ID	Grout ratio (%)	K_{ini} (*kN/mm*)	P_{cr} (*kN*)	P_{ult} (*kN*)	Δ_{ult} (*mm*)	Failure mode*
F9S-HC-76	0	127.42	339.78	424.12	17.33	CC
F10S-PC-76	27	184.50	347.45	500.04	16.00	SC
F11S-FC-76	100	346.65	577.50	975.30	18.67	DT+CC
F9C-HC-76	0	293.84	450.00	611.15	22.67	CC
F10C-PC-76	27	341.65	455.58	757.22	17.33	SC
F11C-FC-76	100	521.92	695.00	1073.01	9.33	DT+CC

*CC: Corner crushing, DT: Diagonal tension cracking and SC: Shear cracks

Table 6-8: Normalized initial stiffness, cracking load, and ultimate load and corresponding displacement expressed relative to results of no grout

Frame ID	Grout ratio (%)	Ratio to results for frame with no grout			
		K_{ini}	P_{cr}	P_{ult}	Δ_{ult}
F9S-HC-76	0	1.00	1.00	1.00	1.00
F10S-PC-76	27	1.45	1.02	1.18	0.92
F11S-FC-76	100	2.72	1.70	2.30	1.08
F9C-HC-76	0	1.00	1.00	1.00	1.00
F10C-PC-76	27	1.16	1.01	1.24	0.76
F11C-FC-76	100	1.78	1.54	1.76	0.41

The principal compressive stress contours developed in the partially grouted infill walls of the steel and RC frames are shown in Figures 6-29 and 6-30. It can be seen that the grout columns acted as stiffeners leading to redistribution of stresses over the entire length of the wall. The infill wall experienced shear cracking over its entire area and failed due to crushing of the masonry at the corners of the wall for both partially grouted masonry infilled steel and RC frames.

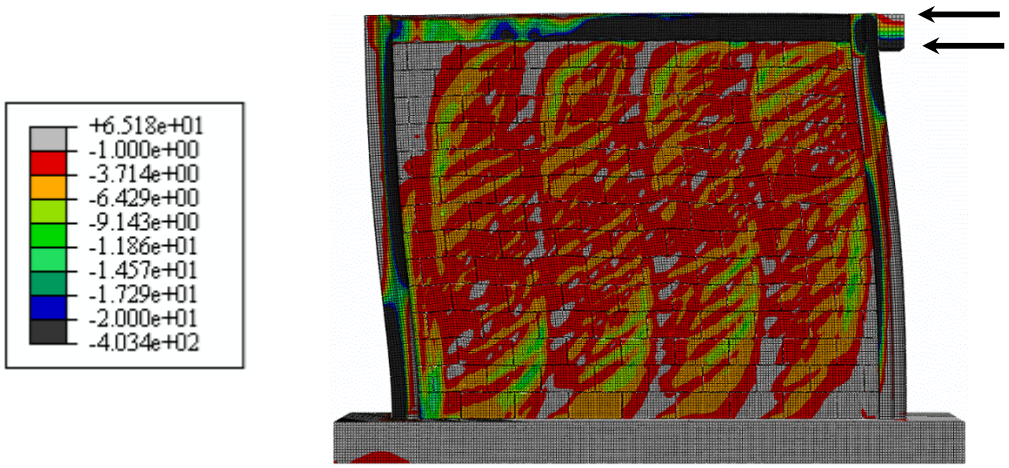

Figure 6-29: Principal compressive stresses at failure load in F6S-PC-76 (partially grouted infilled steel frame) (MPa)

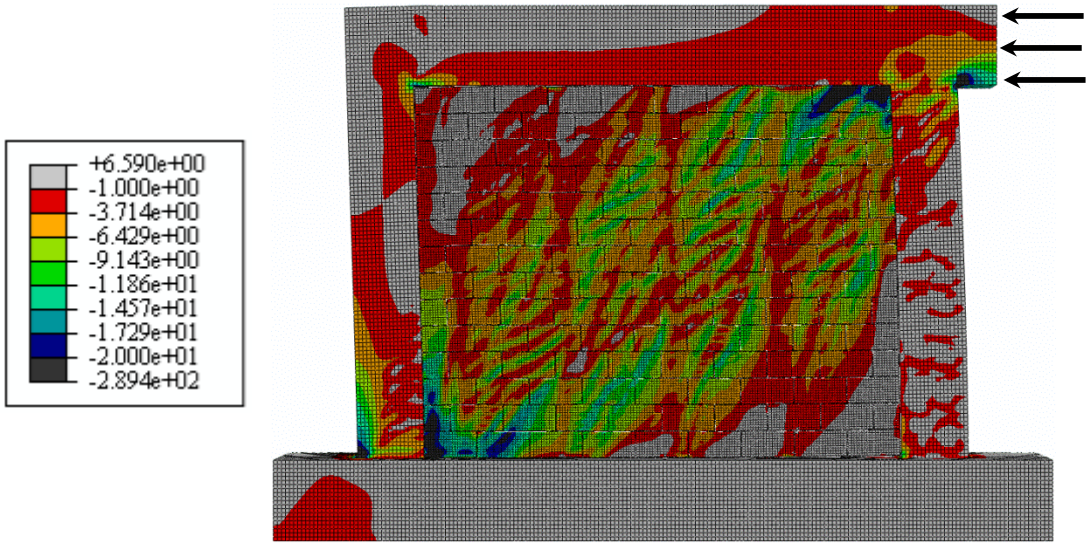

Figure 6-30: Principal compressive stresses at failure load in F6C-PC-76 (partially grouted infilled RC frame) (MPa)

As shown in Figures 6-31 and 6-32, the behaviour of fully grouted masonry infill walls within steel and RC frames resembles the behaviour of hollow infill walls. A diagonal compression strut was formed in the masonry infill followed by a diagonal tension crack as the load increased. The wall was still capable of resisting more load until it failed due to crushing of the masonry at the corners of the diagonal compression strut.

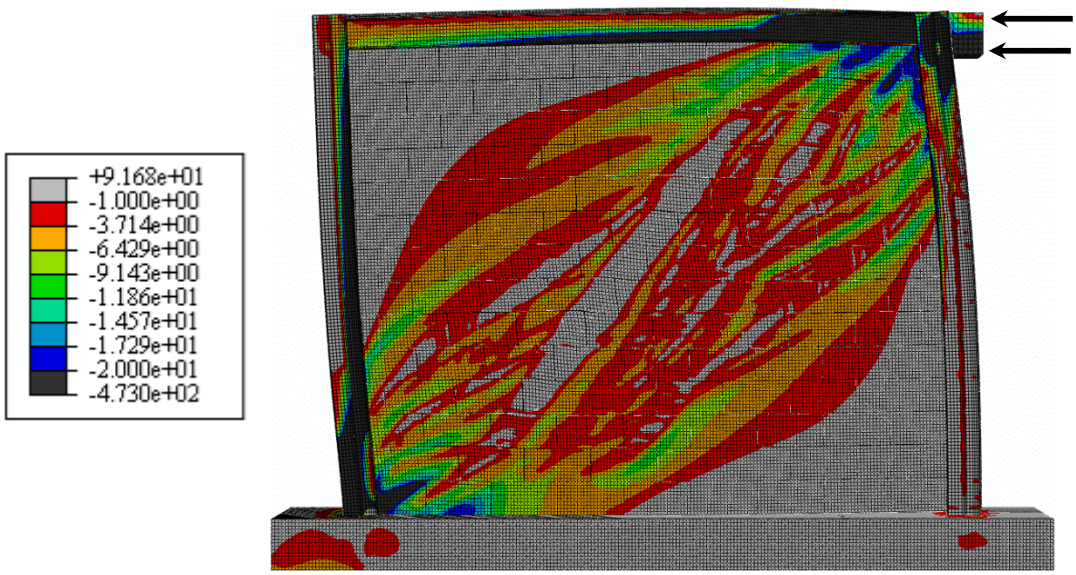

Figure 6-31: Principal compressive stresses at failure load in F7S-FC-76 (fully grouted infilled steel frame) (MPa)

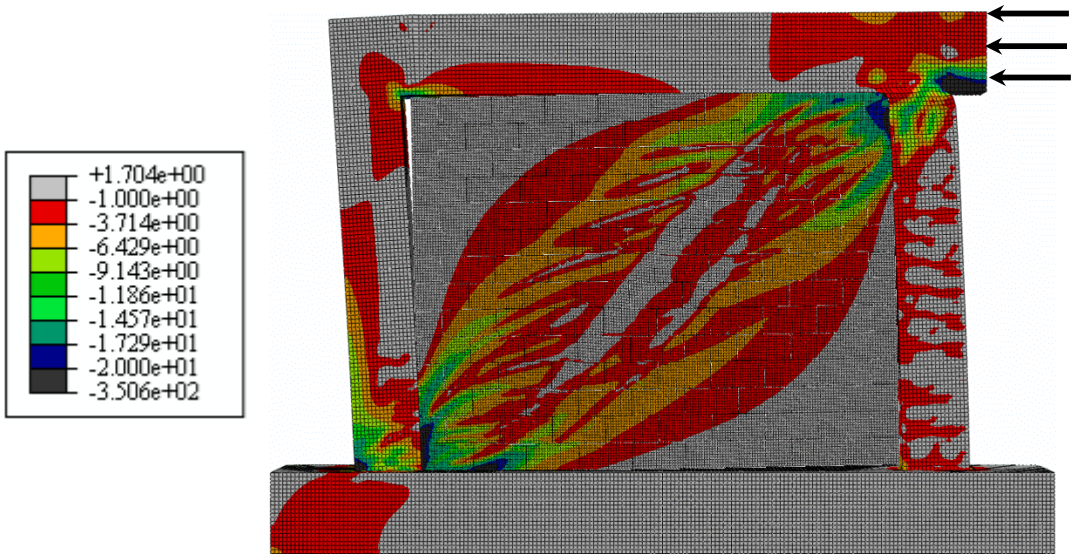

Figure 6-32: Principal compressive stresses at failure load in F7C-FC-76 (fully grouted infilled RC frame) (MPa)

The results of partially grouted and fully grouted masonry infill walls were compared against the results of hollow masonry infilled frames. When 27% of the cores were grouted, the enhancement in the initial stiffness was found to be 45% for the infilled steel frame compared to 17% for the RC frame. For fully grouted masonry infill walls, the increase in the initial stiffness was almost 175% for steel

frames compared to 78% for RC frames. The presence of 27% grout in the masonry did not affect the level at which the cracking load was developed. The first major crack level coincides with the location for hollow infill wall for both steel and RC frames. However, due to the higher stiffness of the fully grouted masonry, the cracking load was increased by 70% and 50% for steel and RC frames, respectively, compared to hollow masonry infilled frames. The increase in the ultimate lateral load for 27% grouted cores was 20% for both types of frames; while the ultimate lateral load was higher by 130% for infilled steel frames and 78% for RC frames for fully grouted infill walls.

In case of steel frames filled with hollow masonry, the stiffness of the infilled frame was improved by the presence of the infill wall which has a much higher stiffness (2902 *kN/mm*) than the frame (3.2 *kN/mm*). No plastic hinge was formed in the frame due to the restrain on the displacement provided by the masonry infill wall. Both the steel frame and the hollow masonry infill wall shared the load until failure in the masonry material took place by crushing at the corner of the developed compression strut.

Due to the excessive cracking in the partially grouted masonry infill walls, the infill wall failed at lower values of the ultimate displacement compared to hollow construction. The reduction in the ultimate displacement was found to be 10% and 25% for steel and RC infilled frames, respectively, compared to hollow construction. Fully grouted masonry infilled frames decreased the ultimate displacement for infilled steel frames by 10%; however, the reduction was almost 60% for infilled RC frames. The cracking of the frame members under lateral loading transferred the lateral load to the masonry infill wall leading to sudden failure at lower displacement levels.

Similar to the steel frame, the presence of the masonry infill wall enhanced the initial stiffness of the RC infilled frame. No plastic hinge was developed in the RC frame in the case of hollow masonry infill wall. The stiffness of the RC frame (22.61 *kN/mm*) was improved by the presence of the infill wall (2902 *kN/mm*) and both members shared the applied lateral load until failure in the infill took place by

crushing of the masonry at corners of the developed compression strut. However, a plastic hinge mechanism was formed in the RC frame in the case of partially and fully grouted masonry infill walls leaving the infill to resist the applied load alone.

6.6. Closure

The effect of the wall aspect ratio, gap size and location, haunched frames, and infill wall stiffness on the behaviour of masonry infilled frames was discussed in this chapter. Reducing the masonry infill wall aspect ratio from 1.0 to 0.50 increased the initial stiffness by 40% and 6% for steel and RC masonry infilled frames, respectively; both, the cracking and ultimate lateral loads, were improved by 70% for steel masonry infilled frames. The cracking load was increased by 7% for RC frames, whereas the ultimate lateral load was improved by 50%.

The presence of a top gap between the frame's beam and infill wall had a small impact on the initial stiffness of the rigid RC frames (less than 7% for 15 mm wide gap), and ultimate lateral load (about 20% for 15 mm wide gap); The cracking load was slightly increased by 10% for masonry infilled RC frames. However, for steel infilled frames having the same gap size, the initial stiffness was reduced by 60%. The reduction in the cracking load and ultimate lateral load was 25% for both masonry infilled RC and steel frames. Full separation gaps led to larger reduction in the initial stiffness, the cracking load, and the ultimate lateral load. Infilled frames can be treated as bare frame when the full gap size is 10 mm or more as the infill wall will have negligible contribution to the initial stiffness and lateral resistance of the system.

Presence of haunches in the frames led to a smooth transition from the linear to non-linear behaviour of the masonry infilled frame. This is attributed to the confinement effect provided by the haunch, and the predefined diagonal strut that transmitted the load to the other corner of the wall. The presence of haunch in the frame improved the initial stiffness by 50% for both steel and RC frames with a haunch size of $600\sqrt{2}$ mm. The cracking load was increased by 10% and 27% for steel and RC frames, respectively; while the ultimate lateral load was improved by 60% and 20% for infilled steel and RC frames, respectively.

Partially and fully grouting of infill walls led to enhancement in the initial stiffness and ultimate lateral load resistance of the system. The mode of failure of the infill wall was affected by the presence of the grout columns, especially partially grouted walls. The grout columns acted as internal stiffeners leading to redistribution of the lateral load over the entire length of the wall. Diagonal tension cracks dominated the failure mechanism in this case. However, a fully grouted wall behaved similar to a hollow masonry infill wall and failed by crushing of the masonry at the corners of the developed diagonal compression strut.

The results of the finite element analysis for masonry infilled steel and RC frames with window and door openings are presented and discussed in the next chapter.

CHAPTER 7

BEHAVIOUR OF MASONRY INFILL WALLS WITH OPENINGS

7.1. Introduction

In this chapter, the behaviour of several finite element models for masonry infilled steel and RC frames with different opening sizes and locations under lateral load is presented and discussed. The opening size varied from a 800×800 mm small window to a 800×2200 mm door openings. The location of the opening varied from the centre of the wall to eccentric towards or away from the lateral load.

7.2. Effect of Opening Size

Four sizes of a centrically located opening were considered: 800×800 mm, 1200×1000 mm, 2000×1000 mm, and 800×2200 mm. These sizes represent, small, medium, large window openings, and a door opening respectively. The masonry infill wall had a height of 2800 mm and an aspect ratio of 0.76 or 0.5. The following sections summarize the results for masonry infilled frames with central openings

7.2.1. Steel Frames with Infills having $h/l = 0.76$

The lateral load-lateral displacement response of masonry infilled frames with different size central openings is shown in Figure 7-1. The initial stiffnesses (K_{ini}), cracking loads (P_{cr}), ultimate loads (P_{ult}), corresponding ultimate displacements (Δ_{ult}) and failure modes are summarized in Table 7-1.

As shown in Figure 7-1, the lateral load-lateral displacement response of masonry infilled frames with openings followed linear pattern till the first crack was formed in the masonry infill wall. Increasing the size of the opening yielded more reduction in the initial stiffness, cracking load and ultimate load. An opening that is 20% of the surface area of the wall led to a reduction of 55% in both initial stiffness and cracking load and 40% in the ultimate load compared to a solid frame filled with a wall. On the other hand, for the same opening size of 20%, the infilled frame underwent 40% more displacement before failure took place.

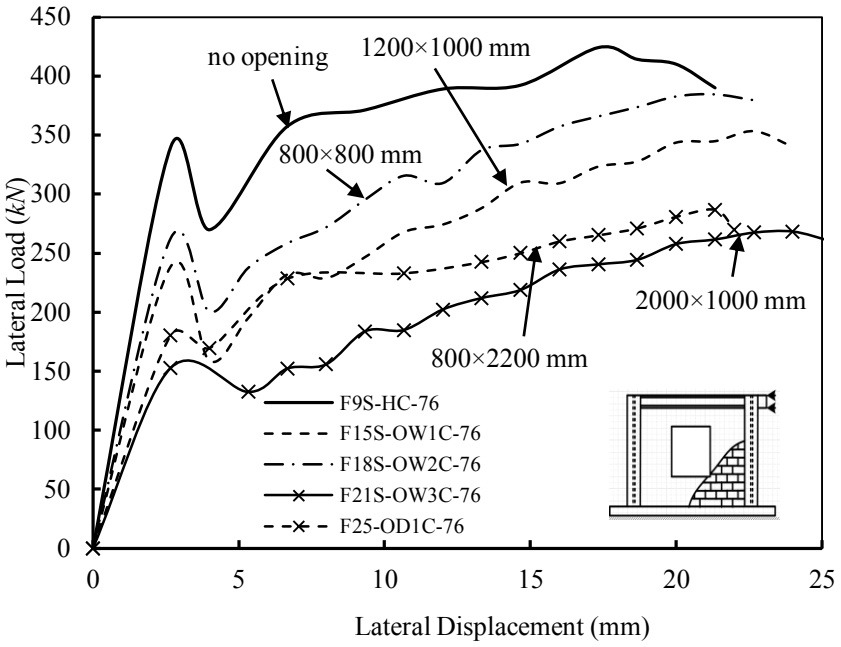

Figure 7-1: Lateral load-lateral displacement response of masonry infilled steel frames with 0.76 aspect ratio and different size central openings

Table 7-1: Summary of the FE results for steel frames with masonry infills having openings and an aspect ratio of 0.76.

Frame ID	Opening size (%)	K_{ini} (*kN/mm*)	P_{cr} (kN)	P_{ult} (kN)	Δ_{ult} (*mm*)	Failure mode*
F9S-HC-76	Solid	127.42	339.78	424.12	17.33	CC
F18S-OW2C-76	6.5	98.36	262.31	384.45	21.33	DT+CC
F15S-OW1C-76	12.0	89.41	238.44	353.33	22.67	DT+CC
F25S-OD1C-76	17.5	67.62	180.32	286.86	21.33	DT+SS
F21S-OW3C-76	20.0	57.25	152.68	268.26	24.00	SS+CC

*CC: Corner crushing, DT: Diagonal tension cracking and SS: Sliding shear

For small window openings of relative surface area of 12% or less (800×800 mm and 1000×1200 mm), the masonry infill wall experienced step-wise shear cracking along the head and bed joints over its entire area. A diagonal strut was formed in spite of the presence of the opening as shown in Figures 7-2 and 7-3, and failure was reached when masonry crushing took place at the corners of the diagonal strut. The vertical component of the developed diagonal strut confined the mortar bed joints and prevented sliding shear. The masonry infill wall restricted the formation of plastic hinges in the frame's members and joints.

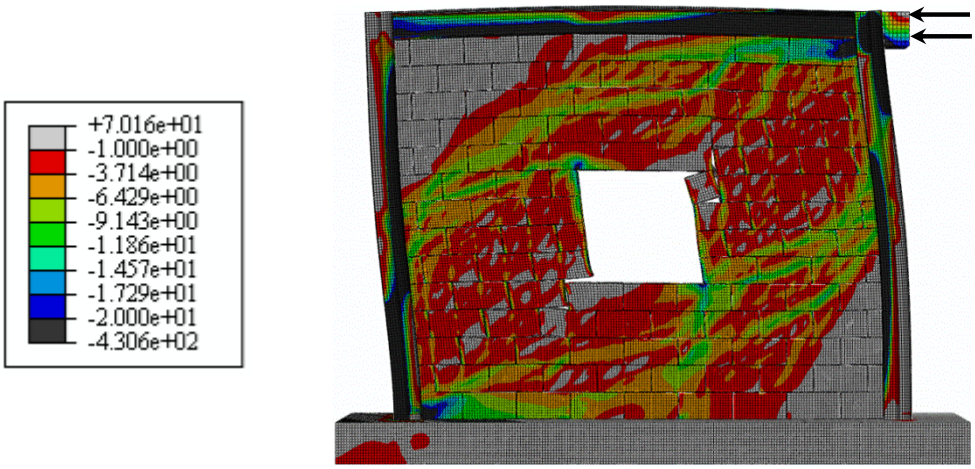

Figure 7-2: Principal compressive stresses at failure load in F18S-OW2C-76 (masonry infilled steel frame with an 800×800 mm central window opening) (MPa)

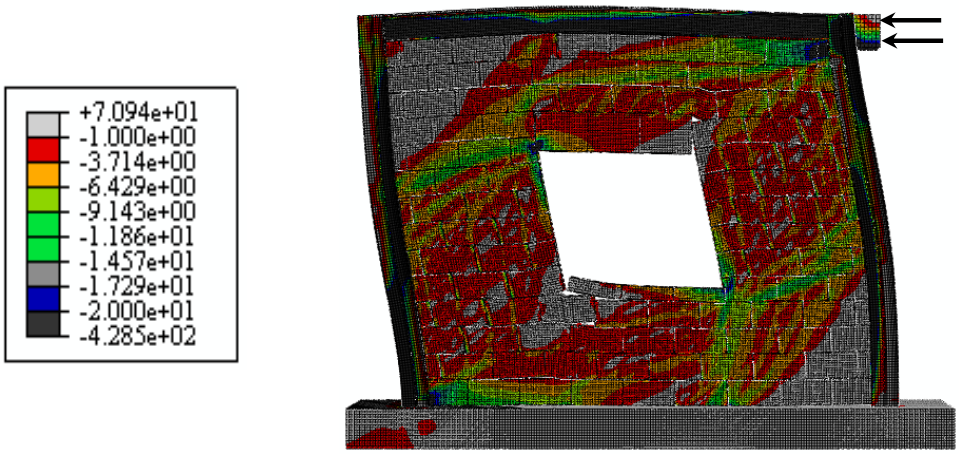

Figure 7-3: Principal compressive stresses at failure load in F15S-OW1C-76 (masonry infilled steel frame with a 1200×1000 mm central window opening) (MPa)

For openings of 17.5% and higher of the surface area of the infill wall, a series of compression struts were developed around the opening. Figure 7-4 shows the developed compression struts in the infill wall for a masonry infilled steel frame with an aspect ratio of 0.76 and an opening of 2000×1000 mm (20 % of the wall surface area). Diagonal cracks were developed from the frame's corner where the

load was applied to the top-right corner of the opening. Sliding shear occurred at the side further from the load at the top of the opening. As shown in Figure 7-4, the intersection of the two struts at the top of the opening further from the load led to the formation of high shear stresses on the mortar joints which led the development of sliding shear at this location. Crushing of the masonry material followed at higher loading levels at the top right (loaded) and lower left corners of the infill wall.

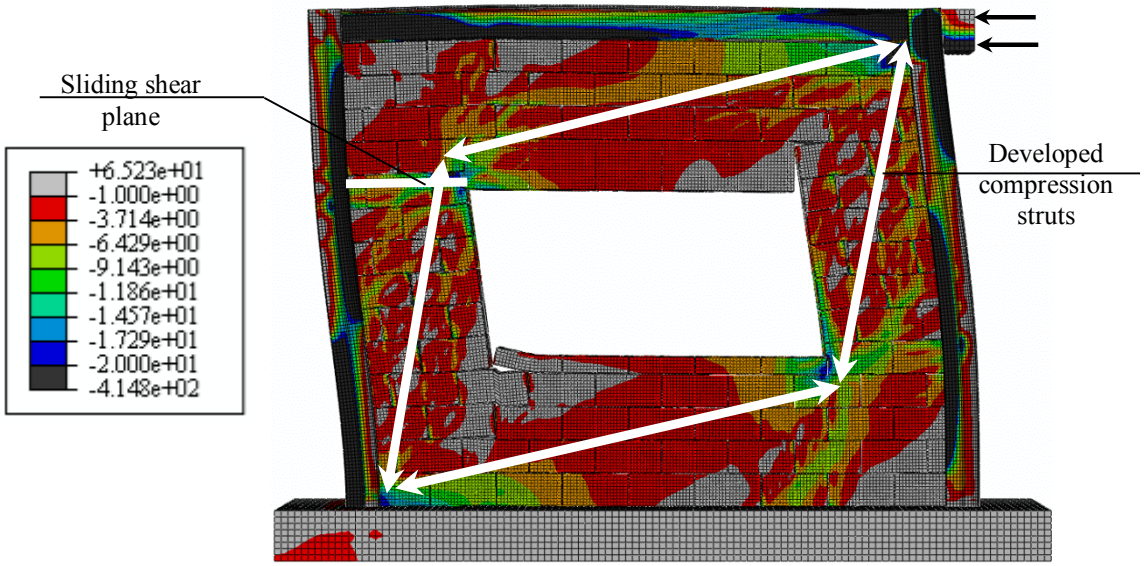

Figure 7-4: Principal compressive stresses at failure load in F21S-OW3C-76 (masonry infilled steel frame with a 2000×1000 mm central window opening) (MPa)

When a door opening of dimensions 800×2200 mm (17.5% of the infill wall surface area) was located in the centre of the infilled steel frame, three compression struts were formed in the infill wall around the opening as shown in Figure 7-5. The presence of a door opening divided the infill wall into two piers connected by a spandrel spanning above the opening. The strut formed in the spandrel had a very small angle of inclination (almost horizontal). The infill wall failed due to sliding shear along a horizontal plane at the level of the top of the opening in the pier further away from the load. The horizontal component of the force in the strut in the spandrel led to the development of high shear stress that exceeded the strength of the mortar joint; and hence, sliding shear failure took place.

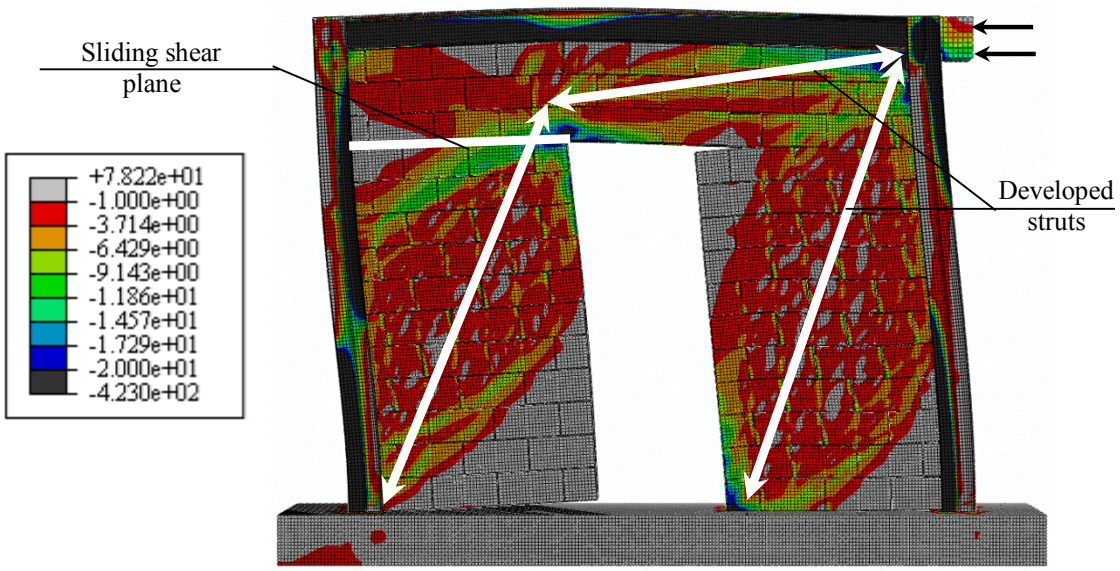

Figure 7-5: Principal compressive stresses at failure load in F25S-OD1C-76 (masonry infilled steel frame with central door opening with 0.76 aspect ratio) (MPa)

7.2.2. Steel Frames with Infills having h/l = 0.5

Figure 7-6 shows the lateral load-lateral displacement response for masonry infilled steel frames with an aspect ratio of 0.5 and different size central openings. The initial stiffness (K_{ini}), cracking load (P_{cr}), ultimate load (P_{ult}) and corresponding displacement (Δ_{ult}) for the different FE models are summarized in Table 7-2.

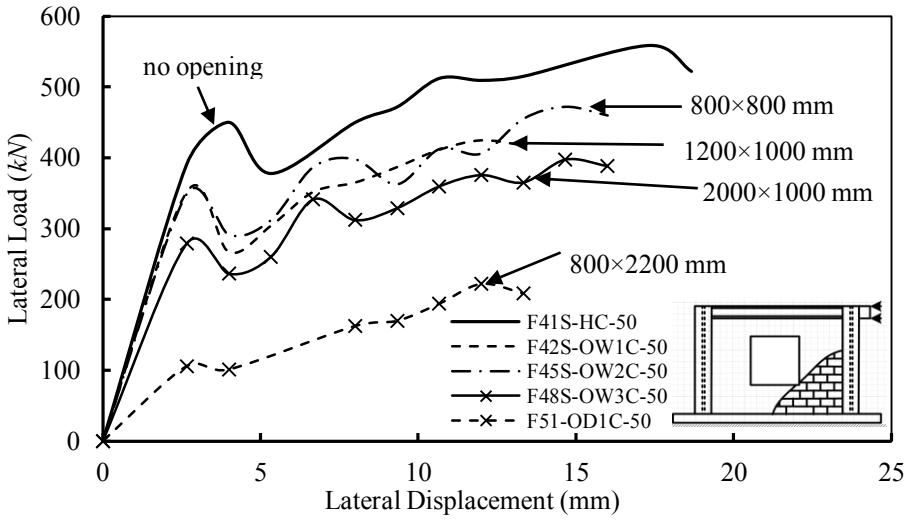

Figure 7-6: Lateral load-lateral displacement response of masonry infilled steel frames with 0.5 aspect ratio and different size central openings

Table 7-2: Summary of the FE results for steel frames with masonry infills having openings and an aspect ratio of 0.5

Frame ID	Opening size (%)	K_{ini} (*kN/mm*)	P_{cr} (kN)	P_{ult} (kN)	Δ_{ult} (*mm*)	Failure mode*
F41S-HC-50	Solid	146.72	450.00	558.55	17.33	CC
F45S-OW2C-50	4.1	131.01	350.00	472.26	14.67	DT+CC
F42S-OW1C-50	7.7	131.83	351.55	424.21	12.00	DT+CC
F51S-OD1C-50	11.2	39.69	105.84	221.83	12.00	SS
F48S-OW3C-50	12.8	104.62	278.98	397.34	14.67	DT+CC

*CC: Corner crushing, DT: Diagonal tension cracking and SS: Sliding shear

Similar to infilled frames with 0.76 aspect ratio, increasing the window opening size led to higher reduction in initial stiffness, cracking load, and ultimate load. A window opening that is 12.8% (2000×1000 mm) of the surface area of the infill wall led to a reduction of 30%, 40%, and 30% in the initial stiffness, cracking load, and ultimate load, respectively, compared to a solid infilled frame. Unlike masonry infilled steel frames with aspect ratio of 0.76, the displacement corresponding to the ultimate load was reduced. For a window opening that is 12.8% (2000×1000 mm) of the surface area of the wall, the reduction in ultimate displacement was 15% less than the solid infilled frame.

In spite of the smaller area of the door opening of dimensions 800×2200 mm (11.2% of the wall's surface area) compared to the 2000×1000 mm window opening of (12.8% of the wall's surface area), the reduction in initial stiffness, cracking load, ultimate load and corresponding displacement was higher. The presence of the door opening led to the formation of only two compression struts in the wall compared to four in case of the window opening. The horizontal strut over the door opening led to higher level of shear stresses leading to failure of the masonry at lower loading levels compared to the window opening.

For small openings of dimensions 800×800 mm and 1200×1000 mm (relative area of 7.7% of the wall surface area or less), the first major crack was a diagonal tension crack. The wall continued to carry more load after the diagonal crack was developed. A single diagonal compression strut was formed in the

masonry infill wall in spite of the presence of a central opening. The infill wall failed due to a mixed mode between diagonal tension cracking and corner crushing in the developed compression strut. Figure 7-7 shows the principal compressive stresses in the masonry infill wall and the development of the diagonal compression strut for infilled steel frame with 800×800 mm central window opening.

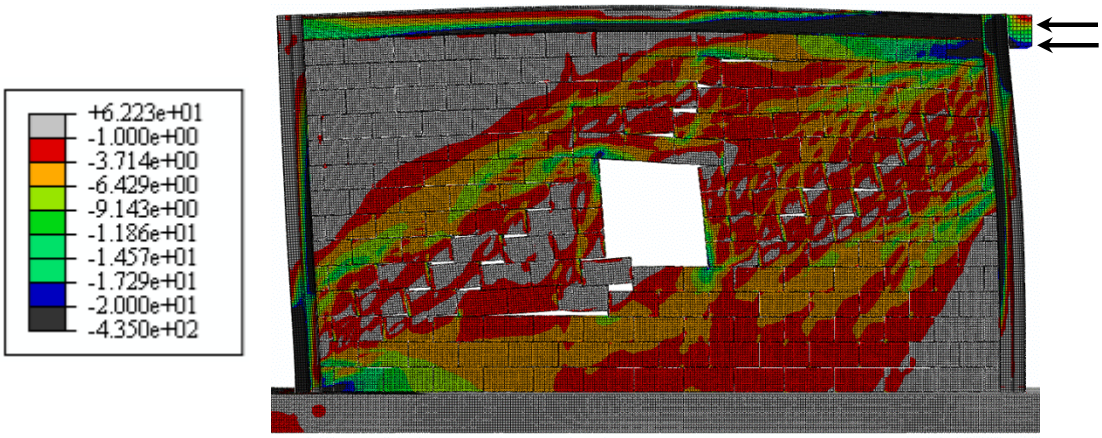

Figure 7-7: Principal compressive stresses at failure load in F45S-OW2C-50 (masonry infilled steel frame with an 800×800 mm central window opening) (MPa)

Similar to infilled frames with 0.76 aspect ratio, a window opening that is 12.8% (2000×1000 mm) of the surface area of the wall in size resulted in the development of a set of compression struts around the opening as shown in Figure 7-8. Diagonal cracks were developed from the corner where the load was applied to the top-right corner of the opening. With continuous loading, the masonry infill wall failed at lower level than the one causing the diagonal cracks due to crushing of the masonry at the loaded and the bottom-left corners.

When a central door opening that is 11.2% (800×2200 mm) of the surface area of the infill wall was introduced in the masonry infill wall, only two compression struts formed as shown in Figure 7-9; the strut formed in the spandrel had a very small angle of inclination (almost horizontal). The infill wall failed due to sliding shear along a horizontal plane at the level of the top of the door opening in the pier away from the load. The high horizontal component of the force in the strut in the spandrel led to the development of high shear stresses that exceeded the

resistance of the mortar joint and led to a sliding shear failure. Corner crushing at the loaded corner followed the development of sliding shear plane at a load level less than the ultimate.

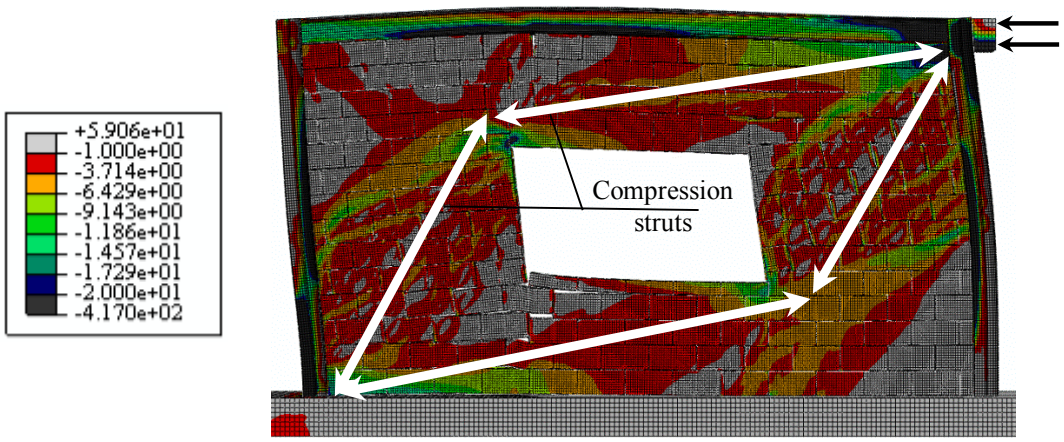

Figure 7-8: Principal compressive stresses at failure load in F48S-OW3C-50 (masonry infilled steel frame with a 2000×1000 mm central window opening) (MPa)

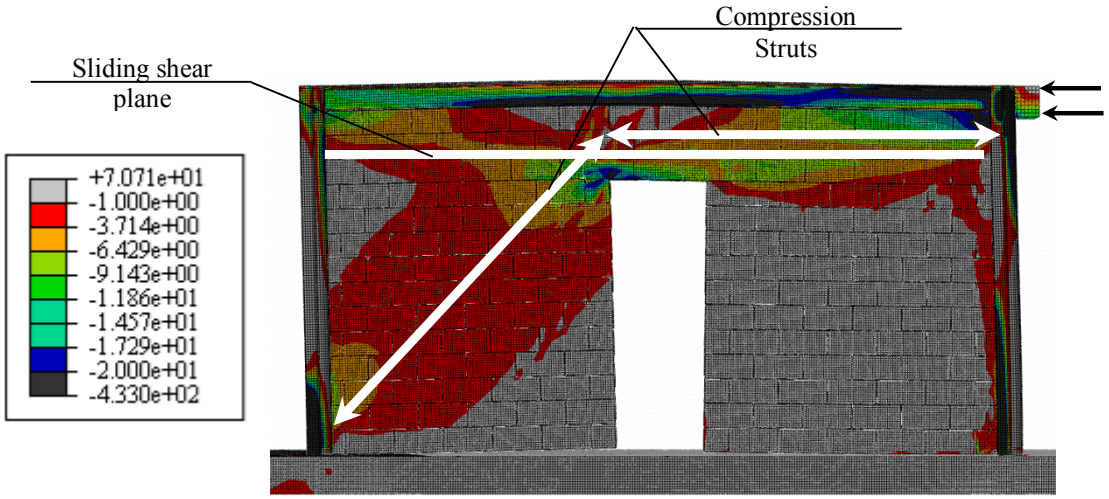

Figure 7-9: Principal compressive stresses at failure load in F51S-OD1C-50 (masonry infilled steel frame with an 800×2200 mm central door opening) (MPa)

7.2.3. RC Frames with Infills having *h/l* = 0.76

The lateral load-lateral displacement response of masonry infilled RC frames with openings is shown in Figure 7-10. A summary of the values of the initial stiffness (K_{ini}), cracking load (P_{cr}), ultimate load (P_{ult}) and the corresponding displacement (Δ_{ult}) is presented in Table 7-3.

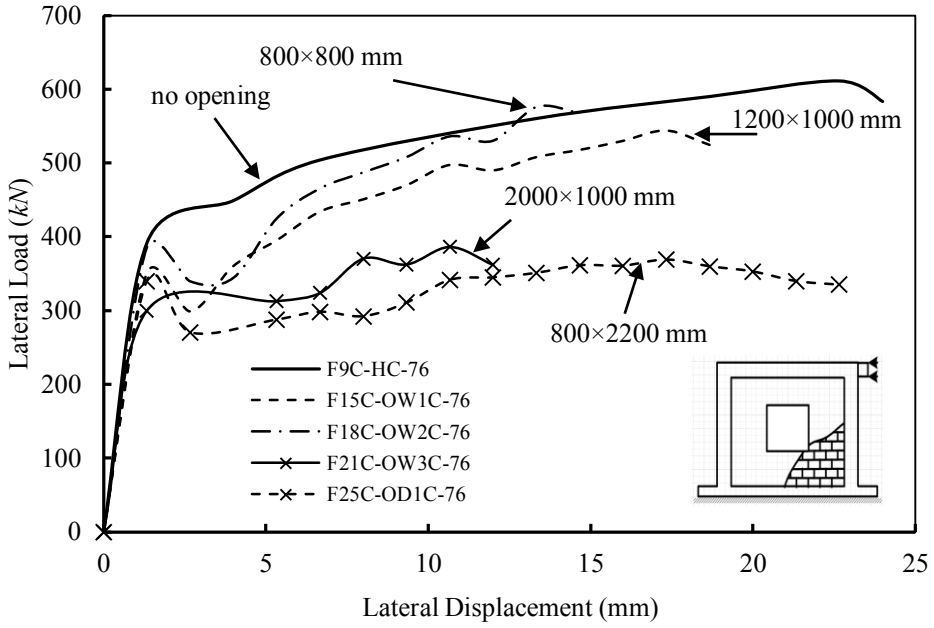

Figure 7-10: Lateral load-lateral displacement response of masonry infilled RC frames with 0.76 aspect ratio and different size central openings

Table 7-3: Summary of the FE results for RC frames with masonry infills having openings and an aspect ratio of 0.76.

Frame ID	Opening size (%)	K_{ini} (*kN/mm*)	P_{cr} (kN)	P_{ult} (kN)	Δ_{ult} (*mm*)	Failure mode*
F9C-HC-76	0	293.84	391.80	611.15	22.67	CC
F18C-OW2C-76	6.5	288.74	385.00	575.62	13.33	DT+CC
F15C-OW1C-76	12.0	262.49	350.00	543.96	17.33	DT+CC
F25C-OD1C-76	17.5	254.98	340.00	369.07	17.33	DT+SS
F21C-OW3C-76	20.0	244.99	300.00	386.12	10.67	SS+CC

*CC: Corner crushing, DT: Diagonal tension cracking and SS: Sliding shear

The presence of openings in the infill wall within the RC frame reduced the initial stiffness, cracking load, and ultimate load of the masonry infilled RC frames.

Larger window openings reduced the stiffness of the infill wall; hence, reduction of the initial stiffness, cracking load of the masonry infilled frame. For a window opening with area 20% of the wall surface area (2000×1000 mm), the reduction was found to be 17%, 23% and 37% of the initial stiffness, cracking load, and ultimate load; respectively, compared to a solid infilled frame. The reduction in the initial stiffness and cracking load was less than the corresponding cases for steel frames due to the higher initial stiffness of the bare RC frame (22.61 *kN/mm*) compared to the bare steel frame (3.20 *kN/mm*) which enables the infilled RC frames to carry more load before cracking of the infill wall. The ultimate displacement corresponding to the ultimate load of the masonry infilled frame was reduced by 50% for the same opening size due to the brittleness of both materials forming the infill wall and the containing frame.

The door opening of dimensions 800×2200 mm had a relative area of 17.5% which is smaller than the 20% relative area of the window opening of dimensions 2000×1000 mm. The reduction in the initial stiffness and cracking load for a door opening was 13% relative to a solid infilled frame; while the reduction for a large window opening was 17% in the initial stiffness and 23% in the cracking load compared to a solid infilled frame; however, the ultimate load was less for infill with door opening than the case of infill wall with large window opening (reduction of 37% compared to 40%). The RC frame's beam-column connection was more rigid compared to the steel frame's. The level of the force in the spandrel was higher leading to development of shear stresses in the mortar joint above the opening on the left pier causing its failure at a lower load compared to an infill with a window opening.

The first cracks in masonry infill walls with 800×800 mm and 1200×1000 mm window openings were diagonal stepwise cracks spanning from the frames' loaded corner to the top-right corner of the opening. A diagonal strut was formed in the masonry infill wall as shown in Figure 7-11 and the masonry infill wall failed due to crushing of the masonry at the corners of the developed strut.

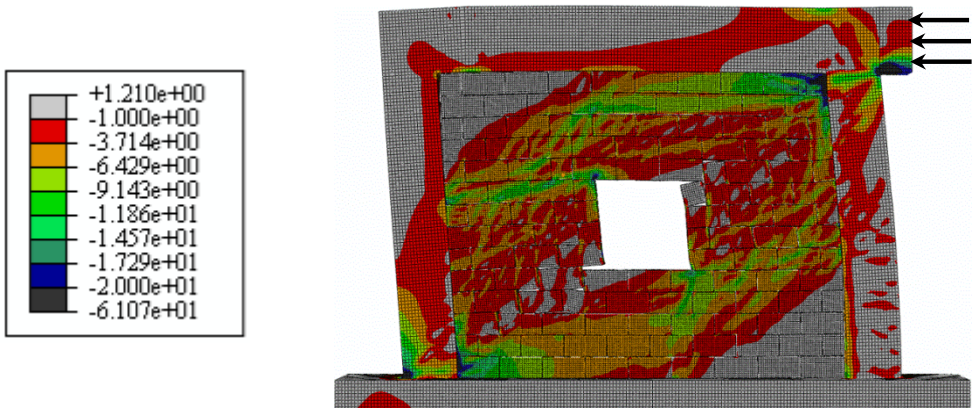

Figure 7-11: Principal compressive stresses at failure load in F18C-OW2C-76 (masonry infilled RC frames with an 800×800 mm central window opening) (MPa)

The presence of a large window opening of dimensions 2000×1000 mm (20% of the total area of the wall) within the masonry infill wall forced the development of a group of struts around the opening, as shown in Figure 7-12, similar to the case of infilled steel frames with the same aspect ratio as shown in Figure 7-12. Diagonal cracking took place in the masonry infill wall at the top corner against the load and the bottom-left corner. With further loading, sliding shear failure occurred at the top of the opening in the pier away from the load. The intersection of the two struts at the top-left corner of the opening led to the formation of a high component of horizontal force and shear stresses in the mortar joint that exceeded the mortar shear resistance. With continuous loading, the crushing of the masonry took place at the masonry corner of against the load at a lower load than the maximum resistance.

When a door opening of dimensions 800×2200 mm (17.5% of the infill wall surface area) was created in the masonry infilled RC frame, cracking began with a vertical crack at the top right corner of the opening. Three compression struts were formed in the masonry infill wall as shown in Figure 7-13. Shear cracks were formed along the diagonal struts in the two piers. The wall failed by sliding shear at the top of the opening in the pier away from the load.

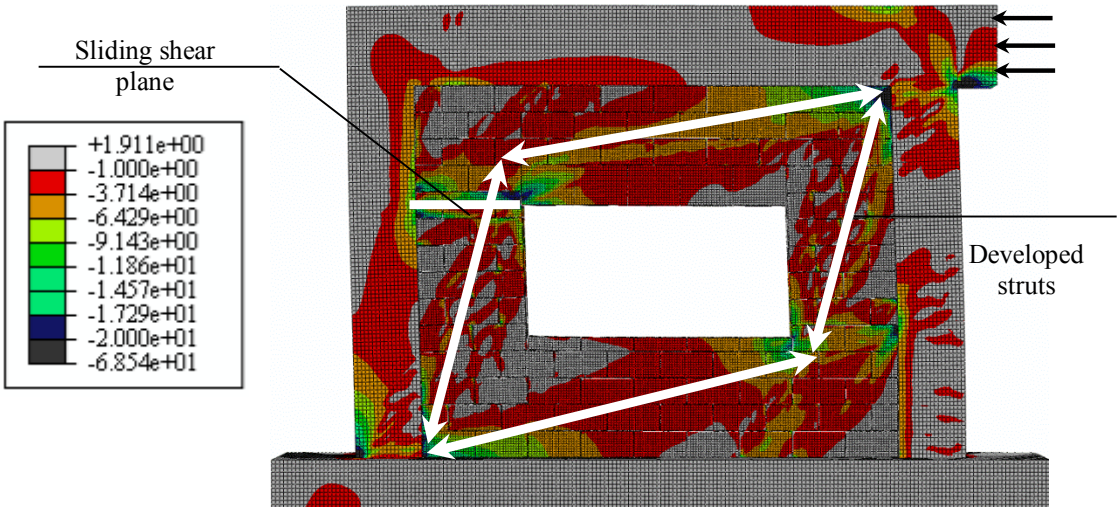

Figure 7-12: Principal compressive stresses at failure load in F21C-OW3C-76 (masonry infilled RC frame with 2000×1000 mm central window opening) (MPa)

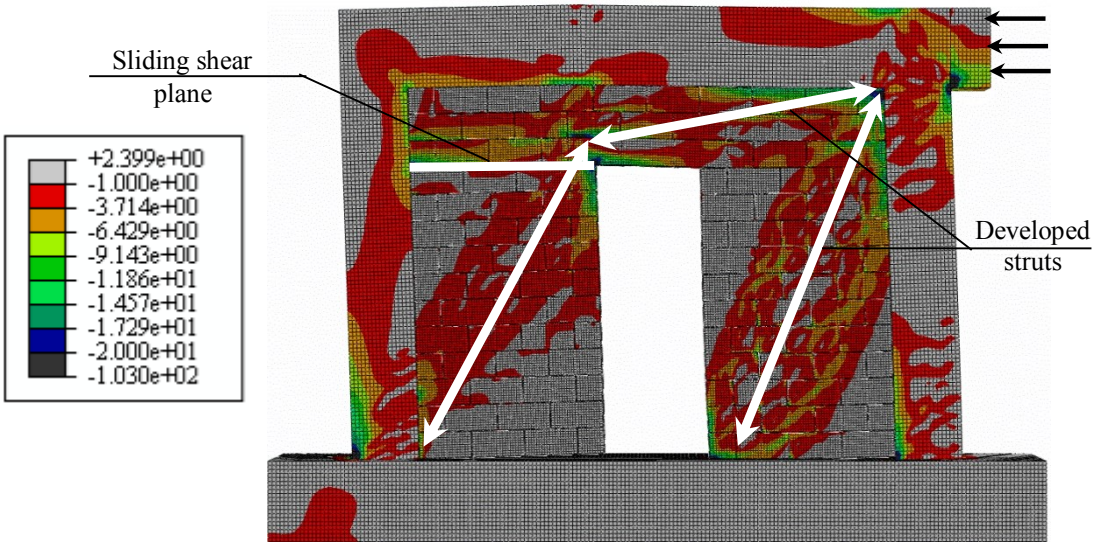

Figure 7-13: Principal compressive stresses at failure load in F25C-OD1C-76 (masonry infilled RC frame with 800×2200 mm central door opening) (MPa)

7.2.4. RC Frames with Infills having $h/l = 0.5$

Figure 7-14 shows the lateral load lateral displacement response for masonry infilled RC frames with aspect ratio of 0.5 and different central opening sizes. The initial stiffness (K_{ini}), cracking load (P_{cr}), ultimate load (P_{ult}) and

corresponding displacement (Δ_{ult}) for the different FE models are summarized in Table 7-4.

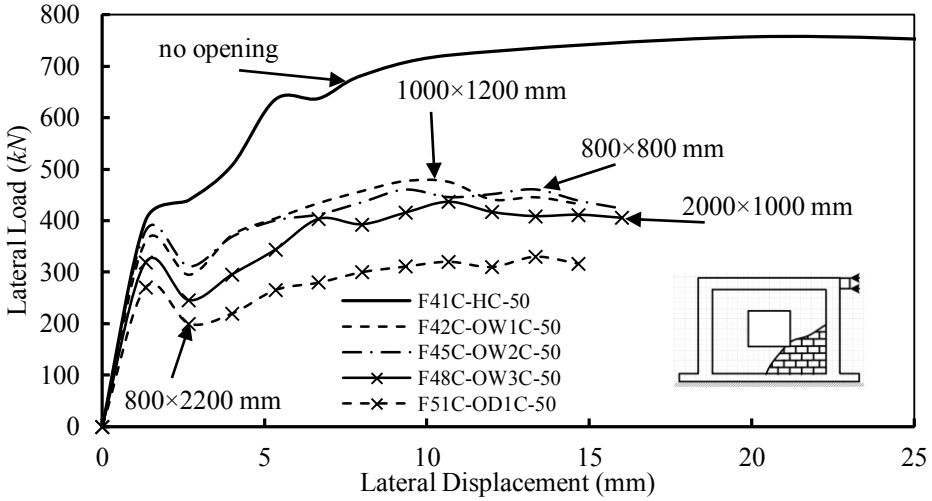

Figure 7-14: Lateral load-lateral displacement response of masonry infilled RC frames with 0.5 aspect ratio and different size central openings

Table 7-4: Summary of the FE results RC frames with masonry infills having openings and an aspect ratio of 0.5.

Frame ID	Opening size (%)	K_{ini} (*kN/mm*)	P_{cr} (kN)	P_{ult} (kN)	Δ_{ult} (kN)	Failure mode*
F41C-HC-50	Solid	299.96	400.00	757.13	20.00	CC
F45C-OW2C-50	4.1	284.98	284.98	460.26	13.33	SS
F42C-OW1C-50	7.7	269.98	360.00	476.84	9.33	SS
F51C-OD1C-50	11.2	203.12	270.84	330.35	13.33	SS
F48C-OW3C-50	12.8	239.10	318.82	436.67	10.67	SS+CC

*CC: Corner crushing, and SS: Sliding shear

For small openings of dimensions 800×800 mm and 1200×1000 mm (less than 7.7% of the infill wall surface area or less) built within RC frames of aspect ratio 0.5, the first major crack took place in the form of stepwise cracking spanning from the frame's top corner towards the load. The wall continued to carry load after these cracks were formed. As shown in Figure 7-15, the masonry infill wall failed due to sliding shear along a plane above the opening in the left side of the infill wall. Sliding shear took place due to lack of the confinement exerted by the frame's beam due to the rigidity of the beam-column connection.

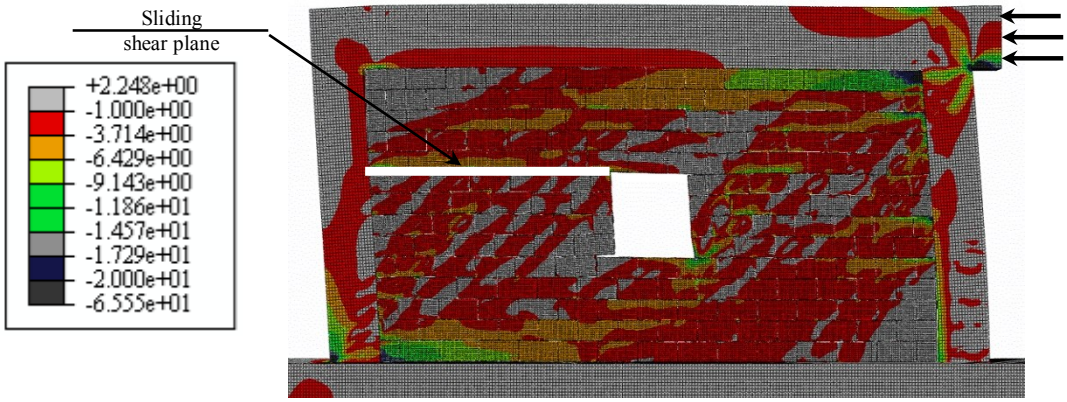

Figure 7-15: Principal compressive stresses at failure load in F45S-OW2C-50 (masonry infilled RC frame with 800×800 mm central window opening) (MPa)

As the relative size of the opening became 12.8% and greater (2000×1000 mm) of the infill wall surface area, four compression struts developed in the wall. Stepwise cracks were formed in the masonry infill wall towards the loaded pier at early stages of loading. The failure of the wall was dominated by sliding shear along a horizontal mortar joint above the opening. With continuous loading, a plastic hinge was formed in the RC frame at the loaded corner at a lower load level than the maximum load leading to failure. Figure 7-16 shows the contours of the compressive stresses formed in the masonry infill wall.

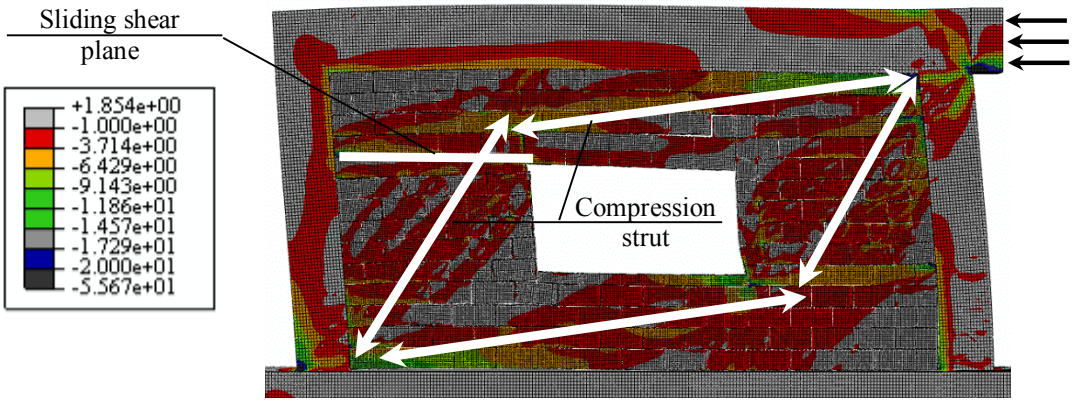

Figure 7-16: Principal compressive stresses at failure load in F48S-OW3C-50 (masonry infilled RC frames with 2000×1000 mm central window opening) (MPa)

The presence of a central door opening within the infill wall resulted in the

development of two struts: a horizontal strut spanning from the loaded corner until the end of the spandrel and a diagonal strut in the pier away from the load as shown in Figures 7-17. The force in the horizontal strut resulted in high levels of shear stresses along the bed joints above the door opening leading to failure of infilled RC frames in sliding shear. Crushing of the masonry at the loaded corner followed the development of sliding shear planes at load lower than the maximum load.

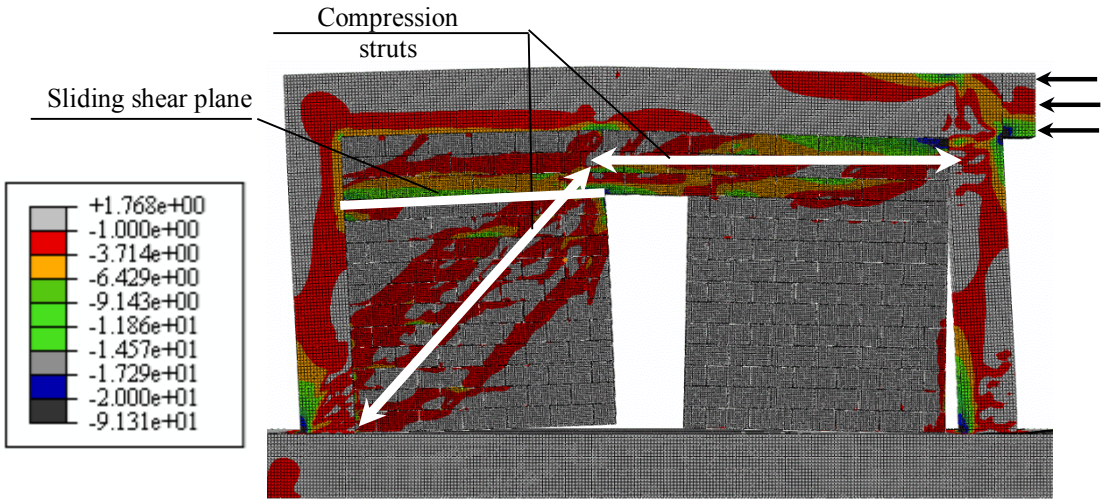

Figure 7-17: Principal compressive stresses at failure load in F51C-OD1C-50 (masonry infilled RC frames with 800×2200 mm central door opening) (MPa)

When the opening size was increased, the reduction in initial stiffness and cracking load increased. For an opening size of 12.8% (2000×1000 mm) of the infill surface area, initial stiffness and cracking load were 20% compared to solid infilled frames; while the reduction in the ultimate load was 40% . The masonry infilled RC frame experienced 47% reduction in the displacement corresponding to the ultimate load for a 2000×1000 mm.

The reduction in the initial stiffness, cracking load, and ultimate load was higher in the case of a door opening even though its relative area (11.2 %) is less than the 2000×1000 mm window opening (12.8 %). In case of a door opening, only two struts were formed in the infill wall leading to sliding shear failure of the wall in the left pier at a lower load compared to an infilled frame with a window opening.

The ultimate displacement corresponding to the ultimate load was reduced only to 33% compared to reduction of 47% in case of a large window opening.

7.3. Effect of Opening Location

To study the effect of the location of the window/door openings with respect to the centre of the masonry infill wall on the in-plane response of masonry infilled frames, the opening was placed at the centre of the wall, towards the load, and away from the load. The following sections summarize the findings for the effect of opening locations.

7.3.1. Small Size Window (800×800 mm)

Figures 7-18 through 7-21 show the lateral load-lateral displacement response for masonry infilled frames having the same opening size but placed at different locations. Table 7-5 is a summary of the initial stiffness (K_{ini}), cracking load (P_{cr}), ultimate load (P_{ult}), corresponding ultimate displacement (Δ_{ult}) and failure mode of the masonry infilled frames.

In case of infilled frames with openings and aspect ratio of 0.5, the 800×800 mm opening interfered with the diagonal strut in a larger area compared to a wall with an aspect ratio of 0.76 as shown in Figures 7-24 and 7-25. The width of the developed strut is dependent on the loading level; at earlier stages, the interference between the opening and the developed strut was minimal which led to minor reduction in the initial stiffness for both steel and RC frames (5% on average) compared to solid infilled frames. With continued loading, the width of the strut increased leading to a reduction in the cracking and ultimate loads of 20% for infilled steel frames; however, due to the rigidity of the RC beam-column connection, the reduction in cracking load was only 8% for infilled RC frames. The ultimate load was reduced by 45% for the infilled RC frames. When cracking was developed in the RC frame's beam-column connection, the frame's load was transferred directly to the infill wall causing its load share to increase; hence, its failure under a lower load compared to solid infills.

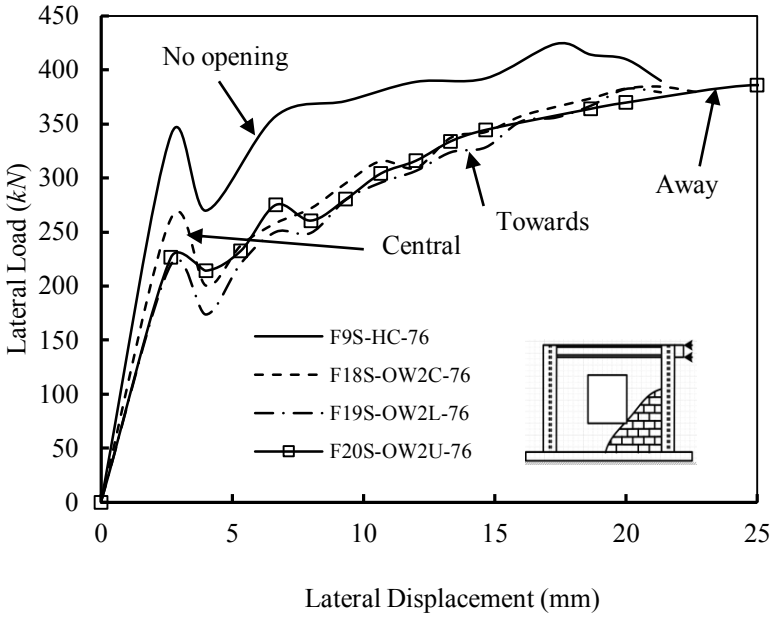

Figure 7-18: Lateral load-lateral displacement behaviour of masonry infilled steel frames with an 800×800 mm window at various locations and a wall aspect ratio of 0.76

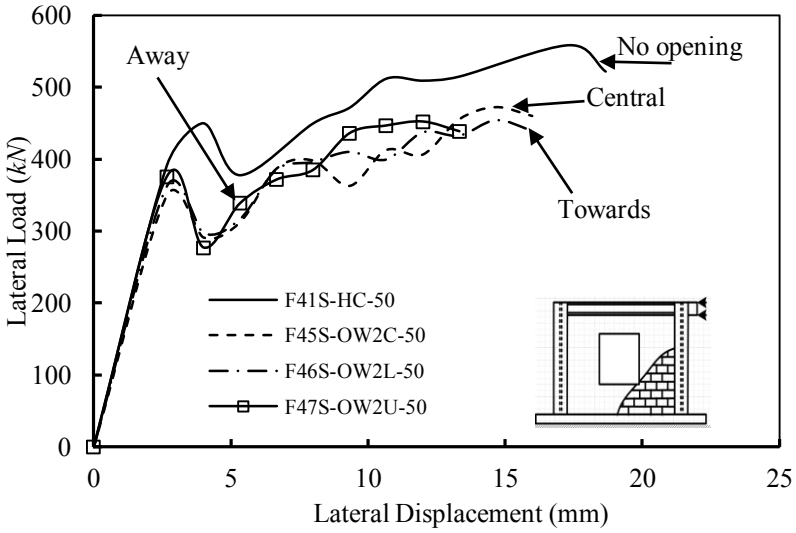

Figure 7-19: Lateral load-lateral displacement behaviour of masonry infilled steel frames with an 800×800 mm window at various locations and a wall aspect ratio of 0.5

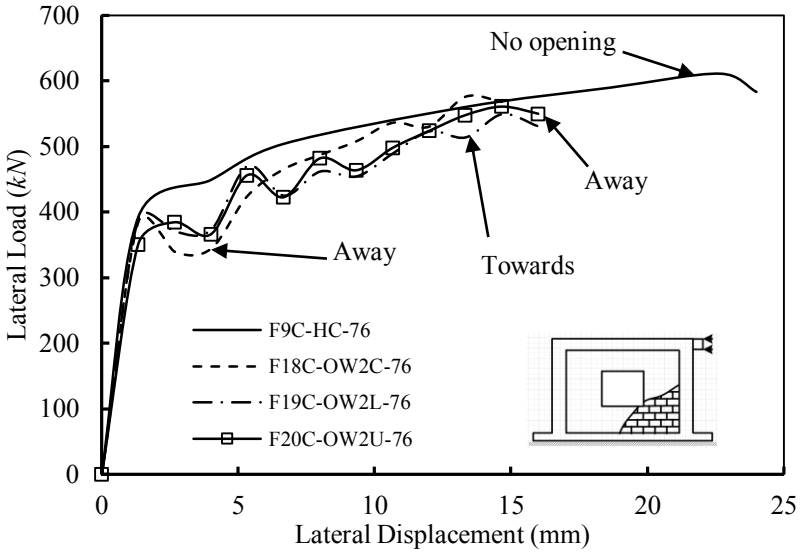

Figure 7-20: Lateral load-lateral displacement behaviour of masonry infilled RC frames with an 800×800 mm window at various locations and a wall aspect ratio of 0.76

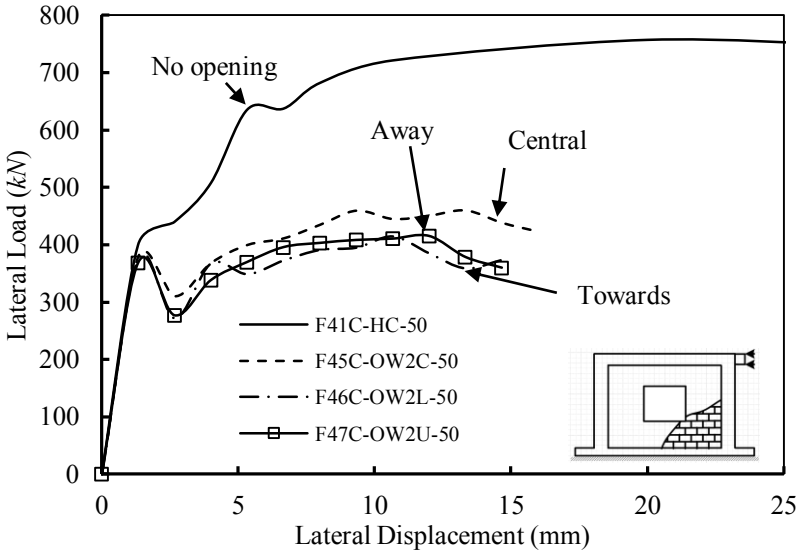

Figure 7-21: Lateral load-lateral displacement behaviour of masonry infilled RC frames with an 800×800 mm window at various locations and a wall aspect ratio of 0.5

Table 7-5: Summary of the FE results for masonry infilled frames with opening placed at different locations

Frame ID	Opening location†	K_{ini} (*kN/mm*)	P_{cr} (kN)	P_{ult} (kN)	Δ_{ult} (mm)	Failure mode*
F9S-HC-76	N/A	127.42	339.78	424.12	17.33	CC
F18S-OW2C-76	Central	98.36	262.31	384.45	21.33	DT+CC
F19S-OW2L-76	Towards	82.38	219.68	382.46	20.00	DT+CC
F20S-OW2U-76	Away	84.92	226.44	386.00	25.00	DT+CC
F41S-HC-50	N/A	146.72	450.00	558.55	17.33	CC
F45S-OW2C-50	Central	131.01	350.00	472.26	14.67	DT+CC
F46S-OW2L-50	Towards	136.02	362.71	454.63	14.67	DT+CC
F47S-OW2U-50	Away	141.00	376.00	452.46	12.00	DT+CC
F9C-HC-76	N/A	293.84	391.80	611.15	22.67	CC
F18C-OW2C-76	Central	288.74	385.00	575.62	13.33	DT+CC
F19C-OW2L-76	Towards	292.88	390.54	549.32	14.67	DT+CC
F20C-OW2U-76	Away	262.75	350.35	560.90	14.67	DT+CC
F41C-HC-50	N/A	299.96	400.00	757.13	20.00	CC
F45C-OW2C-50	Central	284.98	284.98	460.26	13.33	SS
F46C-OW2L-50	Towards	281.99	376.00	415.10	10.67	SS
F47C-OW2U-50	Away	276.38	368.54	415.35	12.00	SS

*CC: Corner crushing, DT: Diagonal tension cracking, and SS: Sliding shear

† Eccentrically towards the load, Away: Eccentrically away from the load

As shown in Figures 7-22 and 7-23, a small eccentric opening of 800×800 mm in the masonry infill wall with an aspect ratio 0.76 did not significantly interfere with a large portion of the developed diagonal compression strut. This limited minor interference resulted in small reduction in the initial stiffness and cracking load (less than 10%) for infilled RC frames regardless of the opening location. The reduction in initial stiffness and the cracking load was 30% for infilled steel frame. The bare RC frame had relatively higher stiffness of 22.61 *kN/mm* compared to the stiffness of the bare steel frame (3.21 *kN/mm*) leading to increasing the load carried by the infilled RC frames over steel ones. The reduction in the ultimate load of infilled steel and RC frames was 10% compared to infilled frames with solid infill walls. When the opening was located away from the load, the ultimate displacement corresponding to the ultimate load was 45% higher than

the case of no opening. The ultimate displacement was reduced by 35% compared to infilled frames with a solid infill wall.

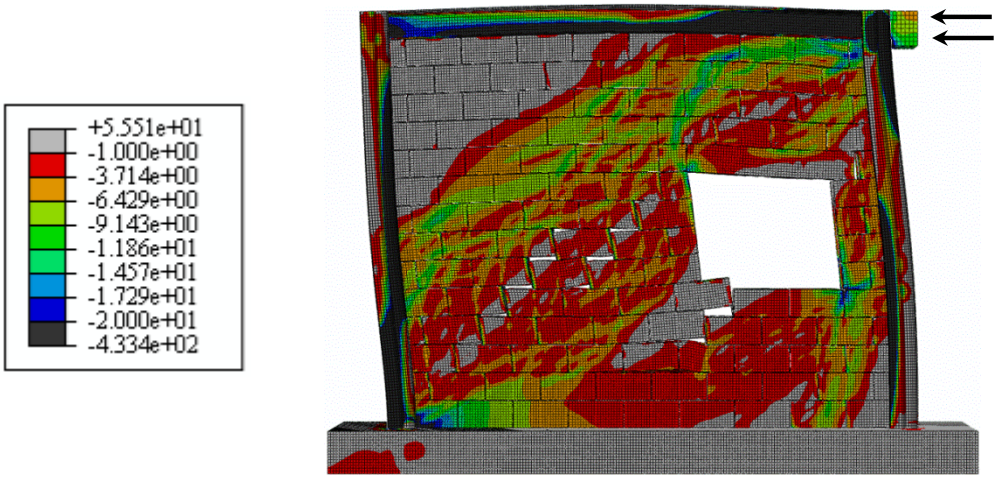

Figure 7-22: Principal compressive stresses at failure load in F19S-OW2L-76 (steel frame with an eccentric 800×800 mm opening and 0.76 wall aspect ratio) (MPa)

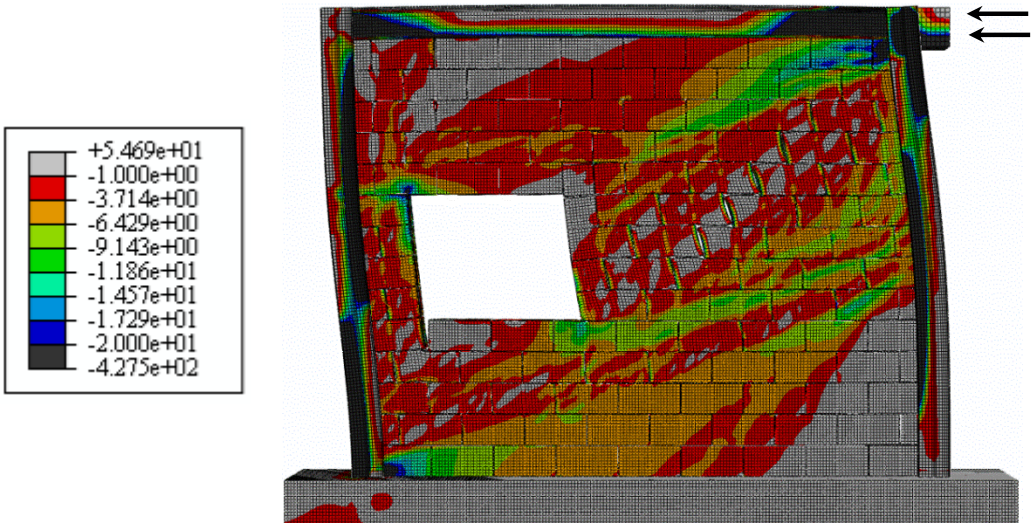

Figure 7-23: Principal compressive stresses at failure load in F20S-OW2U-76 (steel frame with an eccentric 800×800 mm opening and 0.76 wall aspect ratio) (MPa)

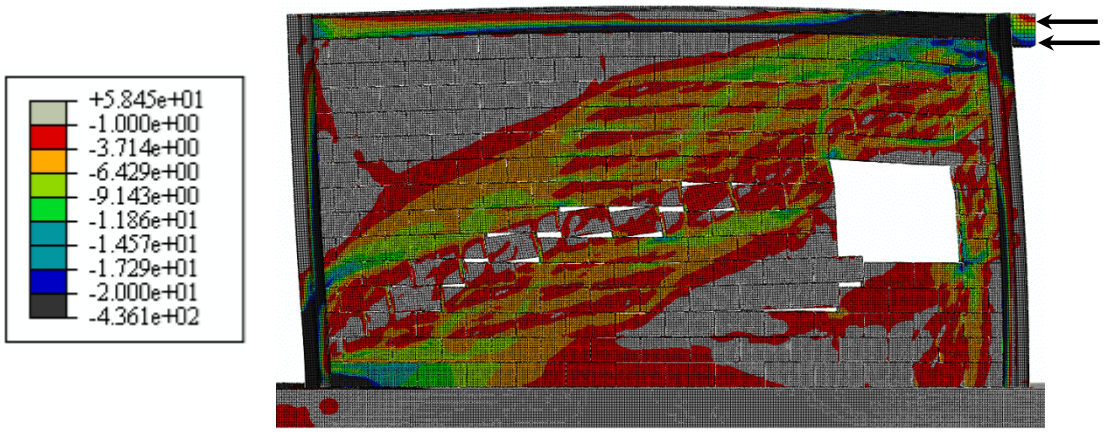

Figure 7-24: Principal compressive stresses at failure load in F46S-OW2L-50 (steel frame with an eccentric 800×800 mm opening and 0.5 wall aspect ratio) (MPa)

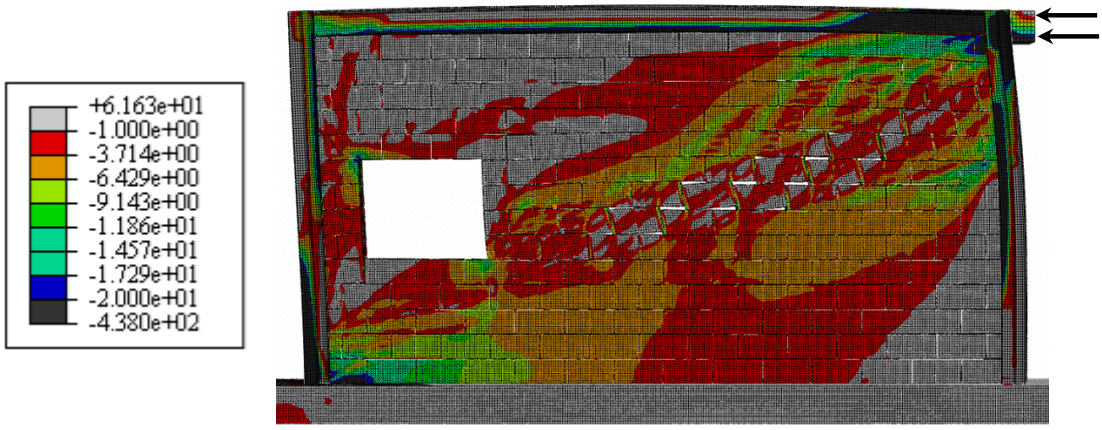

Figure 7-25: Principal compressive stresses at failure load F47S-OW2U-50 (steel frame with an eccentric 800×800 mm opening and 0.5 wall aspect ratio) (MPa)

7.3.2. Medium Size Window (1200×1000 mm)

Figures 7-26 through 7-29 show the lateral load-lateral displacement response for masonry infilled frames having a window opening of 1200×1000 mm placed at different locations. Values for the initial stiffness (K_{ini}), cracking load (P_{cr}), ultimate load (P_{ult}), and corresponding ultimate displacement (Δ_{ult}) of the masonry infilled frames are listed in Table 7-6.

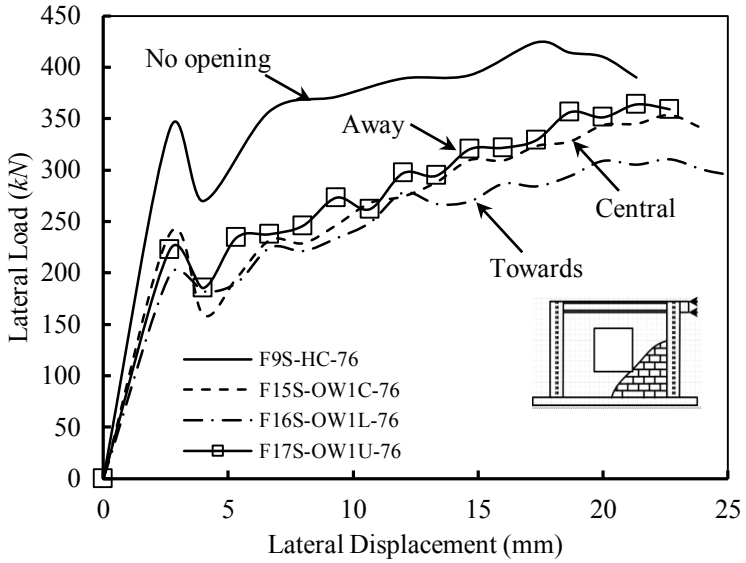

Figure 7-26: Lateral load-lateral displacement behaviour of masonry infilled steel frame with a 1200×1000 mm window at various locations and a wall aspect ratio of 0.76

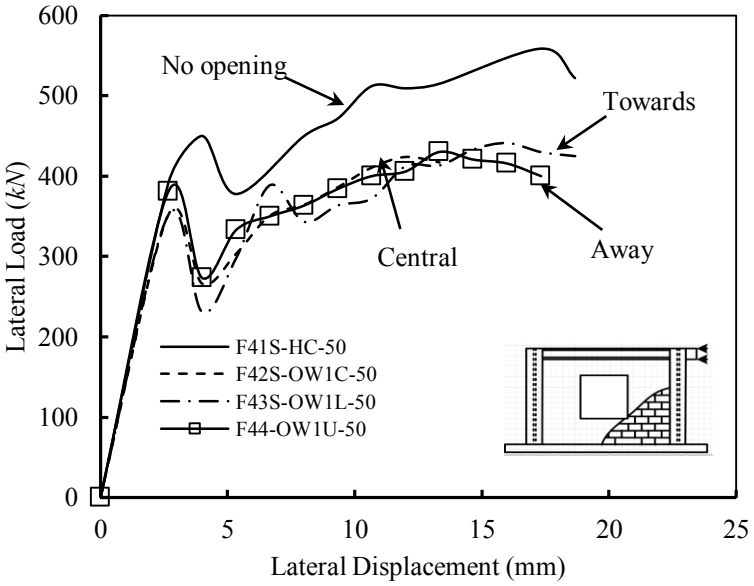

Figure 7-27: Lateral load-lateral displacement behaviour of masonry infilled steel frames with a 1200×1000 mm window at various locations and a wall aspect ratio of 0.5

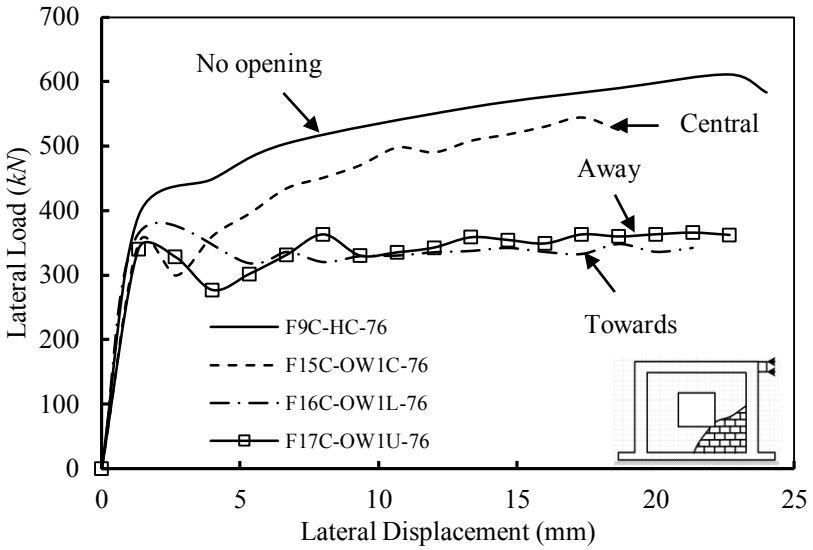

Figure 7-28: Lateral load-lateral displacement behaviour of masonry infilled RC frame with a 1200×1000 mm window at various locations and a wall aspect ratio of 0.76

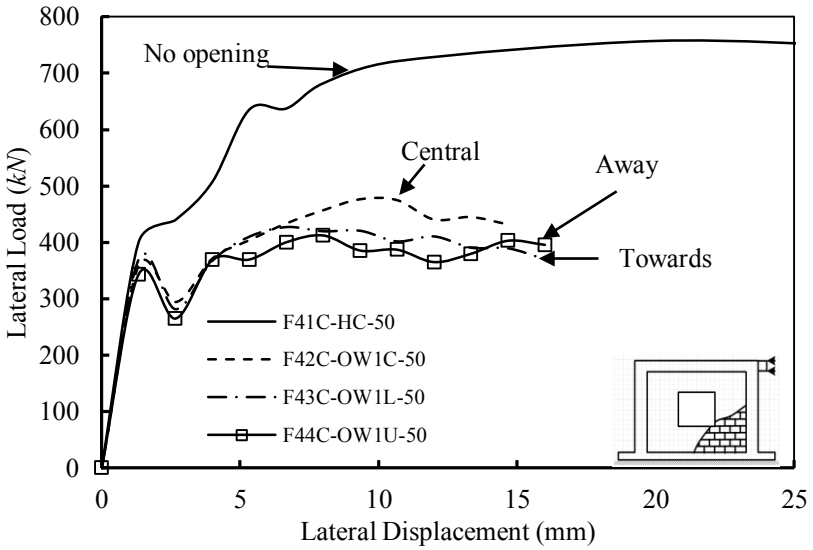

Figure 7-29: Lateral load-lateral displacement behaviour of masonry infilled RC frame with a 1200×1000 mm window at various locations and a wall aspect ratio of 0.5

Table 7-6: Summary of the FE results for masonry infilled frames with opening placed at different locations

Frame ID	Opening location†	K_{ini} (*kN/mm*)	P_{cr} (kN)	P_{ult} (kN)	Δ_{ult} (kN)	Failure mode*
F9S-HC-76	N/A	127.42	339.78	424.12	17.33	CC
F15S-OW1C-76	Central	89.41	238.44	353.33	22.67	DT+CC
F16S-OW1L-76	Towards	74.42	197.07	310.19	22.67	SS
F17S-OW1U-76	Away	83.41	222.43	363.75	21.33	DT+CC
F41S-HC-50	N/A	146.72	450.00	558.55	17.33	CC
F42S-OW1C-50	Central	131.83	351.55	424.21	12.00	DT+CC
F43S-OW1L-50	Towards	131.86	351.62	441.28	17.33	DT+CC
F44S-OW1U-50	Away	142.74	380.63	430.08	16.00	DT+CC
F9C-HC-76	N/A	293.84	391.80	611.15	22.67	CC
F15C-OW1C-76	Central	262.49	350.00	543.96	17.33	DT+CC
F16C-OW1L-76	Towards	274.15	365.53	365.50	1.33	DT+CC
F17C-OW1U-76	Away	255.48	340.65	365.93	21.33	DT+CC
F41C-HC-50	N/A	299.96	400.00	757.13	20.00	CC
F42C-OW1C-50	Central	269.98	360.00	476.84	9.33	SS
F43C-OW1L-50	Towards	277.50	370.00	426.79	6.67	SS
F44C-OW1U-50	Away	257.24	343.01	412.27	8.00	SS

*CC: Corner crushing, DT: Diagonal tension cracking, and SS: Sliding shear

† Eccentrically towards the load, Away: Eccentrically away from the load

For an aspect raito of 0.76, the presence of a medium size opening of dimension 1200×1000 mm towards and away from the load led to the formation of a single diagonal compression strut in the infill wall. Figures 7-30 and 7-31 show the principle stresses in the masonry infill wall at failure. The amount of interference between the opening and the compression strut was almost the same for both cases of opening location. At early loading stages, the interference of the openings with the developed strut was minimal which led to limited reduction in the initial stiffness and cracking load of 10% for infilled RC frames compared to solid infill walls. The width of the diagonal strut increased close to the ultimate load, and the amount of interference between the opening and the diagonal strut increased as a result leading to 40% reduction in the ultimate load. The infill wall failed due to diagonal tension cracking when the opening was located towards the load; hence, the ultimate displacement was less than for the case when the opening was further away from the applied load.

The bare steel frame had less initial stiffness (3.20 *kN/mm*) compared to the RC frame (22.61 *kN/mm*); the wall's share of the lateral load was more than in the case of RC frame. The reduction in the initial stiffness was 17% and 35% when the opening was towards and further away from the load, respectively, compared to a solid infill. On the other hand, the reduction in the cracking load was 56% in the case of an opening located towards the load and 35% for an opening located away from the load compared to a solid infilled frames. The presence of the diagonal tension cracks when the opening was located near the load weakened the infill wall and caused it to fail at lower load level (60% compared to solid infill walls) than when the opening was away from the load (86% compared to solid infill walls). The infilled frame was less stiff when the opening was away from the load and experienced improvement of 23% in the displacement corresponding to the ultimate load compared to solid infill walls.

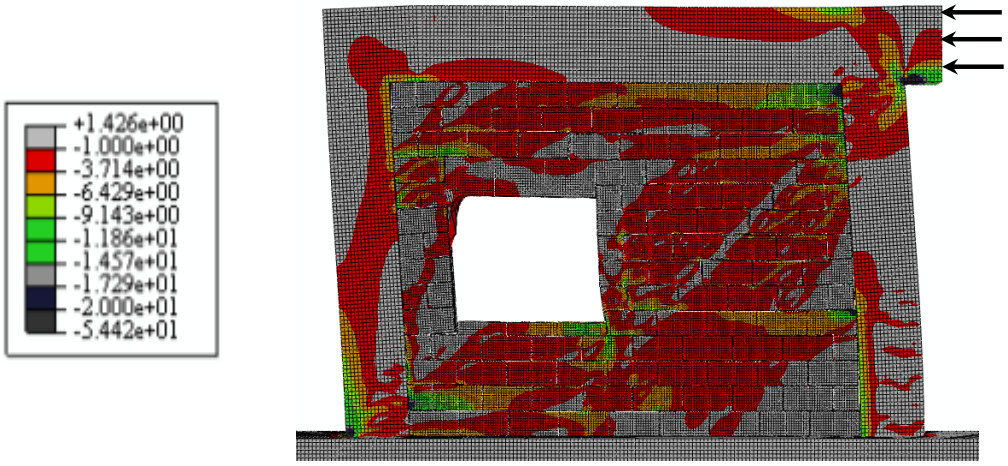

Figure 7-30: Principal compressive stresses at failure load in F17C-OW1U-76 (steel frame with an eccentric 1200×1000 mm opening and 0.76 wall aspect ratio) (MPa)

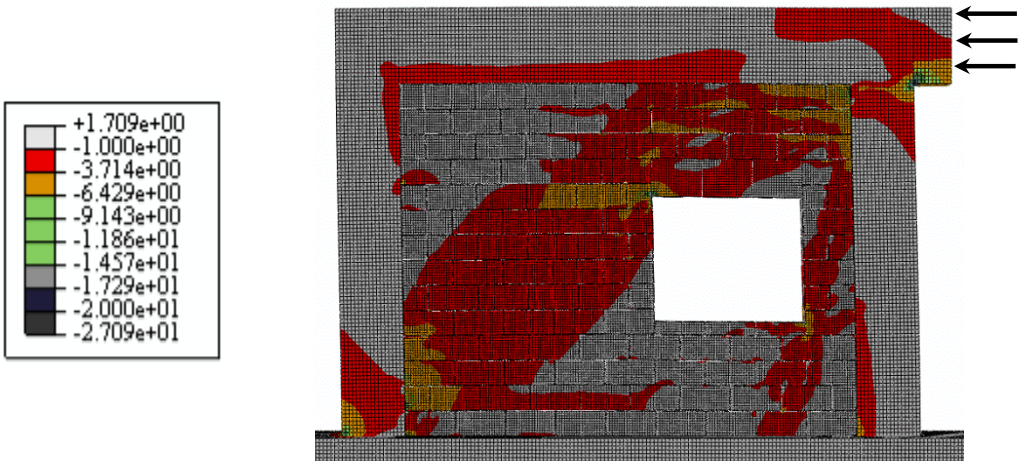

Figure 7-31: Principal compressive stresses at failure load in F16C-OW1L-76 (steel frame with an eccentric 1200×1000 mm opening and 0.76 wall aspect ratio) (MPa)

When the aspect ratio of the masonry infill wall was 0.5, changing the opening location towards and away from the load had a slight effect on the initial stiffness of infilled steel frames compared to a central opening. The reduction was 10% and 3% relative to the behaviour of solid infill wall for an opening towards and away from the loaded side, respectively. The cracking load was 15% lower when the opening was away from the loaded side compared to a solid infilled frame. Placing the opening away from the loaded side and centre of the wall minimized the interference with the developed strut leading to only reduction of 15% in the ultimate load compared to solid infill walls. Figures 7-32 and 7-33 show the principal stresses developed in the infilled steel frames at failure.

The behaviour of RC frames was influenced by the opening location more than steel frames with aspect ratio of 0.5. Unlike infilled steel frames, having the window opening located towards the loaded side had only slight effect on the initial stiffness and cracking load of the system (7% reduction compared to solid infill); the reduction was 14% for openings located away from the load compared to a solid infill. At early loading stages, the width of the compression strut was small and interference with the opening was lesser than when the opening was located towards the loaded side compared to the other two cases. The ultimate load, however, was significantly reduced when the opening was eccentric from the centre

of the wall. The reduction was 45% for both eccentric cases, towards and away from the loaded side.

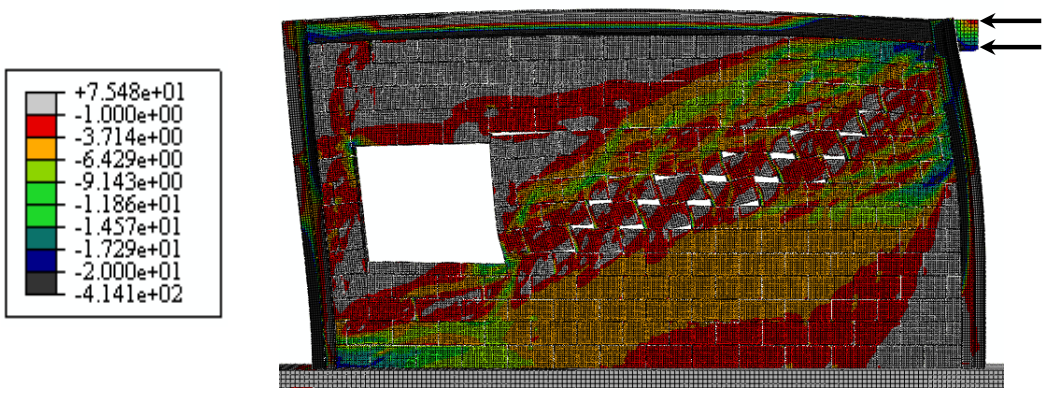

Figure 7-32: Principal compressive stresses at failure load in F44S-OW1U-50 (steel frame with an eccentric 1200×1000 mm opening and 0.5 wall aspect ratio) (MPa)

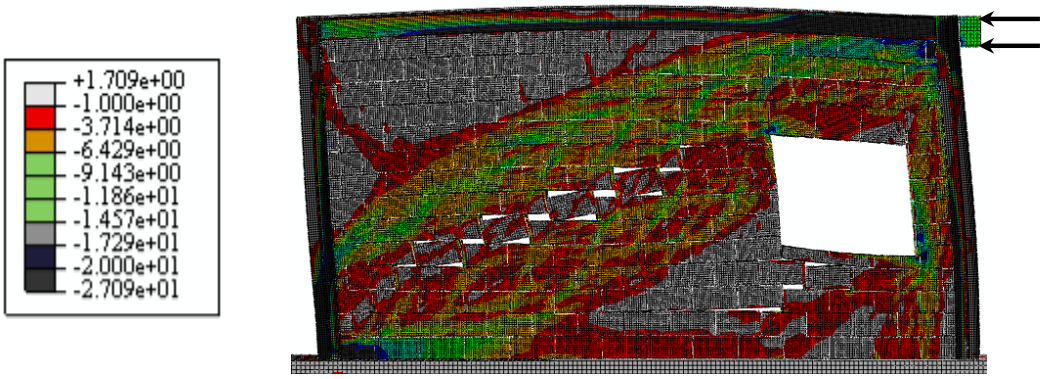

Figure 7-33: Principal compressive stresses at failure load in F43S-OW1L-50 (steel frame with an eccentric 1200×1000 mm opening and 0.5 wall aspect ratio) (MPa)

7.3.3. Large Size Window (2000×1000 mm)

Figures 7-34 through 7-37 show the lateral load-lateral displacement response for masonry infilled frames having a large window opening at different locations. Table 7-7 is a summary of the initial stiffness (K_{ini}), cracking load (P_{cr}), ultimate load (P_{ult}), corresponding ultimate displacement (Δ_{ult}) and failure mode of the masonry infilled frames.

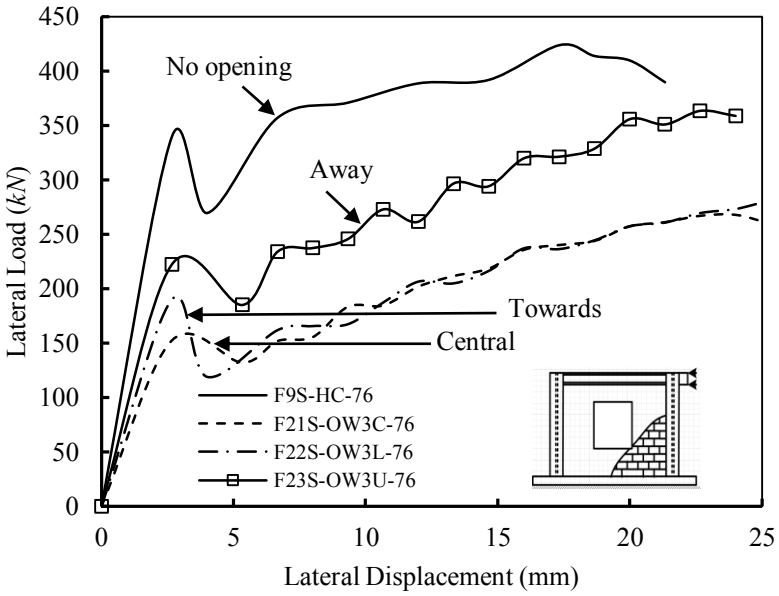

Figure 7-34: Lateral load-lateral displacement behaviour of masonry infilled steel frames with a 2000×1000 mm window at various locations and a wall aspect ratio of 0.76

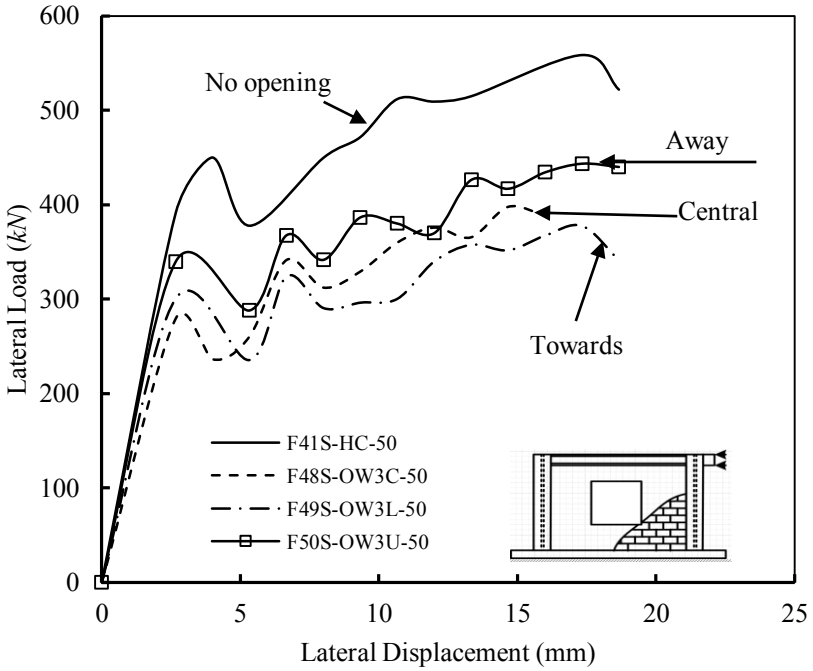

Figure 7-35: Lateral load-lateral displacement behaviour of masonry infilled steel frames with a 2000×1000 mm window at various locations and a wall aspect ratio of 0.5

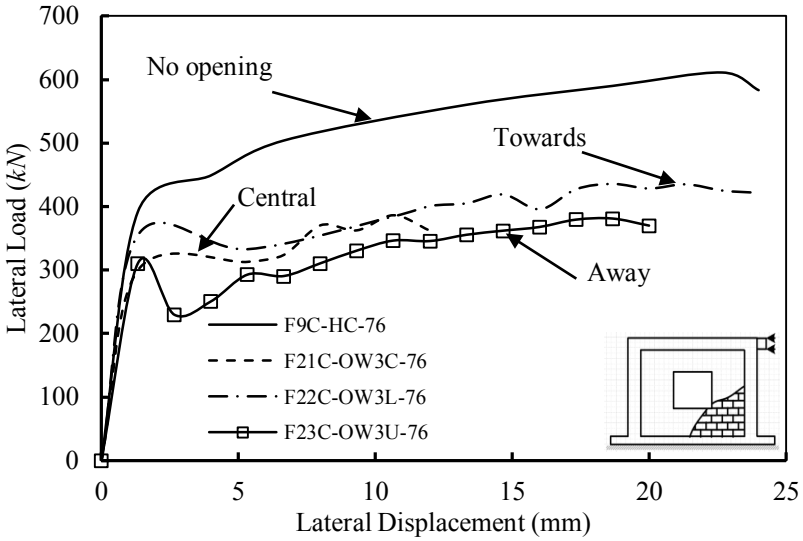

Figure 7-36: Lateral load-lateral displacement behaviour of masonry infilled RC frames with a 2000×1000 mm window at various locations and a wall aspect ratio of 0.76

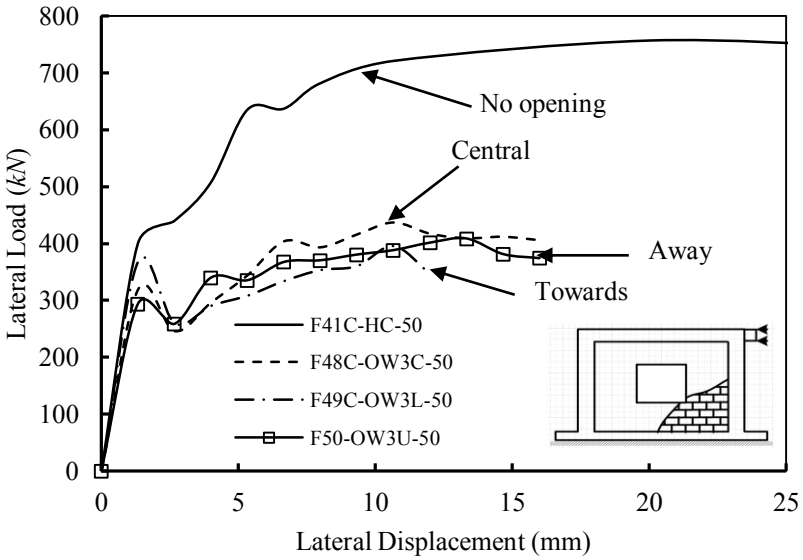

Figure 7-37: Lateral load-lateral displacement behaviour of masonry infilled RC frames with a 2000×1000 mm window at various locations and a wall aspect ratio of 0.5

Table 7-7: Summary of the FE results for masonry infilled frames with opening placed at different locations

Frame ID	Opening location†	K_{ini} (*kN/mm*)	P_{cr} (kN)	P_{ult} (kN)	Δ_{ult} (kN)	Failure mode*
F9S-HC-76	N/A	127.42	339.78	424.12	17.33	CC
F21S-OW3C-76	Central	57.25	152.68	268.26	24.00	SS+CC
F22S-OW3L-76	Towards	71.34	190.25	280.85	25.00	SS+CC
F23S-OW3U-76	Away	65.73	175.29	294.66	24.00	SS+CC
F41S-HC-50	N/A	146.72	450.00	558.55	17.33	CC
F48S-OW3C-50	Central	104.62	278.98	397.34	14.67	DT+CC
F49S-OW3L-50	Towards	112.74	300.63	377.76	17.33	DT+CC
F50S-OW3U-50	Away	127.37	339.66	443.46	17.33	SS+CC
F9C-HC-76	N/A	293.84	391.80	611.15	22.67	CC
F21C-OW3C-76	Central	244.99	300.00	386.12	10.67	SS+CC
F22C-OW3L-76	Towards	266.73	355.65	435.81	18.67	SS+CC
F23C-OW3U-76	Away	232.89	310.54	383.65	18.67	SS+CC
F41C-HC-50	N/A	299.96	400.00	757.13	20.00	CC
F48C-OW3C-50	Central	239.10	318.82	436.67	10.67	SS+CC
F49C-OW3L-50	Towards	276.29	368.42	395.91	10.67	SS+CC
F50C-OW3U-50	Away	220.32	293.78	408.92	13.33	SS+CC

*CC: Corner crushing, DT: Diagonal tension cracking, and SS: Sliding shear

† Eccentrically towards the load, Away: Eccentrically away from the load

For infilled steel frames with wall aspect ratio of 0.76, changing the opening location relative to the centre of the wall had a minor effect on initial stiffness, cracking load, and ultimate load. The reduction in initial stiffness and cracking load was 50% compared to a solid infill. The ultimate load was reduced by 44% compared to solid infilled frames. The infilled steel frame failed due to sliding shear formed from the horizontal component of the strut above the spandrel independent of the location of the opening

For RC frame with the same aspect ratio, initial stiffness and cracking load were reduced by 10% and 20% when the opening location changed from being close to being away from the load. The ultimate load was reduced by 30% and 37% when the opening was towards and further from the load, respectively, compared to a solid infill wall. Similar to steel frames with the same aspect ratio, the infill wall failed due to sliding shear along a bed joint at the top-left corner of the opening. The minor difference in the ultimate load might be attributed to the small

variation of the length of the sliding shear plane. The ultimate displacement was reduced by 18% in the case of eccentric openings.

For infill walls with aspect ratio 0.76, the presence of eccentric opening of 2000×1000 mm led to the formation of set of compression struts around the opening as shown in Figures 7-38 and 7-39. The eccentric nature of the opening led to the formation of small pier having a strut that is almost vertical. The developed strut in the spandrel had a small angle leading to high values of shear stresses along the bed joints in the pier away from the load causing sliding shear failure. Corner crushing of the masonry followed at a lower loading level. A similar behaviour was observed when the opening is eccentric towards the unloaded side. Due to the short length of the pier away from the load, sliding shear dominated the failure of this wall at that location. With further loading, corner crushing at the loaded side took place at loading level less than the ultimate load.

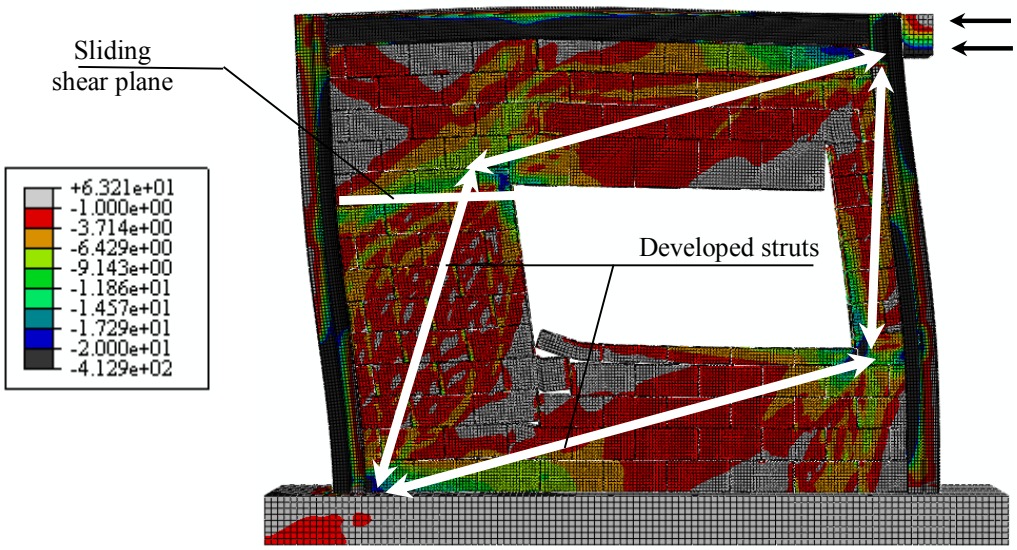

Figure 7-38: Principal compressive stresses at failure load in F22S-OW3L-76 (steel frame with an eccentric 2000×1000 mm opening and 0.76 wall aspect ratio) (MPa)

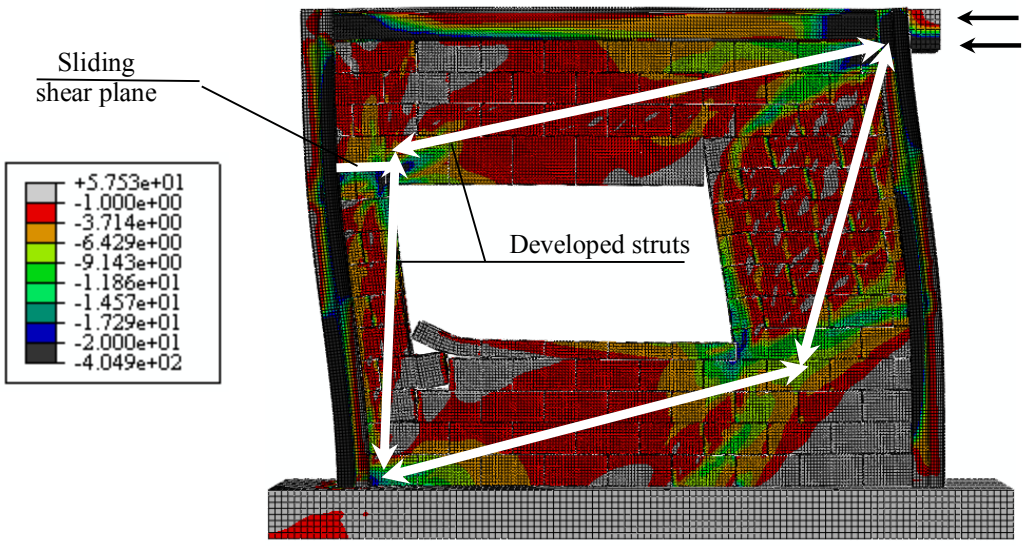

Figure 7-39: Principal compressive stresses at failure load in F23S-OW3U-76 (steel frame with eccentric 2000×1000 mm opening and 0.76 aspect ratio) (MPa)

For infilled steel frames with aspect ratio of 0.5, the presence of an eccentric opening towards the load increased the flexibility of the wall; hence, the initial stiffness of the infilled frame was reduced by 23% compared to solid infilled steel frames. The cracking load was also reduced by 33% compared to solid infilled steel frame. The ultimate lateral load for the case of a central window opening was an average value for the cases when the opening was located towards and away from the load. In the case of an eccentric opening towards the loaded side, the reduction in the ultimate load was 32% of that for solid infilled steel frames; whereas for the case of an opening away from the load, the reduction in the ultimate load was 21%.

When the opening was located away from the load, the infill wall stiffness was higher than when the opening was towards the load leading to reductions of only 13% and 25% in the initial stiffness and cracking load compared to solid infilled steel frames. The ultimate displacement did not experience any reduction in this case compared to the case of solid infilled frame. Figures 7-40 and 7-41show the principal compressive stresses and the developed struts for steel infilled frames with a 2000×1000 mm opening located towards and away from the load, respectively.

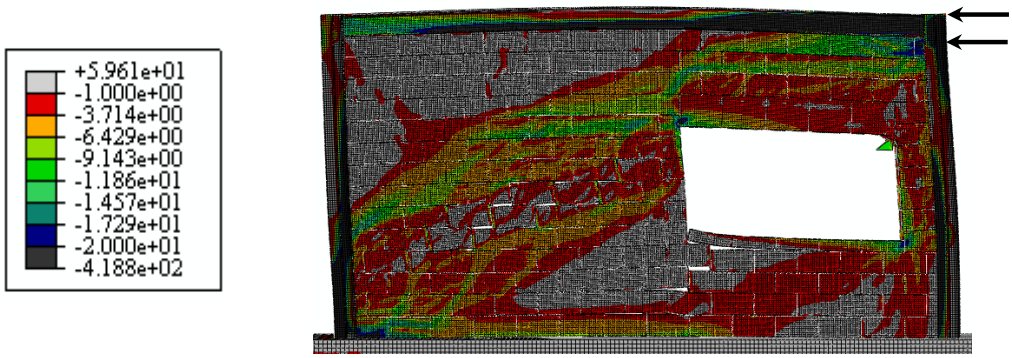

Figure 7-40: Principal compressive stresses at failure load in F49S-OW3L-50 (steel frame with an eccentric 2000×1000 mm opening and 0.5 wall aspect ratio) (MPa)

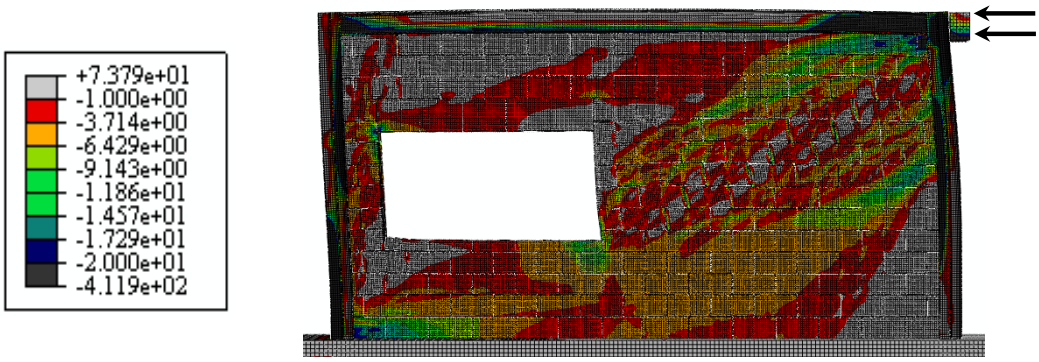

Figure 7-41: Principal compressive stresses at failure load in F50S-OW3U-50 (steel frame with an eccentric 2000×1000 mm opening and 0.5 wall aspect ratio) (MPa)

For RC frame with an infill wall having an aspect ratio of 0.5, the infill wall failed due to sliding shear along bed joints at the top of the window opening. The rigidity of the RC beam-column connection led to the transfer of the load horizontally to the wall. When the opening was located towards the load, the strut in the spandrel formed at almost a horizontal angle leading to a small reduction in the initial stiffness and cracking load of value 8% compared to solid infilled RC frames. However, when the opening was away from the load, the force in the spandrel was lower and the reduction in initial stiffness and cracking load was 27%. The reduction in the ultimate lateral load and corresponding displacement was 48% for both cases of eccentric openings compared to solid masonry infilled RC frames.

The infilled frame was more flexible for the case with the opening away from the load. Figures 7-42 and 7-43 show the principal compression stresses at failure for infilled RC frames with eccentric opening and wall aspect ratio of 0.5.

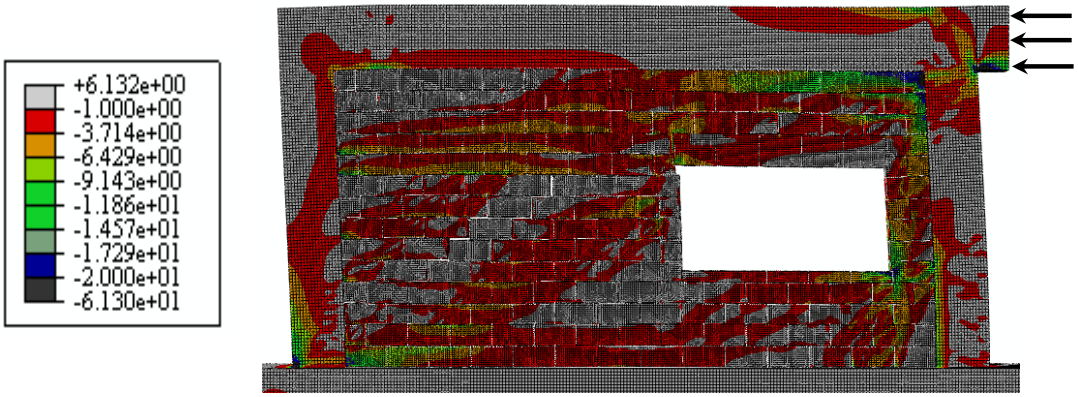

Figure 7-42: Principal compressive stresses at failure load in F49C-OW3L-50 (steel frame with an eccentric 2000×1000 mm opening and 0.5 wall aspect ratio) (MPa)

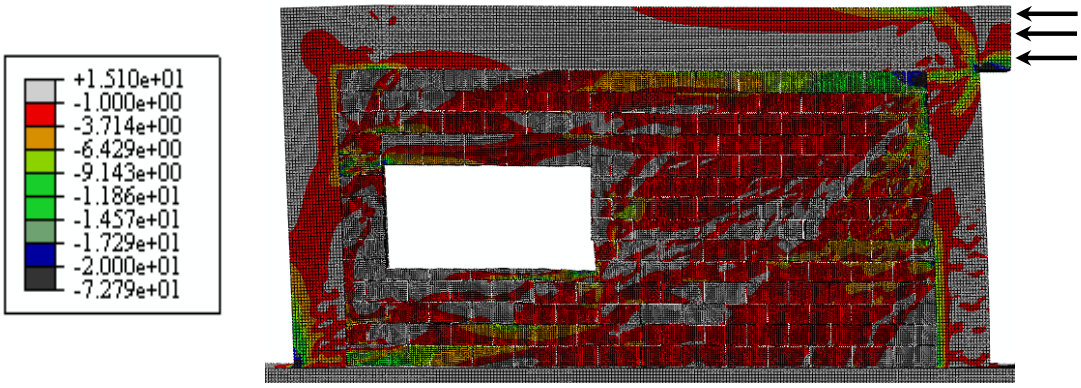

Figure 7-43: Principal compressive stresses at failure load in F50C-OW3U-50 (steel frame with an eccentric 2000×1000 mm opening and 0.5 wall aspect ratio) (MPa)

7.3.4. Door Opening (800×2200 mm)

Figures 7-44 through 7-47 show the lateral load-lateral displacement response for masonry infilled frames having a door opening at different locations. The initial stiffness (K_{ini}), cracking load (P_{cr}), ultimate load (P_{ult}), corresponding ultimate displacement (Δ_{ult}) values and failure modes of the masonry infill frames are summarized in Table 7-8.

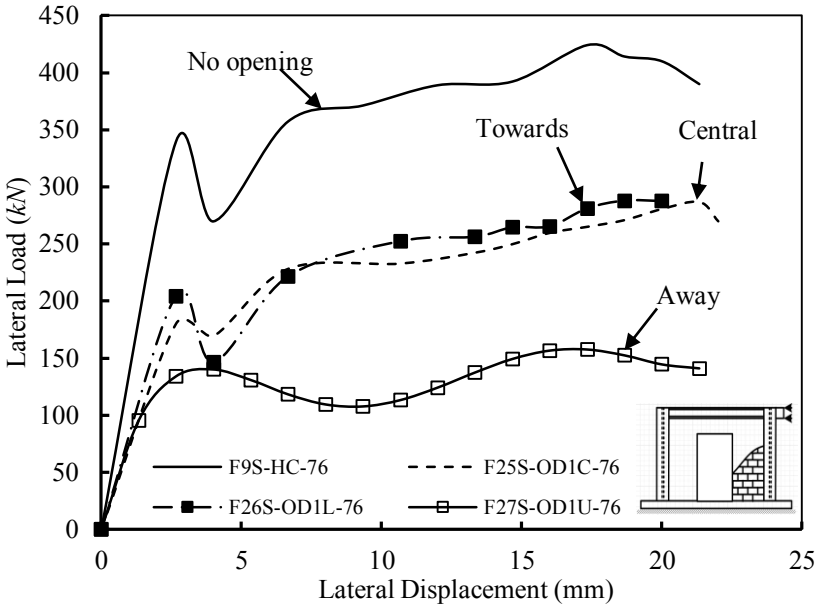

Figure 7-44: Lateral load-lateral displacement behaviour of masonry infilled steel frames with a 800×2200 mm door at various locations and 0.76 wall aspect ratio

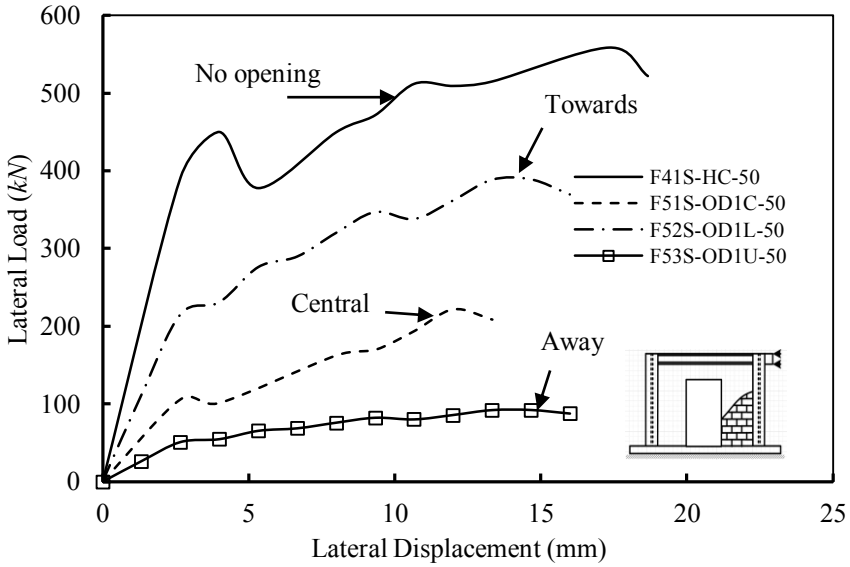

Figure 7-45: Lateral load-lateral displacement behaviour of masonry infilled steel frames with a 800×2200 mm door at various locations and 0.5 wall aspect ratio

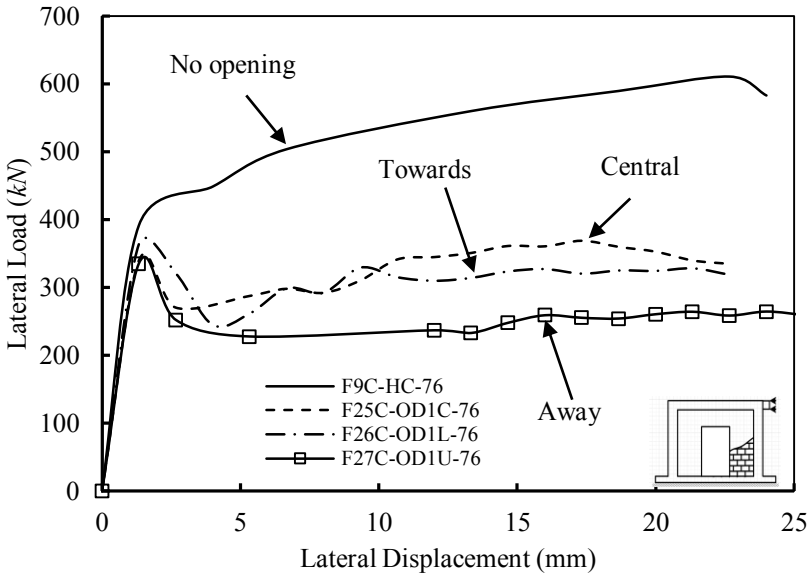

Figure 7-46: Lateral load-lateral displacement behaviour of masonry infilled RC frames with a 800×2200 mm door at various locations and 0.76 aspect ratio

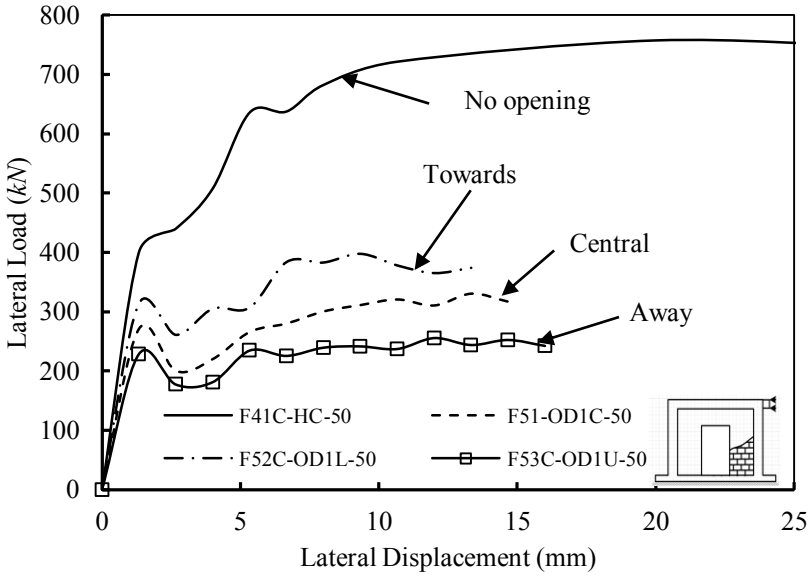

Figure 7-47: Lateral load-lateral displacement behaviour of masonry infilled RC frame with a 800×2200 mm door at various locations and 0.5 wall aspect ratio

Table 7-8: Summary of the FE results and failure mode of for masonry infill frames with different location of an openings

Frame ID	Opening location†	K_{ini} (*kN/mm*)	P_{cr} (kN)	P_{ult} (kN)	Δ_{ult} (kN)	Failure mode*
F9S-HC-76	N/A	127.42	339.78	424.12	17.33	CC
F25S-OD1C-76	Central	67.62	180.32	286.86	21.33	DT+SS
F26S-OD1L-76	Towards	76.66	204.44	287.61	18.67	DT+CC
F27S-OD1U-76	Away	71.51	134.10	157.58	17.33	DT+SS
F41S-HC-50	N/A	146.72	450.00	558.55	17.33	CC
F51S-OD1C-50	Central	39.69	105.84	221.83	12.00	SS
F52S-OD1L-50	Towards	83.98	111.98	389.46	14.67	DT+CC
F53S-OD1U-50	Away	20.00	51.04	92.28	14.67	DT+SS
F9C-HC-76	N/A	293.84	391.80	611.15	22.67	CC
F25C-OD1C-76	Central	254.98	340.00	369.07	17.33	DT+SS
F26C-OD1L-76	Towards	273.25	364.35	364.35	1.33	DT+SS
F27C-OD1U-76	Away	251.73	335.67	335.67	1.33	DT+SS
F41C-HC-50	N/A	299.96	400.00	757.13	20.00	CC
F51C-OD1C-50	Central	203.12	270.84	330.35	13.33	SS
F52C-OD1L-50	Towards	234.85	313.15	397.16	9.33	SS
F53C-OD1U-50	Away	171.41	228.56	255.62	12.00	SS

*CC: Corner crushing, DT: Diagonal tension cracking, and SS: Sliding shear

† Eccentrically towards the load, Away: Eccentrically away from the load

Figures 7-48 and 7-49 shows the principal compressive stresses developed in masonry infilled steel frames having a door opening of 800×2200 mm and wall aspect ratio of 0.76. The presence of a door opening towards the loaded side led to the formation of a single strut in the masonry infill wall, unlike the case of a central opening. The opening interfered with part of the diagonal strut. The reduction in initial stiffness and cracking load was 40% compared to solid infilled steel frames with the same aspect ratio. The reduction in the ultimate load was the same as the case of a central opening (32% reduction compared to solid infilled steel frames). The ultimate displacement was found to be 8% higher than solid infilled frames.

When the opening in the infilled steel frame of aspect ratio 0.76 was away from the load, a diagonal compression strut was formed from the loaded side till the corner of the pier towards the load. The confinement provided by the frame to the infill wall was lost, and the initial stiffness of the infilled system was less than

central door opening and door opening eccentric towards the load (44% reduction compared to solid infilled steel frame). The first crack took the form of stepwise diagonal tension crack along the diagonal strut. The reduction in the cracking and ultimate loads was 62% compared to solid infilled steel frames due to sliding shear formation at the bottom of the pier located towards the load. The ultimate displacement corresponding to the ultimate load was the same as the case of a solid infilled steel frame.

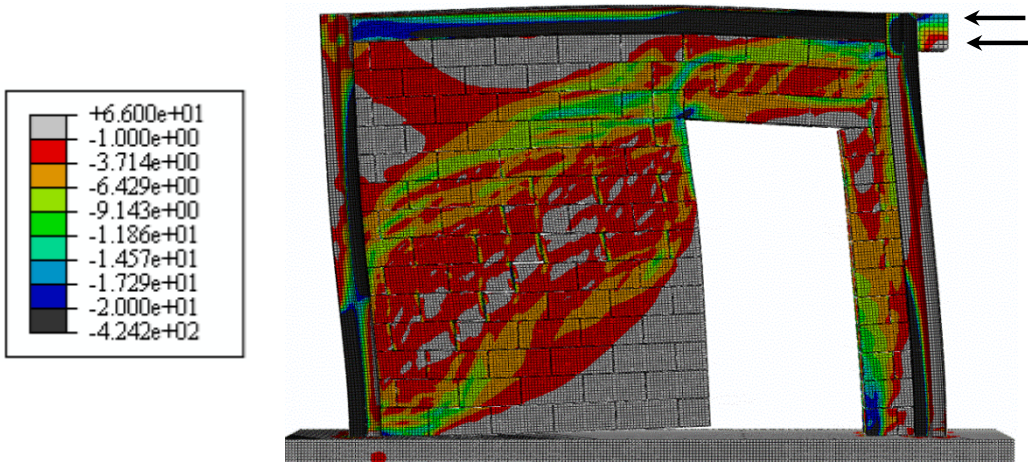

Figure 7-48: Principal compressive stresses at failure load in F26S-OD1L-76 (infilled steel frame with an 800×2200 mm opening and 0.76 wall aspect ratio) (MPa)

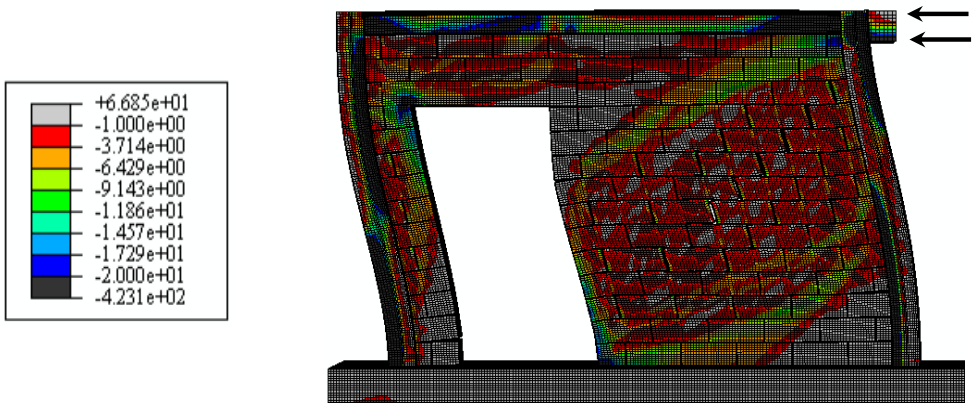

Figure 7-49: Principal compressive stresses at failure load in F27S-OD1L-76 (infilled steel frame with an 800×2200 mm opening and 0.76 wall aspect ratio) (MPa)

Figures 7-50 and 7-51 show the principal compressive stresses for infilled RC frame with wall aspect ratio of 0.76. When the opening was located towards the loaded side, the rigid beam-column connection resulted in the formation of high level of horizontal force in the spandrel above the opening. The infill wall failed due to mixed mode of diagonal tension crack in the pier away from the load and sliding shear along the bed joint at the top of the opening. The reduction in initial stiffness and cracking load was 7% compared to a solid infilled RC frame having the same aspect ratio. The ultimate load was slightly reduced compared to a central opening. The reduction in the ultimate load was 32% compared to solid infilled RC frame. The wall failed in diagonal tension cracking leading to lower ultimate displacement compared to a solid infilled RC frame.

Similar to the steel frame having 0.76 aspect ratio, when the opening was located away from the load, a single diagonal strut was formed in the pier towards the load in the infilled RC frame with the same aspect ratio for a door opening located away from the load. The initial stiffness and cracking load were higher than the case of central door opening. The reduction in the initial stiffness and cracking load was 14% and the reduction in the ultimate load was 45% compared to a solid infilled RC frame. Failure was dominated by diagonal tension cracking followed by sliding shear at the bottom of the pier towards the load. The ultimate displacement coincided with the diagonal tension cracking incidence.

The principal compressive stresses for infilled steel frames with aspect ratio of 0.5 and an eccentric door opening are shown in Figures 7-52 and 7-53.When the door opening was located towards the load, a single diagonal strut was formed in the opening; part of this diagonal strut was interfered by the opening. The initial stiffness of masonry infilled frame was reduced by 43% compared to solid infilled steel frame. The first crack in the infill wall was a stepwise crack at the top loaded corner of the infill wall; the reduction in cracking load was 75% compared to a solid infilled steel frame. The infill wall resisted more load until crushing of the masonry took place at the corners of the developed strut. The reduction in the ultimate load was less than for the case of a central opening (30% reduction compared to a solid infilled steel frame).

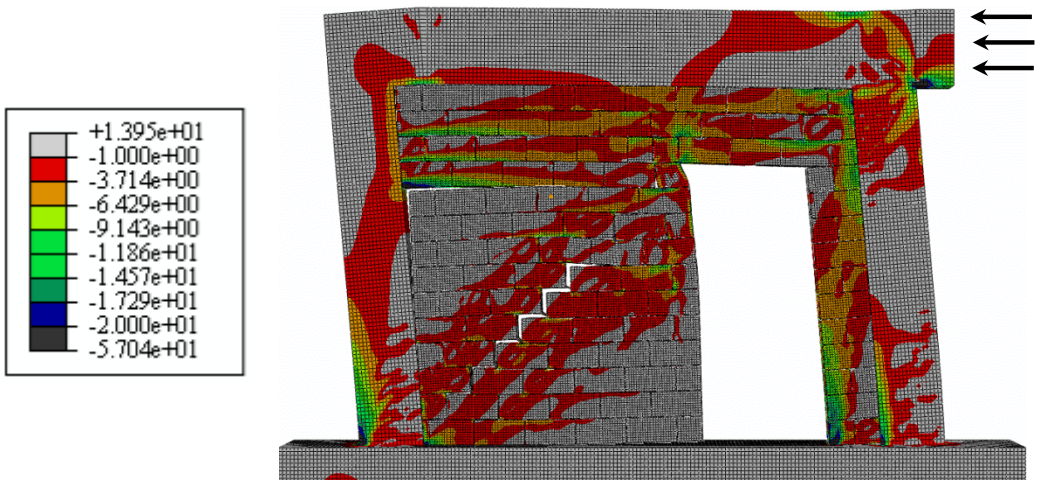

Figure 7-50: Principal compressive stresses at failure load in F26C-OD1L-76 (infilled RC frame with an 800×2200 mm opening and 0.76 wall aspect ratio) (MPa)

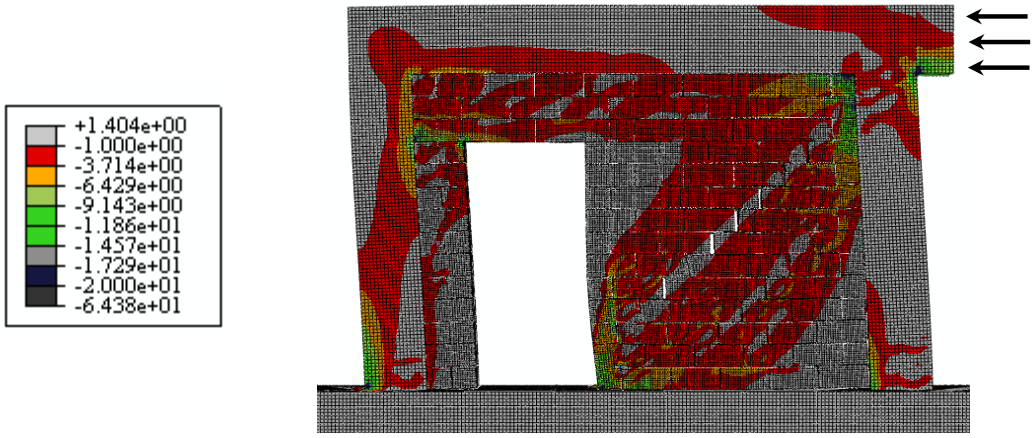

Figure 7-51: Principal compressive stresses at failure load in F27C-OD1L-76 (infilled RC frame with an 800×2200 mm opening and 0.76 wall aspect ratio) (MPa)

When the door opening was eccentric away from the load, a diagonal compression strut was formed in the pier towards the load. The confinement of the steel frame to the masonry infill wall was lost in this case due to lack of contact between the frame and the masonry infill wall. The initial stiffness of the wall was less than the case of opening eccentric towards the load. The reduction in initial stiffness and cracking load was 14% and 12%, respectively, compared to a solid infilled steel frame. Failure of the wall took place in the form of stepwise diagonal

tension cracking along the developed strut followed by sliding shear at the base of the pier towards the load. This mode of failure led to a reduction of 83% in the ultimate load.

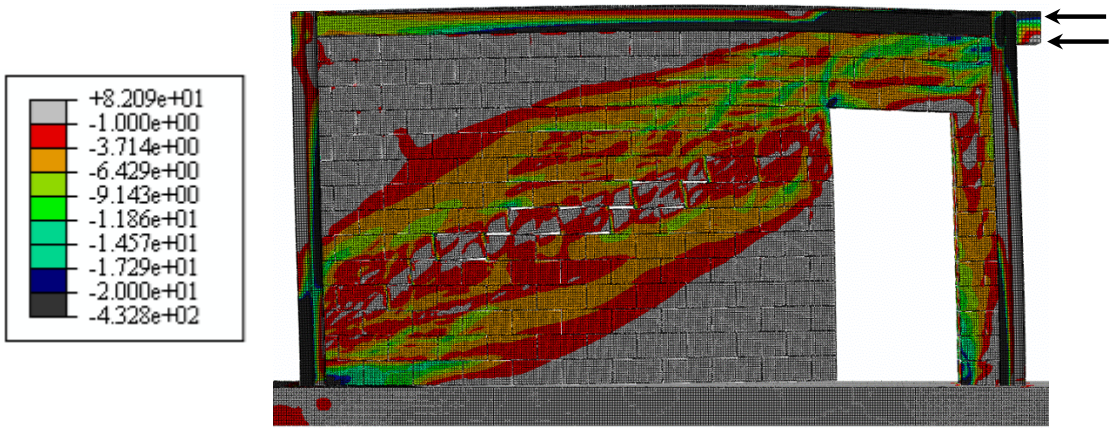

Figure 7-52: Principal compressive stresses at failure load in F52S-OD1L-50 (infilled steel frame with an 800×2200 mm opening and 0.5 wall aspect ratio) (MPa)

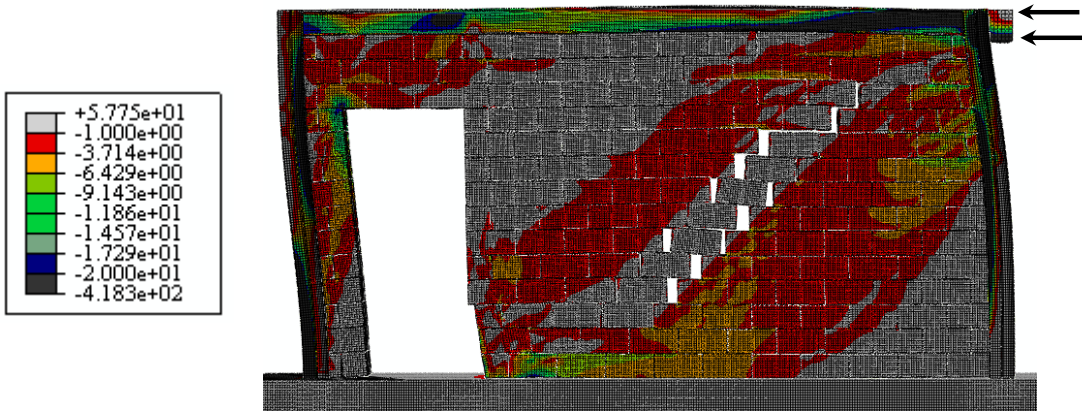

Figure 7-53: Principal compressive stresses at failure load in F53S-OD1U-50 (infilled steel frames with an 800×2200 mm opening and 0.5 wall aspect ratio) (MPa)

Figures 7-54 and 7-55 show the principal compressive stresses acting on a masonry infilled RC frame with an eccentric door opening and an aspect ratio of 0.5. Similar to infilled RC frame with an aspect ratio of 0.76, the rigidity of the beam-column connection of the RC frame led to the development of high horizontal load in the spandrel above the opening for infilled RC frame with an aspect ratio of

0.5 leading to sliding shear along a bed joint at the top of the opening. The initial stiffness and cracking load were less than for the case of a central opening. The reduction was 22% for both the initial stiffness and cracking load compared to a solid infilled RC frame. The ultimate load was almost the same as for the case of central opening as sliding shear was the dominating mode of failure (reduction of 48% in the ultimate load compared to a solid infilled frame).

When the door opening was away from the load, a diagonal strut was formed in the pier towards the load followed by a diagonal tension crack. The initial stiffness and cracking load were reduced more than for the case of central opening due to the lack of confinement provided by the frame to the infill (43% reduction compared to a solid infill wall). The wall failed at a lower ultimate load than the case of central opening (66% reduction compared to solid infill wall), and the ultimate displacement was slightly improved.

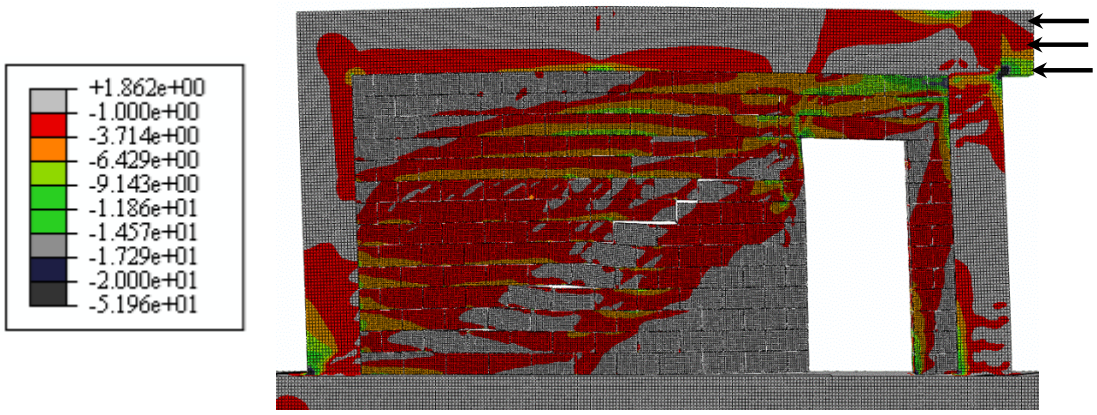

Figure 7-54: Principal compressive stresses at failure load in F52C-OD1L-50 (infilled RC frame with an 800×2200 mm opening and 0.5 wall aspect ratio) (MPa)

Figure 7-55: Principal compressive stresses at failure load in F53C-OD1U-50 (infilled RC frames with an 800×2200 mm opening and 0.5 wall aspect ratio) (MPa)

7.4. Effect of Openings on Stiffness and Resistance

The results of the finite element models with window/door openings were compared against the corresponding case where no opening was introduced. The comparative results are listed in Tables 7-9 through 7-12 for masonry infilled steel and RC frames with different aspect ratios.

Table 7-9: Normalized initial stiffness, cracking load, ultimate load and corresponding displacement for infilled steel frames with openings and $h/l = 0.76$

Frame ID	Opening (%)	Opening location	Ratio to solid infilled frame (F9S-HC-76)			
			K_{ini}	P_{cr}	P_{ult}	Δ_{ult}
F18S-OW2C-76	6.5	Central	0.77	0.77	0.91	1.23
F19S-OW2L-76	6.5	Towards	0.65	0.65	0.90	1.15
F20S-OW2U-76	6.5	Away	0.67	0.67	0.91	1.44
F15S-OW1C-76	12.0	Central	0.70	0.70	0.83	1.31
F16S-OW1L-76	12.0	Towards	0.83	0.44	0.60	0.51
F17S-OW1U-76	12.0	Away	0.65	0.65	0.86	1.23
F25S-OD1C-76	17.5	Central	0.53	0.53	0.68	1.23
F26S-OD1L-76	17.5	Towards	0.60	0.60	0.68	1.08
F27S-OD1U-76	17.5	Away	0.56	0.39	0.37	1.00
F21S-OW3C-76	20.0	Central	0.45	0.45	0.63	1.38
F22S-OW3L-76	20.0	Towards	0.56	0.56	0.66	1.44
F23S-OW3U-76	20.0	Away	0.52	0.52	0.69	1.38

Table 7-10: Normalized initial stiffness, cracking load, ultimate load and corresponding displacement for infilled steel frames with openings and $h/l = 0.5$

Frame ID	Opening (%)	Opening location†	Ratio to solid infilled frame (F41S-HC-50)			
			K_{ini}	P_{cr}	P_{ult}	Δ_{ult}
F45S-OW2C-50	4.1	Central	0.89	0.78	0.85	0.85
F46S-OW2L-50	4.1	Towards	0.93	0.81	0.81	0.85
F47S-OW2U-50	4.1	Away	0.96	0.84	0.81	0.69
F42S-OW1C-50	7.7	Central	0.90	0.78	0.76	0.69
F43S-OW1L-50	7.7	Towards	0.90	0.78	0.84	1.00
F44S-OW1U-50	7.7	Away	0.97	0.85	0.85	0.92
F51S-OD1C-50	11.2	Central	0.27	0.24	0.40	0.69
F52S-OD1L-50	11.2	Towards	0.57	0.25	0.70	0.85
F53S-OD1U-50	11.2	Away	0.14	0.11	0.17	0.85
F48S-OW3C-50	12.8	Central	0.71	0.62	0.71	0.85
F49S-OW3L-50	12.8	Towards	0.77	0.67	0.68	1.00
F50S-OW3U-50	12.8	Away	0.87	0.75	0.79	1.00

Table 7-11: Normalized initial stiffness, cracking load, ultimate load and corresponding displacement for infilled RC frames with openings and $h/l = 0.76$

Frame ID	Opening (%)	Opening location	Ratio to solid infilled frame (F9C-HC-76)			
			K_{ini}	P_{cr}	P_{ult}	Δ_{ult}
F18C-OW2C-76	6.5	Central	0.98	0.98	0.94	0.59
F19C-OW2L-76	6.5	Towards	1.00	1.00	0.90	0.65
F20C-OW2U-76	6.5	Away	0.89	0.89	0.92	0.65
F15C-OW1C-76	12.0	Central	0.89	0.89	0.89	0.76
F16C-OW1L-76	12.0	Towards	0.93	0.93	0.60	0.06
F17C-OW1U-76	12.0	Away	0.87	0.87	0.60	0.94
F25C-OD1C-76	17.5	Central	0.87	0.87	0.60	0.76
F26C-OD1L-76	17.5	Towards	0.93	0.93	0.60	0.06
F27C-OD1U-76	17.5	Away	0.86	0.86	0.55	0.06
F21C-OW3C-76	20.0	Central	0.83	0.77	0.63	0.47
F22C-OW3L-76	20.0	Towards	0.91	0.91	0.71	0.82
F23C-OW3U-76	20.0	Away	0.79	0.79	0.63	0.82

Table 7-12: Normalized initial stiffness, cracking load, ultimate load and corresponding displacement for infilled RC frames with openings and *h/l* = 0.5

Frame ID	Opening (%)	Opening location†	Ratio to F41S-HC-50			
			K_{ini}	P_{cr}	P_{ult}	Δ_{ult}
F45C-OW2C-50	4.1	Central	0.95	0.71	0.61	0.67
F46C-OW2L-50	4.1	Towards	0.94	0.94	0.55	0.53
F47C-OW2U-50	4.1	Away	0.92	0.92	0.55	0.60
F42C-OW1C-50	7.7	Central	0.90	0.90	0.63	0.47
F43C-OW1L-50	7.7	Towards	0.93	0.93	0.56	0.33
F44C-OW1U-50	7.7	Away	0.86	0.86	0.54	0.40
F51C-OD1C-50	11.2	Central	0.68	0.68	0.44	0.67
F52C-OD1L-50	11.2	Towards	0.78	0.78	0.52	0.47
F53C-OD1U-50	11.2	Away	0.57	0.57	0.34	0.60
F48C-OW3C-50	12.8	Central	0.80	0.80	0.58	0.53
F49C-OW3L-50	12.8	Towards	0.92	0.92	0.52	0.53
F50C-OW3U-50	12.8	Away	0.73	0.73	0.54	0.67

7.4.1. Initial Stiffness and Cracking Load

As shown in Figures 7-56 through 7-59, the presence of a window opening within the infill wall led to a reduction in initial stiffness of the infilled system. The reduction is more notable for frames with an aspect ratio of 0.76. An opening with a surface area of 20% of the infill wall surface area within steel frames having an aspect ratio of 0.76 resulted in a reduction in initial stiffness and cracking load of 60% compared to only 20% in case of masonry infill RC frame. The RC frame had higher stiffness (22.61 *kN/mm*) compared to the stiffness of the steel frame (*3.20 kN/mm*). The lesser reduction in the case of RC frames may be attributed to the rigidity of the beam-column connection compared to the steel frame.

For a medium window opening (1200×1000 mm) with a surface area of 12% of the infill wall area and eccentric towards the load, the reduction in initial stiffness was less than for the cases of a central opening and an opening eccentric away from the load. The amount of interference between the opening and the developed diagonal strut is smaller than for the case of central and eccentrically

away from the load which led to stiffer behaviour for the infill wall. The reduction was 17% in this case compared to solid infilled steel frames.

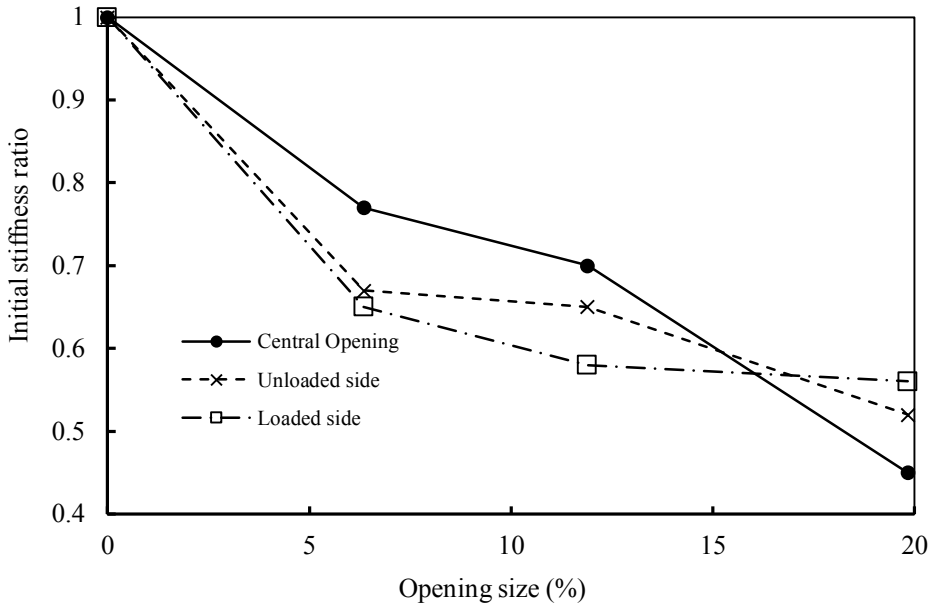

Figure 7-56: Effect of window opening size on the initial stiffness of masonry infilled steel frames with 0.76 wall aspect ratio

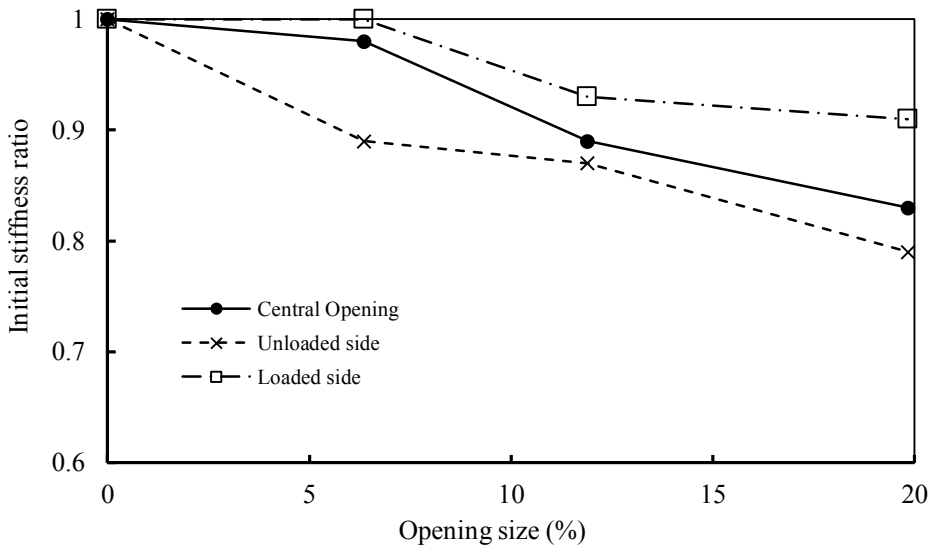

Figure 7-57: Effect of window opening size on the initial stiffness of masonry infilled RC frames with 0.76 wall aspect ratio

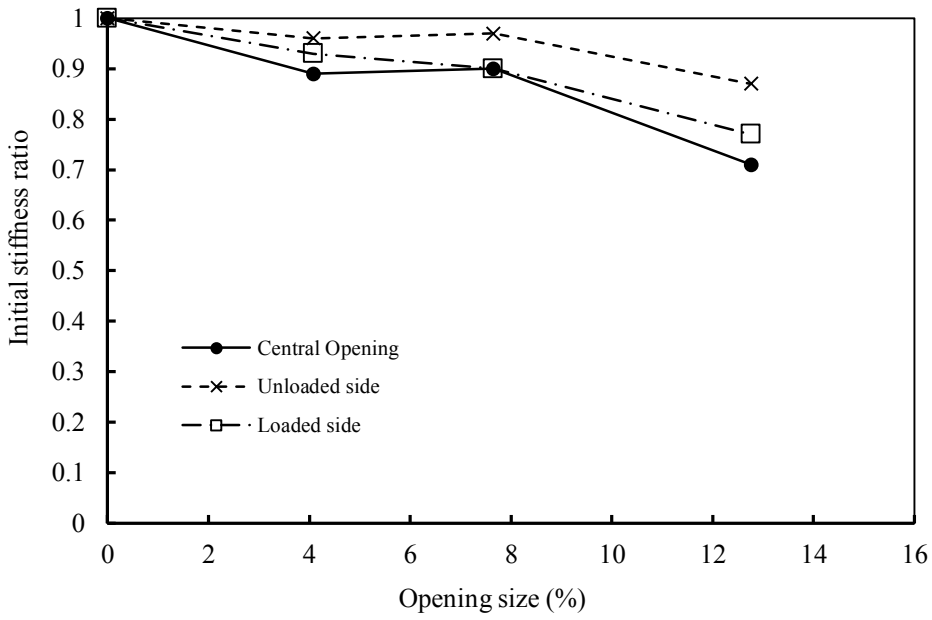

Figure 7-58: Effect of window opening size on the initial stiffness of masonry infilled steel frames with 0.5 wall aspect ratio

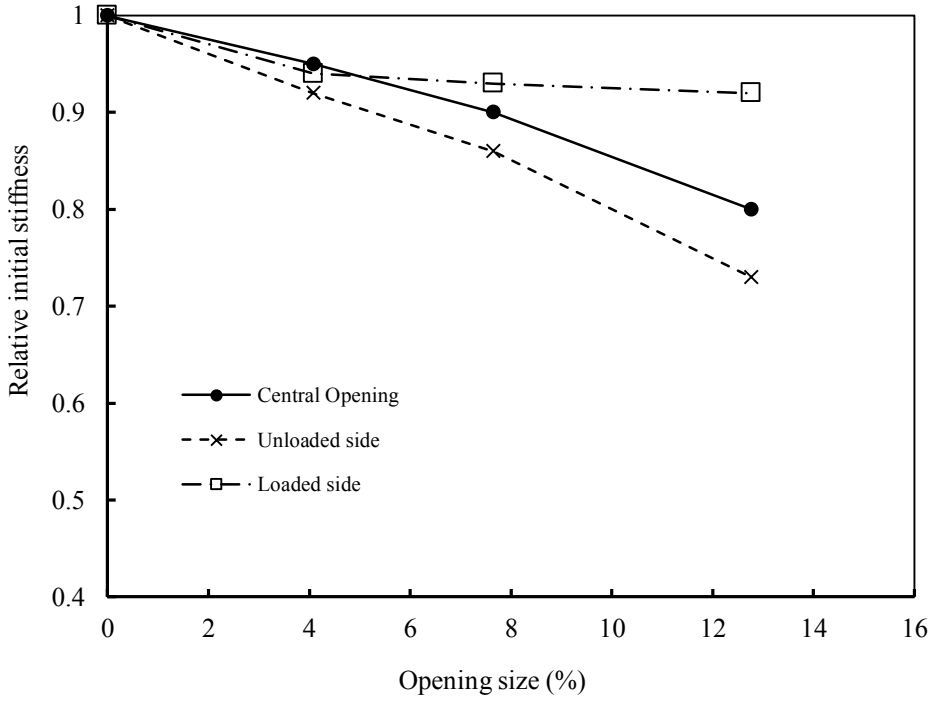

Figure 7-59: Effect of window opening size on the initial stiffness of masonry infilled RC frames with 0.5 wall aspect ratio

When the aspect ratio of the masonry infill wall was 0.5, the effect of opening size and location on the initial stiffness of both infilled steel and RC frames was similar. The contribution of the stiffness of the wall was larger compared to that of the frame. The lateral load was resisted mainly by the infill wall. This led to minor differences in the cracking load between steel and RC frames.

The presence of a door opening within the infilled steel and RC frames reduced the initial stiffness more than a large window opening. Unlike the presence of infilled frame with a window opening, the door opening cut through the entire height of the wall forcing the wall to behave as two separate piers joined by a spandrel, unlike the presence of the window opening.

When a large window opening (2000×1000 mm) was introduced in the infilled steel frame, the reduction in initial stiffness was lesser than when the opening was away from the load. A group of struts were formed around central openings; however, an eccentric opening resulted in the formation of a single diagonal strut, which is stiffer. When the opening was away from the load, the interference with the strut was smaller; and the reduction in initial stiffness was smaller as a result.

7.4.2. Ultimate Load and Displacement

Figures 7-60 through 7-63 show the effect of window opening size on the ultimate lateral load. An opening that is 20% of the infill wall surface area within a steel frame having a wall aspect ratio of 0.76 resulted in a reduction in the ultimate load of 40% for both infilled steel and RC frames.

A door opening that is 17.5% of the infill wall surface area eccentric towards the load did not prevent the development of a single strut in the wall. The interference between the diagonal strut and the opening in this case was minimal leading to reduction in the ultimate load similar to the case of a central opening of the same size (reduction of 32% compared to solid infilled steel frame). When the opening was eccentric away from the load, the diagonal strut did not fully develop. The masonry pier in this case had lesser stiffness as it was not confined by the frame. The reduction in the ultimate load in this case was higher compared to the

cases of a central opening and an eccentric opening towards the load (62% reduction in the ultimate load compared to solid infilled RC frame).

For an infilled steel frame with a large window opening of area that is 20% of the infill wall surface area, the ultimate load was reduced by 34%, 37% and 31% for an opening eccentric towards the load, central opening, and eccentric opening away from the load; respectively. The reduction was higher for the case of a central opening compared to the cases of eccentric openings. The angle of the struts in this case was near horizontal especially for the strut above the opening (in the spandrel) and below the opening, which added high level of shear stresses on the mortar bed joints.

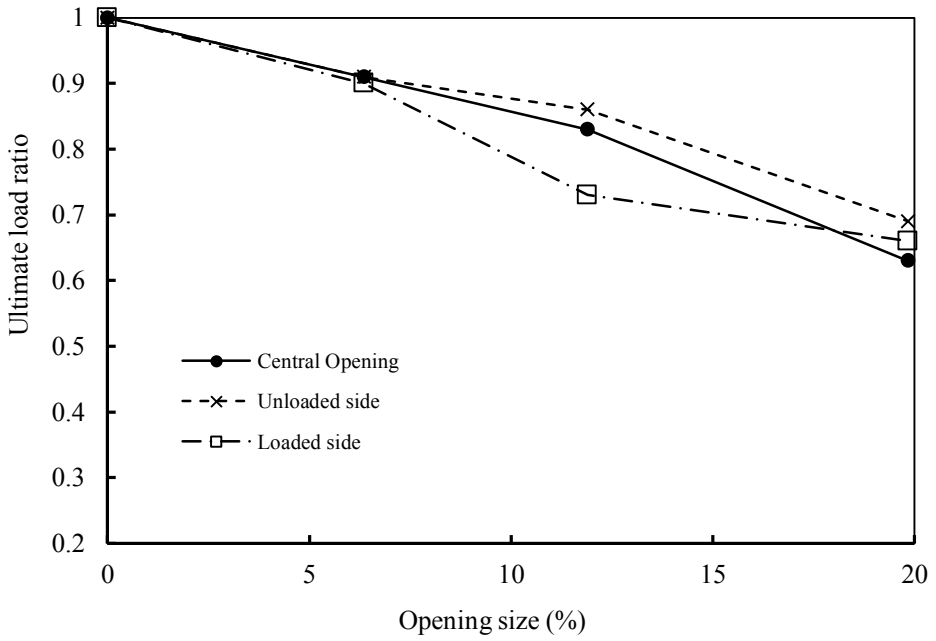

Figure 7-60: Effect of window opening size and location on the ultimate lateral load for masonry infilled steel frames with $h/l = 0.76$

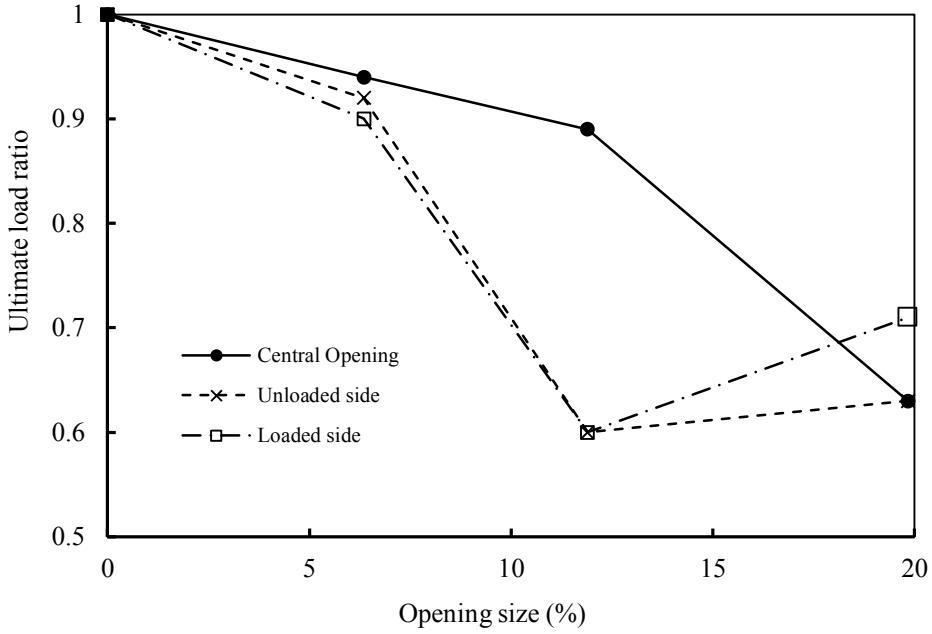

Figure 7-61: Effect of window opening size and location on the ultimate lateral load for masonry infilled RC frames with $h/l = 0.76$

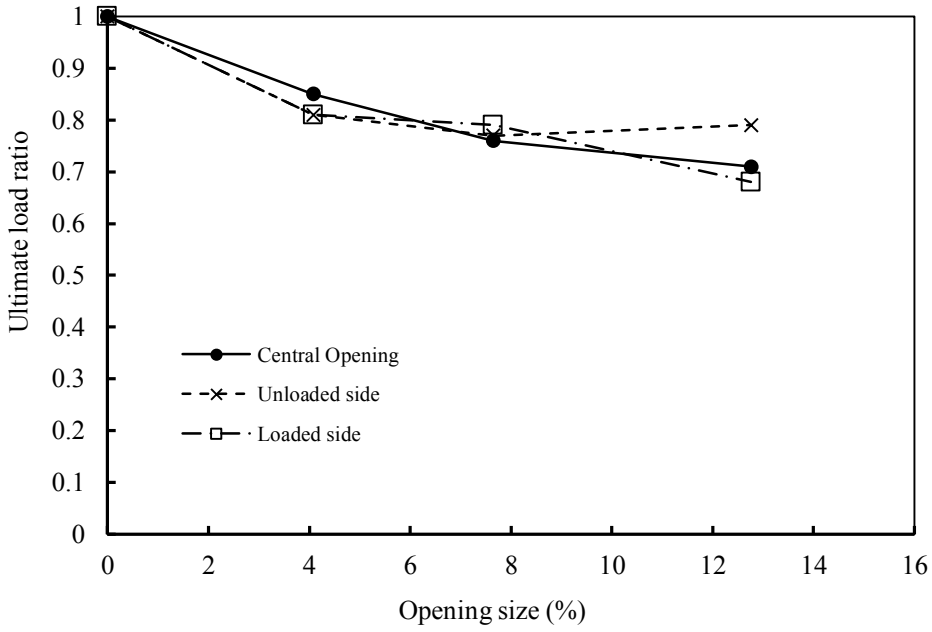

Figure 7-62: Effect of window opening size and location on the ultimate lateral load for masonry infilled steel frames with $h/l = 0.5$

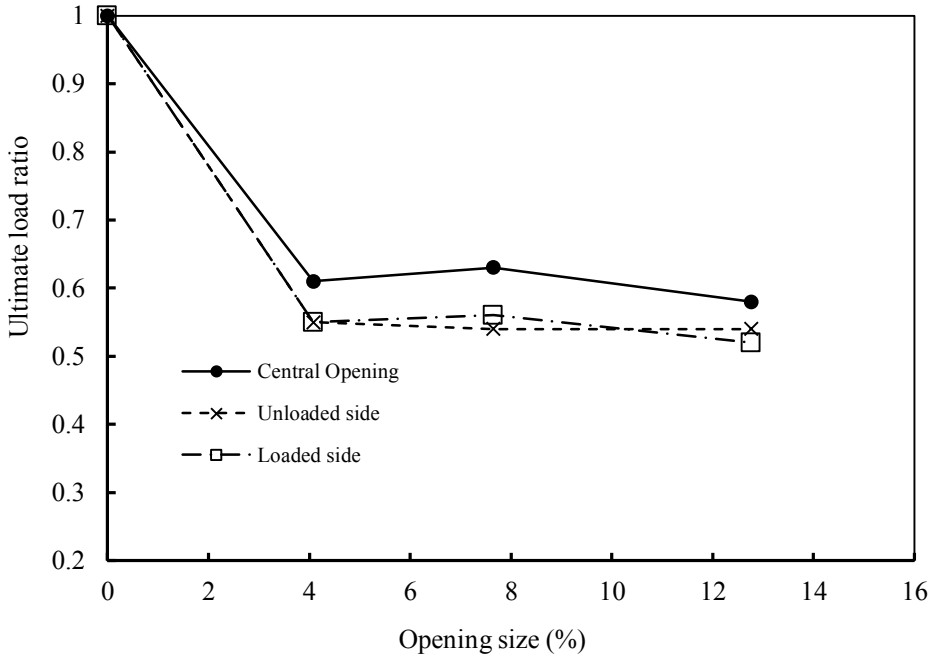

Figure 7-63: Effect of window opening size and location on the ultimate lateral for masonry RC steel frames with $h/l = 0.5$

For infilled RC frames with aspect ratio of 0.5, increasing the size of the window opening led to increasing the reduction of the ultimate load. When a large window opening of area that is 12.8%, the reduction in the ultimate load was reported to be almost 50% for all location. The ultimate displacement corresponding to the ultimate load was reduced by 45% compared to a solid infilled RC frame. The failure mode of the infilled RC frame was independent on the opening location. The infilled frames failed due to sliding shear regardless of the opening location which led to minor difference in the computed value for the ultimate load and corresponding displacement.

For infilled steel frame with a walls with aspect ratio of 0.5, the location of a large opening of area that is 12.8% of the wall surface area did not significantly have an effect on the ultimate load compared to infilled steel frame with a central opening of the same size. The reduction in the ultimate load was 29%, 32% and 21% compared to a solid infilled steel frame for a central opening, eccentric opening towards load, and eccentric opening away from the load; respectively. The

developed diagonal strut in the infill wall had almost the same resistance leading to this minor difference in the ultimate load. The ultimate displacement was reduced by 15% for infilled steel frame with central opening compared to a solid infilled frame.

7.5. Closure

Results of the finite element models for masonry infilled frames with openings were presented and discussed in this chapter. The results have shown that a diagonal strut was formed in the infill wall when the opening size was of 10% or less of the infill wall surface area. For larger window and door openings, a set of compression struts were formed around the opening and transmitted the load through the wall. The presence of an opening led to reductions in the initial stiffness and ultimate lateral load of the infilled frames compared to frames with solid infill walls. The reduction was higher in case of infill walls with lower aspect ratio (0.5).

CHAPTER 8

SUMMARY AND CONCLUSIONS

8.1. Summary

The methodology for calculating the lateral load resistance of masonry infill shear walls according to current design codes and standards are limited to cases that are rare in real construction. None of the current design codes and standards has design provisions for masonry infill shear walls with openings. Although the behaviour of this type of wall has been investigated, there is still significant gap in the understanding of their response; most of the investigations were performed on scaled specimens which do not necessarily represent the true behaviour of the infilled frame system. In addition, the investigations were confined to a few parameters due to time and budget limitations.

This research contributed to filling the gap in knowledge of the lateral load-lateral displacement response of masonry infill shear walls, especially masonry infill walls with openings. The simplified micro-modelling technique was adopted in the current investigation where masonry units were extended by half the thickness of the mortar joint from all sides, and the interface between the units was assigned the properties of the mortar.

Three dimensional finite element technique was used to model masonry infilled steel and RC frames using the simplified micro-modelling approach. The contact between different masonry units and between the masonry infill wall and the containing frame was modelled using a cohesive interface element that follows a traction separation law to model failure in the mortar joints. A commercially available finite element package, ABAQUS 6.10-EF (SIMULIA, 2010), was used to build the models.

Results of 9 steel and 8 RC frames with concrete masonry infilled walls from four major research programs were used to validate the modelling technique. The infilled frames varied in size from full-scale to 1/3 scale and covered solid masonry infill walls and masonry infill walls with window and door openings. The

lateral load-lateral displacement response and failure mechanism of the infilled frames were compared to the corresponding experimental results and were found to be in strong agreement.

The validated modelling technique was used to study the effect of the most influential parameters on the response of masonry infilled frames such as: infill wall aspect ratio, gap size and location between the frame and the infill wall, presence of haunches in the frame, infill wall stiffness, and size and location of openings in the masonry infill wall. The analysis was conducted on full-size steel and RC masonry infilled frames. The sizes and dimensions of these master frames reflect usual length and height of the masonry infill wall for a 3-storey building. The masonry infill wall was 2800 mm in height, and the length varied to reflect different aspect ratios ranging from 1.0 to 0.5. The frames were designed and detailed according to the 2010 NBCC.

In the finite element models, frames were loaded by applying a quasi-static lateral displacement at one of the top corners of the infilled frame system. The corresponding lateral load was computed from the integration of the reactions at the frame base. Dynamic explicit solver in ABAQUS, suitable for analyzing structures with relatively short dynamic response time, was used to carry out the analysis. The lateral load-lateral displacement response and principal compressive stresses at failure were exported from the analysis. The main parameters investigated from the lateral load lateral displacement response were initial stiffness, cracking load, ultimate load and the corresponding displacement.

42 infilled steel frames and 42 infilled RC frames were modelled to study the effect of the parameters listed above on the lateral load response of masonry infilled frame. Among them, 4 masonry infilled steel frames and 4 masonry infilled RC frames were used to study the effect of different aspect ratios (0.5, 0.59, 0.76 and 1.0) on the lateral behaviour. 8 masonry infilled steel frames and 8 masonry infilled RC frames were built to investigate the effect of gap size and location on the lateral response of infilled frames. The sizes of the gap considered were 5 mm, 7 mm, 10 mm and 15mm. Both a top gap between the frame's beam and the

masonry infill wall and a full separation gap were investigated. Four sizes for the frame's haunch were introduced in the infilled steel and RC frames to study the effect of haunched frames on the behaviour. The effect of the stiffness of the infill wall was investigated by considering two grout configurations (fully and partially grouted masonry).

Four opening sizes (800×800 mm, 1200×1000 mm, 800×2200 mm and 2000×1000 mm) were used in the current research to investigate the effect of the opening size and location on the lateral response of infilled frames. The opening was placed at the center of the wall, eccentric towards the load and eccentric away from the load.

8.2. Conclusions

Conclusions drawn from the current research are presented in the next four sections: the first addresses the appropriateness of the diagonal strut width expressions in the current codes and standards, the second section is on the adequacy of the developed finite element technique in estimating the lateral load-lateral displacement behaviour of masonry infilled frames, the third section addresses the findings of the behaviour of solid infill walls, while the fourth addresses the findings of the behaviour of solid infill walls with window and door openings.

8.2.1. Design Codes and Standards

The diagonal strut design equations for masonry infill shear walls in the Canadian standard, the New Zealand standard, and the American code were evaluated using available experimental results. All three design documents failed to provide a consistent estimate for the lateral load resistance. The following conclusions can be drawn:

1. The design expression for masonry infill walls failing due to corner crushing in the current Canadian masonry standard S304.1-04 overestimates the in-plane lateral resistance of infill walls bounded by steel frames by a wide range from 5% to 100%, with an average of one-third.
2. The New Zealand masonry design standard NZS 4230-2004 grossly

overestimates the resistance of masonry walls filling steel frames and failing by corner crushing. It is recommended that a reduction factor of 0.5 be applied to masonry compressive strength, similar to the Canadian standard, to account for the inclined direction of the compressive stresses that develop in the compression strut.

3. The New Zealand standard was the only design document that yielded resistance values that are comparable to the measured resistance for concrete masonry infilled concrete frames.
4. The American code (2011 MSJC) consistently provided lateral load resistance estimates for masonry infill walls that are less than the measured values. However, it extremely underestimated the resistance of concrete masonry infill walls contained by concrete frames which could result in uneconomical designs.

The current design codes/standards expressions should be updated to accurately reflect the behaviour of masonry infilled frames. In the Canadian standard, the equations for the diagonal strut width takes only into account the effect of beam and column stiffness; and not the overall stiffness of the frame (i.e.: the beam-column connection). The 2011 MSJC needs equations for RC infilled frames as the current equations were based on the behaviour of steel frames filled with clay tiles.

8.2.2. Adequacy of the Finite Element Technique

The developed finite element technique, based on the simplified micro-modelling technique was validated against 9 masonry infilled steel frames and 8 masonry infilled RC frames. The following conclusions can be drawn:

1. For solid infill walls, the developed finite element technique was capable of predicting the initial stiffness with an average of 0.99 and a coefficient of variation of 19.06%, cracking load with an average value of 0.93 and a coefficient of variation of 19.53%, and ultimate load with an average value of 0.97 and a coefficient of variation of 4.59% compared to measured experimental values. The displacement associated with ultimate loading

was predicted with an average value of 1.12 and a coefficient of variation of 18.73%.

2. The developed technique succeeded, also, in predicting the initial stiffness, ultimate load, ultimate displacement for infill walls with openings. The initial stiffness had an average of 1.00 and a coefficient of variation of 11.57%. The predicted cracking load had an average of 1.14 and coefficient of variation of 34.53%, while the predicted ultimate load had an average of 0.98 with a coefficient of variation of 4.91%; while the displacement associated with the ultimate load had an average of 1.03 and a coefficient of variation of 15.33%.
3. The finite element technique demonstrated strong agreement with the experimental results; hence, it was used to investigate the effect of the most influential parameters on the lateral load-displacement response of masonry infilled frames.

8.2.3. Behaviour of Solid Masonry Infill Walls

1. The most common failure mechanisms for solid infill walls took the form of diagonal tension cracking and corner crushing. In most models, masonry infill walls failed due to crushing at the corner of the developed strut even after the development of diagonal tension cracks in the wall.
2. A diagonal compression strut was formed in the infill wall regardless of the failure pattern of the masonry infill wall. The width of this strut was not constant and varied significantly with the loading level exerted on the masonry infilled frames.
3. The presence of a top gap between the masonry infill wall and the containing frame did not have significant effect on the ultimate load of the masonry infilled frames. The maximum reduction in the ultimate load for steel and RC infilled frames compared to infilled frames with no gap was found to be 25% for a 15 mm top gap size; the initial stiffness and cracking load in the case of infill steel frames experienced higher reduction of 60% for 15 mm gap compared to infill walls in full contact with the containing frame. This might be attributed to the lower stiffness of the steel frame used.

4. The contribution of the masonry infill wall lateral load resistance should be discounted when a 10 mm full separation gap is introduced between the masonry infill wall and the containing frame. A full separation gap of up to 5 mm will not impact the in-plane behaviour of infilled frames.
5. Haunched frames led to smooth transition from the linear to non-linear behaviour of the masonry infilled frames. The ultimate load was increased by 50% for a haunch size of $600\sqrt{2}$ mm.

8.2.4. Behaviour of Masonry Infill Walls with Openings

1. Sliding shear failure of masonry infill walls with openings is a possible failure mechanism in addition to diagonal tension and corner crushing of masonry. Sliding shear failure is the dominating failure mode for infill walls with large opening sizes and/or small aspect ratios (0.5).
2. A single diagonal strut was formed in the masonry infill wall having a window opening smaller than 10% of the surface area of the masonry infill wall. For large openings, a group of struts was developed in the masonry infill wall around the opening.
3. The presence of a window/door opening within the infill wall led to a reduction in initial stiffness, cracking load, and ultimate lateral load of the infilled frame.
4. The maximum displacement of masonry infilled frames with window or door openings was dependent on the mode of failure. Masonry infill walls failing by diagonal tension cracking had the least displacements compared to the other modes of failure.
5. When a door opening was located away from the load, the developed compression strut was not confined by the frame, and it spanned from the loaded corner to the bottom of the pier towards the loaded side. The initial stiffness of the infilled frames, cracking and ultimate loads were greatly reduced.
6. The best location for an opening in an infill wall is where the interference with the developed compression strut is minimum.

8.3. Recommendations for Future Research

While this research has contributed to understanding of the true in-plane response of masonry infill shear walls, it is recognized that it did not cover all the aspects of the behaviour. The following are recommendations for future research:

1. Although the most practical values for the different parameters have been investigated in this research, the range of the parameters could be widened to include more values such as: stiffness of the frame relative to the infill wall, opening sizes more than 20% of the infill wall surface area located centrically or eccentrically from the centre of the infill wall. Additional analysis is recommended to cover the wide range.
2. Investigating the in-plane response of masonry infill walls under cyclic loading is important but requires the development of material models capable of stimulating the damage and crack development in the masonry infill wall and the containing frame. This aspect of the behaviour was not part of the scope of this research.
3. In most cases, masonry infill walls are subjected to out-of-plane loads which could cause them to crack. It is important that this in-plane behaviour of cracked masonry infill walls be quantified. This analysis was not part of the scope of this research.
4. The size of data, current state of knowledge and complexity of the behaviour of masonry is hindering the effort of developing a simplified design approach for masonry infilled frames with and without openings that can be adopted in design codes and standards. Developing a simplified design approach would enable engineers to properly account for the contribution of masonry infill walls to lateral resistance.

REFERENCES

ACI 318-89. (1989). *Building Code Requirement for reinforced concrete.* ACI, Detroit, Michegan.

Alam, M. S., Nehdi, M., and Amanat, K. M. (2009). "Modelling and analysis of retrofitted and un-retrofitted masonry-infilled RC frames under in-plane lateral loading." *Structure and Infrastructure Engineering,* 5(2), 71-90.

Al-Chaar, G. (2002). "Evaluating strength and stiffness of unreinforced masonry infill structures." US Army Corps of Engineers, Engineering Research and Development Center, Construction Engineering Research Laboratory, Champaign, IL.

Al-Chaar, G. (1998). "Non-Ductile Behaviour of Reinforced Concrete Frames with Masonry Infill Panels Subjected to In-Plane Loading." PhD thesis, University of Illinois at Chicago, Chicago, USA, .

Al-Chaar, G., and Mehrabi, A. B. a. M., T. (2008). "Finite element interface modelling and experimental verification of masonry-infilled R/C frames." *Masonry Society Journal,* 26(1), 47-65.

Al-Chaar, G., Issa, M., and Sweeney, S. (2002). "Behavior of masonry-infilled nonductile reinforced concrete frames." *J.Struct.Eng.,* 128(8), 1055-1063.

AS 3700-01. (2001). *Australian Standards Masonry Structures.* Standards Australia International Ltd, Sydney, NSW, Australia.

Asteris, P. G. (2008). "Finite element micro-modelling of infilled frames." *Electronic Journal of Structural Engineering,* 8 1-11.

Blackard, B., Willam, K., and Mettupalayam, S. (2009). "Experimental observations of masonry infilled reinforced concrete frames with

openings." *ACI Fall 2009 Convention, November 8, 2009 - November 12,* American Concrete Institute, New Orleans, LA, United states, 199-221.

BS 5628-1-05. (2005). *Code of practice for the use of masonry. Part 1, Structural use on unreinforced masonry.* BSI, London, England.

BS 5628-2-05. (2005). *Code of practice for the use of masonry. Part 2, Structural use of reinforced and prestressed masonry.* BSI, London, England.

Chiou, Y., Tzeng, J., and Liou, Y. (1999). "Experimental and analytical study of masonry infilled frames." *Journal of Structural Engineering New York, N.Y.,* 125(10), 1109-1117.

CSA S304.1-04. (2004). *Design of masonry Structures S304.1-04.* Canadian Standards Association, 5060 Spectrum Way, Suite 100, Ontario, Canada.

Dawe, J. L., Liu, Y., and Seah, C. K. (2001). "A parametric study of masonry infilled steel frames." *Can.J.Civ.Eng.,* 28(1), 149-157.

Dawe, J. L., and Seah, C. K. (1989). "Behaviour of masonry infilled steel frames." *Canadian Journal of Civil Engineering,* 16(6), 865-876.

Dawe, J. L., Seah, C. K., and Liu, Y. (2001). "A computer model for predicting infilled frame behaviour." *Can.J.Civ.Eng.,* 28(1), 133-148.

Drysdale, R. G., and Hamid, A. A. (2005). "Masonry Structures Behaviour and Design." Canada Masonry Design Center, Mississauga, Ontario, Canada, 531-562.

El-Dakhakhni, W. W. (2002). "Experimental and analytical seismic evaluation of concrete masonry-infilled steel frames retrofitted using GFRP laminates." PhD thesis, Drexel University, United States -- Pennsylvania, .

El-Dakhakhni, W., Hamid, A. A., and Elgaaly, M. (2004). "Seismic retrofit of concrete-masonry-infilled steel frames with glass fiber-reinforced polymer laminates." *J.Struct.Eng.,* 130(9), 1343-1352.

El-Dakhakhni, W. W., Elgaaly, M., and Hamid, A. A. (2003). "Three-strut model for concrete masonry-infilled steel frames." *J.Struct.Eng.-ASCE,* 129(2), 177-185.

EN 1996-1-1. (2006). *Eurocode 6: Design of masonry structures - Part 1-1: General rules for reinforced and unreinforced masonry structures, EN 1996-1-1:2005.* European Committee for Standardization, Brussels, Belgium.

FEMA 306 (1998). "Evaluation of Earthquake damaged concrete and masonry wall buildings." *Applied Technology Council (ATC-43 project)*, 555 Twin Dolphin Drive, suite 550, Redwood city, California, USA.

FEMA 356. (2000). *Prestandard and Commentary for the Seismic Rehabilitation of Buildings.* Federal Emergency Management Agency, Washington, D.C., U.S.A.

Flanagan, D. P., and T. Belytschko, (1981). "A Uniform Strain Hexahedron and Quadrilateral with Orthogonal Hourglass Control." International Journal for Numerical Methods in Engineering, vol. 17, pp. 679–706.

Flanagan, R. D., and Bennett, R. M. (2001). "In-plane analysis of masonry infill materials." *Pract.Periodical Struct.Des.Constr.,* 6(4), 176-182.

Flanagan, R. D., and Bennett, R. M. (1999). "In-plane behavior of structural clay tile infilled frames." *Journal of Structural Engineering New York, N.Y.,* 125(6), 590-599.

Hassanzadeh, M. (1990). "Determination of fracture zone properties in mixed mode I and II." *Eng.Fract.Mech.,* 35(4-5), 845-853.

Hillerborg, A., Modéer, M., and Petersson, E. (1976). “Analysis of Crack Formation and Crack Growth in Concrete by Means of Fracture Mechanics and Finite element.” *Cement and concrete research*, vol. 6, 773-782.

Kakaletsis, D. J., and Karayannis, C. G. (2009). "Experimental investigation of infilled reinforced concrete frames with openings." *ACI Struct.J.,* 106(2), 132-141.

Kaltakc, M. Y., Koken, A., and Korkmaz, H. H. (2006). "Analytical solutions using the equivalent strut tie method of infilled steel frames and experimental verification." *Canadian Journal of Civil Engineering,* 33(5), 632-8.

Karayannis, C. G., and Chalioris, C.E. and Sideris, K.K. (1998). "Effectiveness of RC Beam-Column Connection Repaired using Epoxy Resin Injections." *Journal of Earthquake Engineering,* 2, No. 2 217-240.

Koutromanos, I., Stavridis, A., Shing, P. B., and Willam, K. (2011). "Numerical modelling of masonry-infilled RC frames subjected to seismic loads." Elsevier Ltd, Langford Lane, Kidlington, Oxford, OX5 1GB, United Kingdom, 1026-1037.

Lanagan, D. P., and T. Belytschko, (1981). “A Uniform Strain Hexahedron and Quadrilateral with Orthogonal Hourglass Control,” International Journal for Numerical Methods in Engineering, vol. 17, pp. 679–706.

Liauw, T. C. (1972). "An approximate method of analysis for infilled frames with and without opening." *Build. Sci.,* 7 233-238.

Liauw, T. C., and Kwan, K. H. (1983). "Plastic theory of non-integral infilled frames." *PROCEEDINGS OF THE INSTITUTION OF CIVIL ENGINEERS PART 2-RESEARCH AND THEORY,* 379-396.

Liu, Y., and Manesh, P. (2013). "Concrete masonry infilled steel frames subjected to combined in-plane lateral and axial loading - An experimental study." *Engineering Structures*, Vol. 52, pp 331-339

Lotfi, H. R., and Shing, P. B. (1994). "Interface model applied to fracture of masonry structures." *Journal of Structural Engineering New York, N.Y.,* 120(1), 63-80.

Lourenço, P. B. (1996). *Computational Strategies for Masonry Structures.* Delf University Press, Stevinweg 1, 2628 CN Delft, Netherland.

Mainstone, R. J. (1971). "On the stiffnesses and strengths of infilled frames." *Institution of Civil Engineers, Proceedings,* Vol. iv 57-90.

Mainstone, R.J., Weeks, G.A. (1971). "The influence of a bounding frame on the racking stiffness and strengths of brick walls." *Proceedings of The Second International Brick Masonry Conference*, SIBMAC, pp. 165-171.

Mann, W. and Müller, H. (1982). "Failure of Shear-Stresses Masonry - An Enlarged Theory, Tests and Application to Shear Walls." *Proceedings of the British Ceramic Society*, Vol. 30, pp. 139-149.

Mehrabi, A. B., Shing, P. B., Schuller, M. P., and Noland, J. L. (1994). "Performance of Masonry-Infilled R/C Frames under In-Plane Lateral Loads." United States.

Mehrabi, A. B., and Shing, P. B. (1997). "Finite element modelling of masonry-infilled RC frames." *Journal of Structural Engineering New York, N.Y.,* 123(5), 604-613.

Mehrabi, A. B., Shing, P. B., Schuller, M. P., and Noland, J. L. (1996). "Experimental evaluation of masonry-infilled RC frames." *Journal of Structural Engineering New York, N.Y.,* 122(3), 228-237.

Mexican Code. (2004). *Complementary Technical Norms for Design and Construction of Masonry Structures.* Mexico City Building Code Ltd., Mexico City, Mexico.

Moghaddam, H. A. (2004). "Lateral load behavior of masonry infilled steel frames with repair and retrofit." *J.Struct.Eng.,* 130(1), 56-63.

MSJC. (2011). *Masonry standards Joint Committee: Building Code Requirements and Specification for Masonry Structures* . Boulder, Colorado; Farmington Hills, MI, Structural Engineering Institute of the American Society of Civil Engineers, Reston, VA, .

NZS 4230. (2004). *Design of Reinforced Concrete Masonry Strucutures.* Standards New Zealand, the trading arm of the Standards Council, Private Bag, Wellington 6140.

Rodrigues, H., Varum, H., and Costa, A. (2010). "Simplified Macro-Model for Infill Masonry Panels." *J.Earthquake Eng.,* 14(3), 390-416.

Saneinejad, A., and Hobbs, B. (1995). "Inelastic design of infilled frames." *Journal of Structural Engineering New York, N.Y.,* 121(4), 634-649.

Shi, G. H. (1988). "Discontinuous deformation analysis: A new numerical model for the statics and dynamics of block systems." PhD thesis, Dept. of Civil Engrg., University of California, Berkeley, California, .

Shing, P. B., Stavridis, A., Koutromanos, I., Willam, K., Blackard, B., Kyriakides, M. A., Billington, S. L., and Arnold, S. (2009). "Seismic performance of non-ductile RC frames with brick infill." *2009 ATC and SEI Conference on Improving the Seismic Performance of Existing Buildings and Other Structures, December 9, 2009 - December 11,* American Society of Civil Engineers, San Francisco, CA, United states, 1117-1128.

SIMULIA (2010). "ABAQUS 6.10 EF-2 Theory Manual." Abaqus, Providence, RI, USA.

Smith, B. S. (1966). "Behaviour of square infilled frames." *J. Struct. Div., ASCE,* 92 381-403.

Smith, B. S., and Carter, C. (1969). "A Method of Analysis for Infilled Frames." *Proceedings of the Institution of Civil Engineers,* 44(SEP), 31-&.

Stafford-Smith, B., and Coull, H. (1991). "Chapter 8: Infilled-Frame Structures." *Tall Building Structures: Analysis and Design,* John Wiley and sons. Inc, New York, USA, 168-183.

Stavridis, A., and Shing, P. B. (2010). "Finite-element modelling of nonlinear behavior of masonry-infilled RC frames." *J.Struct.Eng.,* 136(3), 285-296.

Tasnimi, A. A., and Mohebkhah, A. (2011). "Investigation on the behavior of brick-infilled steel frames with openings, experimental and analytical approaches." *Eng.Struct.,* 33(3), 968-980.

Taylor, R. L. (2007). *FEAP--A finite element analysis program--version 8.1.* Univ. of California at Berkeley, Berkeley, California.

Tiedeman, H. (1980). "A statistical evaluation of the importance of non-structural damage in buildings." *Proc., 7th World Conference on Earthquake Engrg.* 617-624.

Van der Pluijm, R. (1992). "Material properties of masonry and its component under tension and shear." *Proc., 6th Canadian Masonry Symp.* 675-686.

Yàñez, F., Astroza, M., Holmberg, A. and Ogaz, O. (2004). "Behavior of confined masonry shear walls with large openings." Proceedings of the 13th world conference on Earthquake engineering, Vancouver, B.C., Canada, p.14

Zeinkiewicz, O.C. and Taylor, R.L. (2000). *The Finite Element Method.* Butterworth-Heinemann, Oxford, U.K.